MONASH University

4D Image Guided Linac Based Stereotactic Body Radiotherapy Treatment for Primary Renal Cell Carcinoma

Daniel Josef Pham

A thesis submitted for the degree of Doctor of Philosophy at Monash University in 2020

Faculty of Medicine, Nursing and Health Sciences

Table of Contents

Declaration

This thesis contains no material which has been accepted for the award of any other degree or diploma at any university or equivalent institution and, to the best of my knowledge and belief, this thesis contains no material previously published or written by another person, except where due reference is made in the text of the thesis.

Signature:
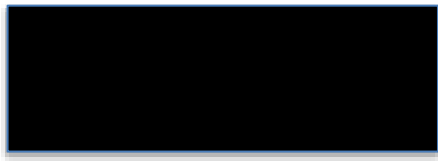
Print Name: Daniel Josef Pham

Date: May 4, 2020

Thesis including published works declaration

I hereby declare that this thesis contains no material which has been accepted for the award of any other degree or diploma at any university or equivalent institution and that, to the best of my knowledge and belief, this thesis contains no material previously published or written by another person, except where due reference is made in the text of the thesis.

This thesis includes five original papers published in peer reviewed journals publications. The core theme of the thesis is stereotactic body radiotherapy for primary renal cell carcinomas. The ideas, development and writing up of all the papers in the thesis were the principal responsibility of myself, the student, working within the Faculty of Medicine, Nursing and Health Sciences at Monash University under the supervision of Professor Michal Schneider and at the Peter MacCallum Cancer Centre under the supervision of Professor Tomas Kron and Dr Farshad Foroudi. Further supervision and mentorship was provided by Dr Shankar Siva. (The inclusion of co-authors reflects the fact that the work came from active collaboration between researchers and acknowledges input into team-based research.)

In the case of chapters 2, 3, 4 and 5 my contribution to the work involved the following:

Thesis Chapter	Publication Title	Status	Nature and % of student contribution	Co-author name (s) Nature and % of Co-author's contribution*	Co-author(s), Monash student Y/N*
2	A Review of Kidney Motion under Free, Deep and Forced-Shallow Breathing Conditions: Implications for Stereotactic Ablative Body Radiotherapy Treatment	Published	90% of study concept, data collection, data analysis/interpretation and input into manuscript writing.	Tomas Kron, input into manuscript 2.5%; Farshad Foroudi, input into manuscript 2.5%; Michal Schneider, input into manuscript 2.5%; and Shankar Siva, input into manuscript 2.5%.	N
3	The use of dual vacuum stabilization device to reduce kidney motion for stereotactic radiotherapy planning	Published	70% of study concept, study design, participant recruitment, data collection, data analysis and manuscript writing.	Tomas Kron, input into manuscript and study design 5%; Colin Styles, input into manuscript, data generation and study design 5%; May Whitaker, input into manuscript and data	N
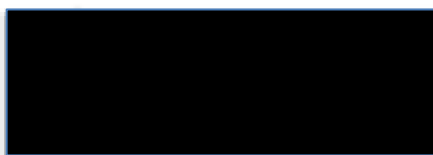
				generation 5%; Mathias Bressel, data analysis and input into manuscript 5%; Kim Dang, data collection; 1%; Thomas Devereux, data collection 1%; Farshad Foroudi, input into manuscript and study design 2%; Michal Schneider, input into manuscript 4%; and Shankar Siva, input into manuscript and study design 2%.	
4	A Phase 1 Study of Stereotactic Body Radiation Therapy for Primary Kidney Cancer: A 3D conformal technique associated with low rates of early toxicity.	Published	80% input into study concept and design, data generation, data collection, data analysis and manuscript writing.	Tomas Kron; input into manuscript, study design and data analysis 5%; Ann Thompson, input into manuscript and data generation 1%; Andrew Lim, data generation 1%; Thomas Devereux, data generation 1%; Farshad Foroudi, input into manuscript and study design 3%; Michal Schneider, input into manuscript 4%; and Shankar Siva, input into manuscript and study design 5%.	N
5	Image guidance and stabilization for stereotactic ablative body radiotherapy (SABR) treatment of primary kidney cancer	Published	70% input into study concept and design, data generation, data collection, data analysis and manuscript write up.	Tomas Kron, input into manuscript and study design 5%; Nicholas Hardcastle, input into manuscript 2%; Mathias Bressel, data analysis and input into manuscript 6%; Sally Soteriou, data generation and input into manuscript 2%; Jason Innes, data generation and input	N

				into manuscript 2%; Farshad Foroudi, input into manuscript and study design 3%; Michal Schneider, input into manuscript 5%; and Shankar Siva, input into manuscript and study design 5%.	

I have renumbered sections of submitted or published papers in order to generate a consistent presentation within the thesis.

Student name: Daniel Pham
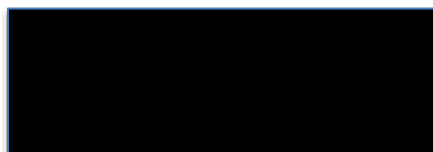
Student signature: **Date:** May 4, 2020

The undersigned hereby certify that the above declaration correctly reflects the nature and extent of the student's and co-authors' contributions to this work. In instances where I am not the responsible author I have consulted with the responsible author to agree on the respective contributions of the authors.

Main Supervisor name: Michal Schneider

Main Supervisor signature: **Date:** May 19, 2020

Publications During Enrolment

I.   **Daniel Pham, Tomas Kron, Farshad Foroudi, Michal Schneider, Shankar Siva**

A Review of Kidney Motion under Free, Deep and Forced-Shallow Breathing Conditions: Implications for Stereotactic Ablative Body Radiotherapy Treatment *Journal of Technology in Cancer Research and Treatment 2014 13(4) pp315-323*

II.   **Daniel Pham, Tomas Kron, Colin Styles, May Whitaker, Mathias Bressel, Farshad Foroudi, Michal Schneider, Tomas Devereux, Kim Dang, Shankar Siva**

The use of dual vacuum stabilization device to reduce kidney motion for stereotactic radiotherapy planning. *Journal of Technology in Cancer Research and Treatment, April 2015 14(2) pp149-157.*

III.   **Daniel Pham, Anne Thompson, Tomas Kron, Farshad Foroudi, Michal Schneider-Kolsky, Thomas Devereux, Andrew Lim, Shankar Siva**

Stereotactic Ablative Body Radiotherapy for Primary Kidney Cancer: A 3-Dimensional Conformal Technique Associated with Low Rates of Early Toxicity. *International Journal of Radiation Oncology Biology and Physics 2014 90(5) pp1061-1068*

IV.   **Daniel Pham, Tomas Kron, Mathias Bressel, Farshad Foroudi, Nicholas Hardcastle, Michal Schneider, Sally Soteriou, Jason Innes and Shankar Siva**.

Image guidance and stabilization for stereotactic ablative body radiation therapy (SABR) treatment of primary kidney cancer. *Practical Radiation Oncology 2015 5(6) e597-e605*

Acknowledgements

It has been my honour to be part of this effort in bringing this protocol to life at Peter Mac as it not only allowed me to work with community leaders but as well be present to see how life-changing it was for patients travelling from all over Australia to receive this treatment. To hear from a 90-year patient how happy and grateful she was about being given an option for treatment made every data crunching session worthwhile. When she asked to keep one of the treatment accessories (vacsheet) after her final treatment, I was humbled by her practical outlook to the entire experience.

This project would not have been possible and successful without the vision of Dr Farshad Foroudi, the tireless energy of Professor Tomas Kron and the charisma of Dr Shankar Siva. Putting all this work together and realising how much was achieved could only have been done with the patience of Professor Michal Schneider, who was always encouraging and kept me on the correct path of this academic journey.

To Farshad who has always thought big and was always supportive and encouraging of those interested in technology and professional development. Your inclusiveness of every member of the department encouraged not only me but others in doing what we never thought was possible.

To Shankar, you brought high energy and leadership to this project. Your ideas, charisma and willingness to support your team members inspired not only me but a gaggle of therapists to get into research and development.

To Tomas, you are an inspiration to not only me but the entire radiotherapy team engaging everyone into meaningful research. Your sense of humour and respect for all made working (and travelling) with you an absolute pleasure. Without your guidance, I would not have been able to see how important the work was to the global community.

To Michal, I wanted to thank you for your patience in guiding me through this entire academic process. It not without a good reason that there is a waiting list of students seeking you as their supervisor. Your insight and feedback always kept me grounded with what a meaningful thesis is meant to be.

I wanted to thank the greater research team Tommy D, Kim Dang, Mathias, Nick, who made my research time at the Mac a truly enjoyable and learning environment. We all learnt from each other and had too many laughs despite all the challenges and difficulties that was pervading the department.

I look back and realise that it was not only a research group at the Mac but truly a multifaceted machine that not many saw for what it was. We developed training workshops, online training programs, national clinical trials that left a large impact within the radiation oncology community. I have never worked with such a dynamic and magnanimous team and feel it is my mission to bring as much of that energy and spirit to my new workplace.

Having said all of this, this thesis would not have been possible without the ongoing support, love and understanding from my wife, Candice. Many of the things I was talking about would not make any sense, but the support was always there. Our areas of expertise are as different as chalk and cheese, and yet Candice would always be able to lend her hand to whatever I was doing. Her design skills made me realise that scientific presentations did not have to be dull and boring as a little presentation makeover can make a huge impact.

Abbreviations

ASR   Age standardised rate

2D   2-dimensional

3D   3-dimensional

4D   4-dimensional

5-FU   5-fluorouracil

AJCC   American Joint Committee on Cancer

BMI   Body mass index

CBCT   Cone Beam Computed Tomography

CT   Computed tomography

DNA   Deoxynucleic acid

FH   Fumarate hydratase

FLCN   Folliculin

GDP   Gross Domestic Product

GTV   Gross Tumour Volume

HDI   Human development index

HGF   Hepatocyte growth factor

HIF   Hypoxia inducing factors

IFN   Interferon-alpha

IGRT   Image-Guided Radiation Therapy

IL2   Interleukin-2

IMRT   Intensity Modulated Radiation Therapy

ITV   Internal Target Volume

LET   Linear energy transfer

MET   Mesenchymal to Epithelial Transition

MLC   Multi-leaf collimators

MR   Magnetic resonance

mTOR   Mammalian target of rapamycin

MV   Megavoltage

PDGF   Platelet-derived growth factors

PORT   Postoperative radiotherapy

PTV   Planning Target Volume

RCC   Renal cell carcinoma

RFA   Radiofrequency ablation

RNA   Ribonucleic acid

RR   Relative risk

SDH	Succinate dehydrogenase
SEER	Surveillance, Epidemiology and End Results
TSC 1	Tuberous Sclerosis 1
TSC 2	Tuberous Sclerosis 2
VEGF	vascular endothelial growth factor
VHL	Von Hippel-Lindau
WHO	World Health Organization
Gy	Gray
BED	Biologically effective dose
eGFR	Estimated glomerular filtration rate
4DCT	4-dimensional computed tomography

List of Figures

List of Tables

15

Chapter 1

General Introduction

1.1 Global incidence and risk factors

Kidney cancer is ranked as the 16th most common cancer globally, presenting itself most commonly in the elderly between 60 - 74 years of age[1]. In countries such as Australia, United States and the United Kingdom the incidence is much higher[2-4] suggesting a link between a higher prevalence of kidney cancer and a region's socioeconomic status[2,5]. Possible explanations for this include an increased utilization rate of diagnostic imaging tools[6,7] contributing to incidental diagnosis of kidney cancers[8-11], as well as lifestyle factors such as smoking[12,13], obesity[14] and hypertension[15,16] which are more common in these regions[17-19]. Hereditary kidney cancers makeup roughly 4% of the incidence[20] and are associated with genetic diseases such as Von Hippel-Lindau disease, Tuberous Sclerosis disease[21] and Birt Hogg-Dube syndrome[22].

In 2018 the estimated number of new kidney cancer cases worldwide was 403 262 which has been projected to reach 650 000 by the year 2040[23]. Despite this increase in incidence for renal cell carcinomas[24], mortality rates have remained relatively unchanged[2,25,26]. Early diagnosis of kidney cancers has shown a pattern of disease downstaging[27,28] leading to more favourable intervention options. From 2004 - 2014 the US National Cancer Database[29] showed that more than 50% of kidney cancer diagnoses were related to small, early-stage disease, with less than 20% of cases presenting with metastatic disease. The 5-year relative survival rate currently is 92.5% for localised disease, 69.6% for regional disease (lymph node invasion) and 12% for metastatic spread of disease[30].

For early stage-localised disease, surgery is the gold standard for management[31-33]. However, for the elderly, those who have co-morbidities, have a single kidney or bulky disease there are limited alternatives for treatment[34]. Historically, radiation therapy has shown little benefit in prolonging survival[35]. However, in recent years, advances in technology and clinical practice have changed this notion. This thesis will focus on the role of radiation therapy as a treatment option for localised kidney treatment. The technical challenges that have limited its use in the past will be discussed and solutions demonstrated to show the efficacy and safety of current radiation therapy treatment.

1.2 Anatomy of the kidney

The kidneys are part of the urinary system involved in the removal of body waste in the bloodstream. They are bilateral organs located in the posterior abdomen with a convex shape that is capped by the adrenal gland and surrounded by fatty adipose tissue. The Gerota's fascia is a layer of connective tissue that encapsulates the kidney and adrenal gland (Figure 1a). Within the internal concave side of the kidney resides the renal hilum with the renal vein, renal artery and ureter exiting the kidney. The smooth outer layer of the kidney is the cortex and the inner part of the medulla which is composed of nephrons used in the filtration and reabsorption of water and amino acids[36]. The glomerular capsule is the site of high-pressure filtration of the blood which produces the nephron filtrate. This is passed through the proximal tubule where most of the reabsorption of metabolites occurs. The filtrate passes through a long descending loop which then ascends forming the loop of Henle before passing out through the renal papilla as urine (Figure 1b).
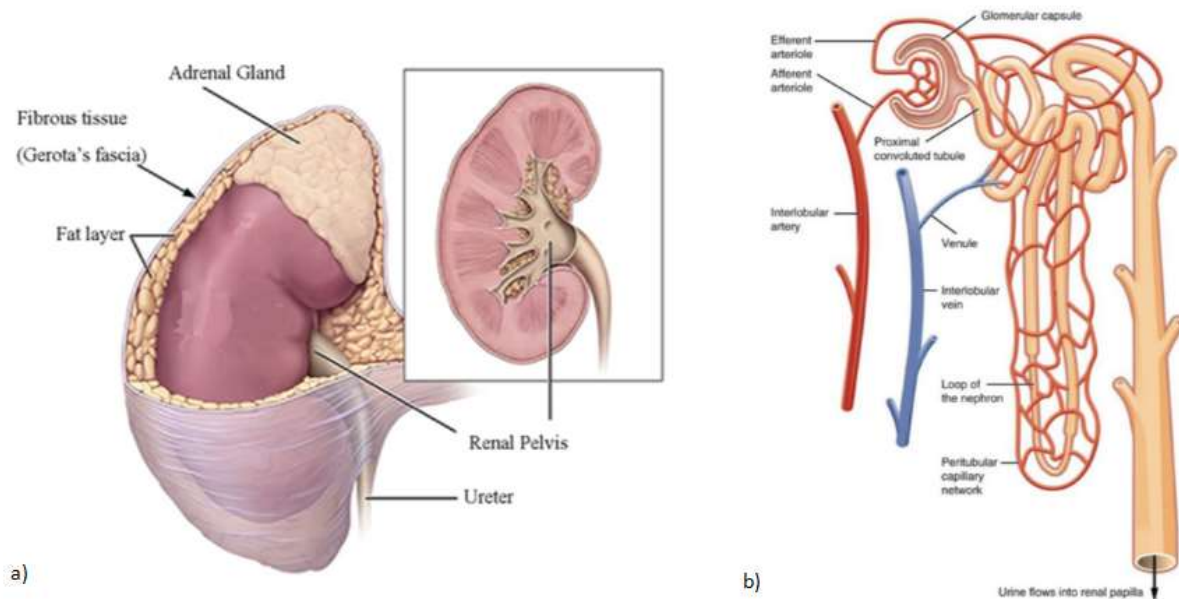
Figure 1. External and internal kidney anatomy and function

1a) The adrenal gland and kidney organ are surrounded by a layer of fatty tissue encapsulated by connective tissue known as Gerota's fascia. The renal pelvis, located at the centre of the kidney, is the location of urine collection[37]. 1b) Connecting between the outer cortex and inner medulla of the kidney are nephrons involved in the reabsorption of water and metabolites. Blood passes through the artery to the arterioles building up high pressure at the glomeruli to facilitate water and amino acid exchange[38].

In the surrounding abdominal cavity is the gastrointestinal system including the stomach, small bowel, large bowel, spleen, liver and pancreas (Figure 2).
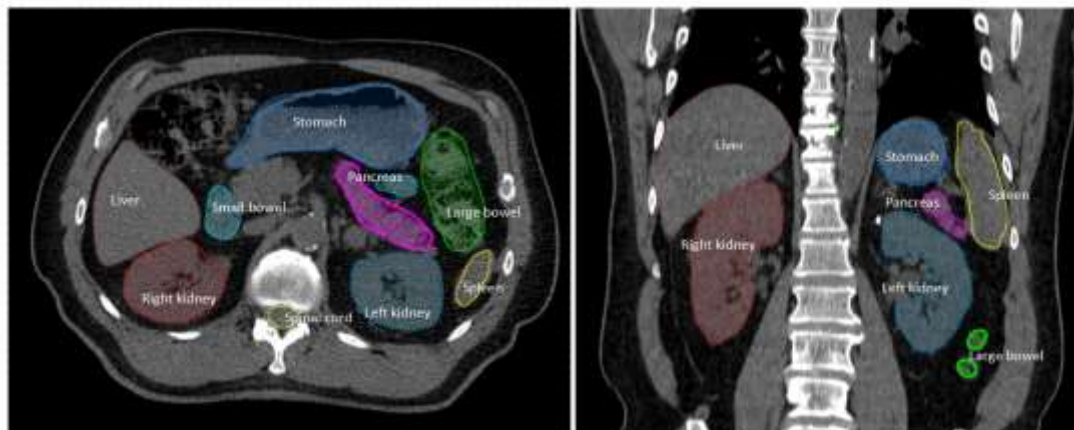
Figure 2. Anatomy of the kidney and surrounding organs.

The right and left kidneys are located in the posterior abdomen with little affixation to bony anatomy. Surrounding radiosensitive organs include stomach, liver, small bowel, large bowel and spinal cord. *Source: Stanford Radiation Oncology Center*

1.3 Kidney cancer classification and staging

Kidney cancers are classified as any neoplasm originating from any part of the kidney tubular epithelium[39]. Over forty histological variations of malignant and benign disease have been identified[40]. Renal cell type cancers that develop within the proximal and distal nephron tubules make up a large proportion of the disease with the most common histology being conventional clear cell carcinoma (73 – 78%), followed by papillary (10.2 - 18%) and then chromophobe type carcinoma (6 - 8.2%)[27,28,40-42]. Kidney cancers are classified according to the American Joint Committee on Cancer (AJCC) TNM staging system which reports the size of the tumour (T), nodal involvement (N), presence of metastatic disease (M) and if available, pathologic grade. Table 1 is a detailed summary of the TNM system to differentiate early and late-stage disease[43].

Table 1. Classification of kidney cancers using the TNM system published by AJCC 8th Edition

Stage	Description
TX	Primary tumour cannot be assessed
T0	No evidence of primary tumour
T1	Tumor 7cm or less in greatest dimension, limited to the kidney
T1a	Tumour 4cm or less (limited to kidney)
T1b	Tumour >4cm but less than 7cm (limited to the kidney)
T2	Tumour greater than 7cm and confined to the kidney
T2a	Tumour >7cm but less than or equal to 10cm
T2b	Tumours >10cm limited to kidney
T3	Tumour extension into major veins or perinephric tissue but not into ipsilateral adrenal gland or the Gerota's fascia
T3a	Tumour grossly extends into renal vein or its segmental branches or invades the pelvicalyceal system, or invasion into perirenal or renal sinus fat but not beyond Gerota's fascia.
T3b	Tumour extends into vena cava below diaphragm

T3c	Tumour extension into vena cava above diaphragm or into walls of vena cava,
T4	Tumour extension into ipsilateral adrenal glands or beyond the Gerota's Fascia.
NX	Regional lymph node cannot be assessed
N0	No regional lymph node
N1	Metastases in regional lymph node(s)
M0	No distant metastases
M1	Distant metastases present

Staging of kidney cancers (Table 2) is done based on tumour size and presence of local and distant node/organ invasion[43].

Table 2. Staging of kidney cancers based on tumour size, nodal involvement and presence of metastatic disease.

Stage	T	N	M
1	T1	N0	M0
2	T2	N0	M0
3	T1 - T2	N1	M0
	T3a - T3c	N0 - N1	M0
4	T4	N0 - N1	M0
	Any T	Any N	M1

Pathological grading of the disease is performed to differentiate slow-growing from faster/more aggressive cancers. The Fuhrman's grading system defines four levels: G1 - well differentiated, G2 - moderately differentiated, G3 - poorly differentiated, G4 - undifferentiated and GX - grade cannot be assessed[44].

1.4 Current standard of care for kidney cancers

Surgery has been the gold standard for early-stage, localised tumours of the kidney[34,45] with 5-year cancer-specific survival rates greater than 95%[46,47]. Small localised tumours less than 4cm in size can be treated with a partial nephrectomy reducing the risk of chronic kidney disease[48] and showing better overall survival

compared to a full nephrectomy[49]. The decision behind the surgical technique is largely driven by the ability to spare as much functional renal parenchyma as possible. As chronic kidney disease has been associated with increased risk in mortality[50], preserving kidney function post-surgery becomes important. A meta-analysis was able to show that in patients with clinically diagnosed T1b and T2b kidney cancers, a partial nephrectomy, compared to a full nephrectomy, resulted in higher post-operative kidney function ($p < 0.001$) and higher all-cause mortality rates (OR = 0.67; $p = 0.005$). This analysis was limited by several differences between the cohorts. Compared to the group of patients that underwent a full nephrectomy, those that had a partial nephrectomy were typically younger of age, had smaller tumours and less likely to be diagnosed with a malignant histologic subtype[51]. For larger T2 to T3 kidney tumours, the benefits of a partial nephrectomy are still indeterminate as studies comparing overall survival between a partial nephrectomy and full nephrectomy, have shown no meaningful survival differences[52-56]. One criticism that has been made about retrospective reports favouring partial nephrectomy over a full nephrectomy, is the possible selection bias made when deciding if a patient is suitable for a partial nephrectomy. A phase 3, randomised control study comparing a full nephrectomy against a partial nephrectomy for T1 to T2 tumours, showed better overall survival for those who underwent a full nephrectomy ($p = 0.03$), however when matched to cancer specific survival, this was no longer significantly different ($p = 0.17$)[57]. For large, bulky and complex tumours a full nephrectomy is recommended[45] providing overall survival greater than 87%[58,59] while maintaining high quality of life with the remaining kidney[60]. Postoperative complications from partial and full nephrectomy include spleen damage, perioperative bleeding, urinary fistula and haemorrhage[57,61] with reported rates between 15 - 33%[61-63]. Contraindications to surgery include age (>80 years), comorbidities, cardiovascular status, deep vein thrombus, obesity, tumour location and poor baseline kidney function[34,45,64-69]. In advanced-staged kidney cancers presenting with metastatic disease, decade-old studies of cytoreductive nephrectomy combined with immunotherapy have shown median overall survival rates of up to 17 months, a significant gain from receiving immunotherapy alone ($p \leq 0.03$)[70,71]. This has set a precedence for the use of cytoreductive nephrectomy combined with systemic therapy, as the standard of care for patients diagnosed with metastatic renal cancers[72-74]. Within this group of patients with advanced, metastatic renal cancers, the role of a full nephrectomy combined with systemic therapy has been questioned by the outcome from more recent clinical trials using modern-day targeted therapies. These studies have shown median overall survival rates between 18.4 to 32.4 months when using targeted-therapy alone, which was either no different or an improvement ($p = 0.03$) compared to treatment that was combined with cytoreductive nephrectomy[75,76]. This is not to discount the role of cytoreductive nephrectomy and systemic therapy for the treatment of metastatic renal cell cancers, as patient selection-criteria for surgery, may have been attributed to the differing study results[77,78].

Thermal ablative therapy is a treatment option for smaller sized kidney tumours (<3cm) and is generally favoured for those who are not suitable for surgery or require less invasive nephron-sparing surgery[34,45,79]. There are two commonly used thermal ablative techniques: radiofrequency ablation (RFA) and cryo-ablation. In RFA, high frequency (375 - 400 kHz) alternating currents are used to generate frictional heat (49 - 60 °C) to an area up to 5cm in diameter[80]. The electrodes are similar in size to blood drawing needles

(15 to 17-gauge) allowing percutaneous insertion with local anaesthesia. The ablative temperature discharged from the electrodes is sufficient to cause cell death by protein denaturation, enzyme dysfunction and cell membrane destruction[81]. During cryo-ablation, probes connected to a source of argon or nitrogen gas generate spherical ice-balls reaching freezing temperatures down to negative 40 °C[82,83]. Individual probes can generate ice-balls with a treatment area up to 4cm in length and by combining multiple probes, can accommodate larger treatment areas[84]. For lesions smaller than 3cm RFA and cryo-ablative techniques have shown 3-year overall survival rates from 80 - 95%[85-89]. However, for larger volumes, there are poorer outcomes due to size limitations of the treatment area[87,88]. One advantage of using thermal ablative techniques is the ability to localise the probe to the tumour using image-guidance systems such as CT, MRI and ultrasound[90]. When treating larger T1b tumours, incomplete ablation can still occur with reported efficacy rates as low as 65%[91]. A new round of ablation can be performed to eradicate any residual disease identified from post-treatment imaging. Similar to surgery, contraindications to this technique include size and location of the tumour, anticoagulation difficulties or spinal deformities that prevent access to the kidney percutaneously[79]. Major complication rates, associated with percutaneous ablation, have been reported to range from 3 to 7.7%[92-94] with overall complication rates as high as 12.2%[94,95]. Some of the serious complications associated with percutaneous ablation includes renal vascular injury, pneumothorax, haemorrhage, thermal injury to the ureter, and bowel injury and infection. Urologic complications are dependent on the size and site of the tumour within the kidney, with large and centrally located tumours contributing to this risk factor[96].

Systemic therapies in the form of targeted therapy, immunotherapy and chemotherapy, have focused on patients diagnosed with metastatic renal cell carcinomas to prolong overall survival[97-99]. During targeted therapy, protein pathways such as those promoting tumour angiogenesis are inhibited[99,100]. Excluding patients diagnosed with Von Hippel-Lindau (VHL) disease, a fault in the VHL gene is present in up to 83% of renal cell carcinomas[101,102]. This gene is considered a tumour suppressor regulating the number of hypoxia-inducible factors (HIF) in the presence of low oxygen conditions[22]. When a defective VHL gene is present, high concentrations of HIF will promote vascular endothelial growth factor (VEGF) and platelet-derived growth factors (PDGF) which can ultimately facilitate tumour angiogenesis[103-105]. Oral drugs such as sunitinib and pazopanib target VEGF and PDGF receptors preventing tumour growth[99,106,107] and have been found to result in partial responses ranging between 16 – 43% and complete responses in 1 to 1.3% of patients[98,107-109]. Survival in these patients can range between eight months up to 29 months[98,107,108]. Another common protein pathway targeted for systemic treatment is the mTOR pathway which has been linked upstream to the production of HIF[110]. Drugs such as everolimus and temsirolimus inhibit the mTOR protein pathway preventing tumour growth[100]. This type of intervention has shown response rates of less than 10% with overall survival gains ranging between 10.9 to 14.8 months. The most common side effects (grade 3 or higher) have been infections, dyspnoea and fatigue, ranging from 5 - 11%[111,112]. Immunotherapy involves the activation of the immune system to target renal cell cancers. Interferon-alpha (IFN) is a drug used to trigger the immune system response, increasing the number of cytotoxic T-cells and natural killer cells to target and destroy kidney cancers[113-115]. Similarly, interleukin-2 (IL2) is a drug that acts to maintain

T-cell activity within the body, promoting immune cell differentiation to target renal type cancer cells[116-118]. For IFN and IL2, response rates in kidney cancer management have varied between 9 - 23.2% for partial responses and 3 - 8.4% for complete responses with overall survival ranging from 13 to 21.1 months. Rates of grade 3 (or higher) toxicity such as hypotension, fatigue, cardiac and gastrointestinal related, have ranged from 8.4 – 56.8%, precluding its use as a modern therapeutic agent[119-122]. Another class of immunotherapy drug are those targeting the immune checkpoint system. During an immune system response, T-cells are regulated by antigens such as cytotoxic T-lymphocytic-associated protein 4 (CTLA4) and programmed cell death protein 1 (PD1). When CTLA4 and PD1 proteins bind to an antigen-presenting cell, T-cell activity is down-regulated. In a healthy immune system, this prevents an autoimmune system response that could harm healthy tissue[123]. However, when renal cancer cells express ligands receptive with CTLA4 and PD1 proteins, the down-regulation of the immune system can allow the tumour to proliferate[124]. Drugs such as Ipilimumab (CTLA4 inhibitor) and Nivolumab (PD1 inhibitor) can bind to tumour PD1 and CTLA4 ligands, preventing the cancer cells from further binding to the associated PD1 and CTLA4 protein. In this way, checkpoint inhibitors allow the immune system response to proceed[125]. The use of Ipilimumab has shown response rates of 12.5%, although grade 3 (or higher) toxicity was seen in 43% of participants[126]. Nivolumab, on the other hand, has shown response rates up to 25% with grade 3 (or higher toxicity) in 19% of patients[127].

Chemotherapy in the management of advanced renal cell carcinomas has shown limited success compared to immunotherapy and targeted therapy[100,128]. Drugs such as 5-fluorouracil (5-FU), capecitabine and gemcitabine act to disrupt DNA and RNA synthesis to prevent tumour growth[129-131] and in phase 2 studies, partial responses to chemotherapy have been relatively small ranging from 3.2 - 11% with overall survival rates between 12 to 23 months[132-135]. Other studies using combination chemotherapy of capecitabine and docetaxel, thalidomide and capecitabine or FOLFOX-4 (fluoro-uracil, folinic acid and oxaliplatin) have shown no response to treatment[136-138], further minimising the support of chemotherapy as a treatment agent.

1.5 Conventional radiotherapy for renal cell carcinomas

Based on retrospective reports from the 1950 - 1960s, 10-year survival rates between 27 - 55% have been observed with postoperative radiotherapy (PORT) compared to surgery alone for which overall survival of 17 - 46% was reported[139,140]. However, in a clinical trial setting, no significant survival benefit was observed for PORT showing 5-year overall survival rates of between 36 - 40% compared to 47 - 65% for surgery alone[139,141]. Pooled analysis of phase 2 studies has shown that PORT can benefit loco-regional control, but provide no improvement in overall survival[35]. Similar poor overall survival results have been observed in studies investigating preoperative radiotherapy versus surgery alone[142,143]. The main limitation of these studies can be attributed to the technology and the technique used at the time. The majority of PORT studies[35] used a 2-field technique (Figure 3a) with no 3D volumetric data to assist with avoiding critical structures (Figure 3b). Based on these techniques, the total dose used in these studies ranged from 24 to 60Gy (1.8 – 2.5Gy per fraction)[35,141,143-145]. The use of a higher total dose to control the tumour was limited by the increased risk of radiotoxicity to the liver and bowel[146]. The importance of dose escalation for tumour

control has been demonstrated in the palliative setting of metastatic kidney disease. Total doses greater than 45Gy have shown better pain response compared to lower doses[147,148]. This effect is more pronounced when high dose per fractions was used[149,150].
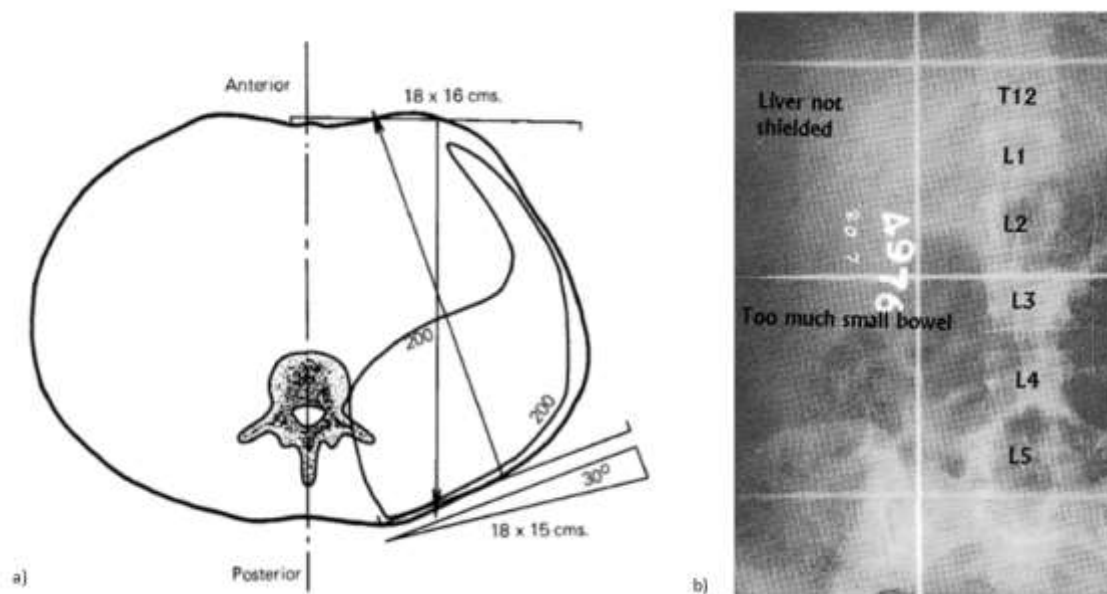
Figure 3. Beam arrangement and example of field border delineation of post operative radiotherapy for kidney cancer

3a) A two-field technique used with some minor angles used to avoid spinal cord dose[139]. 3b) The thoracic (T12) and lumbar spines (L1-L5) were used to define the treatment area. Majority of patients were treated with no further shielding of the liver and small bowel (dark shadow on the film)[146].

1.6 Gastrointestinal toxicity

The anatomy making up the gastrointestinal system is complex, involving many components with various levels of radio-sensitivity[151]. The gastrointestinal system is composed of the pharynx, oesophagus, stomach, duodenum, small intestine, large intestine and the anus. It is a luminal, continuous structure that is segregated into functional regions by sphincters that regulate food content from one area to the next. Food taken in through the mouth passes through the pharynx, down the oesophagus and into the stomach. From the stomach, food moves through the duodenum, small intestine and large intestine by peristaltic motion. Essential fatty acids, iron and mineral are absorbed in the duodenum, whereas carbohydrates, proteins and water are generally re-absorbed in the small and large intestine. The walls of the intestines are made up of several layers, starting with the mucosa, the innermost layer. This layer contains epithelial cells that excrete enzymes and mucus to assist with food breakdown and movement. The next layer is the submucosa which is filled with nerves, blood vessels and lymphatic vessels. The following layer, known as the muscularis externa, contain muscles that are responsible for the peristaltic movement of the gut. The final layer, known as the serosa layer, consists of connective tissue attached to the abdominal wall. Epithelial cells make up the intestinal mucosa and are derived from stem cells located in the submucosa, also known as the crypt region. As cells migrate towards the lumen of the intestinal tract, they differentiate into more specialised

cells such as endocrine, or goblet cells which are involved in mucus and enzyme secretion. These cells have a rapid turnover, ranging between 3 to 5 days, before sloughing to become waste. The high proliferation of these cells makes this region highly sensitive to radiation. Radiation injury to the mucosal layer can cause acute and chronic reactions including inflammation, ulceration and perforation of the gut lining. Bowel inflammation and irritation can lead to diarrhea and vomiting, whereas the damage to enzyme-secreting cells can lead to impairment of bile reabsorption leading to more serious problems[152,153]. Chronic damage to the muscularis externa layer can cause impairment of peristaltic motion causing bloating, abdominal pain and obstruction[154]. Historically, there has been limited success with conventionally fractionated radiotherapy for primary kidney cancers due to dose constraints imposed by the gastrointestinal system. Dose prescriptions from 24 to 60Gy have been used in the post-operative setting with no positive gain in overall survival[146]. Furthermore, with conventional radiotherapy, reports of grade 3 bowel toxicity have been as high as 30.8% and grade 4 at 7.7%[146]. The relationship between bowel toxicity and radiation dosage have been documented by the experience from conventional radiotherapy to abdominal and pelvis targets. Radiation dose tolerance of the bowel organ published almost 30 years ago, indicates a 5% risk of small bowel obstruction, perforation or fistula occurring within 5 years if the entire organ was irradiated to 40Gy. This would increase to a 50% risk if the dose exceeded 55Gy. For partial (1/3) volume irradiation of the bowel, the dose threshold for a 5% and 50% risk of bowel complications was higher at 50Gy and 60Gy respectively[155]. More recent reviews of small bowel obstruction following radiotherapy have also shown the risk to be 2 to 9% when the organ is partially irradiated to over 50Gy[156]. Specific volume-dose thresholds have also been investigated on 40 patients treated for rectal carcinoma. It was found that the risk of grade 3 small bowel toxicity was 59% when more than 125cc of the small bowel received a dose of 40Gy. Similarly, when more than 500cc of the small bowel received 5Gy, a high risk (45%) of grade 3 toxicity was observed. Apart from the effect of high volume irradiation to the bowel, there is still little information on the maximum dose tolerance of this organ[157]. In a review examining the incidence of late small bowel toxicity for patients treated to the pelvis and para-aortic lymph nodes, the authors reported the incidence of grade 3 (or higher) late small bowel toxicity to be 9 (+/-7%) %. Based on pelvic irradiation dose of 50Gy, and considering dose heterogeneity of up to 10%, the authors further recommended a maximum dose of 55Gy to the bowel[158]. In contrast to this, a review of 94 patients treated for various abdominal-pelvic malignancies to doses between 54Gy and 75.6Gy, showed estimated 5-year freedom from grade 3 bowel toxicity of 93.6%. This was despite 49/94 (52%) patients receiving greater than 60Gy to at least 1cc of the small bowel[159].

1.7 Stereotactic ablative body radiotherapy

Stereotactic ablative body radiotherapy (SABR) is the use of hypo-fractionated, high dose per fraction radiotherapy for the curative treatment of cancers[160], which is in contrast to conventional radiotherapy which uses a low dose and high fractionation to achieve the same endpoint of tumour control. In conventional radiotherapy, small daily doses of radiation allow normal tissue to repair sublethal damage and repopulate over the course of treatment. On the other hand, the effect on tumour cells is to redistribute its cell cycle to a more radiosensitive phase and to reoxygenate the tumours' cells, thus increasing

sensitivity to radiation[161]. The high dose and short treatment schedule for SABR result in unrepairable damage to tumour cells leading to necrosis and apoptosis[162-164]. This mode of cell kill with ablative doses has been hypothesised to overcome any inherent radio-resistance believed to exist with kidney cancers[165]. The use of high dose radiotherapy for tumour control has been established since the 1950s in the intracranial setting, with an important emphasis on immobilisation of the head using fixation devices[166,167]. More recently, the extracranial use of high dose radiotherapy has seen success in providing tumour control and survival gains in other anatomical sites such as the lung[168-174] and liver [175-180] for patients who are unsuitable or refused surgery for their treatment. The success has been largely attributed to the technical development in areas of motion management, stabilisation, radiotherapy planning and image guidance.

1.7.1 Motion management strategies

Knowledge of organ motion and strategies to account for this in the planning process is important for determining adequate treatment margins. In conventional treatment planning, generic margins are used which are derived from large sets of data to cover a significant portion of treatment[181-184]. For abdominal and thoracic targets that are subject to motion due to breathing during therapy, generic margins that consider breathing motion can be large, resulting in unnecessary irradiation of critical organs such as lung, liver and the bowel[185,186]. However, by using motion margins specific to each patient, margins surrounding the tumour can be dramatically reduced[184-190]. Individual tumour motion can be measured and visualised using tools such as fluoroscopy[191,192] and four-dimensional computed tomography (4DCT)[188,193,194]. As stereotactic treatment uses large ablative doses in each fraction, reduction of planning margins is crucial in minimising dose to healthy tissue. Organ motion studies of the lung[195-198] and liver[199-203] have shown motion ranges of up to 25mm, prompting further strategies to reduce the total motion. Some popular strategies include the use of breath-hold during treatment[204-206 205,207-210], abdominal compression devices to minimise breathing motion[200,211-216], use of drugs to minimise breathing motion[217], multi-leaf collimator (MLC) tracking[218,219] or the use of fiducial marker tracking during treatment[220-222].

1.7.2 Immobilisation at treatment

Stabilisation during SABR treatment is important to minimise involuntary patient motion since a relatively small motion of 2.9mm can reduce coverage by 6%[223]. Stereotactic specific body frames (Figure 4) that are customised to the patient's contour include stabilisation at the level of the upper arms, abdomen and lower extremities to ensure comfort and reproducibility during each treatment. Accessories such as abdominal compression plates (Figure 4b) and vacuum stabilisation (Figure 4d) can be integrated to further minimise breathing motion. Stability of the lung and liver target when using these devices has shown intrafraction motion of between 0.3mm up to 2mm[224-228].

Figure 4 Examples of inhouse and commercially available stereotactic body frames.

Common elements include a personalised foam body cradle and a diaphragmatic compression device that can be used to apply pressure to the abdomen. (a) In-house stereotactic body frame designed by the Karolinska Institute, Stockholm, Sweden for lung and liver stereotactic treatment[229]. (b) Body Pro-Lok ONE™ with custom body cradle, diaphragm compression, and knee locks[230]. (c) ORFIT™ stereotactic body radiotherapy system with arm, knee, feet foam supports and abdominal compression device[231]. (d) Elekta BodyFIX® dual vacuum system comprised of customised body cradle, vacuum seal over the body and abdominal compression device[232].

1.7.3 Stereotactic body radiotherapy planning concepts

Treatment planning for stereotactic treatment requires the creation of a highly conformal treatment plan to minimise dose to healthy tissue. The use of co-planar and non-coplanar fields is a common strategy to minimise field overlap, facilitating steep dose gradients from the target[233,234]. Figure 5 is an example demonstrating a six-field (coplanar and non-coplanar) arrangement for lung cancer in an anthropomorphic phantom. The dose overlap is reduced in the non-coplanar arrangement resulting in steeper dose gradients.
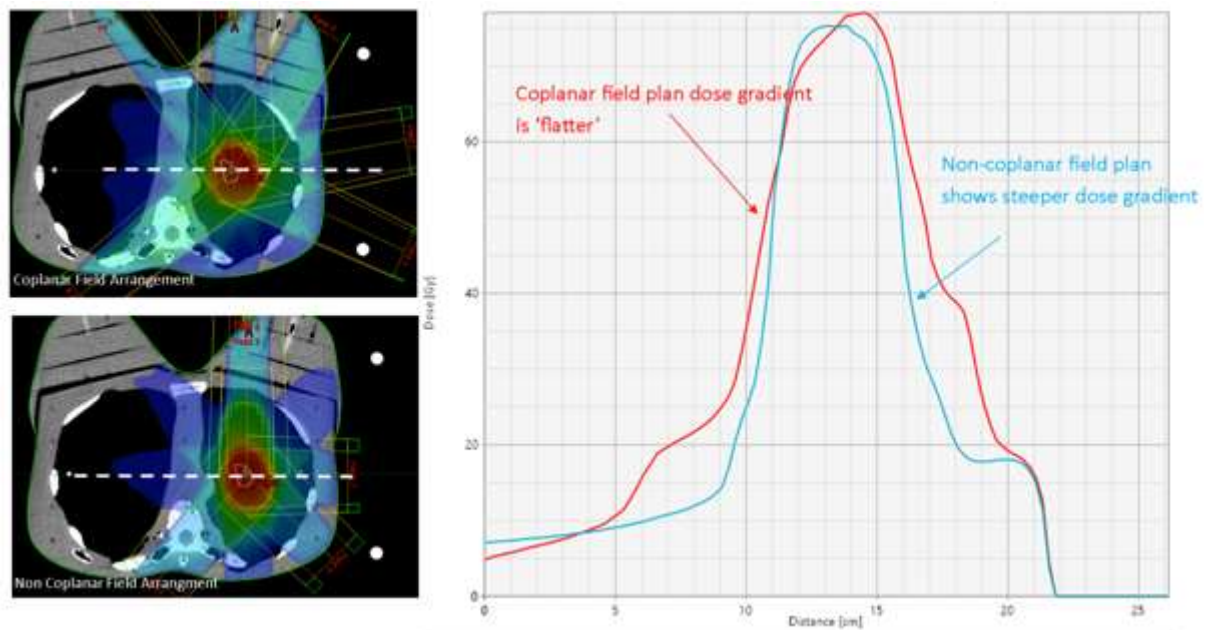
Figure 5. Dose gradient comparison between planar and non-coplanar beams.

A line dose profile through the isocentre shows that a six-field non-coplanar field arrangement can achieve steeper dose gradients than a six-field coplanar arrangement. Overlapping entrance and exit dose in a coplanar arrangement creates high dose tunnels which reduce the dose fall-off effect. *Source: Peter MacCallum Cancer Centre*

In 3D conformal SABR planning, steep dose gradients can be generated by using minimal margins (0-2mm) from the shielding device (MLC/Cones) to the tumour target[235-237]. As the dose drop off is steepest at the region of the penumbra, prescribing to the isodose line of 50 – 80% in this region will create rapid dose fall-off (Figure 6). This is done at the cost of having a heterogenous dose within the target, which is inversely proportional to the prescription point (120 – 150%).
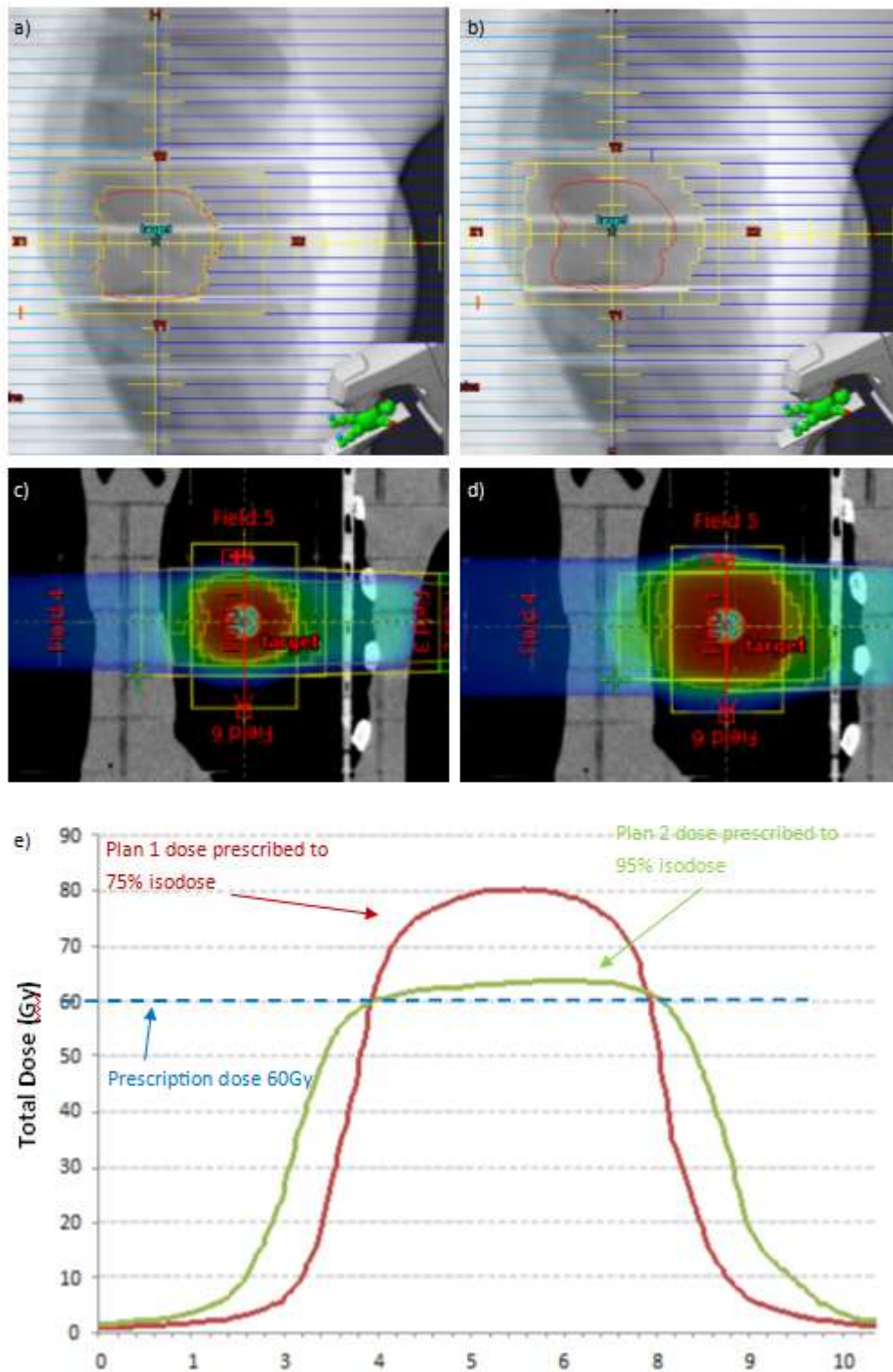
Figure 6. MLC margin generation in 3D conformal planning for stereotactic treatment.

When using a 3D conformal technique during stereotactic planning, the MLC margin around the PTV is small (0-1mm) requiring dose prescription to lower isodose lines (a). In conventional planning, larger MLC margins are applied (5 – 10mm) allowing dose prescription closer to the dose shoulder (b). The distribution around the PTV with a stereotactic type MLC margin is more compact due to the rapid dose fall-off being near the field penumbra (c). The dose fall-off for conventional margins is more gradual as the

dose is prescribed to the shallower dose shoulders (d). The inadvertent effect of prescribing the prescription dose (for example 60Gy) to a lower isodose line is increased heterogeneity within the target (e). *Source: Peter MacCallum Cancer Centre*

This contrasts with conventional planning which prescribes the dose anywhere between 90% - 100% of the dose and has more rounded dose shoulders (Figure 7). The risk with prescribing to the steeper dose gradient is that any geographical misalignment to the target would have a larger dose discrepancy when prescribing to the 50% isodose (steeper slope) than to the 90 – 100% (shallow slope), therefore, having an immobilisation device that minimises intrafraction motion is critical during stereotactic treatment.
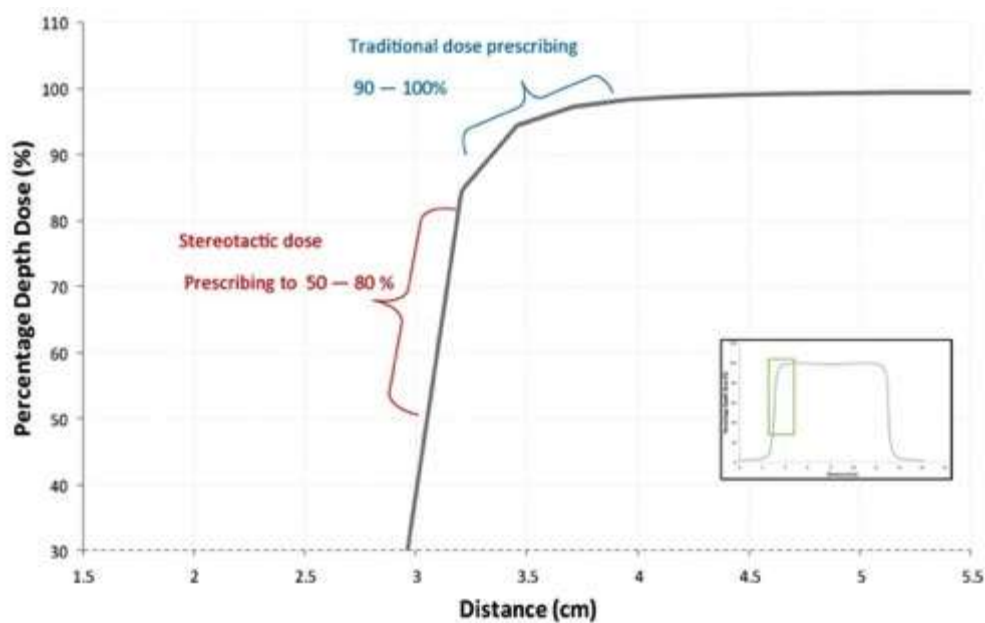
Figure 7. Prescribing dose in stereotactic planning.

Dose prescribing in SABR planning is performed to the field penumbra where the dose gradient is steepest. This allows rapid dose fall-off but also makes dose coverage more susceptible to gross error if target moves. *Source: Peter MacCallum Cancer Centre*

1.7.4 Image guidance

Image guidance systems in radiotherapy typically describe in-room devices that allow verification of the patient's treatment position against a reference image to assess any discrepancy during setup. Modern imaging systems are integrated with the beam delivery system to allow the review of images and correction of the patient position directly before beam delivery[238-241]. Early technology generated 2D planar[239,242] and 3D volumetric[243-245] images that were acquired using the megavoltage treatment beams. The addition of kilovoltage x-ray sources onto linear accelerators[246-248] has allowed superior tissue contrast for improved 2D image quality[249]. This would eventually evolve into cone-beam computed tomography (CBCT) reconstruction to generate 3D volumetric images[250-252], as well as time-resolved 4D CBCT images[253,254]. Other novel imaging systems include the use of ultrasound[255] as a non-ionising alternative, magnetic resonance imaging[256] for superior soft-tissue contrast and positron emission tomography (PET)[257] to localise and semi-quantitate metabolic activity of targets. The integration of imaging during treatment into

clinical practice has allowed a reduction of treatment planning margins[258,259] resulting in improved toxicity outcomes[260-262] and the ability to visualise changes to the tumour volume during the course of treatment[263-267]. These factors have made image guidance a high priority when using stereotactic ablative body radiotherapy for sites such as lung[268-270], spinal cord[224], and liver[271-273].

1.7.5 The current state of renal cell carcinoma and stereotactic treatment

Reports from early 2000 have demonstrated the technical feasibility and safety of SABR for primary kidney cancers on linear accelerators[274-279] as well as particle accelerators[280,281]. Technology at the time relied on the use of rigid, customised body frames and 2D planar imaging to verify target position. The introduction of a robotic arm-based linac (Cyberknife[TM] Accuray, USA) led to studies using fiducial markers inserted near the kidney tumour to track the target during treatment[282-286]. Within the last decade, integration and improved CBCT image quality on linacs have led to the resurgence of treatment on this platform[287-290].

Guidelines and recommendations for the implementation and safe use of SABR have been published and/or endorsed by numerous professional organizations including the American Association of Physicists in Medicine[160], the Australian and New Zealand Faculty of Radiation Oncology[291,292], the Faculty of Clinical Oncology of the Royal College of Radiologists[293], the Canadian Association of Radiation Oncology[294], as well the American Society for Therapeutic Radiology and Oncology [295]. These publications were generated during a period of great interest in stereotactic treatment for lung, liver and spine[296] with emphasis on motion management, stabilisation and image guidance (Table 3). Despite these guidelines, there is little consensus on best practice for SABR treatment of the kidneys[297].

Table 3. A summary outlining key recommendation for stereotactic body radiotherapy treatment made by various professional organisations.

	AAPM	RANZCR	CARO	ASTRO/ASR	UK SABR Consortium
Simulation	Body frames or vacuum moulds personalised to patient position.	Patient specific for comfort over time. Device used based on IGRT system used for treatment. Ideally would encompass entire body.	Near rigid body immobilisation for spine treatment. Chest boards or whole-body mould for abdominal targets. Stereotactic body frames/vacuum bags for lung treatment.	Custom body moulds. Mask, to provide comfort for patient over extended treatment period.	Devices with setup uncertainty ≤5mm (ideally ≤3mm).
Motion Management	Slow CT, 4DCT+MIP, Breath hold, Gating, 4DPETCT	Required to be accounted. This can be done using	Compression for >10mm of motion otherwise breath-hold or fluoroscopy for ITV margins.	Respiratory tracking, abdominal compression.	Motion assessment with 4DCT or fluoroscopy. Compression device, coaching or active breath control, gating with free

		4DCT or other means.			breathing, fiducial/ lesion tracking or ITV. Motion greater than 10mm for lung or 5mm for liver should be controlled.
Planning Imaging	CT or 4DCT with slice thickness 1 to 3mm.	CT or 4DCT with slice thickness 1 to 3mm.	CT or 4DCT with slice thickness 2 to 3mm.	CT, 4DCT or breath hold.	CT with 2 to 3mm slice thickness. 4DCT and MRI with 1 to 2mm slice thickness. CT MIP and average scans.
Treatment Planning	Calculation grid ≤2mm. Algorithm with scatter correction. Five to eight coplanar/non-coplanar or IMRT/VMAT contributing <30% of dose per (static) field.	Inhomogeneity correction. Prescription to low isodoses (≤80%). Calculation grid minimum of 2mm			Calculation grid ≤2mm. Type B or Monte Carlo algorithms.
Image Guidance	Direct target visualisation. 3D volumetric, 2D stereoscopic or fiducial markers.	3D or 2D stereoscopic for target and organs-at-risk verification.	3D or 2D stereoscopic for target and organs-at-risk verification. Fiducial markers. Intrafraction motion verification at mid treatment.		2D kV, 3D volumetric, CBCT, 4DCBCT, MVCT for target visualisation.
Machine QA	1 to 2mm imaging isocentre.	Isocenter ≤2mm.			
Treatment Modality		Linac, Cyberknife, Tomotherapy.	Linac, Cyberknife, Tomotherapy.	Megavoltage or protons.	
Peer Review	Ongoing review of existing QA program.	Multi-disciplinary review at all stages: Pt selection through to planning.	Peer reviewed chart rounds for contours and planning.		Plan reviewed by two oncologists.
Reporting	Prescription conformality (R100), intermediate dose conformality				Prescription conformality (R100), intermediate dose conformality index (R50), homogeneity index.

	index (R50), homogeneity index.				
Additional Training					
Radiation Oncology	SABR specific	SABR specific. Present at treatment	SABR training. Present at minimum first fraction. Medical physicist alternative	SABR specific. Present at treatment.	SABR specific
Medical Physics	SABR specific. Present at first fraction	SABR specific	SABR specific	SABR specific	SABR specific
Radiation Therapy	SABR specific	SABR specific (2 at minimum on treatment)	Part of core SABR team		SABR specific

Abbreviations: AAPM = American Association of Physicists in Medicine; RANZCR = The Royal Australian and New Zealand College of Radiologists; CARO = Canadian Association of Radiation Oncology; ASTRO = American Society for Therapeutic Radiology, ACR = American College of Radiology

In recent years, new literature on SABR for the kidney have been reported describing kidney motion[298,299], kidney stabilisation during treatment[300,301] and as well the use of advanced imaging delivery systems such as the MRI-linac for treatment[302,303]. However, there is still only limited literature on the technical implementation of kidney SABR on a linac. Globally, there are approximately 116 particle accelerators[304], less than 300 Cyberknife[TM] service sites (www.accuray.com) and about 12 000 linear accelerators[304] which makes the linac an ideal platform to provide stereotactic treatment.

1.8 Studies of kidney stereotactic radiotherapy

During the early-2000s, a small number of retrospective reports described the safe use of linac-based stereotactic treatment for primary and metastatic renal cell carcinomas[274-276,278,305]. With a focus on rigid patient stabilisation, abdominal compression, multi-planar and non-coplanar fields, and pre-treatment imaging, these reports were able to demonstrate high rates of local control while showing minimal treatment toxicity.

One of the earliest reports on the use of high dose ablative body radiotherapy for primary renal cell carcinomas came from Staten Island University in New York, USA[274]. This retrospective series comprised of 74 patients diagnosed with metastatic (n =114) and primary renal cell cancers (n = 27). All patients were treated with a short-course, high dose per fraction schedule. The most frequently used prescription was 40Gy in five fractions, and for the primary kidney cancer group of patients, resulted in a 12-month local control rate of 93%. A more detailed series from the same institution described the clinical outcomes for nine patients diagnosed with biopsy-confirmed renal cell carcinoma[275]. The tumour size ranged from 3cm up to 10cm with all but one patient having nodal involvement. Eight patients received a dose of 40Gy in five fractions and one patient a dose of 35Gy in six fractions. All patients were immobilised using a stereotactic body frame and a planning margin of 10mm around the GTV was used for treatment. Patients

were treated on a linac using a mix of static planar and non-coplanar beam angles (4 to 6 fields). At a median follow-up of 26.7 months, 44% of patients were still alive. For those still alive, the median continued follow-up was 57.8 months. Two of nine patients developed nausea and vomiting during treatment, one of which showed signs of radiation injury to the stomach six weeks after treatment.

During the same period, a retrospective series from the Karolinska Institute in Stockholm (Sweden) also showed the effectiveness of high dose radiotherapy for renal cell carcinomas[276]. In this study, eight primary kidney targets and 154 metastatic sites were treated with dose prescriptions ranging from 18 to 48Gy in 2 to 5 fractions. For the primary kidney targets, a dose of 40Gy in five fractions was used for treatment. Patients were immobilised in a stereotactic body frame with an abdominal compression plate used to minimise diaphragm motion to 5mm or less. A planning margin of 10mm in the superior-inferior direction and 5 to 10mm in all other directions was used around the GTV/CTV. A mix of planar and non-coplanar beams (5 to 8 fields) was used to treat the target on a linac. A pre-treatment CT scan was performed with the patient in the stereotactic body frame to verify the kidney tumour position. With a median follow-up of 37 months, the authors reported a local control rate of 98%. The median survival time for patients with 1 to 3 metastatic sites was 37 months, for greater than three metastatic sites; this was 19 months, and for those with inoperable renal cell carcinoma, survival was greater than 58 months. The authors found more effective control when a higher dose was used to treat the tumour. All tumours that showed total regression (n = 48) received a mean biologically equivalent dose (BED) of 110Gy, while tumours that showed local progression (n = 3) received a mean dose of 73.2Gy (BED). The most common side effects (grade 1 to 2) were coughing, nausea and pain. A single grade 5 side effect was reported for the treatment of a metastatic kidney tumour in the pancreas. This same institution also reported the results of a prospective phase 2 study, assessing the safety and efficacy of stereotactic treatment for metastatic and primary renal cell carcinoma[305]. Thirty patients were enrolled in the trial, treating 82 metastatic sites and ten primary kidney tumours. The prescription dose ranged between 5 to 15Gy in two to five fractions. A stereotactic body frame with abdominal compression plate and planar/noncoplanar beam angles were used for treatment[276]. The median survival period was 32 months, with 21% showing total regression of disease. The local control rate, defined as a positive response to treatment, was 98%. Two kidney lesions showed the continued progression of the disease, one of which was attributed to its large size (1136cc). For the other lesion, due to its proximity to bowel and stomach, coverage by the prescription dose was suboptimal. Sixteen patients reported side effects with the most common being coughing, fatigue, skin rash and local pain. The majority (96%) of side effects were of grade 1 and 2. One patient death was reported ten weeks after treatment, the cause of which was cardiac arrest suspected to be related to the treatment of a metastatic renal cell carcinoma in the lung.

Another report originating from the mid-2000s described an approach using 4DCT and IMRT fields to deliver a high-dose treatment to renal cell cancers[278]. This series, consisting of primary (n = 2) and metastatic renal cell carcinomas (n =14), used a prescription dose ranging from 24 to 40Gy in three to six fractions. A 4DCT scanner was used to generate ITV margins, with a 2 to 3mm planning margin to account

for setup errors. Fiducial markers, inserted near the primary kidney cancers, were used for image verification on treatment. Depending on the treatment site, five to 12 conformal arcs or static IMRT fields were used for treatment. At a median follow up of nine months, 12 patients showed partial responses to treatment, no individual showed a complete response, and two patients were found to have disease progression, yielding a local control rate of 87%. In the two patients treated for primary renal cell carcinoma, no change in tumour size was detected during follow-up, and renal function remained unchanged from baseline. No grade 2 or higher toxicity was observed in any patient.

These early retrospective reports were able to show that a high dose, short-course radiotherapy treatment to primary and metastatic kidney cancers can show excellent local control with low rates of treatment toxicity.

One technological development that generated more interest in the use of SABR treatment for primary kidney cancers was the Cyberknife[TM] robotic radiosurgery system. This platform allows highly conformal, high precision and beam tracking for small kidney targets[306,307]. This is achieved using an isocentre-free robotic arm allowing up to 1212 non-coplanar beam angles to target the tumour. The delivery system is integrated with an in-room 2D stereoscopic kV imaging system, allowing dynamic tracking of the beam to the tumour (or fiducial surrogate). The maximum beam aperture of the Cyberknife[TM] system, at 60mm, limits its use to targeting small kidney cancers (5cm or less). For patients diagnosed with small kidney cancers and eligible for fiducial marker insertion, the Cyberknife[TM] system is a viable alternative to a linac-based treatment approach. The feasibility of using robotic surgery combined with fiducial marker tracking has been reported by several studies[282-285,308-310]. Within these reports, a few stand out showing safe dose escalation[283-286] and feasibility for treatment of patients with pre-existing kidney disease[284,308].

The Cyberknife[TM] system, in a single institution prospective study, was used to investigate the feasibility of dose escalation for primary renal cell carcinomas[282,283]. The primary aim was to escalate the total prescription dose before any grade 3 (non-haematological) or higher side effect was observed. With a maximum of three patients per dose level, fifteen patients were recruited into dose arms of 21Gy, 27Gy, 33Gy, 39Gy and 48Gy in three fractions. The mean maximum tumour dimension was 3.4cm, and the largest dimension was 5cm. Gold fiducial markers were inserted into or adjacent to the tumour, and a 3mm margin around the GTV was used for planning. At 12 months, eleven patients showed stable disease, two had a partial response and one patient a complete response to treatment. At greater than 30 months post-treatment, two patients in the low dose arms (21 and 27Gy in three fractions) showed local failure. No acute toxicity greater than grade 3 was reported. Two patients experienced grade 1 nausea and five grade 1 fatigue. Based on these results, the authors proposed for further dose escalation. In a similar study looking at dose-limiting toxicity of grade 3 or higher, 20 patients were recruited into four dose arms of 24Gy, 32Gy, 40Gy and 48Gy in 4 fractions[285]. All patients were stabilised with a vacuum cushion, and CT planned with a GTV to PTV margin of 0 to 3mm. Three fiducial markers were placed around the tumour volume to be used for tracking on treatment. The median tumour volume was 57.9 (ranged from 13.8 to 174.7) cm^3. At 13.6 months follow-up, no patients showed signs of disease progression or recurrence. The 3-year overall survival was 72%

with five patients expiring from non-treatment related illnesses. The study found one patient experiencing a grade 4 duodenal ulcer, which received a maximum point dose of 54Gy. Only one patient reported grade 2 fatigue from treatment. Since the protocol defined dose-limiting toxicity as two or more patients within a single dose arm to experience grade 3 or higher toxicity, the findings in this study also supported further dose escalation. A continuation from the same study reported the outcome for 11 patients recruited into two additional dose arms of 54Gy and 60Gy in three fractions[311]. The median follow-up at 1.7 years, showed local control of 90% with one patient showing disease progression. There was no grade 1 or greater acute gastrointestinal or genitourinary toxicity reported, although one patient did develop a urinary tract infection requiring hospitalisation.

In contrast to the multi-fractionation schedules, single-fraction stereotactic radiosurgery for kidney cancers have also been reported[286]. Forty patients were recruited into a study prescribing 25Gy in one fraction to primary kidney cancers. Forty-five kidney lesions, comprised of renal cell carcinomas (n = 30) and transitional cell carcinoma (n = 15), with a maximum dimension of 4cm, were treated using the Cyberknife™ system. For all patients, three fiducial markers were inserted around the renal parenchyma and used for target tracking on treatment. The reported local control at 9 months was 98%, with 38 of 45 (84%) tumours showing at least a 30% reduction in size. A total of 19 targets showed complete remission, which 13 were of transitional cell type histology and six of renal cell histology. No grade 2 or higher toxicity was observed.

The target tracking functionality on the Cyberknife™ system allows the reduction of the planning margin to preserve as much non-tumour kidney tissue as possible. For kidney cancer patients with chronic kidney disease (CKD), surgery to remove cancer could further deteriorate kidney function. High dose radiotherapy has been shown to minimise the impact on kidney function post-treatment. This is especially important when treating patients with advanced stages of CKD. The American National Kidney Foundation[312] defines five stages of chronic kidney disease based on the glomerular filtrate rate (GFR) of the kidneys: in stage 1 the GFR is greater than 90 ml/min; in stage 2 CKD the GFR ranges from 60 to 89 ml/min; in stage 3, the GFR decreases down to 30 to 59 ml/min; for stage 4, GFR ranges from 15 to 29 ml/min; and for stage 5 CKD, kidney failure (requiring dialysis) is seen with GFR less than 15 ml/min.

Lo *et al* described the outcome for three patients diagnosed with stage 3 to 4 chronic kidney disease, undergoing primary renal cell treatment of 40Gy in 5 fractions[284]. The maximum tumour diameter ranged from 3.6 to 5.7cm. All patients were stabilised in a whole-body vacuum pillow and underwent a CT scan for planning. Planning target volume margins of 1 to 3mm were used around the GTV. Fiducial markers, for target tracking, were used on two patients. For the remaining patient, an abdominal compression device was used to minimise diaphragmatic motion and treatment target verification was made based on alignment to nearby vertebral bodies. Follow-up at 40 months showed all patients alive with no signs of tumour progression, and no toxicities greater than grade 2 reported. As for kidney function, at baseline, each patient had poor kidney function with estimated glomerular filtration rate below 60 ml/min. One patient progressed from stage 4 CKD to stage 5, resulting in kidney failure. The other two patients progressed from stage 3 to

stage 4 CKD though not requiring dialysis. In a more recent report, the Cyberknife[TM] system was used to treat ten patients with stages 2 to 4 of chronic kidney disease[308]. Based on tumour volume and proximity to organs-at-risk, patients received either a single fraction of 24 or 25Gy or received 36Gy in three fractions. The median diameter of the tumour was 2.8 (range 0.9 to 7) cm. A planning margin of 0 to 5mm around the GTV was used for planning. All patients received a single fiducial marker inserted near or inside the tumour for target tracking on treatment. The median follow-up at 27 months showed a local control rate of 92.3% for the 13 lesions that were treated. Disease stability, partial responses and complete responses to treatment were observed in 38.5%, 30.8% and 23.1% of patients respectively. There were no differences in response observed when using a single or multi-fraction prescription. Of the ten patients identified in the report, six had stage 3 CKD, three patients with stage 2 CKD and one patient with stage 4 CKD. At baseline, the mean estimated GFR for the group was 51.3 (+/- 19.7) ml/min and at follow-up (mean of 22 months) was 51.6 (+/- 25.8) ml/min. One grade 1 abdominal pain, and another case of grade 1 diarrhea and abdominal distension was reported.

The Cyberknife[TM] treatment platform provides a highly accurate method of tracking and treating small, localised cancers of the kidney. One caveat with this system is the reliance on fiducial markers to verify the target position before and during treatment. On the other hand, linear accelerators, particle accelerators and helical therapy systems can also provide high accuracy treatment using fiducial[280,281,288] and fiducial-free[287,289,290] treatment. Compared to the Cyberknife[TM] system, these platforms have an integrated 3D volumetric imaging system and can treat large tumours, thereby providing greater treatment flexibility. The following studies are recently published reports using a linac-based approach for kidney SABR treatment.

Chang *et al* described their experience treating 16 patients diagnosed with primary renal cell carcinoma[287]. The dose ranged between 30 to 40Gy in five fractions, with the lower dose used to meet normal tissue constraints. The median tumour size was 4 (range 1 to 14.6) cm. All patients were stabilised using a dual vacuum stabilisation device and underwent a 4DCT to generate an ITV volume with a 5mm PTV margin. Patients were treated using either a step-and-shoot IMRT technique or with VMAT. A CBCT was performed before treatment for target localisation. At a median follow-up of 19 months, five patients showed partial tumour responses, and 11 patients showed stable disease, yielding a 100% local control rate. Apart from one patient suffering from nausea and vomiting after treatment, no other patient experienced grade 2 or higher toxicity. Eleven of 16 patients showed an average GFR decline of 14.4%. Two patients, diagnosed with stage 4 and 5 CKD at baseline, required dialysis post-treatment. In another report focusing on kidney SABR treatment for large masses, a linac was used to treat 11 patients with an average tumour volume size of 9.5cm, ranging from 7.5 to 24.4cm[289]. The dose prescription varied from 25 to 40Gy in five fractions. Patients were stabilised using a vacuum body mould and underwent a 4DCT for ITV margin generation. A planning margin of 5mm was added to the ITV volume, subtracting any overlap with gastrointestinal organs-at-risk, to generate the final PTV volume. Patients were treated using either helical TomoTherapy[TM] with MVCT target verification before treatment, or with a linac using IMRT/VMAT and CBCT image verification for target localisation. The 3-year overall survival rate was 53%, with three deaths

from disease progression. There were five reported cases of grade 1 toxicity, one grade 2 diarrhea and one grade 3 nausea. The grade 2 and 3 toxicity came from the same patient treated for a large tumour with a maximum diameter of 24.4cm. The median baseline GFR value for the patient group was 43.7 (range 21.3 – 73.6) ml/min, and at post-treatment, was measured at 42.3(range 20.5 – 77.2) ml/min, a non-significant change ($p = 0.359$).

Yamamoto et al[288] investigated the use of a linac to treat 14 patients with dose prescriptions ranging from 50 to 70Gy in ten fractions. The median tumour volume was 3cm, ranging from 1.6 to 4.6cm. All patients were immobilised using a full-body vac-loc bag, and nine patients were implanted with a fiducial close to the tumour site. Motion management was based on the amount of displacement observed for the fiducial marker or diaphragm. Six patients with large motion required the use of abdominal compression, and for one patient, a breath-hold technique was used. A variety of planning imaging protocols were used including 4DCT, fast CT and slow-rotation CT. The ITV margin was derived from assessing fiducial marker or diaphragm motion using 4DCT or fluoroscopic imaging. A planning PTV margin of 5mm around the ITV was used for treatment. A combination of CBCT and fluoroscopic imaging were used for treatment verification of the target/surrogate structure. The median follow-up time for all patients was 16.9 months with 100% of lesions responding to treatment. There was no grade 2 or higher toxicity reported. Compared to the serum creatine baseline value of 1.1mg/dl, the post-treatment value of 1.3mg/dl was significantly different ($p = 0.05$). However, the decline in kidney function to clear creatine from the system did not result in any patient requiring dialysis or have a change in hypertension status.

Two studies have described the use of a carbon ion system to treat primary renal cell carcinomas. One study used this to treat ten patients with a median maximum tumour length of 4.3cm, ranging from 2.4 to 12cm[280]. All patients were immobilised using a resin-based custom shell and underwent a non-enhanced planning CT scan. The GTV was the gross, visible disease with a 10 to 15mm CTV margin. For the final planning volume, a 5mm margin was expanded from the CTV. At least one fiducial marker was inserted near to the renal cortex, close to the tumour, which was used for target localisation using 2D image verification on treatment. The beam was gated to treat the target at the exhale phase of the patient's breathing cycle. The dose delivered ranged from 64 to 80Gy (median 72Gy) in 16 fractions. The median follow-up time was 57.5 months showing a 5-year local control rate of 100%. One patient showed a complete response to treatment, six had partial responses, and three showed stable disease. The 5-year overall survival was 74% with patient deaths attributed to non-cancer related illnesses. There were no reports of acute toxicity greater than grade 1. However, there was one grade 4 skin ulceration reported five years after treatment which required a skin flap transplantation. Two patients, with pre-existing diabetic status, showed an increase in blood creatinine levels after radiotherapy treatment. The authors believed that this was due to the progression of the patient's diabetes rather than a side effect of treatment. A continuation from this protocol investigated the feasibility of dose escalation using 66 to 72Gy in 12 fractions[281]. Eight patients were recruited with a median tumour size of 4.3cm, ranging from 2.9 to 8.2cm. All patients had fiducial markers inserted near the tumour and were set up using a custom body mould created from thermal plastic sheets.

A planning CT was used to delineate the GTV, with a further 5mm margin to generate the CTV. An anisotropic PTV margin of 10mm in the superior-inferior direction and 5mm in all other directions was used for treatment. Verification on treatment was performed using kV imaging of the fiducial markers with gated treatment performed at the end-exhale position. At a median follow up of 43.1 months (range 3 to 62 months), one patient had passed away from pneumonia unrelated to treatment. The local control and cancer-specific survival for this group was 100% with only a single grade 1 skin toxicity reported. The measured kidney function before and after treatment showed a mean decrease in estimated GFR of 10.8 ml/min, which did not result in any change in CKD staging.

Linac-based treatment, integrating MVCT imaging and a breath-hold technique, have also been reported[290]. In this study, thirteen patients diagnosed with stage 1 renal cell carcinoma with a median tumour volume of 1.9cm, ranging from 0.9 to 4.3cm, were prescribed a dose of 60 to 70Gy in ten fractions. Each patient was immobilised using dual vacuum stabilisation and underwent multiple self-controlled, breath-hold CT scans. An ITV margin, ranging from 2 to 4mm, was generated based on the reproducibility of the GTV position from each breath-hold scan. A PTV margin of 3mm was expanded around the ITV for treatment. The choice of beam technique was either the use of static fields (5 or more) or five dynamic arcs. Treatment verification was performed by a CT-on-rails system. Twelve patients showed a dose-response and only one patient showing relapse after 1-year post-treatment. The 3-year local progression-free survival was 92.3%, with overall survival at 91.7% at two years, and 71.3% at three years. In terms of toxicity, there was no grade 2 (or higher) side effect reported. The authors also monitored kidney function and found two patients who had CKD progression post-treatment. One patient progressed to stage 5 CKD, eventually succumbing to this disease, and another patient progressed to stage 4 CKD, requiring further dialysis.

In the era of modern targeted therapies, there is interest in the role of kidney SABR in managing metastatic renal cell carcinomas. Cytoreductive nephrectomy, in combination with systemic therapy, has been shown to prolong overall survival compared to those who have system therapy alone[70,73,74]. For patients with comorbidities that are unsuitable for surgery, stereotactic ablative therapy of the entire ipsilateral kidney combined with systemic therapy is a potential management strategy[313]. A prospective phase 1 dose-escalation study of thirteen patients, treating the entire ipsilateral kidney using doses of 20 to 40Gy in five fractions, was able to show minimal grade 3 toxicity and no significant decline in kidney function (at 12 months)[314].

This summary of the literature on kidney SABR treatment span almost two decades, with advances in technology driving further interest in the treatment of this clinical disease. This clinical indication has not only been limited to treatment of primary kidney disease, but as well, the management of oligometastatic spread of renal cell carcinomas[315] .

A variety of delivery systems, motion management tools and image verification systems have been used and is summarised in Table 4.

Table 4. Reported publications of stereotactic body radiotherapy for primary renal cell carcinomas.

Author	Publication Year	Immobilisation	Fiducial Marker	Margin	Motion Management	Planning	Delivery System	IGRT
Beitler[275]	2004	Stereotactic Body Frame	No	GTV + 10mm	Not reported	3DCT	Linac	2D
Wersall[276]	2005	Stereotactic Body Frame with compression plate	No	GTV + 5 to 10mm	Compression plate	3DCT	Linac	NA
Teh[278]	2007	Body Cast	Yes	ITV + 2 to 3 mm	Free breathing	4DCT	Linac (IMRT 5-12 fields)	2D
Nomiya[280]/ Kasuya[281]	2008/2019	Body Cast	Yes	GTV + 10 to 15mm + PTV (5mm)	Gating at 50%	3DCT	Carbon Ion	2D
Kaplan[282]	2010	Not reported	Yes	GTV + 3mm	Tracking	3DCT	Cyberknife	2D
Lo[284] Ponsky[285]	2014/2015	Vacuum Bag + compression belt	Yes	GTV + 1 to 3mm	Tracking	3DCT	Cyberknife	2D
Staehler[286,310]	2010/2015	Not reported	Yes		Tracking	3DCT	Cyberknife	2D
Yamamoto[288]	2016	Stereotactic Body Frame + compression plate	Yes (n = 9)	ITV + 5mm (PTV) ITV from 4DCT, or fluoro	Abdominal compression (n = 6). Breath hold (n = 1)	4DCT (n =5) CT (n = 7) Slow CT (n = 2)	Linac 3DCRT (6MV/15MV)	3D + Fluro
Chang[287]	2016	BodyFix with Dual Vacuum	No	ITV + 5mm	Free breathing	4DCT	Linac (IMRT/VMAT)	3D
Correa[289]	2016	Vacuum body mold	No	GTV + CTV (ipsilateral kidney *or*	Free breathing	4DCT	Linac (IMRT/VMAT) + Tomotherapy	3D MVCT (TomoTherapy)

				GTV alone) + ITV + PTV (5mm)				or 3D CBCT (linac)
Pham [316]/ Siva[317]	2014/2017	BodyFix with Dual Vacuum	No	ITV +5mm	Free breathing (compression)	4DCT	Linac	3D
Funayama[290]	2019	BodyFix with Dual Vacuum	No	ITV (2 to 4mm) + 3mm PTV	Breath hold	CT (breath hold)	Linac (VMAT/Static)	3DMVCT
Senger[308]	2019	Not reported	Yes	GTV + 0 to 5mm	Tracking	CT	Cyberknife	2D

Definitions: ITV = Internal Target Volume; GTV = Gross Tumour Volume; IGRT = image guided radiotherapy; 2D = MV or kV planar imaging; 3D = 3-dimensional volumetric imaging; 4DCT = time resolved CT scan

1.9 Purpose of thesis

The purpose of this thesis was to evaluate the feasibility of using a 4D image-guided linac-based delivery system for stereotactic ablative body radiotherapy treatment for localised kidney lesions. The chapters in this thesis have been divided into subsections of the planning and treatment pathway in order to 1) inform how much kidney motion is affected by breathing instructions, 2) provide a strategy to minimise the kidney motion for treatment 3) define planning technique and metrics that can be used to create conformal and high-quality plans and importantly 4) report the use of motion verification (4D) and 3D kidney target localisation on the linear accelerator. The following aims were chosen to address these four areas:

Aim1: Investigate kidney motion as reported in the literature and categorise the range of motion when undergoing free, deep and/or compressed/shallow breathing. This aim is addressed in chapter 2 in the form of a literature review that compares the evidence of mean/median superior-inferior kidney motion between healthy and cancer-affected kidneys.

Aim 2: Investigate the use of a dual vacuum immobilisation system as a breathing motion management tool. Chapter 3 demonstrates the use of a commercially available immobilisation device to minimise kidney motion by dampening the breathing when using vacuum compression. Ten volunteers underwent vacuum compression and kidney motion was monitored using an ultrasound probe.

Aim 3: Define a 3D conformal planning technique that can be used on a linear accelerator to deliver stereotactic doses with conformal margins and compact dose distribution. Chapter 4 reports the typical beam arrangements used on left and rights stereotactic kidney plans and the planning metrics used to guide plan quality. This chapter also reports on the early toxicity reported for the first 20 patients treated on a linac based SABR protocol for kidney cancers.

Aim 4: Report on the effectiveness of using CBCT imaging to verify the target position directly before, midway and after treatment. Chapter 5 reports on the inter- and intrafraction motion of the kidney during treatment and as well the feasibility of using internal target volume (ITV) margin verification at each fraction. The importance of ITV margin verification is highlighted in a case report describing the dosimetric impact of a change in breathing magnitude for patient planned for kidney SABR treatment.

Chapter 2

A Review of Kidney Motion under Free, Deep and Forced-Shallow Breathing Conditions: Implications for Stereotactic Ablative Body Radiotherapy Treatment

Daniel Pham[1,2], Tomas Kron[1], Farshad F. Foroudi[1], Michael Schneider[2] and Shankar Siva[1]

[1] Division of Radiation Oncology, Peter MacCallum Cancer Centre, St Andrews Place East Melbourne, Victoria, Australia.

[2] Dept of Medical Imaging and Radiation Sciences, Faculty of Medicine, Nursing and Health Sciences, Monash University, Clayton, Victoria, Australia

.

The purpose of this literature review was to summarise reports of kidney motion and categorise the range based on three breathing conditions: free breathing, deep breathing and compressed breathing. This will inform the suitability of using motion management strategies to reduce kidney motion for SABR planning. This chapter is a copy of the manuscript that was accepted for publication[318]. The only modifications made have been to the figures and tables that are embedded within the text and the references that have been moved to the end of the thesis.

Abstract

Motion management strategies are important during stereotactic ablative body radiotherapy for abdominal targets. The kidney is a mobile retroperitoneal organ that moves with respiration. A review of the literature was performed to investigate the reported degree of kidney motion associated with various breathing conditions. A structured search was performed using Medline from January 1970 to May 2013 for all publications describing cranial-caudal kidney motion. Relevance to radiotherapy practice was reviewed based on any breathing instructions and/or immobilization equipment that could affect breathing pattern. Studies were categorized under three types of breathing conditions: Forced-shallow, breath-hold/deep and free. A total of 25 publications were identified describing cranial-caudal kidney motion with a combined total of 415 participants. Three publications described forced-shallow breathing using prone positioning or abdominal compression plates. Prone positioning, compared to supine positioning, did little to minimise kidney motion, however use of compression plates can result in kidney motion of less than 5 mm. Eight publications described deep breathing/breath hold techniques that showed average kidney motion ranging between 10mm - 40mm. Fifteen publications investigated kidney motion under free breathing with the majority reporting mean motion of less than 10mm. Kidney movement of up to 8.1mm in the anterior posterior direction and 6.2mm laterally were reported with no indications that breathing technique can influence the extent of this motion. In summary, kidney movement is complex, and consideration should be made to ensure that motion management strategies provide the desired radiotherapy benefit. There are limited publications on the effectiveness of abdominal compression on reducing kidney motion which warrant further investigation in this area.

2.1 Introduction

Renal cell carcinoma (RCC) is the 9th most common cancer in the US. In 2010, approximately 320,000 men and women had a diagnosis of cancer of the kidney and renal pelvis The disease is becoming more prevalent, with an annual increase in incidence of 2.8%[319]. Surgery has been considered the gold standard for the management of primary RCC[320] with conventional radiotherapy offering limited utility due to dose limitation from surrounding organs at risk[321]. However, developments in the field of stereotactic ablative body radiotherapy (SABR) treatment for extracranial targets are changing the limitations seen in conventional treatment. Delivery of high ablative doses was shown to be safe and well tolerated by patients treated for lung and abdominal cancers[322,323]. The role of SABR treatment for primary kidney cancers is emerging with a recent review of the literature for SABR treatment in primary kidney tumors showing two year local control rates of between 86% - 100% with a concurrent incidence of grade 3 toxicities of less than 4%[324]. Whilst early reports of safety and efficacy appear promising, strategies to account for respiratory induced motion of the kidneys are limited. The purpose of the present review is to summarize cranial-caudal kidney motion under three breathing conditions 1) Forced- shallow whereby equipment has been used to try to dampen abdominal based breathing 2) deep/breath hold whereby participants have been instructed to take deep breaths and/or hold their breath and 3) free whereby no breathing coaching or devices are used to control breathing

Anatomy of the Kidney

The kidney is a retroperitoneal organ measuring approximately 12 x 6 x 3 cm in size, surrounded by perinephric adipose tissue and bounded by Gerota's fascia[325]. The renal pelvis lies approximately at the level of the 2nd lumbar vertebrae and is not anchored to any bony anatomy. The right and left kidneys are in close proximity to different organs of varying radiosensitivity. The anterior portion of the right kidney is intimately associated with the inferior portion of the liver, whereas the left kidney is positioned inferior to the stomach and is in close proximity to the spleen. The second and third part of the duodenum, a particularly radiosensitive organ, enters the retroperitoneum and runs antero-medially to both kidneys. These structures are organs that need to be carefully assessed for toxicity when delivering SABR doses to the kidney.

Motion Management Strategies in Radiation Therapy Treatment

Motion management has seen a resurgence of interest with advances in image guidance technology used in parallel in the delivery of ablative doses of radiation for lung and abdominal targets. The American Association of Physicists in Medicine have published recommendations on the use of management strategies including motion encompassing, respiratory gated, breath hold, forced shallow breathing and respiration synchronized within the Task group 76 Report[326]. These techniques can be implemented at a number of different stages in the radiotherapy planning pathway providing various motion management

goals. Respiration synchronized delivery is based on patient training using visual-audio aides to replicate breathing motion at simulation to be carried out over the course of treatment[327]. Breath hold delivery aims to replicate the position of a mobile target by creating a freeze on respiratory motion. This can be self guided by patients[328] or can use oral devices that mechanically hold expiration[209]. Force- shallow breathing is based on equipment that can dampen the range of motion. Devices such as abdominal compression plates and body vacuums can limit the depth of abdominal based breathing reducing abdominal organ motion[329]. In the absence of breathing regulation devices or breath coaching programs, motion encompassing techniques can use time resolved 4-dimensional computed tomography (4DCT) scanners to show the extent of organ motion in a 3D image [330]. This allows radiotherapy planning margins to incorporate the extent of tumor motion. Similarly, 2D fluoroscopic imaging can be used to determine the maximum and minimum range of motion in order to incorporate this motion into planning margins[191].

2.2 Method

A review of the literature was conducted using MEDLINE (pubmed.gov) from Jan 1970 to May 2013. The following expressions were used for the search: [exp kidney/ or kidney$.af.] AND [exp motion/ or exp movement/ or motion.af. or move$.af. or displace$.af.] AND [exp respiration/ or breath$.mp.] Articles were excluded when animals or material phantoms were used to investigate kidney motion and if they were published in a language other than English. Direct reporting of kidney motion in the superior inferior direction was required for inclusion into this review.

2.3 Results

A total of 216 citations or papers were retrieved by the search including non-english articles. Twenty-five publications met the inclusion criteria for this review. This resulted in a total of 415 participants who were either healthy volunteers or had been diagnosed with cancer of various body sites. A review of the methodology from these publications allowed the authors to determine the breathing categories for publications to be assigned. For studies that performed repeated testing on the participants using multiple techniques, the result for each individual breathing technique was summarized separately. A variety of imaging modalities was used to measure kidney motion including ultrasound, film radiographs, magnetic resonance imaging (MRI) and 4DCT.

Kidney Motion during Forced-shallow Breathing

Three publications were found describing forced-shallow breathing achieved from either the use of a compression device[212,331,332] or from prone positioning[331,332]. A summary of the mean and range of superior-inferior kidney motion is described in Table 5.

Table 5. Summary of publications reporting crania-caudal kidney motion during forced/shallow breathing.

Author (year)	Site of Disease	Patient Number	Imaging*	Aide	Right Kidney Mean (range) (mm)	Left Kidney Mean (range) (mm)
Heinzerling et al. 2008 [212]	Lung/Liver cancer	10	4DCT	ACP[a] medium pressure	4.7 (3 - 7.5)	4.6 (2 - 9.2)
Kim et al. 2007 [331]	Volunteers	9	4DCT	Prone	11.7 (SD +/-11.7)	12.2 (SD +/-6)
Lee et al. 2004 [332]	Liver cancer	3	4DCT	Prone + RMRD[b]	18.1 (14 - 24.3)	12.5 (7 – 17)

[a] Abdominal compression plate [b]RMRD – In-house developed Respiratory Motion Reduction Device. *4DCT = 4-Dimensional Computed Tomography

The use of a stereotactic body frame with a compression plate at a moderate setting to dampen abdominal motion was investigated by Heinzerling et al[212]. The authors showed that this equipment was able to create a mean reduction in lung and liver tumor motion of 37.5% compared to free breathing (p = 0.0001). Cranial-caudal motion of the right and left kidney motions were also reduced by an average of 38.2% and 39.5% respectively. However, when compared to the range of kidney motion without the compression device, the authors reported no statistical significance. Similarly, when comparing the effect between moderate and high abdominal compression, the authors did not report a significant reduction in kidney motion. In the absence of commercial devices, prone positioning has been investigated as a means to dampen breathing. Kim et al[331] compared prone and supine positioning to evaluate reduction in abdominal organ motion in nine healthy volunteers. They showed a 25% reduction in cranial-caudal motion for the liver dome (p = 0.015) and a 35% reduction for the pancreatic head (p = 0.036). For the right and left kidneys however, in the supine position the average motion was 12mm and 13.9mm respectively and when prone, the motion was 12.2mm and 11.7 mm respectively. The reduction was not significant for the right kidney (p = 0.859) or the left kidney (p = 1.0). In the study by Lee et al[332] the impact of prone and supine positioning on organ motion was also investigated. The authors showed that whilst prone, the average diaphragm motion was 12mm and when supine, the average was 16mm. With further use of a customized compression device in the prone position, diaphragm motion showed a mean motion of 3mm (SD ±0.9) The investigators did not report any difference in kidney motion according to positioning. However, the average kidney motion was similar to the study by Kim et al[331] at 18.1mm for the right and 12.5mm for the left kidney. In a separate study investigating the impact of supine and prone positioning on adrenal gland motion[333], a fiducial marker was implanted around the adrenal gland for nine patients diagnosed with metastatic disease to this site. The average cranial-caudal motion when the patients were supine and prone were 11.0 mm (p= 0.962) in both positions.

Kidney Motion During Deep Breathing/Breath Hold

Eight publications where found describing kidney motion under deep breathing[334-337] or from breath-hold instructions[336,338-341]. No external devices were used on the abdomen. For a "Deep" technique participant were told to breathe regularly but deeply. A "Hold" technique refers to participants instructed to hold/suspend their breath at the beginning and end of the breathing cycle. A summary of the mean and range of cranial-caudal kidney motion is described in Table 6.

Table 6. Summary of publications reporting crania-caudal kidney motion during deep breathing

Author (year)	Site of Disease	Patient Number	Technique^	Imaging*	Right Kidney Mean (range) (mm)	Left Kidney Mean (range) (mm)
Wysocka et al. 2010[341]	Stomach	22	Hold	CT	Median 16.8 (1.5-53.1)	17.2 (1.3 – 59.9)
Draney et al. 2005[340]	Volunteers	7	Hold	MRI	13.2	10.1
Aruga et al. 2000[338]	Pancreas/Liver	10	Hold	CT	18 (7 - 26)	16 (0 - 23)
Ahmad et al. 1997[337]	Abdominal	8	Deep	Radiographs	11 (3 - 21)	17.7 (1 - 32)
Balter et al. 1996[339]	Lung/Abdominal	9	Hold	CT	18	18
Schwartz et al. 1994[335]	Upper thoracic/head and neck cancer	14	Deep	MRI	16 (3 - 39)	14 (6 - 39)
Moerland et al. 1994[334]	Volunteers	14	Deep	MRI	- (10-86)	- (10-66)
Suramo et al. 1984[336]	Not described	50	Deep	Ultrasound	40 (20-70)	41 (20-70)
		50	Hold	Ultrasound	19 (10-40)	19 (10-40)

*Imaging Systems: MRI = Magnetic resonance imaging, CT = Computed tomography ^Hold: Participants instructed to hold their breath after inspiration/expiration; Deep: participants instructed to breathe regularly but deeply.

One of the earliest studies reporting the range of kidney motion under deep breathing was performed by Suramo et al[336]. This study on 50 patients using ultrasound imaging, showed mean motion of 40mm for both the right and left kidney. The maximum kidney excursion reported in this group was reported to be up

to 70mm for both kidneys. This is similar to the range reported by Moerland et al[334] who used MRI to show that under deep breathing, kidney motion could be up to 86mm for the right kidney and 66mm for the left kidney.

In contrast, a study by Schwartz et al[335] using MRI on 14 participants, showed maximum motion of 39mm for both kidneys. Similarly, Ahmad et al[337] using radiographs on eight participants reported maximum motion of 21mm for the right kidney and 32mm for the left kidney. The main difference between the publications by Suramo et al[336] and Moerland et al[334] over Schwartz et al[335] and Ahmad et al[337] is the investigated patient population. Suramo et al [336] measured kidney motion on patients coming in for a routine ultrasound appointment (no specified disease/illness) while Moerland et al[334] evaluated healthy volunteers. On the other hand Schwartz et al[335] measured kidney motion in patients with either thoracic or head and neck cancers due for radiotherapy treatment, similar to Ahmad et al[337] who used data from patients due for whole abdominal radiotherapy treatment. The tumor location could potentially restrict the total range of organ motion due to compromised breathing volume in lung cancer patients or post surgical changes in abdominal cancer patients[203] The mean kidney motion reported by Schwartz et al[335] was 16mm on the right and 14mm on the left. Ahmad et al[337] also reported similar motion of 11mm for the right kidney and 17.7mm for the left kidney. The average kidney motion in deep breathing is similar to that found when instructed to breath hold. Five studies[336,338-341] used breath hold techniques to describe average motion of between 13.2 – 19mm for the right kidney, and between 10.1 – 19mm for the left kidney. Deep breathing and breath hold techniques have been used to investigate replication of kidney position within the abdomen. The study by Schwartz et al[335] used deep breathing to show that the mean deviation of the superior and inferior kidney borders was within 3mm from the original position. Suramo et al[336] showed that right and left kidney organ position could be replicated within 4mm with breath holding instructions. This kidney position could be further replicated to within 1mm when a wooden bar was used to guide the patients' breathing by tapping the patient's abdomen at regular intervals. Wysocka et al[341] used repeated free breathing, inspiration breath hold and expiration breath hold CT scans to quantify both abdominal organ motion as well as interfraction organ placement. The median displacements of the kidneys from a reference position during free, inspiration hold, and expiration hold breathing techniques were 6.6, 4.4 and 5.4mm respectively for the right kidney and 6.1, 5.7 and 6.2mm respectively for the left kidney. In a separate study looking at the role of respiratory gated treatment in primary kidney RCC, Stam et al[299] used cine MRI imaging on 15 patients to examine the reproducibility of kidney position under free breathing and breath hold conditions. Compared to breath hold, free breathing was able to reproduce the kidney position within 2mm for 80% of the participants.

Kidney Motion During Free Breathing

Fifteen publications where found that described kidney motion under free breathing whereby no equipment to influence breathing was given to the participant[212,298,331,334,342-352]. A summary of the mean and range of cranial-caudal kidney motion is described in Table 7.

Table 7. Summary of publications reporting crania-caudal kidney motion during free breathing

Author (year)	Site of Disease	Patient Number	Imaging*	Right Kidney Mean (range) (mm)	Left Kidney Mean (range) (mm)
Tai et al. 2013[351]	Pancreatic Cancer	10	4DCT	5.7 (SD +/- 3.2)	7.1 (SD +/- 3.1)
Hallman et al. 2012[349]	Liver/pancreatic	18	4DCT	6 (0 - 11)	4.5 (0 - 16.7)
Siva et al. 2012[350]	Liver/lung/	62	4DCT	7.7 (1.1 - 19.2)	7.9 (1 - 36)
Gawthrop & Gill 2012[346]	Lymphoma/stomach/ Adrenal	5	4DCT	13 (SD +/-0.5)	12 (SD+/-0.8)
Song et al. 2011[298]	Volunteers	10	MRI	8.9 (4.4 - 15.5)	8.5 (5.6 - 13.9)
Goldstein et al. 2010[348]	Pancreatic cancer	30	4DCT	7.2 (1.7 - 13.8)	6.4 (2.2 - 11.1)
Heinzerling et al. 2008[212]	Lung/Liver cancer	10	4DCT	7.6 (4.3 - 12.4)	6.2 (2.9 - 10.6)
Kim et al. 2007[331]	Volunteers	9	4DCT	13.9	12
van Sörnsen de Koste et al. 2006[352]	Lung/Abdominal cancer	54	4DCT	9	9.8
Giraud et al. 2006[347]	Liver/Lung cancers	8	4DCT	7.3	9.8
Brandner et al. 2006 [343]	Eligible for radiotherapy	13	4DCT (audio[a])	13	11
Boucher et al. 2004[342]	Volunteers	8	4DPET	12 (3.5 - 18.8)	11.1 (3.5 - 17.1)
Bussels et al. 2003[344]	Pancreas/volunteers	12	MRI	- (max 16.1)	- (max 16.9)
Moerland et al. 1994[334]	Volunteers	14	MRI	- (4 – 35)	- (2 – 24)
Davies et al. 1994[345]	Volunteers	9	Ultrasound	11 (SD 4)	-

[a] Audio feedback for breathing synchronization used **Imaging Systems: MRI = Magnetic resonance imaging, 4DPET = 4-Dimensional Positron Emission Tomography; 4DCT = 4-Dimensional Computed Tomography

Free breathing measurements are taken with no specific breathing instructions or immobilization equipment over the abdomen to intentionally dampen the range of abdominal based breathing. Eight of the fifteen publications reported mean kidney motion of less than 10mm for both the left and right kidneys [212,298,347-352]. From this group, Siva et al [350] and van Sornsen de Koste et al [352] with a combined series of 116 participants reported average kidney motion of 7.7 and 9.8mm respectively. Five publications [331,342,343,345,346] showed average kidney motion ranging from 11mm to 13mm. The study by Brandner et al [343] reported right and left motion of 13mm and 11mm respectively with the aide of an audio device to guide breathing inspiration and expiration. This is an aide that is calibrated to suit the patients' own level of comfort rather than to achieve a specified motion range. Davies [345] attempted to quantify organ motion by classification of participants into chest or abdominal based breathers. The authors noted that there was a trend for abdominal breathers to have larger kidney motion (average motion 10mm - 16mm) compared to chest breathers (average motion 9mm).

Kidney Motion in Pediatric Patients

Two publications were found describing kidney motion for pediatric cases with and without general anesthesia[353,354]. A summary of the mean and range of motion is described in Table 8.

Table 8. Summary of publications reporting crania-caudal kidney motion in paediatric patients

Author (year)	Site of Disease	Patient Number	Imaging*	Aide	Right Kidney Mean (range) (mm)	Left Kidney Mean (range) (mm)
Nazmy et al. 2012[353]	Neuroblastoma (mean age 4 +/-1.6)	9 (mean age 4 +/-1.6 yrs)	CBCT	General Anesthesia	(4 – 10)+	(4 - 8) +
Pai et al. 2012[354]	Neuroblastoma/ Hodgkins/ Soft tissue sarcoma/wilms	11 (mean age 4 , range 2 to 8 years)	4DCT	General Anesthesia	1.9 (0.6 - 3.7)	1.7 (0.7 - 3.4)
		9 (mean age= 12, range 9 to 18 years)	4DCT	Free breathing	3.9 (1.5 -6.3)	3.07 (0.8 - 4.6)

*4DCT = 4-Dimensional Computed Tomography; CBCT = Cone Beam Computed Tomography + Interfraction motion of the kidney position reported.

The use of general anesthesia in radiation oncology is limited to pediatric cases and with the reduced tidal volume effect during anesthesia[355,356] can potentially act as a method to reduce kidney motion. Pai et al[354] analyzed kidney motion data for children undergoing anesthesia (2-8 years of age) and showed that kidney motion for this age group was less than 2mm for both the right and left kidneys. The older age group (9 – 18 years of age), not under general anesthesia, showed mean motion of 3.9 and 3.07mm for the right and left kidneys respectively. While there was a statistically significant difference in motion between these two groups (p =0.0075) indicating reduced kidney motion during anesthesia, the authors also found a significant correlation with age. For every increase in age by one year there was an increase in kidney motion of 0.12mm on the left (p=0.0187) and 0.15mm on the right kidneys (p=0.0323). The increased kidney motion in the older age group could be due to the age effect rather than the anesthesia effect. The study by Nazmy et al[353] used cone beam CT to image kidney position on different treatment fractions among children with a mean age of four years. The mean displacement of the kidney position from the planning CT was 10mm for the right and 8mm for the left kidneys.

Lateral and Anterior/Posterior Kidney Movement

Due to the size, shape and location of the kidney, the movement of the kidneys is not limited in the cranial-caudal direction but can be more complex. A large range of motion in the lateral and anterior posterior direction has been reported for the kidney with little evidence to suggest breathing technique can affect the absolute range of motion (Table 9).

Table 9. Summary of publications reporting lateral and anterior/posterior kidney motion

Author (year)	Breathing Type	Mean Left Right Motion (mm)		Mean Anterior Posterior Motion (mm)	
		Left Kidney	Right Kidney	Left Kidney	Right Kidney
Kim et al. 2007[331]	Controlled (Prone)	2	0.1	0.1	2
Lee et al. 2004[332]	Controlled (Prone)	1.4	2.6	3.1	4.2
Wysocka et al. 2010[341]	Breath Hold	Median 1.6	Median 1.5	Median 5	Median 4.5
Draney et al. 2005[340]	Breath Hold	-	-	2.3	6.3
Aruga et al. 2000[338]	Breath Hold	0.8	1.2	0.3	2.9
Tai et al. 2013[351]	Free	0.9	0.8	2.8	3.3

van Sörnsen de Koste et al. 2006[352]	Free	0.6	0.6	1.2	2.6
Giraud et al. 2006[347]	Free	3	4.7	8.1	6.7
Brander et al. 2006[343]	Free	1.4	1.4	4.4	6.1
Bussels et al. 2003[344]	Free	6.2	4.8	5.3	-

Prone positioning[331,332] showed average lateral kidney motion of less than 3mm with mean anterior posterior motion of up to 4.2mm. Similarly, breath hold techniques[338,340,341] showed average lateral kidney motion of less than 2mm with average anterior posterior motion of both kidneys between 0.3 – 6.3mm. Free breathing techniques[343,344,347,351,352] also showed lateral motion between 0.6 – 6.2mm and larger average anterior-posterior motion of up to 8.1mm. Differences in cranial-caudal movement of the individual kidney poles have also been reported in two studies[335,346]. Gawthrop & Gill[346] reported average superior kidney pole motion of 12.3mm compared to inferior kidney pole motion of 6.7mm. Schwartz et al[335] showed that in the left kidney the superior pole average motion of 14mm compared to the inferior pole with an average of 17mm.

2.4 Discussion

One of the earliest reports on stereotactic body radiotherapy was from the Karolinska institute in 1994 [229] describing the design and use of a stereotactic body from for lung and liver stereotactic treatment. Since then this technique has been increasingly used internationally. In the United States, a survey among more than 500 physicians showed a dramatic increase in use of SABR treatment over a 10-year period. In 2000, less than 10% of the surveyed physicians where using this technique, whereas in 2010 more than 60% had adopted the technique into the clinic. Of the top five most common sites for treatment, four were targets that are subject to potentially significant motion induced error (lung, liver, pancreas and adrenal glands). Within this group of physicians prescribing SABR treatment, the majority of respondents addressed motion management with gating and/or abdominal compression techniques. For the non-users of SABR, 62.6% agreed that lack of necessary equipment limited a protocol for SABR treatment[296]. SABR treatment has become more popular due to the increased implementation of advanced imaging technology that can capture organ motion. A 2009 report on use of advanced imaging technology in the United States[357] showed that from 2006 to 2009 there was an almost doubling of the use of 4DCT imaging in radiation oncology. The rapid adoption of this technology into the radiotherapy department stems from the ability to provide time resolved CT data that can be used for dose planning as well as to accurately describe organ motion.

The role of other imaging modalities is limited in radiotherapy planning due to resource availability. Technologies such as MRI are commonly used to assist in delineation of immobile soft tissue structures[358], and with further developments in motion based MRI imaging[359] their role as non-ionizing imaging technology will increase. In this review a variety of technologies were employed to observe kidney motion. Ultrasound and MRI were commonly seen in the older publications, but the development of 4DCT in the early 2000 has resulted in 4DCT as the dominant technology used to quantify organ motion in more recent publications. Nevertheless, the variety of imaging techniques and the type of equipment does not appear to influence the degree of kidney motion reported.

SABR treatment for primary RCC is a relatively new indication with few reports of motion management strategies. Staten Island University Hospital and The Karolinska Institute have published studies using standard CT imaging with the stereotactic body frame to compress diaphragm motion[275,276]. A minimum of 10mm margin around the gross tumor volume (GTV) was used for the planning target volume. The National Institute of Radiological Sciences in Japan also did not use 4D CT imaging for target delineation. Instead, a margin of 15 – 20mm was added to the GTV and used alongside iridium needles for target verification[280]. One report from the Methodist Hospital in Houston[360] described the use of 4DCT in the planning process, however, this was for treatment using a gating technique. The Peter MacCallum Cancer Center in Australia has described the use of 4DCT imaging with vacuum immobilization for stabilization in a patient undergoing SABR treatment to a kidney target. Pre-treatment verification of breathing depth to ensure consistency with the breathing motion seen in planning was a requirement for treatment[361].

The sparing of non-tumor tissue is an important priority in SABR delivery. Unlike conventional planning, heterogeneous dose distribution is a main feature of this technique. A target that has minimal motion will therefore ensure a highly conformal dose to the tumor target. There are, however, resource implications in the use of motion management equipment. Implementing motion management techniques can lead to an extension of the overall treatment time. In one study, the additional time requirement when using stabilization equipment was reported to be up to 40 minutes (12). This extra time burden may not be suitable for a SABR program associated with an ageing patient population that have difficulties in maintaining a fixed position for an extended period of time.

2.5 Conclusion

In the context of SABR delivery for primary kidney targets, the range of motion of the kidney under different breathing conditions can be complex. Cranial-caudal kidney motion under forced-shallow breathing has been shown in one publication to be on average less than 5mm [212]. The use of prone positioning as a compression strategy does not seem to affect kidney motion as it appears to be unchanged from kidney motion during free-breathing which has reported motion ranges of less than 10mm [212,298,347-352]. Not surprisingly, under deep breathing and breath holding the average right and left kidney motion is almost double that of free-breathing, with a majority of publications reporting motion between 10mm and 20mm. Complex kidney motion is also seen for both the right and left kidneys with the mean anterior

posterior motion ranging between 0.1mm up to 8.1mm. Lateral motion of the kidney appears to be less of an issue with the majority of publications reporting a lateral motion mean of less than 2mm. There are a limited number of publications describing effectiveness of techniques/equipment that can minimize kidney motion, warranting further investigation into this area.

2.6 Literature review update

An update of the literature review was performed using the OVID Medline database for the period since the publication of the review outlined above. The new search criteria included publications between 2013 to October 2019 with the following expressions used for the search: [exp kidney/ or kidney$.af.] AND [exp motion/ or exp movement/ or motion.af. or move$.af. or displace$.af.] AND [exp respiration/ or breath$.mp.].

A total of 114 publications were found within the database from the period of 2013 to October 2019. After exclusion of articles not involving humans, case reports and non-reporting of cranial-caudal motion of the kidney, a total of 16 additional articles were deemed relevant to the literature review. These included 356 adults and 74 paediatric cases. The imaging modalities employed for these studies were similar to those previously reported with 4DCT, ultrasound, CT/CBCT and MRI used to quantify cranial-caudal kidney motion.

Of the 16 additional papers updated for the literature review, twelve articles published results detailing kidney motion under free-breathing conditions, six reports on forced/shallow breathing conditions and two articles on paediatric kidney motion. No reports were identified describing kidney motion under deep breathing conditions.

Kidney Motion Under Free-Breathing

Under free-breathing conditions, seven studies[302,362-367] reported average kidney motion between 10mm and 24.8mm. Five studies showed 10mm or less of motion[362,368-372]. Table 10 is a summary of the means and standard deviations of kidney motion observed in those studies.

Table 10. Summary of publications (2013 to October 2019) reporting crania-caudal kidney motion during free-breathing

Author (year)	Site of Disease	Patient Number	Imaging	Aide	Right Kidney Mean (standard deviation) (mm)	Left Kidney Mean (standard deviation) (mm)
Yamashita (2014)	Lung, oropharyngeal, liver	20	4DCT	Free	11.1 (+/- 4.8)	

Tai (2013)	Pancreas	10	4DCT	Free	5.7 (+/-3.2)	7.1 (+/- 3.1)
Jung (2013)	Liver	11	4DCT	Free	median 12 (range 6-23)	median 15 (range 8-31)
Pham (2014)	Healthy	9	US	Free	14.8 (+/-7.8)	16 (+/-11.4)
Damato (2014)	Gynecologic	6	4DCT	Free	9.9 (range 4.5 – 18.7)	
Bohris (2015)	Healthy	10	US	Free	12 (range 6-18)	
	Kidney Stone	10			10 (range 4-16)	
Abhilash (2016)	Healthy/stones/cysts/RCC	110	US	Free	24.5 (+/- 6.4)	17(+/-3.6)
Harrogate (2016)	Kidney stone	41	US	Free	7.7(+/- 2.9)	
West (2017)	Liver/Kidney cancer	13	4DCT	Free	Median 10 (range 4 - 16)	8 (range 2 - 18)
Cusumano (2018)	Kidney cancer	4	4DCT/MRI	Free	5 (+/2.9) (4DCT) 7 (+/-2.4) (MRI)	
Van Gelder (2018)	Liver/Pancreas cancer	15	4DCT	Free	6.9 (+/-1.0)	6.1 (+/-2.5)
Prins (2019)	Kidney cancer	15	MRI	Free	12.3	

Kidney Motion Under Shallow Breathing

Shallow breathing in five publications reported kidney motion between 4mm and 8.1mm[300,362,367,371,373]. One study reported an average kidney motion greater than 12mm[364]. Table 11 is a summary of the means and standard deviations of kidney motion as reported in these studies.

Table 11. Summary of publications reporting crania-caudal kidney motion during Forced/Shallow breathing

Author (year)	Site of Disease	Patient Number	Imaging	Aide	Right Kidney Mean (standard deviation) (mm)	Left Kidney Mean (standard deviation) (mm)
Sonier (2014)	Primary Kidney	30	4DCT	Vacuum (n = 28) ACP (n = 2)	8.1 (+/-4.33)	
Pham (2014)	Healthy	9	US	Vacuum	12.8 (+/-6)	14.4 (+/-11.8)
Pham (2015)	Kidney	32	4DCT	Vacuum	8 (+/-4)	6 (+/-3)
Bohris (2015)	Healthy	10	US	ACP + Oxygen	8 (range 3-11)	
	Kidney Stone	10			7 (range 3-11)	
West (2017)	Kidney/Liver	31	4DCT	ACP	Median 6 (range 2 -10)	Median 4 (range 2 - 10)
Van Gelder (2018)	Liver/Pancreas cancer	15	4DCT	Pneumatic Belt	6.3 (+/-1.7)	5.2 (+/-2.4)

Two studies compared kidney motion under abdominal compression and free-breathing conditions[362,364]. Bohris *et al*[362] designed a compression plate to sit above the participant's navel. An ultrasound transducer was angled from the patient's side to capture the superior-inferior motion of the kidney. Under abdominal compression, the average kidney motion was 8mm compared to free-breathing at 12mm ($p = 0.001$). A similar setup using ultrasound also showed a significant reduction in kidney motion when under vacuum compression[364]. However, this was effective for only 6/9 (67%) participants. Two of nine (22%) participants showed less than 1mm change in kidney motion and 1/9 (11%) showed an increase of 8.2mm in kidney motion when under vacuum compression. Two studies reported kidney motion for patients undergoing kidney SABR treatment[300,373]. In both studies, 4DCT imaging was used to quantify kidney motion with the patient immobilised under dual vacuum immobilisation. Sonier *et al* reported mean superior-inferior kidney

motion of 8.1 (+/4.3) mm. In contrast, our group measured kidney motion at the superior, mid and inferior poles of the left and right kidney[373]. For the right kidney, the superior, mid and inferior kidney pole motion averaged 8 (+/4) mm, 5 (+/-3) mm and 6 (+/3) mm respectively. For the left kidney, the superior, mid and inferior kidney pole motion averaged 6 (+/3) mm, 5 (+/4) mm and 5 (+/3) mm respectively. A similar study also measured the cranial-caudal motion of the superior and inferior poles of the right and left kidneys[301]. In this study, a compression belt with an air bladder that was inflated to 60-80 mmHg was investigated to determine its effectiveness in reducing kidney motion. Under compression, the superior and inferior poles of the right kidney showed a median motion of 6 (range 2 – 10) mm and 4 (range 0 – 8) mm respectively, and for the left kidney, the median motion was 4 (range 2 – 10) mm and 4 (range 0 – 8) mm respectively. Compared to free-breathing, the addition of compression was able to reduce the left superior kidney poles by 2mm ($p = 0.047$). The right kidney, while under compression, also showed a median reduction of 2mm, but this was not statistically significant ($p = 0.051$). One of 13 patients (7%) in this study showed an increase of 4mm in kidney motion when under compression. In another study comparing the effectiveness of abdominal compression to reduce organ motion, a pneumatic compression belt was used to limit breathing motion[367]. Fifteen patients underwent repeated 4DCT scans, with and without the compression belt. Four of 14 (28%) and 6/14 (42%) patients showed a reduction in left and right kidney motion respectively. Two of 14 (14%) patients showed an increase in the left and right kidney motion. Overall, the authors did not find a significant change in kidney motion (p-value not reported).

Kidney Motion in Paediatric Patients

Two new studies[374,375] have reported on the interfraction kidney displacement in paediatric cases (Table 12).

Table 12. Summary of publications reporting crania-caudal kidney motion in paediatric patients

Author (year)	Site of Disease	Patient Number	Imaging	Aide	Right Kidney Mean (mm)	Left Kidney Mean (mm)
Huijskens (2015)	Lung, Abdomen, Spinal Cord	39	CT/CBCT*	Free breathing (n = 37) Anaesthetised (n = 2)	0.5	1.5
Uh (2017)	Abdominal tumours	35	MRI	Free breathing (n = 18)	4.7 (95% CI 3.5 – 5.9)	4.8 (95% CI 3.3-6.2)

Anaesthetised	2.3 (95% CI 1.8-2.8)	1.6 (95% Ci 1.1 - 2.1)
(n = 17)		

*CBCT imaging was used for verification at pre/mid and post treatment

The study cohort of 39 patients had a median age of eight years (range 1.6 to 17.8). Only two patients were anaesthetised during imaging[374]. Kidney motion was measured using CBCT imaging to calculate the positional displacement from the planning CT. This is a limitation of the study which does not accurately measure the intrafraction motion of the kidney. In another publication, thirty-five patients with a median age of nine years (range 1 – 20) underwent 4D MRI imaging for treatment planning[375]. Patients aged eight years or less (with the exception of one twelve-year-old) were anaesthetised. The authors found a strong correlation between age and patient height with the peak-to-peak superior-inferior motion of the kidneys (p = <0.001).

There is renewed interest in quantifying organ motion as imaging technology becomes readily available. This review has discussed a large body of evidence indicating a wide variation of superior-inferior kidney motion among individuals. Stabilisation devices, to manage breathing motion, can reduce kidney motion for radiotherapy planning[301,376], an effect similarly shown in other clinical sites[212,216,225,329]. Two new studies recording superior-inferior kidney motion based on the superior, central and inferior pole suggests independent motion in these areas[301,373]. Further investigation into this geographical independence could inform future studies on asymmetric planning margins. Compared to adults, kidney motion in paediatric patients continue to show relatively small amounts of motion[374,375].

A limitation with using compression devices to regulate kidney motion is the occasional risk of increasing kidney motion[301,364]. This effect has also been seen in other clinical sites[226,329,377], highlighting a need to closely monitor the use of compression devices as a motion management tool.

Chapter 3

The use of dual vacuum stabilization device to reduce kidney motion for stereotactic radiotherapy planning

Daniel Pham[1,2], Tomas Kron[3], Colin Styles[4], May Whitaker[5], Mathias Bressel[6], Farshad Foroudi[7], Michal Schneider[2], Thomas Devereux[1], Kim Dang[1] and Shankar Siva[7]

[1] Department of Radiotherapy Services, Peter MacCallum Cancer Centre, Melbourne, Australia.

[2] Department of Medical Imaging and Radiation Sciences, Monash University, Melbourne, Australia.

[3] Department of Physical Sciences, Peter MacCallum Cancer Centre, Melbourne, Australia.

[4] Barwon Health, Melbourne, Australia.

[5] Department of Radiation Oncology, Royal Prince Alfred Hospital, Sydney, Australia.

[6] Centre for Biostatistics and Clinical Trials, Peter MacCallum Cancer Centre, Melbourne, Australia.

[7] Division of Radiation Oncology, Peter MacCallum Cancer Centre, Melbourne, Australia.

As the previous chapter has highlighted, kidney motion can vary greatly among individuals. Strategies to minimise breathing motion can influence kidney motion including the use of abdominal compression devices. In this chapter, the Elekta^{TM} dual vacuum stabilisation device was investigated to explore if increased vacuum compression could reduce kidney motion by restricting breathing. This chapter is an exact copy of the manuscript that has been published[364]. The only modifications made have been to the figures and tables that were embedded within the text and the references which have been moved to the end of the thesis. This has allowed a consistent format for this thesis.

Abstract

Abdominal stereotactic ablative body radiotherapy is aided by motion management strategies to ensure accurate dose delivery as targets such as the kidney are easily influenced by breathing motion. Commercial devices such as compression plates and dual vacuum technology have been demonstrated to reduce the motion of lung and liver tumors. The aim of this study was to evaluate the effectiveness of a dual vacuum system in reducing kidney motion as well to investigate any relationship between abdominal wall motions with kidney motion. Ten healthy volunteers were set up with and without vacuum compression (Elekta BodyFIX^{TM}) to simulate free and dampened breathing. Ultrasound imaging was used to visualize kidney motion at the same time an abdominal surface marker was monitored using infrared imaging (Varian, Real Time Position Management). The resulting kidney and abdominal motion tracks were imported into motion analysis (Physmo^{TM}) and custom built software (Matlab, Mathworks, MA, USA) to calculate amplitude of motion independent of shifting baselines. Thirty-four kidney datasets were available for analysis, with six datasets unable to be retrieved. With vacuum compression six out of nine participants showed a mean reduction of kidney motion ranging between 1.6 mm - 8 mm ($p < 0.050$). One participant showed an increase in motion of 8.2 mm ($p < 0.001$) with vacuum compression. Two participants showed no significant change (< 1 mm) in kidney motion. No relationship was observed for abdominal wall motion and motion changes in the left kidney ($r = 0.345$, $p = 0.402$) or right kidney ($r = 0.527$, $p = 0.145$). Vacuum compression reduced kidney motion in the majority of participants; however larger breathing motion can also result from its use. No pattern emerged regarding which patients may benefit from vacuum immobilization as abdominal wall motion was not found to be an adequate surrogate for kidney motion.

3.1 Introduction

Stereotactic ablative body radiotherapy (SABR) in primary kidney targets have shown tumor control rates of between 80 - 100% at 2 years[324]. Implementation of an optimal stereotactic program for kidney targets is reliant on effective motion management techniques as reports of mean kidney motion are varied, ranging from less than 10 mm[212,347,348,350,352] up to 40 mm[336]. The American Association of Physicists in Medicine (AAPM) have developed guidelines on motion management strategies summarizing their findings in the AAPM Task Group Report[160]. In this report one of the more common strategies to reduce organ mobility is to induce shallow breathing through abdominal compression. This strategy has been popularized in a number of clinical settings including lung and liver treatment. Devices such as abdominal compression plates[200,212,329,378,379], dual vacuum technology[329] and abdominal straps[331] have been demonstrated to reduce target volume and as well reduce dose to critical structures such as the healthy lung [380] and liver[381]; however no study has directly examined the impact of abdominal compression on kidney motion. In this study an investigation is made into the effect of dual vacuum compression on kidney motion as visualized by ultrasound. We hypothesized that at high levels of vacuum compression, breathing motion will be dampened and hence reduce the superior inferior kidney motion. As a secondary objective, we investigated whether internal kidney motion was associated with abdominal wall motion, as assessed by an abdominal surrogate maker.

3.2 Materials and Methods

Participants

The research protocol was approved by our institution's ethics committee. Ten healthy volunteers were recruited consecutively from within our institution. The group consisted of five females and five males with a mean age of 34.1 years (range 22 – 65 yr). All participants were able to tolerate being set up in a supine position with their arms up for a session that would last approximately one hour. No specific instruction for breathing was given.

Equipment

The BodyFIX™ system (Elekta, Stockholm, Sweden) was used in this study to provide dual vacuum compression over the abdomen. This device is composed of a T-shaped body support system that can be molded onto a patient's body profile (Figure 8).

Figure 8. Dual vacuum immobilization using the Elekta BodyFIX® system.

Composed of a) BodyFix® dual cycle pump, b) BlueBAG™ for custom body molds c) Coversheet . *Source: Peter MacCallum Cancer Centre*

A plastic coversheet was placed over the participant, leaving the head and neck uncovered, whilst at the same time isolating the region of the upper body to mid waist underneath the coversheet. A closed environment was ensured by sealing the coversheet to the vacuum formed body bag that is connected to a dual cycle pump via a tube that is fed under the coversheet. By activating the vacuum pump, air underneath the coversheet can be evacuated to different pressure levels ranging from 0 up to a maximum of 100 mbar or the maximum pressure tolerated by the participant.

Ultrasound

A portable ultrasound system (B&K Falcon, Herlev, Denmark) was set up to visualize the kidneys using an abdominal transducer (6 - 3 MHz). In order to make a recording of the superior inferior kidney motion, the ultrasound system used a video output connection to a laptop (IBM: Armonk NY) for a live video recording of 300 seconds. Operation of the ultrasound was performed by an experienced radiologist with specialist training using ultrasound.

Abdominal Surface measurement

Abdominal motion measurements were performed using the Varian Real-Time Position Management™ (RPM) system (v. 1.6, Varian Medical System, Palo Alto, California, USA). This is composed of an infrared tracking camera and a two-point reflective marker (Figure 9).
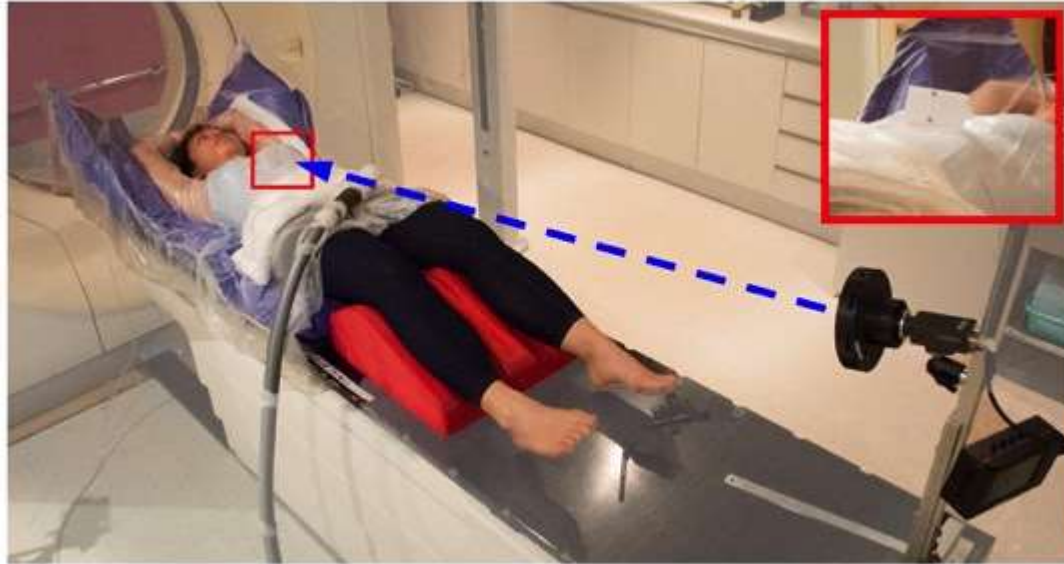
Figure 9. Participant setup in the dual vacuum system with a two-point surrogate marker (inset) on the abdomen.

Infrared camera used to monitor and record abdominal motion. *Source: Peter MacCallum Cancer Centre*

The position of the marker box was midline at the point of greatest motion, allowing any anterior-posterior motion that occurred to be detected by the infrared camera. The displacement of the marker box was recorded by the RPM software for a period of 300 s. This measurement was initiated simultaneously with the beginning of each kidney recording, and for the final analysis the first and final 30 s of RPM recording was removed to exclude any bias introduced at the beginning and end of each setup change. Hence, the evaluable measurements were taken over a 240 second period.

Measurement Order

All participants were first set up in the BodyFIX system in order to determine the maximum pressure setting comfortably tolerated. Once this was defined an ultrasound video recording was performed on the kidneys in the following order: right kidney with no vacuum pressure applied; right kidney with vacuum pressure applied; left kidney with vacuum pressure applied; left kidney with no vacuum pressure applied.

Motion Analysis

On each video recording, the kidney motion was measured using open-source video motion analysis software (Physmo-Video Motion Analysis Package, San Francisco, CA. http://physmo.sf.net). Each kidney video recording was imported into this software which subsequently converted each second of video into four frames. An experienced dosimetrist used a marker tool in the software to localize the most superior head of the kidney in each frame. For each video set, a file containing the spatial location of each marker at each time point was exported into Microsoft Excel for further analysis. Due to the inherent baseline shift associated with manual operation of the transducer, the Excel file containing the kidney motion data was imported into a previously described customized software[382] developed using Matlab™ (Mathworks, Natick Massachusetts). This software was used to calculate a series of motion amplitudes indicating the cranial caudal motion of each kidney video recorded under each breathing condition. The software was designed to analyze five parameters that characterize a breathing track: inhale and exhale amplitude, frequency of breathing asymmetry of the breathing period and a mean variable baseline; the software calculates a baseline for each inhale/exhale cycle, providing a moving baseline for the entire breathing track. In our current investigation the ability of the software to quantify an amplitude value from a shifting baseline that is a characteristic for each breathing period removed the bias associated with manual handling of the transducer.

Statistical Analysis

IBM SPSS Statistics software (v. 21.0, Chicago, IL) was used to analyse the data with statistical significance set at $p = 0.05$. Each participant was analysed separately. The mean amplitude of kidney motion with and without the vacuum immobilization, as well as the mean amplitude of abdominal motion with and without the vacuum immobilization were each compared using an independent samples t –test. Spearman's Rank correlation was used to investigate the relationship between kidney motion (mm) and the change in abdominal surface motion (%), as well as the relationship between the change in kidney motion and vacuum pressure setting (mbar).

3.3 Results

A total of forty kidney motion datasets and abdominal breathing traces from ten volunteers were acquired and recorded. However, due to a necessary hardware upgrade of the laptop used for data storage, a total of five kidney and abdominal datasets from two volunteers were unable to be retrieved for analysis leaving only nine participants available for analysis. Based on an extended time lapse between the data measurement and data analysis as well as subsequent unavailability of equipment and personnel, it was decided to not repeat or collect new data. The full data from eight participants was available for comparison of left kidney motion and abdominal motion with and without vacuum compression. Similarly, data for nine participants were available for comparison of right kidney and abdominal motion with and without vacuum compression.

Participant motion and manual operation of the ultrasound transducer probe meant that visualization of the kidney was not possible for the entire recording in each participant. Visualization of kidney motion averaged 230 s (range 105 – 300 s) and for the final analysis the first and final 30 s of the video was removed to exclude any bias introduced at the beginning and end of each setup change.

In this group of volunteers, the mean pressure level achieved using the dual vacuum compression was 74.3 mbar (range 63 – 100 mbar) with an aim to reach 100 mbar or what was tolerated by the participant.

Kidney Motion with and without the Vacuum Pressure

The mean superior-inferior kidney motion without the vacuum immobilization was 16 mm (range 8.2 – 45.0 mm) and 14.7 mm (6.8 – 33.4 mm) for the left and right kidneys respectively. The mean superior-inferior kidney motion during vacuum immobilization was 14.5 mm (range 7.2 – 43.0 mm) and 12.8 mm (range 7.2 to 27.0 mm) for the left and right kidneys respectively. Figure 10 demonstrates the mean right and left kidney motion with and without dual vacuum immobilization. The line of identity represents no difference in kidney motion with and without dual vacuum immobilization. As a group average the vacuum effect was not found to be statistically significant for left kidney ($p = 0.781$) nor for the right kidney ($p = 0.566$).
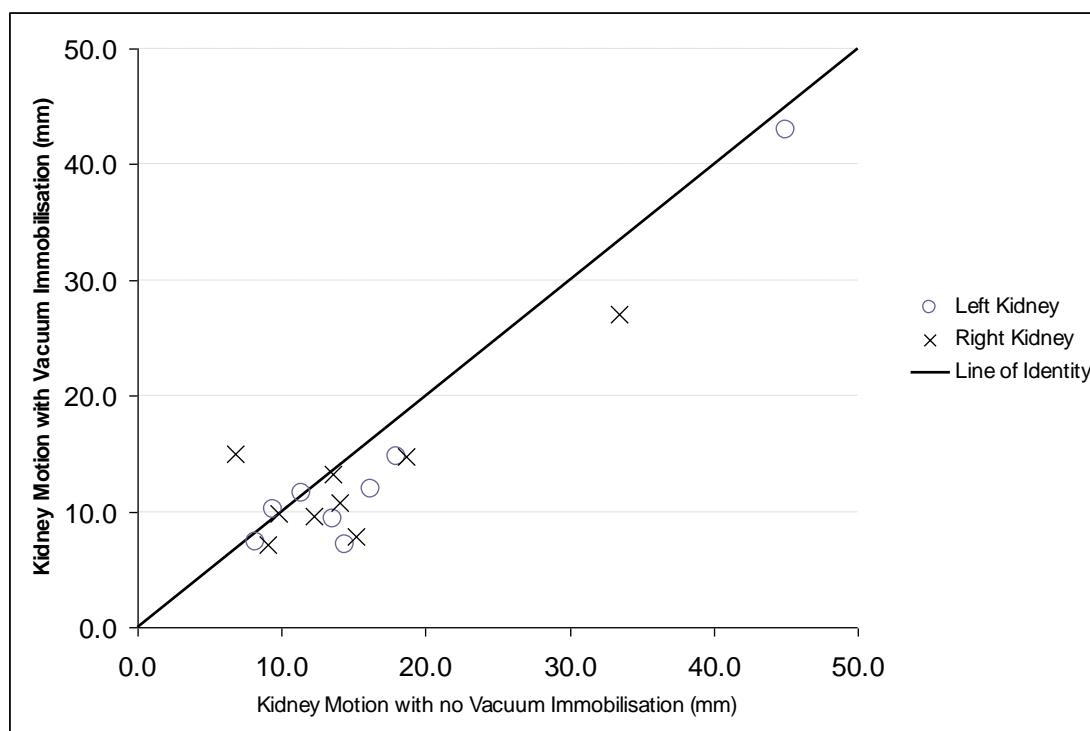
Figure 10. Kidney motion (mm) with and without dual vacuum immobilization.

Analysis of individual effects of the vacuum compression showed that of the nine participants, seven showed a significantly different motion on at least one kidney as a result of the vacuum compression. When immobilized using the dual vacuum system four of eight participants showed left kidney reduction ranging

from 3.2 mm up to 8.0 mm (p <0.001 to p = 0.020). Right kidney motion change was observed in seven of nine participants. Reduction of motion was observed in six of these nine with values ranging from 1.6 up to 6.2 mm (p <0.001 to p = 0.033). One of the nine participant showed a mean increase in right kidney motion of 8.2 mm (p<0.001). In two participants the mean difference of the kidney motion with and without the vacuum compression was less than 1 mm which was not found to be statistically significant. A summary of the individual results can be seen in Table 13.

Table 13. Summary of superior inferior kidney motion with and without dual vacuum immobilization.

Participant	Sex	Kidney	Kidney motion with vacuum compression (mm) Mean (±SD)	Min	Max	Kidney motion without vacuum compression (mm) Mean (±SD)	Min	Max	Mean Difference* (95% CI)	p-value
1	Female	Left	7.2 (±2)	3	12.2	14.4 (±3)	8	24	-8 (-8.2 to -6)	<0.001
		Right	7.8 (±2.8)	3	16.4	15.2 (±2.2)	7.2	23	-7.4 (-8.4 to -6.2)	<0.001
2	Female	Left	Data not available			8.2 (±2.8)	4.4	14.6	-	
		Right	15 (±1.6)	12.4	17.4	6.8 (±1.8)	4.4	10.4	8.2 (7.2 to 9.2)	<0.001
3	Female	Left	9.4 (±5.8)	3.4	33.8	13.6 (±7.2)	5	36.6	-4 (-6.6 to -1.4)	0.003
		Right	10.8 (±5)	5.4	37.4	14 (±7.4)	6.4	36.8	-3.2 (-5.6 to -0.6)	0.012
4	Male	Left	7.4 (±3.4)	3.2	17.8	8.2 (±4.4)	3.4	18	-0.8 (-2.4 to 0.8)	0.362
		Right	13.2 (±6.2)	3.4	29.2	13.6 (±7.8)	5	39	-0.4 (-3.4 to 2.6)	0.794
5	Male	Left	43 (±11.8)	22.2	63.2	45 (±3.8)	41.2	49.4	-2 (-15.2 to 11.2)	0.738
		Right	27 (±7.2)	11.4	41.6	33.4 (±10.4)	16.4	65.2	-6.2 (-12 to -0.4)	0.033

#	Gender	Side	Without vacuum Mean (±SD)	Min	Max	With vacuum Mean (±SD)	Min	Max	Difference (95% CI)*	p
6	Male	Left	11.6 (±3.4)	4.8	16.8	11.4 (±4.8)	6	35.6	0.2 (-2.2 to 2.8)	0.854
		Right	9.6 (±2.6)	4.4	19	12.2 (±3.6)	5.4	18.2	-2.6 (-4.4 to -0.6)	0.010
7	Male	Left	10.2 (±1.4)	7.8	12.4	9.4 (±2.4)	5.8	16.2	0.6 (-0.6 to 1.8)	0.279
		Right	9.8 (±2.8)	6	14	9.8 (±2.2)	5	15.2	0 (-1.6 to 1.4)	0.922
8	Female	Left	14.8 (±5.8)	5	28.2	18 (±7)	8.4	47.4	-3.2 (-5.8 to -0.6)	0.020
		Right	14.8 (±6.2)	5	39	18.6 (±8.2)	8.8	60.6	-3.6 (-6.4 to -0.6)	0.013
9	Male	Left	12 (±3)	5	20.8	16.2 (±9.4)	5.8	46.2	-4 (-6.4 to -1.6)	0.001
		Right	7.2 (±2.4)	5	15.8	9 (±3.4)	4.2	19.6	-1.6 (-2.8 to -0.4)	0.015
Total		Left	14.4 (±11.8)			16 (±11.4)			-1.6 (-13.5 to 10.4)	0.781
		Right	12.8 (±6)			14.8 (±7.8)			-1.9 (-8.9 to 5.1)	0.566

*Negative value indicates reduced kidney motion with vacuum compression; positive value indicates increased kidney motion with vacuum compression.

Abdominal Motion with and without Vacuum Pressure

During ultrasound imaging of the left kidney, the abdominal motion measured for the group of participants without the vacuum compression averaged 6.1 mm compared to 4.7 mm when under the vacuum compression. This mean group difference of 1.37 mm however was not found to be statistically significant (p = 0.289). Similarly, when imaging the right kidney, the abdominal displacement without vacuum compression was 8.2 mm compared with 6.9 mm with the vacuum compression, which was again not found to be statically significant (p = 0.416). Looking at the effect of vacuum compression on individuals, the RPM device was able to detect reduction of abdominal motion ranging from 1 mm up to 3.7 mm. One outlier showed an increase in abdominal motion of 8.2 mm. A summary of the individual results can be seen in Table 14.

Table 14. Summary of abdominal surface displacement in the anterior posterior direction with and without the abdominal compression

Participant	Sex	Kidney	Abdominal displacement with compression (mm) Mean (±SD)	Abdominal displacement without compression (mm) Mean (±SD)	Mean Difference* (95% CI)	p-value
1	Female	Left	2.9(±0.37)	5.3(±0.2)	-2.4 (-2.7 to -2.1)	<0.001
		Right	2.6 (±0.8)	6.2(±1.2)	-3.5 (-3.9 to -3.2)	<0.001
2	Female	Left	Data not available		-	-
		Right	15.1(±1.6)	6.9(±1.9)	8.2 (7.3 to 9.1)	<0.001
3	Female	Left	3.4(±0.8)	6.9(±3.8)	-3.5 (-4.6 to -2.5)	<0.001
		Right	10.5(±1.7)	13.2(±1.5)	-2.7 (-3.5 to -1.9)	<0.001
4	Male	Left	3.1(±0.9)	4.1(±1.3)	-1 (-1.5 to -0.5)	<0.001
		Right	5.3(±2.1)	7.9(±2.7)	-2.7 (-3.8 to -1.6)	<0.001
5	Male	Left	3.7(±0.4)	3.6(±0.6)	0.1 (-0.2 to 0.5)	0.460
		Right	3.6(±0.6)	4.6(±0.8)	-1 (-1.6 to -0.5)	0.001
6	Male	Left	3.4(±0.8)	6.9(±3.8)	-3.5 (-4.6 to -2.5)	<0.001
		Right	3.6(±0.5)	6.8(±1.4)	-3.2 (-3.6 to -2.8)	<0.001
7	Male	Left	8.7(±0.4)	7.7(±1.1)	1 (0.6 to 1.4)	<0.001
		Right	8.2(±1.6)	9.2(±1.3)	-1 (-1.5 to -0.5)	<0.001
8	Female	Left	3.1(±0.9)	4.1(±1.3)	-1 (-1.5 to -0.5)	<0.001
		Right	5.5(±1.9)	7.9 (±2.7)	-2.5 (-3.6 to -1.4)	<0.001
9	Male	Left	9.5(±1.5)	10.2(±2.2)	-0.7 (-1.4 to 0.2)	0.115
		Right	7.6(±2.1)	11.3(±1.31)	-3.7 (-4.5 to -3)	<0.001
Total		Left	4.7 (±2.7)	6.1 (±2.3)	-1.4 (-4.1 to 1.3)	0.289
		Right	6.9 (±4.0)	8.2 (±2.7)	-1.3 (-4.7 to 2.1)	0.416

*Negative value indicates reduced abdominal motion with vacuum compression; positive value indicates increased abdominal motion with vacuum compression.

Relationship between Abdominal Motion and Kidney Motion

Observation of the dual vacuum effect on the left kidneys showed that in four of the eight participants a significant reduction in abdominal motion also showed a significant reduction in left kidney motion. For the remaining participants, three showed a significant reduction in abdominal motion but no significant reduction in kidney motion and one participant showed no change in abdominal motion and kidney motion. As to the effect of the vacuum compression on the right kidneys, out of nine participants, six showed a significant reduction in abdominal displacement as well as a significant reduction in kidney motion this was also observed for one participant had an increase in abdominal motion with a significant increase in kidney motion. In two participants a significant reduction in abdominal motion was not associated with a significant reduction in kidney motion. Despite these observations, Figure 11 shows that changes in abdominal displacement was not correlated with a change in left kidney motion ($r = 0.345$, $p = 0.402$) or for right kidney motion ($r = 0.527$, $p = 0.145$).
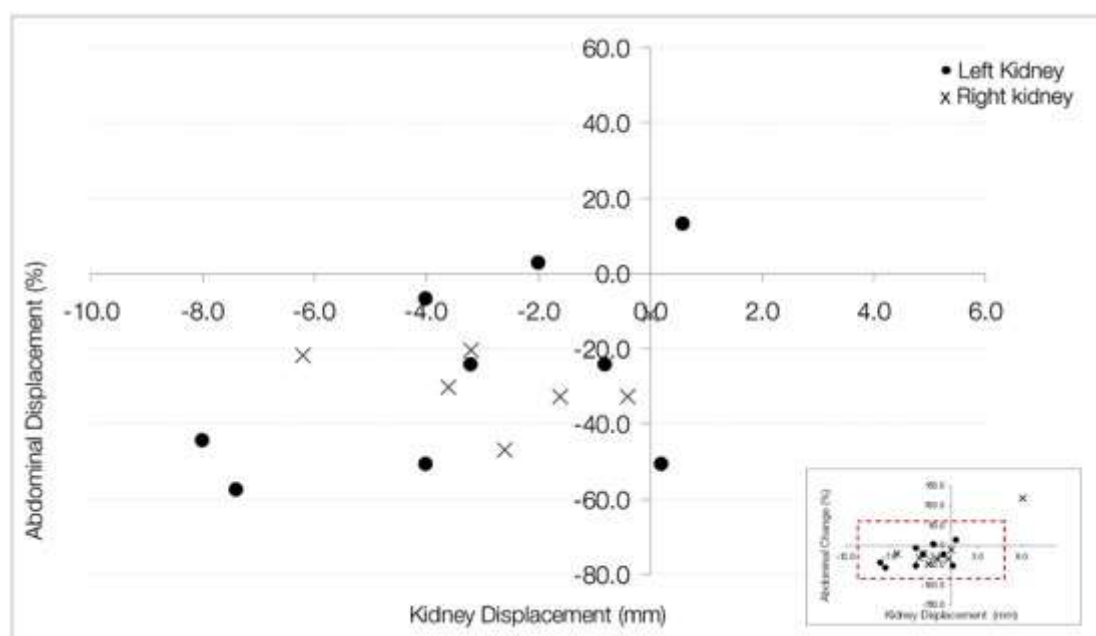
Figure 11. Relationship between kidney motion change and abdominal motion change.

A negative value indicates an increase and positive value an increase. An outlier (inset) is seen showing increase kidney motion associated with increased abdominal motion.

Relationship between Kidney Motion and Vacuum Compression

Figure 12 shows the relationship between vacuum pressure and kidney motion change. A significant correlation was observed ($r = 0.70$, $p = 0.002$) indicating that an increase in vacuum compression pressure can further decrease kidney motion.
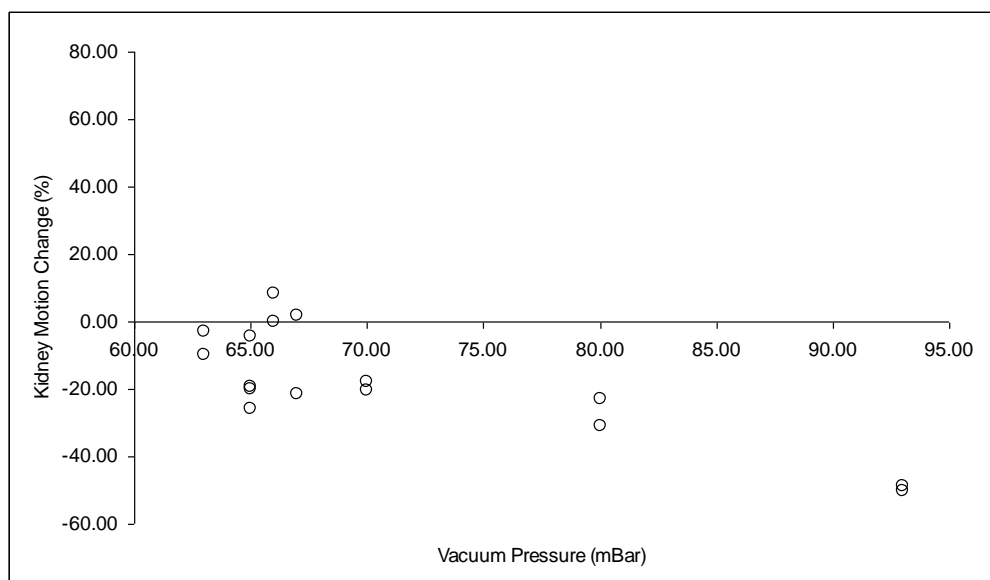
Figure 12. Relationship between vacuum pressure and kidney motion change.

A negative value indicates a reduction and positive indicates increase.

3.4 Discussion

In the context of primary kidney SABR, a small number of publications have described a variety of motion management techniques including the use of a stereotactic body frame (SBF) to reduce diaphragm motion[275,276] and 4DCT based planning for gated treatment[360]. In terms of the usefulness of abdominal compression strategies to reduce kidney motion, Heinzerling et al[212] demonstrated that using the SBF together with the compression plate on a high pressure setting can result in a mean kidney motion of less than 5 mm in the superior inferior direction. Other investigators have looked at prone positioning to minimise breathing motion, with little effect seen on the reduction of kidney motion[331,332].

In the present study we were able to demonstrate that a dual vacuum system was able to reduce kidney motion in a majority of healthy volunteers. Of the nine evaluable volunteers, six demonstrated mean kidney motion reduction of between 1.0 mm up to 8.0 mm, two showed no changes and one showed a mean increase in kidney motion of 8.2 mm. The effects of abdominal compression causing an increase in target motion have previously been demonstrated in the dual vacuum system as well as in the use of the abdominal compression plate. Han et al[329] showed that among 24 patients undergoing lung SABR treatment, one patient had a 27% increase in lung tumor motion when under dual vacuum compression with a mean pressure of 94 mbar (range 60 – 100 mbar). This has also been observed in the study by Siva et al[383] which showed that vacuum compression (ranging between 60 – 80 mbar) increase tumor motion (56%) in one (of 12) patient undergoing SABR treatment in the lung. Another study by Baba et al[377] showed with vacuum compression (pressure set at 80 mbar) in a series of 55 tumors (from 53 patients), two showed an increase in cranio-caudal motion of greater than 3 mm, 38 tumors showed no change and 15 showed greater than 3 mm of motion. In the study by Bouilhol et al[379] the use of a compression plate showed an increase in lung

tumor motion of up to 18% in five (of 27) individuals. These are important observations as the goal of abdominal compression equipment is to reduce the internal target volume margin.

A secondary part of our analysis was to use external surrogate measurements to predict kidney motion changes. The Varian RPM device has traditionally been used for 4DCT scanning and gated treatment[384] by monitoring abdominal wall displacement as a surrogate for breathing motion. In our study we have demonstrated that its placement on the abdomen can be used to detect millimeter changes associated with vacuum compression. This has two potential benefits, the first being a reassurance during the simulation process that the abdominal compression device is dampening breathing motion rather than increasing motion. The second benefit is to set the compression device for each patient to a level that will result in a specific abdominal motion change. In this study we found no statistical significance in the correlation between the change in abdomen displacement and reduction of left and right kidney motion. We believe that this may be a limitation based on the small number of participants involved in this study; our previous investigation of the correlation between abdominal displacement and kidney motion[350] demonstrated a stronger correlation existing between right kidney and abdominal wall (r = 0.36, p = 0.004) compared to a weaker correlation between left kidney and abdominal wall (r = 0.24, p = 0.056). Nevertheless, a mean reduction of over 5 mm in the kidneys was observed when the vacuum compression was used to reduce the abdomen displacement from 22 % to 48 % of its original range.

In SABR planning, PTV expansion is generally in the order of 5 mm and so an ITV reduction of this amount can provide dosimetric advantages. This has been shown in the liver SABR setting by Molinelli et al[381] who demonstrated that a 5 mm reduction in the superior-inferior direction of the PTV can result in a 20% reduction in healthy liver dose as well as facilitate dose escalation. Another means of targeting specific kidney reduction is to categorize abdominal pressure into moderate or high-pressure compression. The dual vacuum device pressure settings range from 0 (no pressure applied) up to 100 mbar. In our department there is no protocol for pre-determined pressure settings as the final pressure applied will depend on the level tolerated by individual patients. A motion management protocol that is able to differentiate a high or moderate pressure on the patient in order to reduce target motion by a clinically significant amount can be useful as patient comfort and setup time can be improved with less pressure applied. While we were able to observe a correlation between a larger pressure setting and a larger reduction in kidney motion, any effect of pressure levels on individual patients is beyond the scope of this study. This moderated pressure effect has been investigated by Heinzerling et al[212] who used an abdominal compression plate with two pressure settings: moderate and high compression to reduce mean motion of lung and liver tumors by 37.2 % and 49.2 %, respectively, compared to no compression. The effect on left kidney motion, however, was not shown to be statistically significant compared to free breathing and showed a greater reduction of 32.8 % at the moderate setting compared to only 16.4 % at a high compression.

There were a number of limitations in this study including the use of healthy volunteers to investigate kidney motion. The effect of large tumors in the kidney and any fixation to abdominal structures is not yet known. Similarly, the use of ultrasound imaging to record kidney motion can be subjected to operator bias

as baseline shifts will occur if the transducer probe is moved. The customized software used in this study was able to calculate the kidney amplitude displacement, taking into account a moving baseline; we have assumed that this shifting baseline is due to the operator rather any baseline shifting occurring physiologically.

This study has shown that dual vacuum compression can provide variable benefit towards kidney motion reduction. Despite observing no effect as well as an increased effect on kidney motion, we have previously demonstrated that dual vacuum immobilization can reduce patient intrafraction motion to be less than 2mm (p = <0.001)[226] which is important in stereotactic treatment that utilize small margins and treatment appointments that can last up to 1 hour. If the purpose of the compression device was to reduce target volume motion, we recommend that the use of abdominal compression devices be carefully assessed on patients, with consideration as to what kind of effect will occur when pressure is applied to the abdomen. Our clinical practice is to use vacuum compression for the purpose of stabilization in thoracic and abdominal based stereotactic treatment. Based on this study, close observation and verbal communication with patients when determining the optimal pressure setting is advised. The same pressure setting used for planning CT and each treatment should be maintained.

Further studies focusing on the design and use of abdominal compression devices at various degrees of compression can become informative in using dual vacuum devices to reduce target motion by a clinically specific amount or simply as an immobilization device to limit intrafraction body movement not related to breathing.

3.5 Conclusion

We were able to demonstrate a reduction in kidney motion using dual vacuum technology in the majority of participants however the cumulative data does not show a kidney motion reduction effect when using vacuum compression. As a means to reduce target motion the effect of dual vacuum compression can vary per individual. This is important as certain patients may demonstrate increased respiratory induced motion under vacuum compression, which can preclude the use of compression devices as this will increase internal target volume margins. Abdominal surface markers can be used to assess changes caused by the vacuum compression device, however in this study abdominal surface motion was not demonstrated as an adequate surrogate for kidney motion and should be further investigated before routine clinical implementation into the stereotactic kidney radiotherapy workflow.

Chapter 4

Stereotactic Ablative Body Radiotherapy for Primary Kidney Cancer: A 3-Dimensional Conformal Technique Associated with Low Rates of Early Toxicity

Daniel Pham[1,2], Ann Thompson[1], Tomas Kron[3,5], Farshad Foroudi [4,5], Michal Schneider Kolsky[2], Thomas Devereux[1], Andrew Lim[1] and Shankar Siva[4,5]

[1]Department of Radiotherapy Services, Peter MacCallum Cancer Centre, Melbourne, Victoria, Australia.

[2]Department of Medical Imaging and Radiation Sciences, Monash University, Melbourne, Victoria, Australia.

[3]Department of Physical Sciences, Peter MacCallum Cancer Centre, Melbourne, Victoria, Australia.

[4]Departmnet of Radiation Oncology and Cancer Imaging, Peter MacCallum Cancer Centre, Melbourne, Victoria, Australia.

[5]Sir Peter MacCallum Department of Oncology, Melbourne University, Melbourne, Victoria, Australia.

The radiotherapy planning process is used to design a beam arrangement that generates high dose conformality to the planning volume while avoiding significant dose to surrounding critical structures. This next chapter describes the most common beam geometry used to target left and right kidney cancers. The R50 plan quality metric, which describes intermediate-dose conformality, is investigated for any relationship with target volume size. The acute toxicity outcome for the first 20 patients treated on a linac based SABR protocol will also be presented. This chapter is a copy of the manuscript that was accepted for publication[316]. The only modifications made have been to the figures and tables that are embedded within the text and the references which have been moved to the end of the thesis.

Abstract

Purpose/Objective Stereotactic body radiation therapy (SBRT) is a novel treatment approach for the management of primary renal cell carcinoma (RCC). We describe our 3D-conformal planning approaches and report early toxicities with this technique.

Methods/Materials This is an analysis of a phase I trial of SBRT for primary inoperable RCC. A dose of 42Gy/3fx was prescribed to targets ≥5cm, whereas for <5cm 26Gy/1fx was used. All patients underwent a planning 4DCT to generate a planning target volume (PTV) from a 5mm isotropic expansion of the internal target volume. Planning required a minimum of 8 fields prescribing to the minimum isodose surrounding the PTV. Intermediate dose spillage at 50% of the prescription dose (R50%) was measured to describe the dose gradient. Early toxicity (<6 months) was scored using the Common Terminology Criteria for Adverse Events (v4.0).

Results From July 2012 - August 2013 a total of 20 patients (median age 77 years) were recruited into a prospective clinical trial. Eleven patients underwent fractionated treatment and nine patients a single fraction. For PTV targets <100cc the median number of beams used was eight (2 non-coplanar) to achieve an average R50% of 3.7. For PTV targets >100c the median beam numbers used was 10 (4 non-coplanar) for an average R50% value of 4.3. The R50% was inversely proportional to decreasing PTV volume (r= -0.62, p= 0.003) and increasing total beams used (r = -0.51, p = 0.022). Twelve of 20 patients (60%) suffered ≤grade 2 early toxicity, whilst 8/20 (40%) patients were asymptomatic. Nausea, chest wall pain and fatigue were the most common toxicities reported.

Conclusion A 3D-conformal planning technique of 8-10 beams can be used to deliver a highly tolerable stereotactic ablation to primary kidney targets with minimal early toxicities. Ongoing follow-up is currently in place to assess long-term toxicities and cancer control.

4.1 Introduction

The gold standard for the management of primary renal cell carcinoma (RCC) has been total nephrectomy, or, in suitable cases partial nephrectomy. The use of external beam radiation therapy has been limited by the perceived radioresistance of RCC to conventionally fractionated radiation therapy. Within the last decade developments in stereotactic body radiation therapy (SBRT) have allowed for precise delivery of very high dose per fraction treatments. In the context of RCC, SBRT can provide two- year local control ranging from 84%-100%[324]. This can be achieved using linear accelerator-based SBRT treatments with additional tools such as direct soft tissue pretreatment imaging, immobilization and motion management (4D CT or compression devices). For a robust stereotactic program these are minimum requirements that have been stipulated by a number of consensus guidelines[160,226,385]. Whilst stereotactic dosimetric benchmarks have been published[386], this guide was developed for lung targets which may not be directly applicable due to small lesion sizes and targets being typically located a distance away from serially arranged organs at risk (such as spinal canal, small bowel). As such it is important to investigate and review stereotactic planning dosimetry criteria for larger targets in the abdominal body site.

In this paper we present our initial planning experience of patients recruited into a phase 1 study of SBRT for primary RCC. This is an interim analysis of the study based on the recruitment made within the first year of the trial opening. Our aim was to analyse the characteristics of 3D-conformal planning approach for the first 20 patients with emphasis on relationship between size of target volume, beam numbers used and intermediate dose indices. The dose to organs at risk will also be reported as well as the early toxicity observed among the patients during follow up.

4.2 Methodology

Patient Recruitment

Patients enrolled into an ethics approved pilot study for primary RCC (FASTRACK ClinicalTrials.gov ID NCT01676428) were included in this study. This is a phase 1 study investigating the feasibility and safety of treatment of primary renal cell carcinoma using SBRT on a conventional linear accelerator. For gross tumour volumes (GTV) of 5cm or greater in maximal diameter a dose of 42Gy was prescribed in three fractions. For a GTV of less than 5cm in maximal diameter a radiosurgery dose of 26Gy in one fraction was prescribed. All patients underwent a 4D CT scan on a Brilliance 16 slice CT scanner (Philips Medical System, Netherlands) using the Philips bellows to reconstruct the data into 3mm slices that was were binned into 10 phases of breathing. Patients were placed supine in a dual vacuum stabilisation system (BodyFIX™; Elekta Medical Intelligence, Stockholm, Sweden.). An average pressure of 72 mbar (50 – 100) was used to immobilize patients using both the thoracic and pelvic setup. The averaged CT dataset was reconstructed into a 3mm slice dataset that was imported into Eclipse (v11.03) (Varian Medical System, Palo Alto, USA) for contouring and dose calculation. The maximum inspiration and expiration, and maximum intensity projection datasets were used to define the internal target volume (ITV) with a 5mm isotropic planning

target volume (PTV) margin applied to the ITV. All patients were planned on an Eclipse v11.03 workstation using the analytical anisotropic algorithm (AAA; v 11.03) for the final dose calculation.

Planning Objectives

A minimum number of eight fields was part of the planning guidelines using a mixture of 6 and 18MV beams. For each field, the multi-leaf collimators (Millenium 120 MLC; Varian Palo Alto) were assigned to close outside of the PTV with 0 - 1mm margin to achieve rapid dose fall-off by prescribing to a lower isodose line (generally between 75 – 85%). The planning objective was for 99% of the PTV to receive the full prescription dose.

Treatment Time

The treatment time was taken from MOSAIQ™ record and verification system (Sunnyvale, CA) and was based on the time taken to deliver all fields as well as to perform pre, mid and post treatment CBCT imaging. The setup time was not included. All beams were delivered with a dose rate of 600MU/min on a Varian Trilogy Linear accelerator.

Conformity Indices Calculation

PTV conformity index (R100%) and intermediate dose spillage (R50%) was calculated by converting isodose values into contours to generate dose cloud volumes using the treatment planning system inbuilt functions. The dose clouds used in this study were measured twice for each patient using two different dose calculation algorithms; the AAA (Type B algorithm) as well as the pencil beam convolution algorithm (PBC; v11.03; Type A algorithm). Compared to the PBC algorithm, the AAA has a superior ability to model lateral electron scatter and it was of interest to investigate any differences in intermediate dose volume. To evaluate the conformity of the prescription dose to the target, an R100% value was calculated by deriving the ratio of the volume of the prescription dose relative to the PTV volume. This was repeated to evaluate the spillage of the intermediate dose (R50%) by measuring the volume of the 50% isodose line relative to the PTV volume. The R100% and R50% value were calculated using the RTOG definition [160]

$$R100\% = (\text{volume of 100\% prescription dose})/(\text{PTV Volume})$$

$$R50\% = (\text{volume of 50\% prescription dose})/(\text{PTV Volume})$$

Toxicity assessment

The toxicity assessment data from patient clinic reviews at one month, three months and six months post treatment were used to assess early treatment side effects. The assessment template used was the Terminology Criteria for Adverse Events v4.0 (CTCAE) and the greatest early toxicity change from baseline assessment was used to indicate any treatment related side effects.

4.3 Results

From July 2012 to August 2013 a total of 20 patients with primary RCC were enrolled into the FASTRACK study. No patients were excluded due to target proximity to small bowel/ renal pelvis or collecting system. The characteristics of this group of patients are described in Table 15.

Table 15. Patient Characteristics (Total N = 20)

Characteristic	Value
Age	
Median (range)	77 years (41 – 91)
Site	
Left Kidney	10
Right Kidney	10
Sex	
Male	15
Female	5
Dose Prescription	
42Gy in 3 fractions	9
26Gy in 1 fraction	11
PTV Length (Volume cm^3)	
3 – 5 cm (22.7 – 52.1)	5
5 – 7 cm (62.3 – 116.7)	7
7.1 – 9 cm (164.2 – 222.5)	8

All patients received treatment planned as per the intention to treat, with Table 16 showing a summary of the planned target and volume constraints as well as the achieved median (range) of dose to the target volumes and organs at risk.

Table 16. Dose constraints used for planning in both single and fractionated prescription and the resultant dosimetry for all patients (N = 20)

	26Gy in 1Fx		42Gy in 3Fx	
Organ	**Planned Limit**	**Achieved Median (Range) (Gy)**	**Planned Limit**	**Achieved Median (range) Gy**
PTV	D99 = 26Gy	27.5 (26 – 28.1)	D99 = 42Gy	41. (32 – 45.4)
	Min	30.1 (28 – 34.8)	Min	42.8 (32.3 – 50.6)
ITV	Max	34.1 (33 – 38.8)	Max	56.6 (50.6 – 60.7)
Spinal Canal	12 Gy point dose*	8.1 (3.9 – 9.3)	18Gy point dose	16.3 (7.9 – 17.8)
Skin (5mm subcutaneous)	18Gy (max dose)	11.4 (9.5 – 13)	24Gy	23.5 (18.2 – 27.1)
Small bowel	30cc < 12.5Gy	11.2 (7.9 – 17.8)	D0.035cc < 30Gy	25.3 (14.4 – 29.9)
	30cc ≤12.5Gy	6.5 (0.4 – 9.3)	No constraint, report D30cc	14.3 (8.9 – 17.9)
Stomach	-	0.5 (0.1 – 9.0)	<30Gy	10.4 (0.6 – 21.0)
Liver	700cc ≤ 15Gy	0.1 (0 – 0.3)	700cc ≤ 15Gy	0.6 (0.4 – 13.66)
Large bowel (No constraint, for reporting only)	10cc	9.6 (1.1 – 13.1)	10cc	21.5 (11.6 – 38.7)
	1cc	12.6 (8.4 – 18.6)	1cc	27.5 (13 – 45.3)
	0.035cc	13.9 (8.8 – 24.6)	0.035cc	31.6 (13.2 – 50.9)
	Dose to Specific Volume	**Median Dose (Gy) (Range; No. of Patients)**	**Dose to Specific Volume**	**Median Dose (Gy) (Range; No. of Patients)**
	D10cc > 12.5Gy	13.1 (n = 1)	D10cc > 30Gy	38.7 (n = 1)

Specific dose to large bowel exceeding 30Gy (in 3fx) or 12.5Gy (in 1 fx)	D1cc > 12.5Gy	14.4 (12.6 – 18.6; n = 6)	D1cc > 30Gy	38.9 (33 – 45.3; n = 3)
	D0.035cc>12.5Gy	16.5 (13.1 – 24.6; n = 7)	D0.035cc> 30Gy	32.7 (31.5 – 50.9; n = 7)

*Point dose as reported by Eclipse TPS which is the dose to 10^{-6} cubic centimetres.

All patients were able to complete planning and treatment with no deviations from the protocol mandated prescription dose. For the entire group the median beam number employed was nine (range 6 – 13). A summary of the typical coplanar and non-coplanar beam angles used for left and right sided kidney targets are shown in Figure 13.
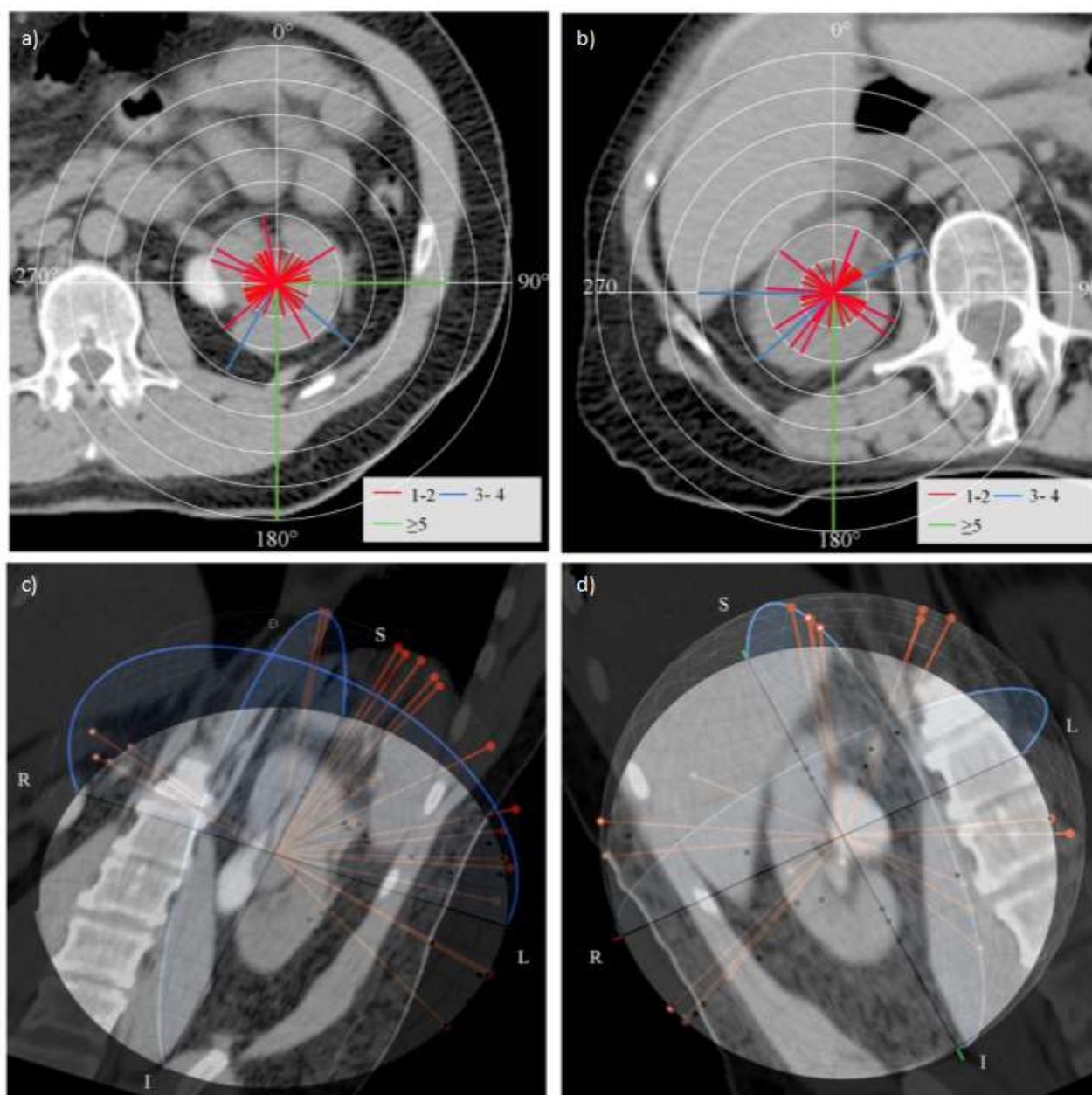
Figure 13. Typical beam arrangements used for 3DCRT planning.

Panels a) and b) shows a circular histogram distribution of frequency of coplanar beam angles used. With bowel located anteriorly, posterior and contralateral oblique fields are commonly used to avoid these critical structures. Panels c) and d) shows a 3D 'stereonet' distribution of the non-coplanar beam angles used. The distribution for left kidney targets shows a favouring of superior/ipsilateral oblique fields to avoid more medially located bowel. For right kidney targets inferiorly located non coplanar angles are commonly used to avoid healthy liver and bowel.

The median PTV volume for single fraction targets was 52.5cc with a median of six (range 8 – 9) coplanar and two (range 0-3) non coplanar angles used. For multi-fraction targets the median PTV volume was 171.9cc with a median of six (range 8 -13) coplanar and four (range 2 - 9) non coplanar angles used. As the PTV volume increases a significant trend to increase the total number of beams was observed (r = 0.61, p

= 0.004). This increase is largely driven by the extra number of non-coplanar fields required (r = 0.48, p = 0.03).

Treatment Time

All patients successfully completed treatment. The median time to image and deliver all fields was 44min (interquartile range 42min to 52min 30sec) for fractionated treatment and 48min (interquartile range 41min to 51min 30sec) for single fraction treatment. Of this time the median time spent on the image guidance component (assessment of breathing motion and target localisation) was 24min and 30secs (interquartile range 22 to 28 minutes).

Conformity Indices

The mean conformity of the prescribed dose (R100%) to the PTV was 1.22 (range 0.98 – 1.35) and 1.25 (range 1.1 – 1.38) calculated using the PBC and the AAA algorithm respectively. There was no statistically significant difference between the values calculated (p = 0.231).

Target volume size, number of beams used and the R50% volume showed significant association during the planning. Figure 14 shows that as the number of beams increase, the volume of the intermediate dose trends towards reduction (r = - 0.51, p = 0.022).
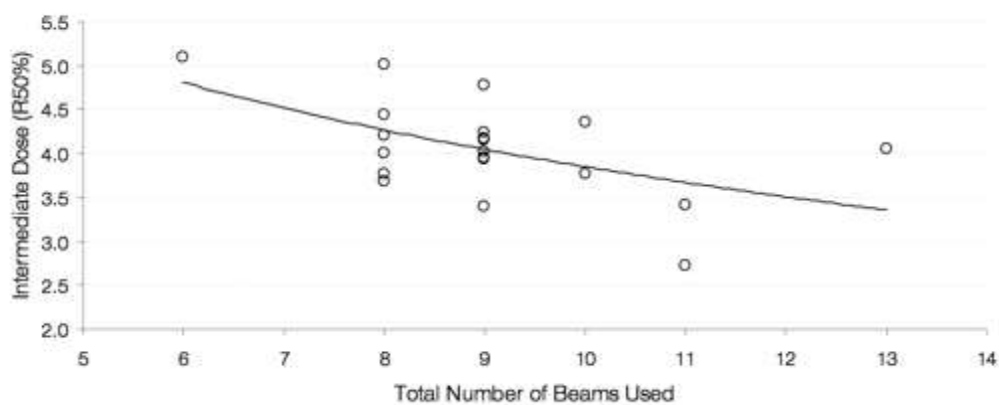
Figure 14. Relationship between the total number of beams used and ratio of the intermediate dose (R50%).

A significant correlation existed: r = - 0.51, p = 0.022 showing that a larger number of non-opposing fields will maximise dose fall-off beyond the PTV target.

Figure 15 shows the intermediate dose spillage achieved for the 20 patients using both AAA and PBC calculations.
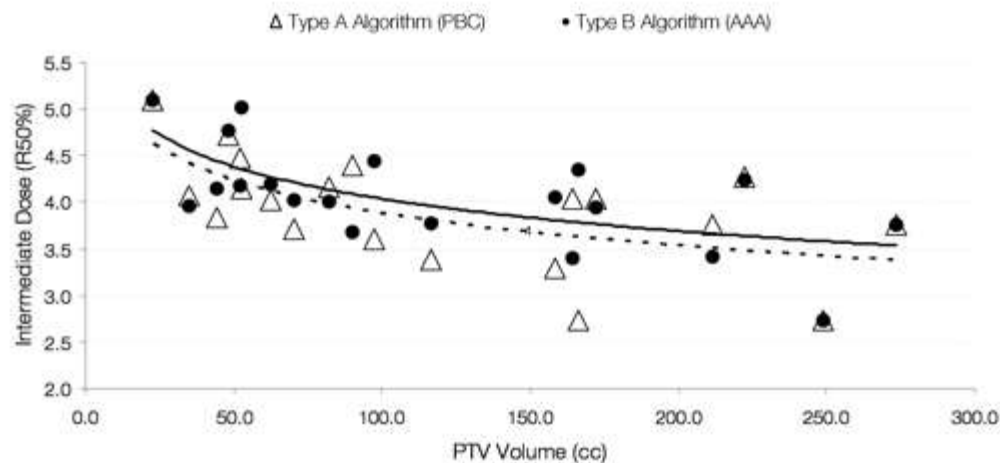
Figure 15. Relationship between the size of the intermediate dose (R50%) relative to size of PTV volume.

The R50% values for the first 20 FASTRACK patients have been calculated using an Analytical Anisotropic Algorithm (Type B) and a Pencil Beam Convolution (Type A) algorithm. A significant trend was observed for the size of the R50% value and for a Type B algorithm (r= -0.62, p = 0.003) as well for a Type A algorithm (r = -0.54, p = 0.014).

There was a significant trend for the R50% value to decrease with increasing PTV size (AAA: r = -0.62, p = 0.003; PBC: r = -0.54, p = 0.014). The mean R50% value calculated by AAA was 4.04 compared to 3.99 by PBC showing no significant difference (p = 0.24). In order to summarise our data a comparison of the R50% value between fractionated (large targets, >100cc) and single fractions plans (small targets < 100cc) was made. For targets over 100cc in size the mean R50% value was 3.7 (±0.5), whereas for targets <100cc it was 4.3 (±0.4). These values were found to be significantly different (p = 0.03)

Early Toxicity

Within the six-month assessment period, 12 of 20 patients (60%) reported treatment side effects of Grade 1-2 intensity. The remaining patients did not report any treatment related problems. In the single fraction group, fatigue (in 7 of 11 patients, 73%) was the most commonly symptom reported, after which dermatitis, chest wall pain and nausea followed. In the multi-fraction group, fatigue and chest wall pain were most commonly reported (in 5 of 9 patients, 56%). No grade 3 or 4 toxicities were reported during the follow up period. A breakdown of the reported toxicities is summarised on Table 17.

Table 17. Toxicity grade within six months of treatment completion for fractionated and single fraction prescriptions (Total N = 20).

Total Prescribed Dose of 26Gy in 1 fraction

Pt	Dyspnoea	Nausea	Diarrhoea	Gastritis	Chest Wall Pain		Fatigue	Dermatitis	Hematuria	Asymptomatic
1										1
2	1	2					2	2		
3					1		1			
4		1	1				1	1		
5								1		
6							1			
7										1
8					1					
9		2			1		1			
10										1
11										1
Total pt No.	1	3	1	-	3		5	4	-	4

Total Prescribed Dose of 42Gy in 3 fractions

	Dyspnoea	Nausea	Diarrhoea	Gastritis	Chest Wall Pain		Fatigue	Dermatitis	Hematuria	Asymptomatic
12					1		2			
13							1			
14					1					
15		1		2	1		2	2		
16										1
17										1
18		1			1		1			
19										1
20										1
Total Pt. No.	-	2	-	1	4		4	1	-	4

In total, 12/20 patients suffered toxicity from treatment

At baseline assessment, four patients were identified with hematuria ranging between Grade 1 up to Grade 3. At six months post treatment, the patient with Grade 3 baseline hematuria reported Grade 1 hematuria, the two patients with Grade 1 hematuria showed bleeding resolution and the patient with Grade 2 hematuria showed no change in symptoms. No patient had changes in anti-hypertensive drugs or developed hypertension at the time of reporting.

4.4 Discussion

An analysis of novel treatment techniques is an important component for a comprehensive quality assurance program. As part of our stereotactic service, we reviewed the planning technique for the first 20 patients recruited into this trial. The first objective in the review was to analyse intermediate dose fall-off. Several publications have examined optimal beam arrangements to achieve rapid dose fall off[387-389] which is a feature that differentiates SBRT planning from the conventional fractionated treatment techniques. While our group of patients is inadequately powered to create class solutions as had been done for other clinical sites[390] we felt that it was important to evaluate the technique for any trends and to develop planning guides. SBRT protocols tend to describe the minimum number of beams to be used; however, there is little evidence to suggest the optimal number of beams and the possible benefits when using more beams. In our study we found that with larger volumes more beams were used to achieve rapid dose fall-off. This is an important parameter in SBRT treatment for lung normal tissue as low dose can contribute to pulmonary dysfunction[391]. For stereotactic treatment in the liver this is also an important parameter as reduction of the dose to the liver will reduce the risk of radiation-induced liver disease[392,393]. For treatment of renal cancer, the consequences of rapid or slow intermediate dose fall have yet to be reported. Plan assessment goals such as intermediate dose spillage therefore can be used to produce high quality treatment plans. One of the earlier co-operative clinical trials that imposed planning requirements was the North American Radiation Therapy Oncology Group RTOG 0236 trial for medically inoperable non-small cell lung cancer. As part of planning quality index, intermediate and high dose conformity indices were used to evaluate dose fall off[386]. A table with expected range of conformity indices against PTV volumes was used. However, there were limitations with these guidelines as treatment plans were submitted with no inhomogeneity corrections. These older guidelines need to be implemented with caution as modern day planning systems will have heterogeneity corrections in place for more accurate dose calculations. Recalculation of the dosimetry with heterogeneity correction in place can show a larger expected value in the R50% conformity index as reported by Xiao et al[394] who reassessed the dosimetry on a select group of participants from the RTOG 0236 trial. These expected conformity indices can again be quite different as shown by the quality assurance working party report behind the European co-operative Phase III stereotactic lung trial for operable lung cancer patients. In this report Hurkman et al[395] showed that under heterogenous conditions, the plan optimisation process can lead to even larger expected intermediate dose spillage The contribution of scatter modelling was highlighted by Hurkman whom was able to show that with smaller target volumes the volume of intermediate dose spill can deviate as much as 30% between treatment planning system algorithms. Our comparison between a Type A and Type B (superior electron

scatter modelling) algorithm did not show a significant difference in the 50% dose conformity index which will be due to the relatively homogeneous tissue in the abdomen. Despite this our range of values is still comparatively larger than the reported values from the RTOG 0236 trial which assumes tissue unit density. This could be explained by several factors including:

1) Location of the target area. Surrounded by serial organs such as the bowel, stomach and spinal cord, there is a need to distribute the intermediate/high dose away from these structures thus leading to a reduced ability to maintain a wide hinge angle between fields

2) Our dose prescription requirements of 99% of the volume to receive at least 100% of the dose. Optimisation to achieve this level of coverage in heterogenous conditions will require more dose input in the target area.

From this study we would recommend for kidney PTV less than 100cc the use of 6 coplanar and 2 non co-planar angles to achieve 50% conformity index of less than 5. For PTV over 100cc, 6 coplanar and 4 non co-planar angles can achieve 50% of less than 4.

In future SBRT clinical trials, benchmarking standards such as conformity indices can be set in place to ensure plans of comparable dosimetry. Both abdominal and lung targets will require different standards due to the nature of the treatment region. Primary RCC poses specific planning challenges which mean that suggested lung conformity guidelines cannot be directly extrapolated. Several factors will contribute to this difference including the lower lung density treatment region which will lend to larger conformity indices per unit volume compared to abdominal targets where there is more dense tissue and hence less scatter distance. Target volume size, target clinical site, and planning system used are parameters that will influence the expected R50% value.

Improvement of our kidney SBRT program is an ongoing process as we await long term toxicity data. Our findings of early toxicity within the first six months are not dissimilar to findings in the literature. Beitler et al[275] observed three of nine patients with some form of early toxicity (nausea, vomiting) relating to SBRT treatment of the kidneys. Wersall et al[276] reported that 23/58 (39%) patients reported a treatment related side effect. This study, however, was not limited to primary kidney targets but also to metastatic sites in abdominal and thoracic organs. The most common side effects observed were nausea, pain and coughing. Nomiya et al[280] reported on the use of carbon ion technology for irradiation of primary kidney targets for 10 patients. Apart from a single incidence of late grade 4 skin toxicity, they authors did not observe any early toxicity > Grade 2 based on their technique. Svedman et al[279] also reported minor Grade 1- 2 toxicity of transient nausea, fatigue and local pain in four of seven (57%) patients.

The largest planning challenge we have found is from the presence of highly mobile bowel (small and large). Our protocol has pre-defined limits on dose to small bowel. However, at present have no specific constraint for large bowel, as there is limited robust evidence to suggest a dose constraint for ascending and descending colon. Expert consensus guidelines have previously defined similar constraints to that of small bowel, with a three fraction dose constraint in the order of 30Gy[160,396,397]. From this study we have reported

the irradiated dose to large bowel at various volumes which have used dose levels modelled after small bowel constraints (Table 16). Our technique has in general taken a conservative stance to unnecessarily irradiating the large bowel, however, in some scenarios, this has not always been possible. While our data suggests that there may be greater tolerance of the large bowel to radiation dose compared to small bowel, this is still an area that warrants further investigation.

4.5 Conclusion

Our analysis of planning approaches of 20 SBRT kidney treatments using a 3D conformal treatment, has shown that 8-10 planar and non-coplanar fields will provide intermediate dose spillage unique from that of the lung setting. Our values have shown no toxicity for seven patients, and in the remaining minimal toxicity no greater than Grade 2 within the first 6 months after treatment. Ongoing follow up is necessary to assess long term toxicities within this group of patients.

Chapter 5

Image guidance and stabilization for stereotactic ablative body radiotherapy (SABR) treatment of primary kidney cancer

Daniel Pham [1,2], Tomas Kron[3,4], Mathias Bressel[5], Farshad Foroudi[4,6], Nicholas Hardcastle[3], Michal Schneider[2], Sally Soteriou[1], Jayson Innes[1] and Shankar Siva[4,7]

[1]Department of Radiation Therapy Services, Peter MacCallum Cancer Centre, Melbourne, Australia.

[2]Department of Medical Imaging and Radiation Sciences, Monash University, Melbourne, Australia.

[3]Department of Physical Sciences, Peter MacCallum Cancer Centre, Melbourne, Australia

[4]Sir Peter MacCallum Department of Oncology, University of Melbourne, Melbourne, Australia

[5] Department of Biostatistics and Clinical Trials, Peter MacCallum Cancer Centre, Melbourne, Australia.

[6] Department of Radiation Oncology, Olivia Newton-John Cancer Centre/Austin Health, Melbourne, Australia

[7] Division of Radiation Oncology and Cancer Imaging, Peter MacCallum Cancer Centre, Melbourne, Australia.

As the planning process uses small planning margins, steep dose gradients and extremely heterogeneous dose distributions, the room for error on treatment is very small. Direct visualisation of the target and verification of the planning margins is therefore critical to the success of SABR treatment. This final chapter shows the use of CBCT imaging to verify inter and intrafraction variation of the target and as well, the ability to verify planning ITV margins on treatment. This chapter is a copy of the manuscript that was accepted for publication[373]. The only modifications made have been to the figures and tables that are embedded within the text and the references which have been moved to the end of the thesis.

Abstract

Purpose: Stereotactic ablative body radiotherapy for primary kidney cancer treatment relies on motion management that can quantify both the trajectory of kidney motion and stabilize the patient. A prospective ethics-approved clinical trial of stereotactic treatment to primary kidney targets was conducted at our institution. Our aim was to report on specific kidney tumour motion and the inter/intra fraction motion as seen on treatment.

Methods and Materials: Patients with tumor size less than 5cm received a dose of 26Gy in one fraction and those with tumor size greater or equal to 5cm received 42Gy in three fractions. All patients underwent a 4DCT planning scan, immobilized in a dual vacuum system. A conventional linear accelerator cone beam CT was used for pre, mid and post treatment imaging to verify target position.

Results: From July 2012 to October 2014 a total of 33 targets from 32 consecutive patients (24 males/8 females) were treated. Seventeen targets were prescribed 26Gy/1fx and the remaining 16 targets received 42Gy/3fx. Kidney motion at each of the poles was not affected by the presence of tumour (p = 0.875) nor was the motion statistically different from the corresponding contralateral kidney pole (p=0.909). The mean 3D displacement of the target at mid and post treatment was 1.3mm (SD± 1.6) and 1.0mm (SD±1.3) respectively. The maximum displacement in any direction for 95% of the fractions at mid and post treatment was 3mm or less.

Conclusion: In summary, stereotactic ablative body radiotherapy of primary kidney targets can be accurately delivered on a conventional linear accelerator with protocol that has minimal intra-fractional target motion.

5.1 Introduction

A difficulty in the delivery of stereotactic ablative body radiotherapy (SABR) for primary kidney targets is respiration associated organ motion. Kidney motion in the superior inferior direction can vary from less than 5 mm up to 70 mm depending on shallow or deep breathing conditions[318] . Even free breathing situations can be associated with a wide range of motion anywhere between 4.5 mm to 13 mm[318]. Published kidney treatments in the SABR setting have reported the use of 3D CT planning with population based PTV expansions to account for motion[275,276,280] or the measurement of fiducial markers to verify motion and position[278]. In these studies, tumor local control has been reported to be up to 100% at 2 years. With availability of modern, motion management equipment, new areas are under investigation (i.e. breath hold)[299]. The use of 4D CT for Internal Target Volume (ITV) margin generation relies on the replication of patients' breathing range at each session. The verification of breathing motion can be achieved through fluoroscopic imaging, 4D CBCT or dynamic MRI[202,398,399].

In this study we investigated protocol feasibility for the delivery of stereotactic radiotherapy to primary kidney cancers on a conventional linear accelerator equipped with 3D volumetric imaging. Our aim was to develop a process that can inform future image guidance protocols in this stereotactic setting. For this study, our primary objectives were to 1) describe kidney motion and determine any relationship with affected and unaffected kidneys 2) assess inter- and intrafraction kidney motion at treatment using a dual vacuum immobilisation system for daily treatment and 3) to investigate tools to assess on-line the variation of breathing changes on a per fraction basis. Furthermore, as a secondary objective, we wanted to investigate any relationship between kidney motion and diaphragm motion in order to inform gating protocols.

5.2 Method

Patients recruited into an ethics approved single centre prospective observational study of patients with primary kidney renal cell carcinoma treated with extra cranial stereotactic treatment were selected for analysis. Patients were eligible if deemed inoperable or declining surgical treatment. Tumors greater or equal to 5cm in maximum diameter were prescribed a dose of 42 Gy in 3 Fractions (14 Gy per fraction) and tumors less than 5 cm, 26 Gy in 1 fraction. The prescription chosen are based on biological dose modelling that indicate RCC may be inherently radioresistant to conventional dose fractionations. Using the linear quadratic model[400] radiosensitivity of RCC have been observed in laboratory to vary with α/β values estimated to be 2.6 Gy or 6.9 Gy depending on the cell lines[401]. The biologically equivalent doses (BED) in 2 Gy fractions for $\alpha/\beta = 6.9$ Gy is 123 Gy and 127 Gy for the prescription of 26 G/1 fx and 42 Gy /3 fxs respectively. For the higher $\alpha/\beta = 2.6$ Gy, the BED in 2 Gy fractions is 286 Gy and 268 Gy for the prescriptions 26 G/1 fx and 42 Gy /3 fx respectively. Patients were required to provide informed consent for study treatment.

Simulation/Planning

Patients were positioned supine with their arms above their head and a dual vacuum immobilization system (BodyFIX, Elekta Stockholm, Sweden) was used to minimise kidney motion and stabilize the patient. We have previously demonstrated that there is a potential to minimise kidney motion in the majority of patients [364] using this vacuum immobilization. This technique uses a plastic drape that is fitted over the patient's body. A vacuum pump is used to evacuate the air underneath to create a seal immobilizing the patient. The pressure can be raised to a threshold that can cause reduction to the depth of breathing. Each patient underwent a helical 4D time-resolved CT scan (Brilliance Big Bore, Philips, Cleveland, USA) with CT datasets retrospectively binned into 10 breathing phases. All scans were performed in free breathing with no specific instructions for breathing.

We have previously described our treatment planning process[316]. In brief, the averaged 3D dataset and the maximum intensity projection, maximum exhale (generally 50 – 60%) and maximum inhale breathing dataset were imported into a treatment planning system (Eclipse Varian, Palo Alto, USA) for organs at risk and target volume marking. The ITV was delineated on the MIP (Maximum intensity projection) and the contour used on the average CT data set using the maximum intensity projection and maximum expiration/inspiration data sets assess the motion range of the gross tumor volume. A 5 mm isotropic margin from the ITV was used to generate the PTV. A 3D conformal plan was generated using between 7-11 coplanar and non-coplanar beam directions with 6 MV or 18 MV x-rays where appropriate. In order to achieve a rapid dose fall off, 0 to 2 mm MLC margins were used around the PTV with the prescribed dose normalised to the surrounding isodose line (75% - 85%) that covered 99% of the PTV target volume.

ITV Margin Verification

Treatment was delivered on a linear accelerator with 3D volumetric imaging capabilities (Varian On Board Imager v1.4, Palo Alto, USA). Pre treatment verification required an orthogonal kV pair of images to localize the patient's position using bony anatomy. Following this, a cone beam CT (CBCT) was performed at the level of the diaphragm to quantify the right diaphragm motion range by measuring the width of the probability density function (PDF), as described by our group previously[402] as well as by Guckenberger et al[272]. To summarize, a line profile tool that graphically displays the CT Hounsfield unit variation along the drawn line is used to display changes in lung density. The blurred region over the diaphragm is displayed as a gradient as the pixel varies across from the liver to the lung interface. Due to the limitations of the CBCT field-of-view (16cm length) a second CBCT was performed at the level of kidney for target matching. To perform the target match, the kidney from the maximum expiration and maximum inspiration dataset were outlined.

Measurement of Kidney and Diaphragm Motion at Planning CT

The ten breathing phases (0 - 90%) derived from the planning CT were imported into a contouring program (MIM Software™ v 6.5, Cleveland, USA) for the left and right kidney contours to be automatically

propagated across each breathing phase. For the reporting of organ motion, the kidney was divided into equal thirds. The most superior point of the kidney represented motion of the superior pole, the centroid co-ordinate of the kidney represented the mid pole and most inferior point as the inferior pole. Using these three reference points the maximum cranio-caudal motion could be calculated for the superior, inferior and mid pole of the left and right kidney. This measurement does not consider any rotation that may occur in the kidney. To measure right diaphragm motion, the most superior location of the diaphragm at each breathing phase was also recorded.

Kidney Motion at Treatment

CBCT imaging was used to localise the target position at treatment. All CBCT matches were performed after localisation to the bony anatomy in the surrounding target region (i.e. spinal vertebrae, ribs). The shift that was required to match the structure to the imaged soft tissue kidney volume was recorded in the anterior/posterior (AP), medial-lateral (ML) and superior-inferior (SI) direction. This data, captured on our record and verification system (MOSAIQ 2.4, Elekta Stockholm), was retrieved for further analysis. To quantify total displacement, the 3D vector (square root of the sum of the squares of the shift) in the AP/ML/SI direction was calculated. All pre treatment and mid treatment images were reviewed online with an action threshold of 0mm. All post treatment images were reviewed offline.

Data Analysis

Mean differences in motion between each individual pair of kidney poles were tested using paired t-tests. Kidney poles presenting with a tumor were compared to the respective contralateral kidney pole without a tumor. Finally, the motion from kidney poles with a tumor greater or larger than 5cm were compared to those with tumor smaller than 5cm. Spearman correlation (r.) was used to assess the relationship between magnitude of change to breathing motion and displacement of the kidney target. For all analysis a p-value of < 0.05 was considered statistically significant. All tests were performed using SPSS 21 (IBM; Chicago, IL, USA).

5.3 Results

From April 2012 to October 2014, a total of 33 kidney targets from 32 patients were treated according to study protocol. The demographic characteristics of the patients are outlined in Table 18.

Table 18. Summary of patient demographics (n = 32)

Characteristic	Value
Age	
Median	77 years
Range	41 – 91 years

Sex	
Male	24 (75%)
Female	8 (25%)
Prescription	
42Gy in 3 fractions	16 (48%)
Average Size* (range)	59.1mm (45 – 75)
26Gy in 1 fraction	17 (52%)
Average Size* (range)	38.8mm (21 -53)

* size = maximum dimension of tumor

Due to limited research licensing availability with MIM Software™, analysis of total kidney motion was only performed on the first consecutive 20 patients. Motion was assessed in both kidneys on 20 consecutive patients except for one patient with single kidney due to a previous nephrectomy of the right kidney.

Right and Left Kidney Motion as Measured using 4D Planning CT

Figure 16 shows the mean and standard deviation of kidney motion at each individual kidney pole.
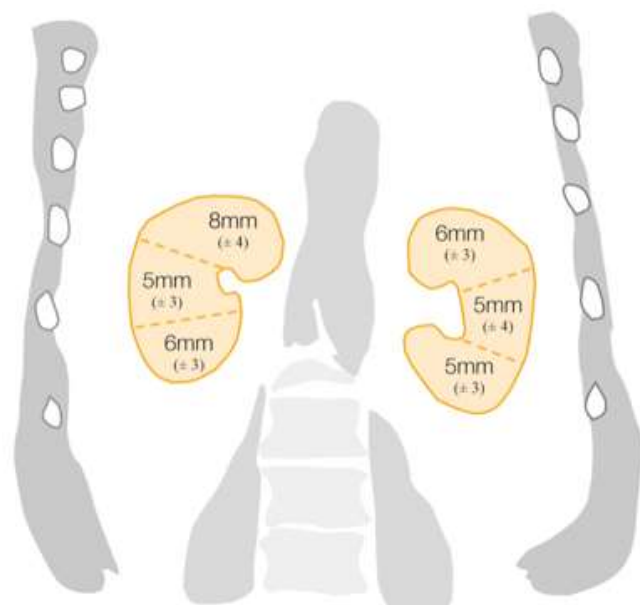

Figure 16. Summary of superior inferior mean kidney motion (standard deviation).

Measured on the 4D CT dataset taken from three areas of measurement: superior kidney pole, inferior kidney pole and central kidney.

For the right kidney, the mean difference in cranial-caudal motion between the superior and mid pole was 3.0mm (95% CI: 0.7 to 5.2mm; p = 0.011) and between the superior and inferior pole was 2.5mm (95% CI: 0.8 to 4.1mm; p = 0.005). The mean difference between the mid and inferior pole was -0.5mm (95% CI: -2.0 to 0.9mm; p = 0.471). In the left kidney, the superior pole showed a mean difference of 1.2mm against the mid (95% CI: -0.8 to 3.3mm; p = 0.219) and 0.9mm against the inferior poles (95% CI: -1.1 to 2.9mm; p = 0.367). Between the mid and inferior poles, the mean difference was -0.3mm (95% CI: -2.2 to 1.5mm; p = 0.703). Between the right and left kidneys, the difference in motion of the superior poles was 1.6mm (95% CI: -1.5 to 4.7mm; p = 0.299), the mid poles -0.2 (95% CI: -1.9 to 1.6mm; p = 0.807) and inferior poles 0.3mm (95% CI: -1.7 to 2.4mm; p = 0.714).

Kidney Motion in the Presence of Tumor

Among these 20 patients, there were a total of three (15%) superior pole, 10 (50%) mid pole and seven (35%) inferior pole tumors. For all cases the mean motion of the poles with a tumor present was 5.7mm compared to its corresponding contralateral pole which was 5.8mm (p = 0.909). The mean motion of the kidney poles with a large tumor (≥5cm) was 5.8mm compared to 5.6mm for poles with smaller tumors (<5cm), a difference of 0.2mm which was not statistically significant (95% CI: -2.8 to 3.2mm; p = 0.875).

Kidney Motion and Right Diaphragm Motion

The relationship between diaphragm motion and kidney motion was assessed by first measuring the amount of organ displacement from a breathing phase to the following phase i.e. 0 to 10%, 10 to 20% etc. Figure 17A and 17B is a graphical display of the displacement of the right and left kidney relative to the right diaphragm when transitioning from one breathing phase to the next (where 0% is generally maximum inhale and 50% maximum exhale).
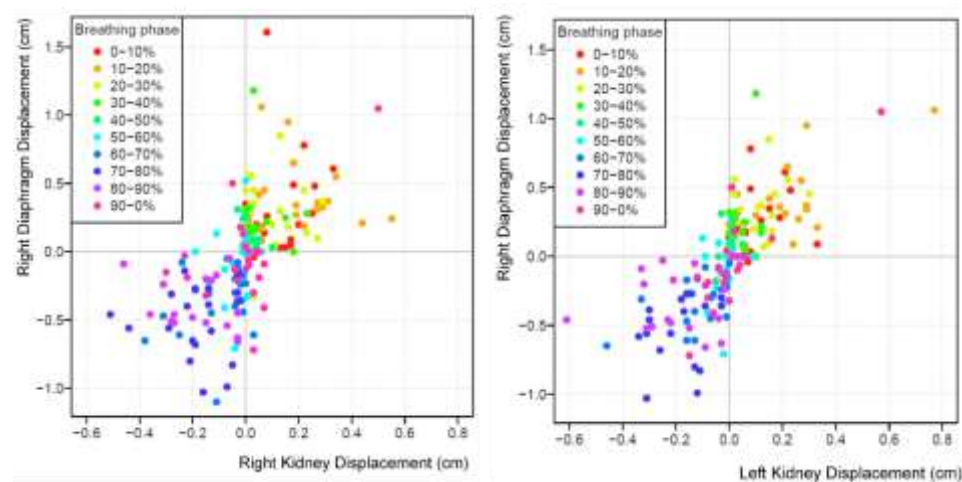
Figure 17. Displacement of the right (A) and left (B) kidney against displacement of right diaphragm per breathing phase (from 0 - 90%)

Around the exhalation phases 40-50, 50-60 and 60-70%, minimal motion (0 to 2mm) was seen for 19/19 (100%) of all right kidneys and 19/20 (95%) of left kidneys. This is in comparison to the inhalation phases 90-0%, 0-10%, 10-20% whereby 15/19 (74%) of right kidneys and 16 /20 (80%) of left kidneys achieved minimal motion (0 to 2mm). Medium kidney displacement (between 3 – 5 mm) was predominantly at the 20% breathing phase. The largest motion of over 5mm was usually seen at the 80-90% breathing phase. Similar to the kidney motion, the right diaphragm showed the least motion (0 to 2mm) predominantly at the 50-60% breathing phase for a majority of patients (16/20).

Interfraction/Intrafraction Motion as Observed at Treatment

A total of 65 pre-treatment and mid-treatment CBCT images were acquired for target verification. Post-treatment CBCT were not imaged for two patients leaving 63 available images for analysis. The mean (standard deviation) shift was recorded for the SI/ML/AP and from this the 3D displacement was calculated (Table 19).

Table 19. Mean (standard deviation) of localization shifts to the target kidney.

	Superior/inferior (mm)	Medial/lateral (mm)	Anterior/posterior (mm)	3D Displacement (mm)
Pre treatment	-0.2 (±4.1)	0.7 (±2.2)	-0.1 (±3.4)	4.7 (±3.3)
Mid treatment	0.0 (±1.5)	0.1 (±1.0)	0.0 (±1.0)	1.3 (±1.6)
Post treatment	-0.3 (±2.4)	0.1 (±0.8)	0.2 (±0.9)	1.0 (±2.5)

Figure 18 is a summary of the magnitude of displacement in each individual direction. The intrafraction motion for 95% of fractions at mid and post-treatment was 2mm or less for all directions except cranial-caudal which was 3mm or less. Inter-fractional variation of the kidney from planning showed that the difference for 95% of fractions was between 4 to 7mm.

Figure 18. Frequency histogram showing the pre/mid and post treatment displacement of the kidney target.

Superior/inferior (A), medial/lateral (B) and anterior/posterior (C) direction.

Changes in Diaphragm Motion and 3D Target Motion

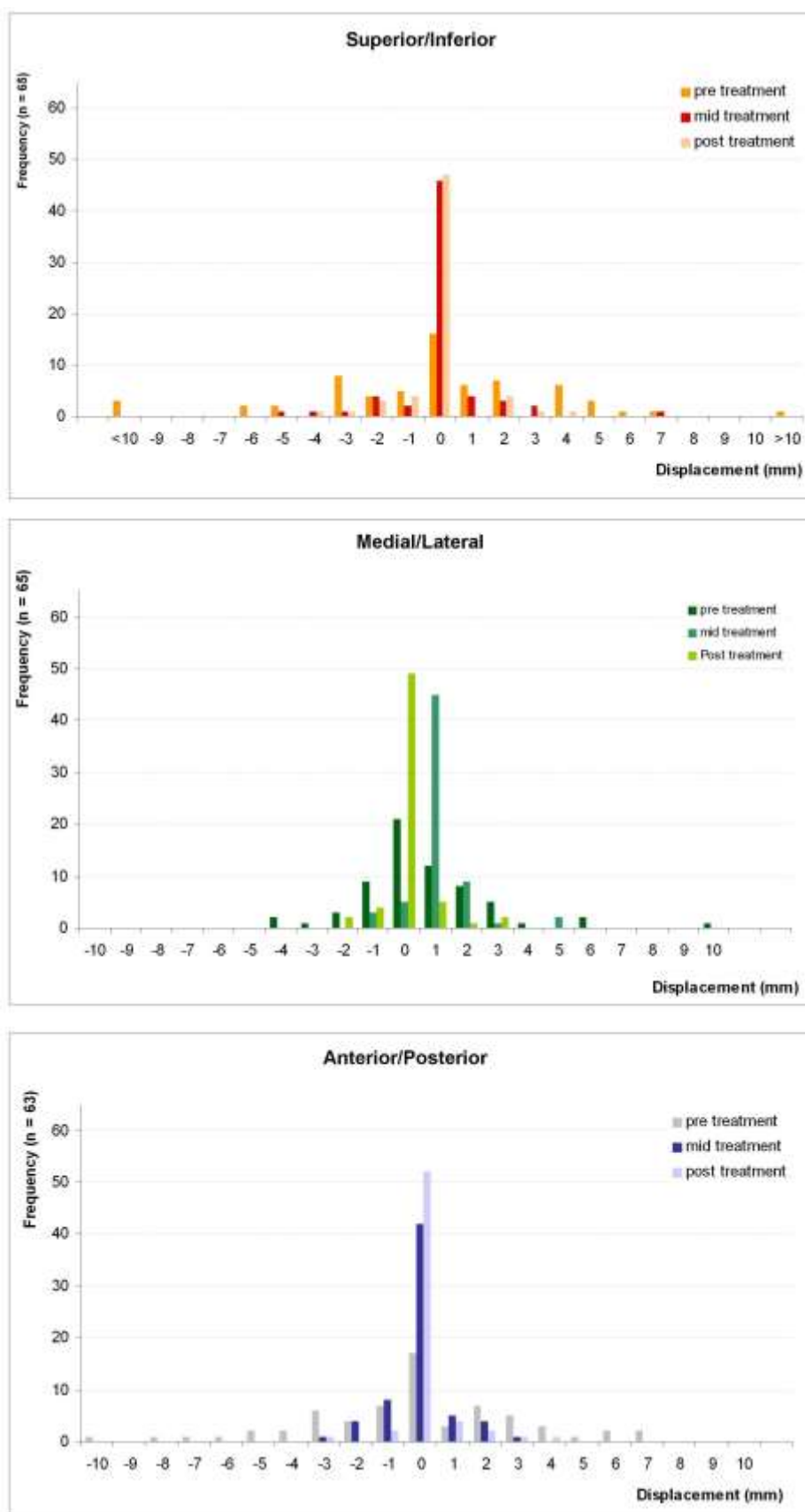The average width of the probability density function of the right diaphragm measured at planning CT was 18 mm (std. dev. $\pm$ 7). The mean difference at fraction one showed a PDF width of -0.3mm (95% CI: -1.8 to 1.3mm; p = 0.758); at fraction two, the mean difference was 1.5 mm (95%CI: -1.4 to 4.4mm; p = 0.290); and for fraction three, -1mm (95% CI: -3.2 to 1.0mm; p = 0.308). On one occasion was breathing motion different by 23mm. For this patient, planning simulation recorded motion of 39mm and at mock up, the value was found to be at 16mm. This was found to be a misunderstanding of breathing instructions given and has been described in further detail elsewhere[403].

The median mid treatment CBCT time taken from pre treatment imaging was 30min (interquartile range: 25min – 35min). The median post treatment CBCT time from pre treatment imaging was 44min 30sec (interquartile range: 40min – 51min 15sec). Relative to the planning position, the mean 3D displacement of the target at mid treatment CBCT was 1.2mm (STD $\pm$ 1.6mm) compared to 2.1mm ($\pm$ 2.7mm) at post treatment (p = 0.003). Pre treatment changes in breathing motion, showed a significant relationship with mid treatment 3D displacement (r_s = 0.278, p = 0.025) and post treatment 3D displacement (r_s = 0.363, p = 0.003).

5.4 Discussion

In this paper we have shown the feasibility of a free breathing motion management protocol for kidney stereotactic ablative body radiotherapy. We have also described and evaluated kidney motion making this a unique report on kidney motion in the presence of a tumor mass. This has potential implications for margin design for healthy and cancer affected kidney. This protocol is able to show small kidney target motion, minimal intrafraction motion and strategies to identify large changes to target motion prior to treatment delivery. Such a protocol is feasible on a conventional linear accelerator with minimal early toxicities as we have previously reported[316].

The use of dual vacuum immobilization under free breathing conditions has shown a small variation in kidney motion measurements. When looking at motion of the superior pole our findings were comparable if not less than the 7.7mm and 7.9mm which we previously published on 62 patients with a mix of diagnosis[402]. Van Sörnsen de Koste in a study of 54 patients, also used the apex of the kidney showing mean motion was 9 and 9.8mm on the right and left respectively. In studies that have utilised centroid motion, Heinzerling[212] described the use of an abdominal compression plate to show mean displacement of right and left kidneys to be 4.7 and 4.6mm respectively. Our own study shows motion of the midpole (centroid) to be very similar with mean displacement of 5mm. Whilst the aim of our study was not to

evaluate the effectiveness of the vacuum immobilisation to minimise kidney motion, in other studies that have used no compression devices, mean centroid motion of the right kidney have been 6 and 7.2mm, and on the left 4.5 and 6.4mm[348,349] findings that are similar if not larger to our own measurements.

We have investigated kidney motion showing a statistically significant difference in motion between the superior and inferior poles on the right kidney but not on the left kidney. This difference in motion of the right kidney would suggest either deformation or rotation to occur with breathing motion. Around the left kidney are the stomach and bowel, whereas the liver over the right kidney is a less compressible structure and could explain this difference in motion between the left and right kidney. A smaller study of five patients by Gawthrop & Gill[346] reported similar motion differences between the superior and inferior poles of the right and left kidneys. Their report showed average superior motion of 13 and 12mm in the right and left superior kidney poles respectively. This is in comparison to the inferior right and left kidney poles which showed average motion of 7 and 6mm respectively which the authors also attributed to a form of deformation or rotation occurring with kidney motion.

In our study the presence and size of the tumor were factors that did not show any statistical difference in motion between the patient's unaffected kidney. A recent publication by Sonier et al[404] on kidney motion of patients treated for kidney/adrenal SBRT using vacuum immobilisation reported average centroid motion of 8.1mm (+/- 4.3) in the superior/inferior motion which is similar to our reported data. Furthermore, their findings also saw localisation data at pre mid and post treatment to be within 2.1mm at 95% of occasions. This is similar if not smaller than our reported intrafraction motion of 3mm or less on 95% of fractions at mid and post treatment. Whilst the treatment time was not reported in Sonier's (2014) publication, compared to our study, the use of VMAT/IMRT treatment technique and smaller dose per fractionation (30-40Gy/5fx) could potentially contribute to a shorter treatment duration thus reducing the magnitude of intra-inter fraction motion reported. In comparison to other SABR protocols, intrafraction motion data from Foster et al[405] reported on the intrafraction motion outcome on over 260 patients stabilised with a stereotactic body frame. In this study Foster (2013) was able to show vector displacement of less than 2 mm on thoracic, abdominal and pelvic sites.

In our current protocol for kidney stereotactic treatment, we verified our ITV expansion at the time of IGRT by assessing patient breathing through a PDF measurement. While the majority of fractions (95%) showed mean breathing changes of less than 2mm to that planned, a few patients did show breathing changes from 10mm up to 23mm. While no formalized coaching strategy was in place, therapists were advised to query with the patient if large changes in breathing (over 10mm) was detected. Sleepiness/drowsiness[217], difficulty breathing with vacuum compression[364] or mis-communicated breathing instructions[403] are some factors that can contribute to changes in breathing amplitude and thus should be points of investigation if large discrepancies do appear. Whilst not available in our current protocol, dynamic tumor tracking or continuous monitoring of breathing would be ideal for future protocols. On one occasion in our study did post treatment imaging show a large displacement (17mm) of the kidney target (Figure 19) due to breathing change.

A) Planning CT with kidney (cyan) and ITV (red) contoured.

B) Fraction 2 pretreatment CBCT showing 5mm posterior displacement of the kidney target.

C) Fraction 2 post treatment CBCT showing 17mm inferior displacement of the kidney target. Left diaphragm displaced inferiorly (arrow) suggests a baseline shift in breathing amplitude occurring at some point after mid treatment imaging.

Figure 19. Example from a treatment fraction showing change in kidney target position due to breathing change.

Offline review of post treatment CBCT imaging showed the target position had changed despite no bony anatomy change. In the post treatment CBCT the more inferior position of the diaphragm would suggest a form of baseline shift/breath hold occurring thus displacing the kidney position. Whilst no obvious factor could be determined why the patient's breathing changed during the treatment, it is important nonetheless to monitor potential geographical misses. We have in a previous study shown the ability of an abdominal surface marker to detect changes in breathing[364] which can be used to continually monitor patient's breathing throughout the course of treatment. The correlation we found with pre-treatment breathing changes and mid/post treatment kidney displacement could potentially initiate continuous monitoring of breathing changes to minimise geographical misses with a change in breathing.

Gated treatment offers a smaller target volume for treatment thus reducing the dose to critical organs. The insertion of tumor markers to facilitate respiratory gated treatment however can lead to various complications[217] and in patients that are not suitable for surgery will not be feasible. The role of fiducial-free tracking [406] therefore becomes an attractive option whereby the ability to use a soft tissue surrogate to track the position of the kidney. Our previous investigations have shown an association between the magnitude of motion of the right diaphragm and the right kidney[402,407]. In this study we have explored the range of motion of the right diaphragm and the left and right kidney at specific breathing phases. We have shown that the trajectory of motion of the kidney from the 40% through to 70% breathing phase can be $\leq$ 2 mm in a majority of patients. This provides confidence in using these breathing phases for defining the duty cycle for gated treatment. Future soft tissue tracking strategies can potentially uses the right diaphragm dome as a soft tissue marker which also showed minimal motion around the exhale phases.

5.5 Conclusion

Stereotactic treatment on a conventional linear accelerator with vacuum immobilisation can maintain average kidney target motion of less than 6mm. Pre and mid treatment stabilisation at 95% of fractions can be maintained within 3mm or less for average treatment delivery time of <50mins (not including setup). With vacuum immobilisation, breathing replication can be maintained within 2mm for a majority of patients however there are cases where large changes in breathing can occur at pre and post treatment. We advise that for SABR treatment, verification of this is part of the image guidance protocol.

Chapter 6

Discussion

Technological advances over the last two decades have led to the rapid adoption of stereotactic ablative body radiotherapy techniques globally[296,408-410]. These techniques have been used to treat tumours of the lung[171,173,411], liver[412,413], spine[414,415] and more recently, of the kidneys[324]. Conventional radiotherapy for primary renal cell carcinomas has been ineffective in improving overall survival[146]. This has been attributed to the radio-resistant nature of the tumour[401,416], preventing a sufficient dose of radiation to be used without causing severe toxicity to nearby organs. Developments in radiotherapy systems, motion management tools and image guidance systems have led to many institutions utilising a wide range of strategies for kidney SABR treatment (Table 4). Despite this global utilisation, there is minimal consensus on the best approach for high-dose radiotherapy of the kidney[297]. This thesis used the expert literature from lung, liver, spine SABR treatment, and recommendations from national and international SABR guidelines to define a kidney-specific SABR protocol focusing on motion management, dose conformality, and image-guidance. This protocol formed the technical component of the FASTRACK (Focal Ablative Stereotactic Radiosurgery for Cancers of the Kidney) study which examined the feasibility of linac-based SABR treatment of the kidneys. The final report from this study showed an 89% rate of technical feasibility based on 33 of 37 patients able to complete their radiotherapy treatment[417](Appendix 9.7). Of the four patients who were unable to meet the primary endpoint, two patients were not able to achieve bowel dose constraints safely, one unable to complete their final treatment fraction due to social circumstances and the fourth passed away before treatment could be started. Pathological confirmation of disease was available in 30 of 33 (90%) tumours, with the most common histology being clear cell carcinoma type (88%), followed by papillary/chromophobe type (9%), and a small proportion of mixed histology type (3%). All patients who received and completed treatment had a median follow-up of 24 months. Four patients had partial responses, and 28 had stable disease. One patient, at 28 months post-treatment, progressed locally with the distant progression of the disease. The 2-year freedom from local progression, distant progression, and overall survival was 100%, 89%, and 92% respectively. Post-treatment, one patient experienced grade 3 transient fatigue and no patient experienced grade 4 or 5 toxicity.

This discussion will, using examples from the literature and the work presented in this thesis, highlight the advantages and disadvantages of motion management, patient stabilisation, treatment planning, and image guidance techniques that have been used for kidney SABR treatment. This discussion will also present some of the literature on kidney SABR side effects, with a focus on gastrointestinal (GI) treatment toxicity. Finally, current and future developments for the role of kidney stereotactic treatment will be discussed.

6.1 Kidney motion management techniques

Motion management, in the kidney SABR setting, has been implemented using techniques such as abdominal compression to reduce kidney motion, large planning margins to account for motion, use of patient-specific ITV motion margins, breath-hold, or fiducial marker tracking for motion compensation. The following section will summarise the use of these strategies for kidney SABR planning.

The literature review in chapter 2 showed that the average superior-inferior kidney motion can range between 4 to 76mm depending on the breathing intervention involved. The wide range of kidney motion emphasises the importance of a protocol to accurately define and, if possible, to minimise the tumour motion for treatment. The work outlined in chapter 3 demonstrated that a dual vacuum immobilisation system could act as a compression device to reduce kidney motion by 1.8 to 8mm. This is similar to using a pneumatic compression belt[301] or an abdominal compression plate[212] to reduce kidney motion. One caveat in using compression devices is the possibility of an increase in target motion. We observed this for one participant in our study, described in chapter 3, and have also found similar experiences in the literature for one study investigating kidney motion[301] and others for lung tumour motion[211,226,329,377]. Within these reports, the number of participants who had an adverse increase in target motion ranged from 4 to 18%. Identification of individuals who cannot tolerate abdominal compression could be done by monitoring changes in breathing when compression is applied. In chapter 3, we described the feasibility of using the Varian RPM system to monitor changes in abdominal motion which could be used as an indication of breathing motion changes. Another strategy would be to use fluoroscopic imaging to directly assess changes in diaphragm motion when under abdominal compression[418]. Patient comfort, with any abdominal compression device, should be another consideration when using this motion management strategy. In a study comparing the dual vacuum compression system and an abdominal compression plate[329], patients were asked to rate their preference for either set up. Most patients (15/24, 63%) preferred the abdominal compression plate, rating it more comfortable. As these patients' opinion was based only on their level of comfort during the simulation process, a different opinion may have been made if the patient was able to rate their experience of the device over the entire course of treatment. In one report of lung stereotactic radiotherapy [419], a small number of patients experienced anterior chest wall tenderness after three treatments using an abdominal compression plate. An over-the-counter analgesic was prescribed to manage the pain which resolved shortly after the course of treatment. For shorter courses of SABR treatment, an abdominal compression plate may be manageable for patients. However, for extended five or more fraction SABR treatments, this may cause increased pain/discomfort as treatment progresses. As renal cell carcinoma manifestations are often in the elderly[1], the significance of patient preference and tolerability with motion management devices requires further investigation.

Three kidney SABR studies[275,276,280] have used planning PTV margins of 5 to 15mm around the GTV to account for setup uncertainty, including breathing-attributed motion. In these studies, abdominal compression was applied to limit the magnitude of kidney motion. The literature review in chapter 2 showed that median kidney motion could be 5.4mm (range 4 – 8mm) when using compression plates[212,301,362] or

8.1mm (range 6 – 14.4mm) when using dual vacuum compression[364,373,420]. This suggests that generic planning margins of 10mm or greater can be used in combination with abdominal compression devices. However, with the abundance of motion management options in the modern-day clinic, other means of estimating target motion should be considered before resorting to generic planning margins. Within this thesis, and in more recent linac-based SABR studies, patient-specific motion inclusive ITV margins were derived from 4DCT scans[278,287-289]. Not only does a 4DCT provide an accurate assessment of the kidney motion, but it also provides an opportunity to triage the most suitable motion management approach. For example, if a tumour was seen to move 10mm or less, then a motion inclusive ITV margin could be used. If tumour motion was seen to be greater than 10mm, then a respiratory-gated protocol could be used for treatment. A gating solution has been demonstrated[280] treating the 50% breathing phase. This exhale phase of the breathing cycle, was shown to be the most stable breathing phase in our study (chapter 5), demonstrating the least amount of motion. One limitation with using 4DCT imaging for planning is the presence of motion artefacts caused by breathing irregularity[421,422]. The reported frequency of a motion artefact appearing through the target volume have been reported to be as high as 30% in the lung and mediastinal treatment setting[423]. Motion artefacts appearing through the kidney tumour (Figure 20) can misrepresent the extent of motion, thereby requiring either a new 4DCT scan to be done, continuation with the use of a (larger) planning margin around the GTV or the use of a surrogate structure to estimate the ITV margin. The feasibility of using the right diaphragm as a surrogate motion structure for the right and left kidneys were investigated by our institution[402](Appendix 9.3). In a retrospective analysis comparing the 4DCT motion of the right diaphragm and the right and left kidneys of 71 patients, a correlation between the right diaphragm and right kidney ($p = 0.001$) was seen, but not between the right diaphragm and left kidney ($p = 0.76$). It was also identified that the magnitude of the right diaphragm motion was almost twice that of the right kidney, suggesting a disproportional motion relationship between these two organs. The use of the diaphragm to generate a kidney ITV margin was mentioned by Yamamoto *et al* [288], but there was no further elaboration behind this particular decision. Based on our institutional report of kidney motion characteristics[350], an ITV margin generation based on the right diaphragm motion for the right kidney would be acceptable. Any correlation between the left diaphragm and the kidneys or the right diaphragm and the left kidney requires further investigation.
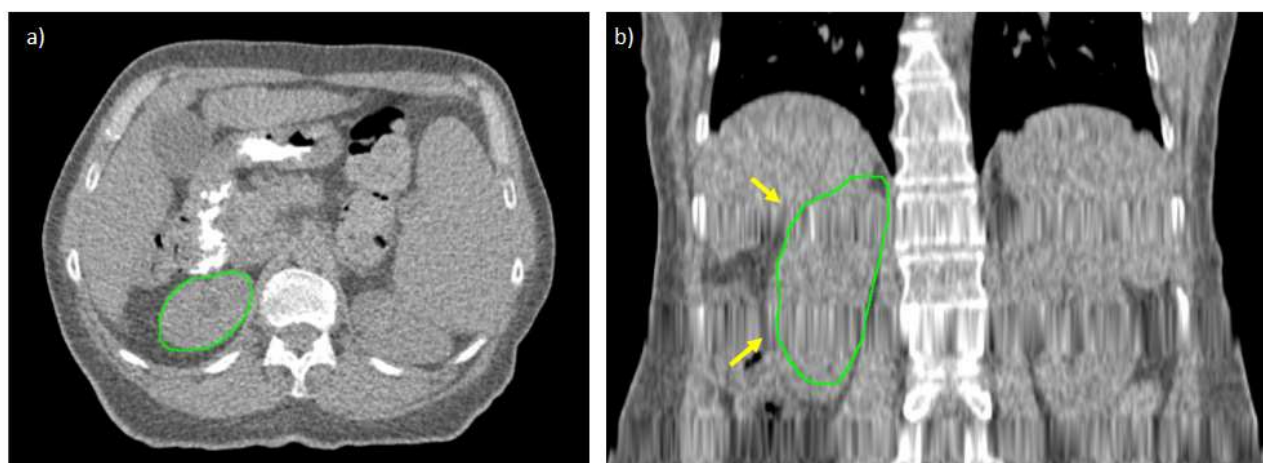
Figure 20 Motion artefacts on 4DCT images

Kidney volumes can be accurately delineated on axial planes (a). However, in the presence of 4DCT motion artefacts (b) quantifying total kidney motion can be difficult. *Source: Stanford Radiation Oncology Center*

The use of tumour tracking as a motion management technique for kidney SABR treatment has been reported by several institutions[282-285,310,311]. Fiducial markers, inserted near the kidney tumour, were used as surrogates of the target for treatment. In the Cyberknife[TM] treatment system, dynamic tracking of the fiducial marker can minimise intrafraction motion uncertainty, thereby allowing the use of reduced PTV margins around the GTV. As a surrogate structure, the fiducial marker placement must be located near the target. The kidney motion study in chapter 5 and in another report from the literature[301], suggests that kidney displacement can be different between each pole. This could lead to misrepresentation of the fiducial marker motion and the tumour if each were in separate kidney poles. Furthermore, the additional complications-risk from the procedure inserting the fiducial marker and the potential for seed migration may limit its feasibility for patients[424-426]. The use of fiducial markers for image guidance can also limit the type of imaging system, such as CBCT, which can introduce artefacts around the target region[427,428].

A breath-hold technique commonly used for liver and lung SABR treatment[204,205,208,210,429], has also been reported for stereotactic treatment of the kidney. Funayama *et al*[290] used a self-controlled breath-hold protocol to treat 13 patients. Each patient underwent repeated 3D breath-hold scans to derive an ITV margin of 2 to 4mm based on the consistency of tumour position. On-treatment target verification utilised a CT-on-rails system, allowing fast image acquisition under breath-hold. The challenge with this technique is whether a patient can hold their breath for the duration of the beam delivery. The authors did not report on the total treatment time. However, they did describe their planning technique which used either multiple (>5) static fields or five conformal arcs for treatment. All 13 patients in this study were able to complete their treatment, but whether this can be implemented across other patient cohorts is still unknown. For prolonged breath-hold treatments, there is the risk of kidney centroid drift. This has been shown in a study using cine MRI to visualise kidney motion under free-breathing and breath-hold conditions[299]. The authors found that compared to free-breathing, repeated breath-holds of up to 20 minutes showed a wider range of kidney displacement.

In summary, numerous motion management strategies have been used for SABR treatment of the kidney. A summary of the advantages and disadvantages of these strategies are listed in Table 20. Considering the aging population of those diagnosed with renal cell carcinoma, the use of a vacuum compression system combined with 4DCT imaging to generate patient-specific ITV margins is an uncomplicated approach with minimal disadvantages. Compression plates/belts may be unsuitable for the elderly as would fiducial marker insertion, due to any pre-existing comorbidities. The role of breath-hold for treatment could provide an opportunity to reduce planning motion margins, however, further investigation is required regarding patient suitability and treatment delivery efficiency.

Table 20. Summary of motion management strategy advantages and disadvantages.

	Advantage	Disadvantage
Abdominal compression	Can reduce kidney motion, thereby minimising treatment margins[212,301,364].	In small percentage of patients, can increase motion[211,226,301,329,364]. May not be comfortable for the elderly[329,419].
Motion inclusive ITV from free breathing	Personalised to patient's free breathing[278,287-289,316]. Based on free breathing reproducibility.	Irregular breathing patterns can produce motion artefacts[421-423].
Fiducial marker	Tumour tracking for treatment can be used[282-285,310,311].	Seed migration[424]. Risk associated with procedure[425,426] Seed may not represent true position of target[301,373]. Artefacts with CBCT may hinder image quality[427,428].
Breath-hold	Small motion margin required[290]. CBCT imaging shows no motion artefacts[210].	Breath-hold drift over time[299]. Reproducibility of breath hold position[299].

6.2 Stabilisation and intrafraction motion

The reduction of planning margins in SABR treatment relies on stabilisation devices that can minimise involuntary patient motion during treatment[160]. With reduced planning margins, small intrafraction motion

can increase the dose to surrounding critical structures and/or decrease the target coverage[223]. The dual vacuum system is composed of a body cradle customised to fit around the patient's body. Plastic drapes, fitted anteriorly over the patient, are evacuated to create an air-tight vacuum. In our kidney SABR protocol, the use of this device for treatment was able to confer less than 2mm of intrafraction motion, thereby supporting our use of a 5mm PTV margin. Stereotactic-specific body immobilisation systems used for lung and liver treatments have reported similar intrafraction motions, ranging from 0.7 to 2.3mm[224-227,329,430]. One important consideration with the dual vacuum immobilisation system is the additional time required for patient setup. One investigation found that the average setup time for the dual vacuum system was longer at 40 (+/-21) minutes compared to the compression plate, which took on average 33 (+/-10) minutes ($p = 0.04$)[329]. A similar study also showed longer setup times of 7.9 (+/- 1.3) minutes when using the dual vacuum system compared to the vacuum cushion alone, which took on average of 2.2 (+/- 0.4) minutes to set up ($p = 0.021$)[430]. The overall treatment duration is important from the clinical perspective, as with increased treatment time, there is a risk of increasing patient motion. This has been shown in one investigation examining intrafraction lung tumour motion over time[268]. In this study, the mean intrafraction motion of the tumour was 2.2 (+/- 1.2) mm within 34 minutes, and after 34 minutes, the mean tumour displacement was 5.3 (+/- 3.0) mm. In the context of SABR planning, which uses small PTV margins, the authors emphasised the importance of using either mid-treatment imaging to verify the position of the target volume or strategies to reduce the overall treatment time. This study, however, had relatively small patient numbers (n = 28) and was investigating motion in patients undergoing lung SABR treatment. A similar study used mid-treatment CBCT imaging to investigate intrafraction motion for 133 patients undergoing treatment for lung SABR. At a mean mid-treatment acquisition time of 20:05 (+/- 6:10) minutes, 94% of fractions were within the +/-5mm margin[227]. Whether or not a similar problem exists with kidney SABR treatment requires more in-depth investigation. In our report in chapter 5, the median treatment time was 44 minutes and 30 seconds (interquartile range: 40 – 51 minutes, 15 seconds). The mean intrafraction and post-treatment motions were 1.3 (+/-1.6) mm and 1.0 (+/- 2.5) mm respectively. In a similar study using CBCT to localise kidney motion mid-SABR treatment, the mean intrafraction motion for kidney and adrenal targets in the left-right, superior-inferior and anterior-posterior directions were 0.63 (+/-0.74) mm, 1.08 (+/-1.38) mm and 0.70 (+/-1.00) mm respectively[420]. One limitation of these two reports is the small number of patients analysed (n = 62 in total for both studies). However, if combined with the experience from lung intrafraction motion studies, short treatment times could remove the necessity of mid-treatment CBCT imaging. One way of reducing the delivery time is to use volumetric arc therapy for treatment. This has been shown in a planning study comparing the treatment time between a 7 to 9 field IMRT technique and a single arc VMAT technique[431]. In each technique, the coverage to the PTV target was similar, as were the maximum doses to the small bowel, large bowel, duodenum, spinal cord and stomach which all met the protocol constraints. The average treatment delivery time for the static IMRT technique was 13 (+/- 2.6) minutes compared to an average of 4 (+/ 0.9) minutes for a VMAT technique ($p <0.05$). Faster treatment delivery, however, is not a guarantee that intra-fraction motion will not occur during any part of the treatment delivery process. Investigations using cine MRI imaging to visualise kidney motion, have

observed baseline drifts occurring at both the beginning and the end of imaging. One study used a 1.5T MRI to monitor kidney motion over 25 minutes for 15 patients diagnosed with renal cell cancers[302]. Within the first 200 seconds of imaging, most patients showed a small baseline drift of less than 5mm. One patient showed a drift of over 12mm which continued to increase to over 20mm after the 10-minute imaging mark. For a selected number of patients, the baseline drift that occurred at the beginning of imaging would eventually stabilise by the 25-minute mark. In a similar study, a 1.5T MRI was used to compare kidney motion under breath-hold and free breathing conditions. The authors observed that at gating windows of 5mm or less, the average gating efficiency was optimal when using baseline-corrected breath-hold, followed by free breathing and the least ideal when using breath-hold (with no baseline correction)[299]. These two MRI studies highlight the limitations of using mid and post-treatment imaging strategies for verification. As this process is performed at discrete time points, the behaviour of the kidney cannot be established outside of these imaging times. Real-time imaging technology, such as continuous MRI imaging, can mitigate this motion shift by providing visualisation of kidney position during treatment[303]. An alternative method would be to monitor breathing changes during treatment. Body-surface imaging can be used to continuously monitor patient breathing changes during treatment. This has been used to estimate baseline shifts occurring in lung stereotactic treatment[432]. Further studies correlating body-surface motion against the left and right kidney motion would help to validate its role for kidney SABR treatment.

6.3 Treatment planning

Plan quality metrics in stereotactic radiotherapy planning were first proposed by the Radiation Therapy Oncology Group (RTOG) to benchmark treatment plans generated for patients enrolled in clinical trials of intracranial radiosurgery[433]. These metrics included assessing the minimum isodose covering the target relative to the prescription dose (quality of coverage index), the ratio of the maximum dose in the target to the prescription dose (homogeneity index) and the ratio of the volume of the prescription isodose relative to the target volume (conformity index). Other indices have also been proposed to describe the conformity of the dose overlapping with target and healthy tissue[434], with the gradient index (GI or R50), describing the dose fall-off beyond the target volume, being important in plan quality assessment[435]. In stereotactic ablative body radiotherapy planning, plan metrics such as the conformity index and gradient index (R50) have been recommended to guide the planning process[436,437]. A small R50 value is ideal as it represents a steep dose gradient generated by the low entrance and exit dose from each beam used. On the other hand, a large R50 value indicates either high dose contribution from each treatment field or excessive field overlap on entry and exit of the body. The R50 value can help guide the plan to use more treatment fields or to adjust beam angles to minimise dose overlap. This metric has been recommended for evaluating stereotactic plans of the lung and liver[160] and was first used in the RTOG 0236[386] trial of lung stereotactic radiotherapy to benchmark each patient plan enrolled in the study. The values from this trial ranged from 3.9 to 2.9, which was dependent on the target volume size. One limitation with these values, proposed by the RTOG 0236[386] trial and recommended by AAPM SBRT Task Group 101 report[160], was that it did not consider heterogeneity within the plan. With heterogeneity not accounted for tumours in the lung, or any target

surrounded by or adjacent to air, the dose distribution misrepresents the behaviour of electrons scattering in the air[438]. The impact of heterogeneity correction on the R50 value is demonstrated in several reports proposing new values for treatment plan benchmarking. Xiao *et al* [394] recalculated the treatment plans with heterogeneity correction for twenty patients, originally submitted to the RTOG 0236 study. The authors found a larger ratio of the R50 criterion ranging from 7 to 3.5. The RTOG 0813 study for centrally located lung tumours, generated R50 values for plans with heterogeneity correction enabled, showing a maximum of 5.9 and a minimum of 2.9 depending on the tumour volume[439]. The ROSEL study[395], comparing lung SBRT to surgery, proposed R50 values ranging from 8 to 6 when using older dose calculation models (Type A algorithm), and values ranging from 12 to 6 when using more advanced algorithms (Type B algorithm) that were able to model lateral electron transport. In an Australian multi-institutional analysis of 65 patients receiving lung SABR treatment to 85 targets, R50 recommendations ranging from 13.2 (for small targets) to 6 for volumes greater than 40cm^3 were made[234]. The study methodology consisted of more than one-half of the plans generated using a 3D conformal technique, and the remainder using a mix of VMAT and static IMRT techniques. The median R50 value for the 3D conformal techniques was 6.44 (range 5.62 – 7.74) compared to the IMRT/VMAT plans which had a significantly larger median R50 value of 7.25 (range 5.15 – 9.12) (p = 0.001). This difference in R50 value was attributed to the 3D conformal plan using combinations of planar and non-coplanar angles to avoid beam paths overlapping. The UK National Radiotherapy Trials QA Group have also proposed R50 values for lung and non-lung body sites[440]. According to this report, for lung sites, the R50 should range from 7 to 5, and for non-lung sites, the values should be from 5.5 to 4.5. Using the experience from lung SABR protocols with R50 guidelines, parameters such as calculation model, technique (VMAT or 3D conformal) and presence of heterogeneous media (such as air) can impact on the expected gradient index value. For these reasons, directly using R50 constraints based on lung SABR plans for abdominal targets may not be suitable. A summary of proposed R50 values from different institutions/trials is presented in Table 21.

Table 21 Recommended gradient index (R50) based on target volume size as proposed by RTOG 0236 study[394,441], RTOG 0813 study[439], ROSEL study[395], UK National Radiotherapy Trials QA Group[440], and the Peter MacCallum Cancer Centre/Northern Sydney Cancer Centre (PMCC/NSCC)[234].

Planning target volume, PTV (cc)/Max tumour dimension (cm)	RTOG 0236		RTOG 0813	ROSEL	UK National Radiotherapy Trials QA Group		PMCC/NSCC
	Lung (no heterogeneity correction)	Lung (with heterogeneity correction)	Lung	Lung (Type A algorithms)	Lung	Other	Lung
1.8 (2)	<3.9	<7	<5.9	<12 (<8)	7	5.5	<13.2
3.8 (2.5)	<3.9	<5.8	<5.5				

7.4 (3)	<3.9	<5.4	<5.1			
13.2 (3.5)	<3.9	<5.3	<4.7			<8.4
21.9 (4)	<3.8	<5.2	<4.5	<9 (<7)	5.5	4.5	<9
33.8 (4.5)	<3.7	<5.0	<4.3			
49.6 (5)	<3.6	<4.8	<4.0	<6 (<6)	5	4.5	<6
69.9 (5.5)	<3.5	<4.5	<3.5			
95.1 (6)	<3.3	<4.1	<3.3			
125.8 (6.5)	<3.1	<3.7	<3.1			
162.6 (7)	<2.9	<3.5	<2.9			

In chapter 4, plan quality analysis of the first 20 patients treated on the FASTRACK trial yielded a mean R50 value of 3.7 (+/-0.5) for targets less than 100cc in size and 4.3 (+/-0.4) for targets larger than 100cc in size. Compared to the R50 guidelines defined by the UK National Radiotherapy Trials QA Group[440] for non-lung sites, the R50 values reported in this thesis were within the expected value of less than 4.5 for volumes greater than 40cc in size. When compared to the RTOG 0236/0813[439,441] benchmark for volumes larger than 95.1cc, our values were larger at 4.3. But when compared to other institutions and clinical trials[234,395,440], these values were within the expected range (<5). It could be possible that differences in surrounding organs-at-risk can limit the field geometry for kidney targets compared to lung targets, thereby limiting the dose gradient achievable. In a retrospective study comparing R50 values for stereotactic lung plans against the RTOG 0813 R50 benchmarking values, 21/52 (40%) VMAT plans, limited to coplanar beam angles, failed to meet the RTOG study requirements. This is in comparison to 4 of 53 (7%) plans not meeting the requirement when using a mix of planar and non-coplanar beam angles[442]. For techniques such as VMAT which is often performed without non-coplanar angles, high-quality plans generated for fast treatment delivery can come at the cost of the R50 value. In another VMAT SABR lung study evaluating dose gradients for tumour volumes between 95cc to greater than 163cc (n = 18), the R50 value ranged from 3.61 to 3.72. This was much larger than that defined by the RTOG 0813 study with an expected range of 3.9 to 3.3[443]. This suggests that R50 metrics may need to re-consider the role of co-planar VMAT techniques and put less focus on non-coplanar beam arrangements.

There are limited studies which have published R50 values in the context of kidney SABR planning. In one particular planning study, fifteen patients with a mix of IMRT (co-planar and non-coplanar) and VMAT plans were generated for analysis[431]. The PTV volumes ranged from 14.4cc to 281.3cc. The authors found that for IMRT plans, the average R50 value was 5.6 (+/-2.32) compared to the VMAT technique which averaged 5.04 (+/-2.01). These values were much larger than our own and are most likely due to the use of a coplanar VMAT technique. SABR studies for other abdominal targets have also reported R50 values

similar to our own. In one study treating 35 patients for adrenal gland metastases, the median R50 value was 4 (range 3.1 - 9.1). Thirty-nine targets with a median volume of 50cc (range 7.9 - 352.9cc) were treated using either a VMAT or IMRT (coplanar/non-coplanar) approach[444]. Another study analysed planning metrics for 15 patients diagnosed with pancreatic tumours with an average PTV size of 135cc (ranging from 58.4 to 320cc)[445]. Treatment plans were generated using either a 9-field static IMRT (coplanar) or a single arc VMAT. The authors found that for an IMRT and VMAT technique, the mean R50 value was 4.5 (range: 3.6 - 5.3) and 4.3 (range: 3.1 – 5.9) respectively. More interesting, when VMAT plans were re-optimized to maximise sparing of the duodenum, the R50 value increased to a mean of 4.7 (range: 3.7 – 6.1) which was significantly larger when not purposely sparing the organ ($p < 0.05$). This finding suggests that dose constraints and proximity of the target to nearby critical structures can influence the R50 conformality of a plan. This could be the reason why R50 values in IMRT and VMAT plans are higher than what has been reported in our patient series.

With IMRT and VMAT technologies becoming more readily adopted for radiotherapy treatment[446-448], this approach would suit kidney stereotactic treatment as it would allow more conformal dose distribution around critical structures. In doing so, the expectations of R50 values could change. Using R50 values from lung studies to benchmark abdominal SABR plans would not be appropriate as differences in surrounding tissue constraints and tissue inhomogeneity can influence the dose gradient. Current literature on R50 values for kidney SABR targets should be used as guides rather than strict benchmarking requirements. Larger case series are needed to properly analyse any R50 trends with volume size, the technique used and proximity to organs at risk.

6.4 Image guidance and treatment

Similar to studies of kidney stereotactic treatment on a linac[288-290], the protocol from this thesis utilised CBCT imaging to visualise kidney tumour position directly before treatment. In the absence of fiducial markers implanted near the tumour, there is little evidence to support the use of bony anatomy as a surrogate for kidney position. Conventional treatment with large planning margins has used the 12th thoracic vertebrae down to the 5th lumbar vertebrae to identify the treatment area[35]. In a report describing kidney SABR treatment using the Cyberknife[TM] machine, the authors used vertebral body alignment for the kidney in one patient who did not have fiducial markers. The authors justified this approach by using abdominal compression to minimise kidney motion[284]. In chapter 5, we reported an average correction of 4.7 (+/-3.3) mm from the bony anatomy registration (2D imaging) to the kidney target. This may suggest a close relationship between the kidney position and nearby bony anatomy. However, there were still individuals requiring a shift greater than 10mm to correctly match to the kidney tumour. In a similar study reporting localization accuracy for kidney and adrenal targets, the 95% confidence interval for CBCT correction required for treatment was less than 2.1mm and less than 0.8 degrees[420]. These two reports suggest that bony anatomy, as a surrogate for kidney tumour position, is possible with a PTV margin of 5mm. The use of bony anatomy verification should only be used under specific conditions such as minimal kidney motion at planning, presence of abdominal compression, and if possible, ability to verify breathing amplitude on

treatment against the planning value. One advantage of cone-beam CT imaging is the ability to verify ITV margins at treatment. As CBCT acquisition is acquired over multiple breathing sequences, motion artefacts can appear on the reconstructed image. In chapter 5, we reported the use of the probability density function (PDF) of the right diaphragm/liver as a surrogate for ITV motion margin. For all but one patient, the mean difference in breathing motion from planning to treatment was less than 2mm. The patient who had a large difference in breathing amplitude underwent a new planning scan with corrected breathing instructions. Quantifying the PDF of the right diaphragm was first described by Guckenberger et al[272] to verify liver ITV margin before treatment. In this study, eleven patients with 13 tumours were treated with either a single (26Gy or 30Gy) or three fraction (37.5Gy or 45Gy) regimen. All patients underwent a 4DCT for planning with a 3D conformal technique using five to seven planar/non-coplanar beams. A CBCT was acquired before and after treatment to localise to the liver volume, and as well, to quantify any PDF differences between planning and treatment. The authors found no systematic difference between the mean planning, pre-treatment and post-treatment breathing amplitude values at 11 (+/-5) mm, 11 (+/-5) mm and 12 (+/-4) mm respectively. Verification of ITV (or breathing margins) has to date been performed in a limited fashion using fluoroscopic imaging[449,450] and 4D CBCT for lung tumours[199,451,452]. The image quality of 4D CBCT is still susceptible to motion artefacts, thereby limiting its use in the abdominal setting[453,454]. Beyond our implementation of ITV verification for kidney SABR treatment, there has still been little work done to investigate the role of margin verification for kidney stereotactic treatment. Our case report, presented in the Appendix 9.2, highlights the impact of a change in breathing amplitude. A large change in breathing motion, not only changed the location of the target but also deformed the PTV, consequently affecting the coverage and dose to nearby bowel structures.

Margin verification is only required in studies that use a motion-inclusive planning protocol. Tumour tracking or gating protocols do not need this as motion is compensated actively by either continuous beam tracking of the target[278,282,285], or by selectively treating to a specific phase of the breathing cycle[280]. The effectiveness of these protocols is dependent on fiducial markers acting as tumour surrogates. Kilovoltage imaging systems, such as the Cyberknife™ (Accuray, USA) and Novalis® (Brainlab®, Germany) systems have floor-mounted imagers that allow continuous imaging of the target, regardless of the patient position during treatment. Fiducial marker insertion has its own risk of complication including abdominal pain, haemorrhage and seed migration[425,455]. Brook et al[424] examined the safety profile and technical success of CT and ultrasound-guided percutaneous insertion of fiducial markers into 188 patients. Of the 38 patients who had one or two fiducials inserted near the kidney, two (5%) experienced a minor complication (small haematoma) and one a major complication (bleeding) which required hospitalisation. The author's measure of technical failure was based on reports of seed migration outside of the intended targeted region which would render it unusable for stereotactic treatment. In the kidney study group, 3 of 38 (7.8%) patients showed seed migration resulting in a 92.2% technical success rate. There are advantages and disadvantages when using fiducial markers for treatment verification. The eligibility for fiducial marker insertion, risk of complication and seed migration need to be weighed against the overall treatment benefit. The role of fiducial markers on the linac is limited, especially when CBCT imaging is available for target localisation.

CBCT imaging not only provides direct visualisation of the target, but also provides additional information on the position of surrounding organs-at-risk which may have changed from planning. Similarly, a breath-hold protocol requires no ITV margin verification. Funayama *et al*[290] used a breath-hold protocol for kidney stereotactic treatment on a linac combining it with fast CT-on-rails imaging for target volume localisation. CT-on-rails allow image acquisition at a rate of five seconds per slice[456], as opposed to CBCT imaging which can take between one to two minutes depending on the imaging protocol and vendor used[456]. This longer image acquisition time can limit the feasibility of using CBCT for verification of kidney targets under breath-hold treatment. The effectiveness of breath-hold CBCT is not always guaranteed as shown in the report by Zhong *et al*[457]. In this study, 121 patients were screened for the feasibility of lung SABR treatment with breath-hold using the Active Breathing Controller (Elekta, Sweden). Patients were excluded if target motion was less than 5mm or if they were unable to maintain a breath hold of at least 40 seconds. Of the 121 patients, only 83 (68%) patients were eligible for a breath-hold treatment. In a similar study, Eccles *et al*[208] used the Active Breathing Controller (Elekta, Sweden) to assist with breath-hold for liver stereotactic treatment. The study was able to qualify 21 of 34 (62%) patients for a breath-hold based protocol. A breath-hold strategy for kidney stereotactic treatment would benefit from using fast treatment delivery techniques, such as VMAT, combined with ultra-high dose rates of 1200 to 2400 monitor units per minute. This has been shown in a study describing a lung VMAT breath-hold technique combined with a high dose rate of 2400 MU/min (10MV flattening-filter-free beam) to deliver a single dose of 25Gy in an average of 241 seconds[458].

Real-time visualisation of the kidney target can also negate the use of ITV verification. The integration of cine MRI imaging on a linac can provide continuous organ motion assessment. For the kidney target, tracking and correcting for its displacement can bring the motion margin down from 6.1mm to 1.5mm[302]. In one of the first reports of kidney stereotactic treatment on an integrated MR-linac, Rudra *et al* [303] treated a kidney lesion with a 5mm PTV margin around the gross tumour volume. The PTV margin operated as a treatment boundary, stopping the beam if the tumour moved beyond this threshold (Figure 21).
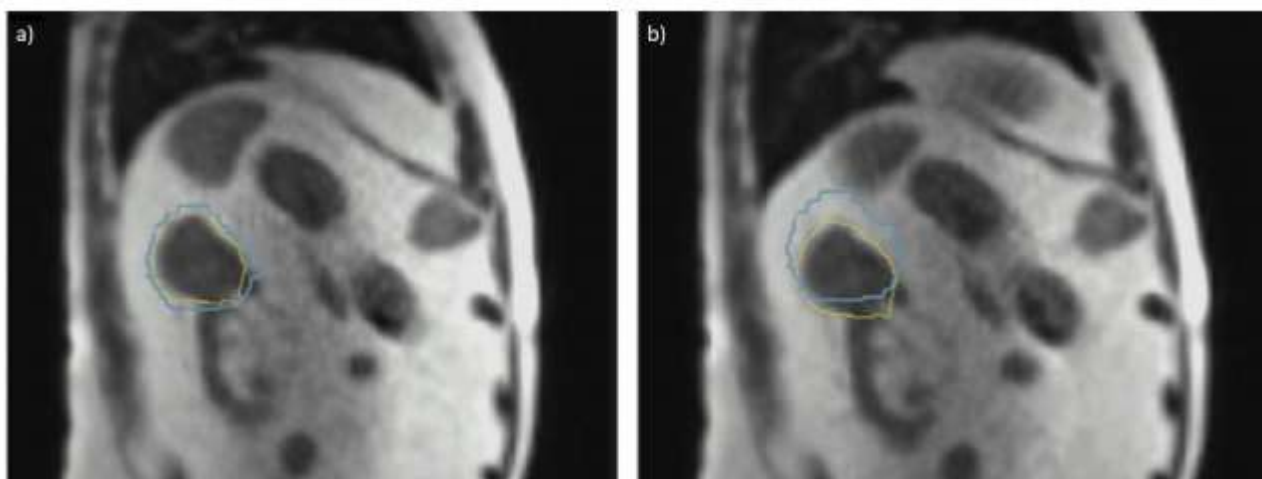
Figure 21. Real-time MRI imaging (0.35T) of a left kidney lesion on an integrated MRI-linac (Viewray, California).

A gating boundary was defined (light blue) for the GTV (a). If the GTV was found to be outside of this boundary, the beam would turn off (b)[303].

Image verification for kidney stereotactic treatment is important as the use of single or small treatment fractions leave little room for error. A linac-based treatment approach can utilise integrated CBCT imaging technologies to visualise not only kidney position but as well as screen for any breathing amplitude changes. CBCT imaging, however, is still limited by acquisition performed at specific time points. Continuous target verification, as is the case with fiducial marker tracking, can further reduce planning margins. New technologies, such as the MRI-linac, allow continuous volumetric image acquisition without the need for fiducial markers. This is a developing area of interest and can potentially be used to generate further understanding of intrafraction kidney motion.

6.5 Side effects of treatment

In chapter 4 we have discussed the acute toxicity observed in the first 20 patients treated on the FASTRACK study. Within the first six months after treatment, there was no toxicity higher than grade 3 reported. Twelve of 20 (60%) patients reported some side effect, while the remaining were asymptomatic. The most common side effects reported were chest wall pain, nausea and tiredness. The final report from the FASTRACK study showed that the most common side effect observed post-treatment was grade 1 chest wall pain (n = 15) followed by grade 1 nausea (n = 14)[317]. The risk of injury from chest wall pain has been reported in patients undergoing stereotactic radiotherapy for lung tumours[459-463]. An analysis of 48 patients treated for lung stereotactic radiotherapy to a dose of 60Gy in 3 fractions, showed 10 (21%) patients reporting grade 1 chest wall pain, and 6 (12.5%) reporting grade 2 pain[461]. The authors found a significant correlation between the volume of chest wall receiving 30Gy and 60Gy, recommending a constraint of V30 to $\leq$30cm^3 and V60 to $\leq$3cm^3 to predict a 10 to 15% risk of late chest wall toxicity. In a similar study using a dose of 21 to 60Gy in three to five fractions, a 30% risk of severe chest wall toxicity was observed when the chest wall received more than 30Gy to 35cm^3 of its volume[463]. Other kidney SABR publications have not detailed

incidences of chest wall pain[150,274-280,282,284-288,305,464]. The incidences in our study were all grade 1 (mild discomfort) which may have been under-reported by these other studies, concerned more with grade 2 or higher toxicity[278,280]. When comparing our results with stereotactic radiotherapy for liver targets, a small number of publications have reported incidences of chest wall pain ranging from 2 to 14% (Table 22).

Table 22. A summary of publications reporting chest wall pain after liver/kidney stereotactic treatment

Author	Patient No.	Dose	Incidence	Technique
Pham et al[316]	20	26 – 42Gy (1 or 3 fx)	7 (35%)	3D CRT
Chang et al[465]	65(multi-institution)	22 – 60Gy (1 – 6 fx)	2 (3%)	3DCRT (Arcs/Static field)
Goodman et al[466]	26	18 – 30Gy (1 fx)	2 (7%)	Cyberknife™
Scorsetti et al[467]	61	75Gy (3fx)	1 (2%)	VMAT
Lee et al[178]	68	27.7 - 60Gy (6 fx)	2 (3%)	3DCRT/IMRT
Meyer et al[468]	14	35/40Gy in 1 fx)	2 (14%)	3DCRT/IMRT

In our cohort of patients, posterior chest wall pain was reported ipsilateral and contralateral to the target. Our reported planning technique shows a predominantly posterior beam arrangement using contralateral-oblique beams[316]. Posterior-oblique angles, passing through the vacuum bag could be a contributing factor to the chest wall pain. The vacuum bag is filled with radio-translucent beads which provide minimal beam attenuation. However, with enough transmission depth through the bag, the photon build-up effect could be negated, resulting in higher skin dose. This effect has been shown in a phantom study investigating the influence of immobilisation devices on skin dose. At a depth of 1mm below the surface of a water phantom, a 6MV beam passing through 1.5cm, 4.5cm and 6.5cm of BodyFix™ bag could increase the peak dose by 23%, 39% and 41% respectively[469]. The same effect has also been shown to increase to 101% of the peak

dose when larger field sizes are used[470]. The authors in these studies suggested introducing air gaps, less dense material or higher energies to reduce the dose close to the skin surface.

In stereotactic treatment of the kidneys, the risk of severe gastrointestinal toxicities can become a contraindication for radiotherapy treatment. In the FASTRACK study, two patients enrolled into the trial were unable to proceed with their treatment due to the proximity of the kidney lesion to the bowel, preventing a suitable SABR plan to be generated[317]. Studies of SABR treatment to the liver and pancreatic cancers, using a dose of 45Gy in three fractions, have reported grade 3 ulcerations and mucositis to the stomach, colon and duodenum. The plan dosimetry showed that these areas of grade 3 toxicity received more than 30Gy[471,472]. These findings suggest that, in the SABR setting, there is a maximum dose sensitivity to the bowel. In a single-fraction, dose-escalation study for pancreatic cancers, the use of 15 to 25Gy in one fraction treated for 15 patients, did not show any grade 3 toxicity. As part of the planning objective, the authors kept 50% of the dose away from the contralateral wall of the duodenum. This resulted in a mean dose of 14.5Gy and 22.5Gy to 50% and 5% of the duodenum respectively[473]. In a separate study investigating bowel-dose toxicity, 12/73(16.4%) patients, after receiving single-fraction SABR treatment to the pancreas, experienced grade 2 to 4 bowel toxicity. The authors found that a maximum dose of less than 23Gy to the duodenum showed a toxicity rate of 12% compared to 49% when exceeding 23Gy. Other predictors of (grade 2 to 4) toxicity were the duodenum volume receiving 15Gy and 20Gy which should be kept below 9.1cc and 3.3cc respectively in order to decrease the risk from 52% to 11%[474]. Dose-volume-histogram (DVH) risk maps have also been modelled to evaluate the risk of gastrointestinal toxicity[475,476]. In one such study, the treatment and outcome data from 175 patients, treated with SABR to various abdominal targets in one to five fractions, was used to generate bowel toxicity risk estimations. Within the dataset, there were seven incidences of grade 3 or higher gastrointestinal toxicity. Based on the maximum and volumetric dose to 5cc and 2cc of the bowel, the authors used normal tissue complication probability models to generate small bowel toxicity risk maps based on various fractionation schedules. For a single fraction regimen, a low risk (1.4%) of small bowel toxicity is considered when a maximum dose of 12Gy (to the bowel) is used. On the other hand, a high risk (8.2%) of toxicity is present if the maximum dose to the bowel is planned to 19Gy. Similarly, for a three fraction SABR protocol, low risk (3.6%) is considered when the maximum bowel dose is kept to less than 25.2Gy, whereas a high risk (7%) is seen when 30Gy is used.

There have been limited reports of gastrointestinal toxicity after stereotactic treatment to primary kidney cancers. In one study reporting the treatment for primary and metastatic renal cell carcinomas, one case of grade 4 gastric haemorrhage and one case each of grade 3 diarrhoea and stomach haemorrhage was reported[276]. The grade 4 toxicity was from an individual receiving treatment to a metastatic lesion in the pancreas which was located adjacent to stomach and duodenum. In another report, a single case of grade 4 duodenal ulcer was reported. The dose received to the duodenum was 54Gy over four fractions[285].

Despite the vast literature on bowel toxicity, there is minimal consensus for maximum and volumetric dose constraints for the gastrointestinal tract. In studies of kidney SABR treatment, not only were there variations

in dose constraints to the bowel, there were differences in bowel-organ structure delineation. Studies that used five fraction prescriptions have published a maximum dose constraint to the small bowel ranging from 25Gy to 35Gy with the volume receiving 5cc to be less than 18 to 25Gy[284,287,289,303]. Studies reporting three to four fraction prescriptions reported small bowel maximum dose constraints between 21 to 30Gy[276,278,285,308,317]. For single fraction prescriptions, the maximum dose to the bowel was reported to be between 13.9Gy and 19Gy[308,317]. The AAPM Task Group Report 101[160] for stereotactic treatment, recommended small bowel dose constraint to receive no more than 32Gy in five fractions and no more than 12.4Gy in one fraction. In the IROCK consensus statement, the maximum dose to small bowel in five fractions was 30Gy. For single fraction treatment, there was no maximum point dose defined, but there was a recommendation for no more than 20cc to receive 14Gy, and the circumferential volume to receive less than 12.5Gy[297].

Some institutions define the bowel constraint to a single continuous organ[279,288], whereas others separate the bowel into the duodenum, small bowel and large bowel[284,287,303]. Table 23 is a summary of these published constraints, grouped according to the total fraction number. Included in this table are the International Radiosurgery Consortium for Kidney (IROCK) consensus statement summarising dose constraints to organs at risk[297], the AAPM SBRT Task Group 101 organ dose constraint recommendations[160], and a SABR normal tissue constraint recommendation based on findings from the modern literature[477].

Apart from one study, which defined specific constraints for the duodenum, small bowel, large bowel and stomach[287], the specification of dose constraints to each of these organs vared across other studies[276,278,282,284,288,289,303,305,308,317]. Historical literature has indicated that the duodenum is the most radiosensitive gastrointestinal structure followed by the small intestine and then the large intestine[478]. Whether this sensitivity is still valid in high-dose ablative therapies requires further investigation. When the tumour target is adjacent to the duodenum, small bowel and large bowel, the manner in which organ dose constraints are defined can affect the final dosimetric outcome of the plan. Dose constraints imposed on the bowel as a single contiguous organ is considered a more conservative planning approach than when planning with dose constraints to each of the duodenum, small bowel and large bowel. When the planning volume abuts or overlaps with bowel structures, there is a lesser need to sacrifice PTV coverage to meet dose-volume constraints for three organs rather than the one. An example of this is seen in Figure 22.
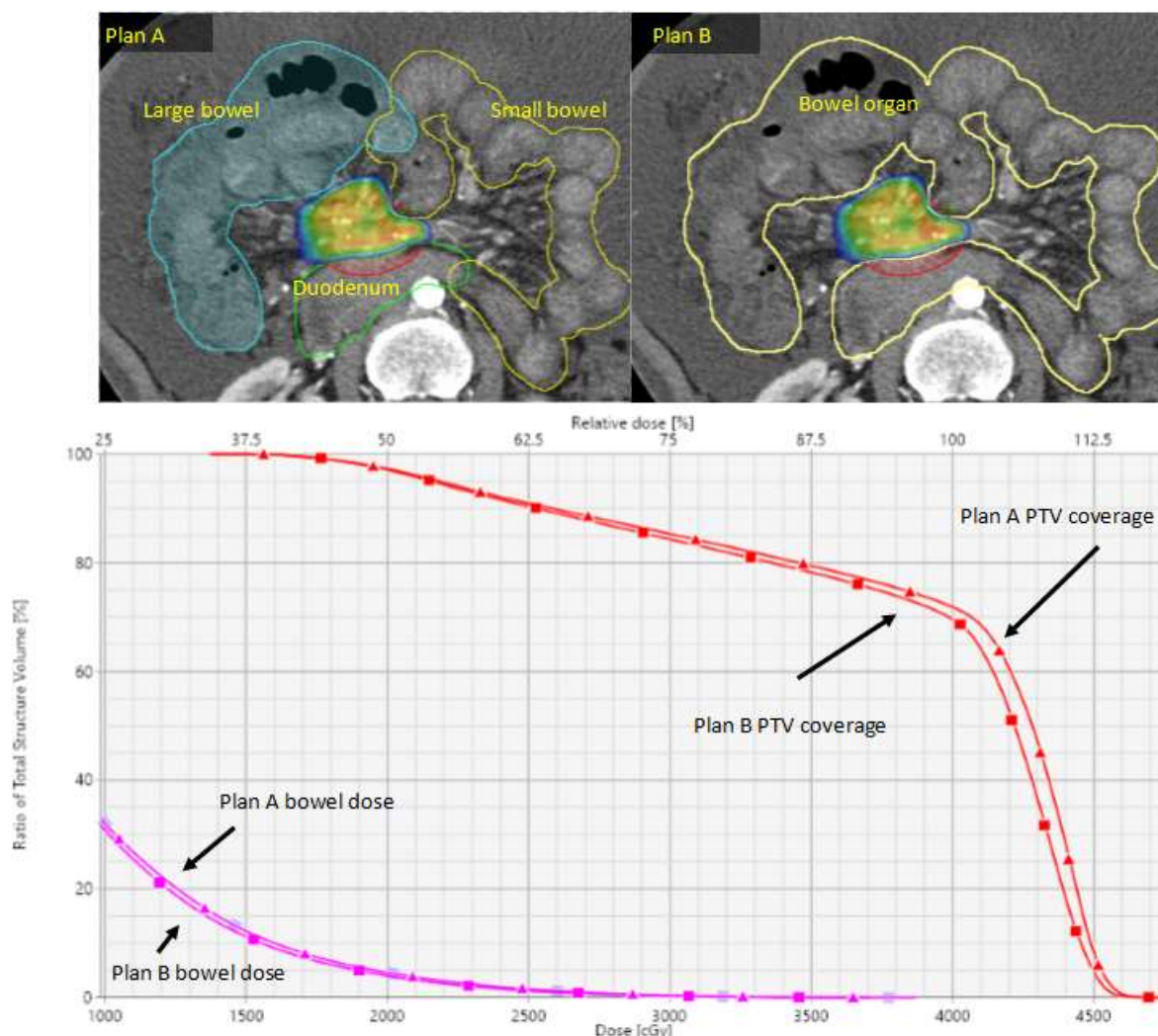
Figure 22. PTV coverage is less likely to be sacrificed when organ constraints are defined to specific sub-organs rather than to a single organ.

In this example, the constraint for gastrointestinal structures (duodenum, small bowel, large bowel or the bowel organ) is for 1cc to receive 33Gy or less. Plan A has been optimised so that the maximum dose to 1cc of the small bowel, duodenum and large bowel are at 31.8Gy, 32.9Gy and 31.8Gy respectively. The dose to 1cc of the bowel organ (sum of small bowel, duodenum and large bowel) is at 34.1Gy. The minimum volume receiving 100% of the dose is 72%. Plan B on the other hand, has been optimised so that 1cc of the bowel organ receives 32.9Gy. The coverage to the PTV is less than plan A, with only 69% of the volume receiving 100% of the dose. The dose to the small bowel, duodenum and large bowel is 29.8Gy, 32.3Gy and 30.4Gy respectively. *Source: Stanford Radiation Oncology Center*

Despite the relatively low incidences of bowel toxicity from kidney SABR treatment[479], there has been a concern with the cumulative toxic effect of antiangiogenic drugs with high-dose ablative therapies causing severe gastrointestinal related toxicities[480]. Targeted therapies aim to inhibit vascular endothelial growth factors (VEGF) from preventing tumour vasculature expansion. However, as VEGF plays a role in wound healing, its use after SABR treatment may inhibit the recovery of any small bowel injury caused by the radiation[480,481]. A review of abdominal SABR studies combined with antiangiogenic drugs (sorafenib and bevacizumab) identified four studies using prescriptions of 8 to 60Gy in one to five fractions. Late grade 3 to 5 bowel toxicity, within the treatment area, occurred as early as one week, and up to 17.2 months, after

treatment[480]. One report, documenting the use of SABR treatment to abdominal targets (28 to 60Gy in one to five fractions), identified 76 patients treated for 84 primary and metastatic lesions. Twenty-seven of 76 (35%)patients received a VEGF inhibitor before and within 13 months of completing radiotherapy treatment. Seven patients, all receiving the combination radiotherapy and systemic therapy, suffered from grade 3 to 5 gastrointestinal ulceration or perforation at a median of 4.6 months post-radiotherapy treatment[481]. Having said this, other reported series of targeted therapies combined with abdominal SABR treatment, have reported no grade 3 or higher gastrointestinal toxicity. This is despite more than 37% of patients receiving a VEGF inhibitor within 2 years (before and/or after) of treatment[475].

These examples from the literature show that the gastrointestinal system is sensitive to the maximum dose received and total-volume irradiation. However, there is still a gap in the literature with specific threshold doses levels. Maximum dose definitions can be expressed as dose-per-pixel, dose to 1cc of volume, or dose to 0.03cc or 0.35cc of volume, making dosimetric comparisons across studies challenging. Another challenge with quantifying dose-response assessment of the gastrointestinal system relates to the position of the organ at planning and treatment. Any changes from the time of planning to the time of treatment are unlikely to be captured without proper imaging tools to verify the organ[482]. 2D imaging of fiducial markers provides no volumetric information to assess changes in bowel anatomy. Cone beam CT image quality, providing valuable soft-tissue information, can be degraded by bowel gas[483,484]. The MR-linac, with superior soft tissue definition compared to CBCT imaging[485], has the potential to be used to investigate dose-response relationships of bowel structures[303,482].

Table 23. Summary of published dose constraints used in reports of SABR treatment for primary kidney cancers. Included are recommendations from IROCK[297], AAPM TG 101[160], Pollom *et al*[477] and from the work reported in this thesis[316].

Organ	Author	Fractions	Volume (cc)	Dose (Gy)	Max Dose (Gy)
Colon	Benedict [160]	1 fx	20cc	14.3	18.4
Duodenum	Benedict [160]	1 fx	5cc	11.2	12.4
Duodenum	Benedict [160]	1 fx	10cc	9	
Jejunum/ileum	Benedict [160]	1 fx	5cc	11.9	15.4
Large bowel	IROCK [297]	1 fx	alara		
Large bowel	IROCK [297]	1 fx			
Large bowel	Pham [316]	1 fx	10cc	9.6	
Large bowel	Pham [316]	1 fx	1cc	12.6	
Large bowel	Pham [316]	1 fx	0.035cc	13.9	
Small bowel	IROCK [297]	1 fx	<20cc	14	
Small bowel	IROCK [297]	1 fx	circumference	<12.5	
Small bowel	Senger [308]	1 fx	<5	10	19
Small bowel	Pham [316]	1 fx	30cc	12.5	
Stomach	IROCK [297]	1 fx	<10cc	11	
Stomach	IROCK [297]	1 fx	<5cc	22.5	
Stomach/intestine	Yamamoto [288]	10 fx	1	71	

Organ	Reference	Fx	Volume	Dose	Max/BED
Stomach/intestine	Yamamoto [288]	10 fx	10	52	
Stomach/intestine	Yamamoto [288]	10 fx	100	43	
Colon	Benedict [160]	3 fx	20cc	24	28.2
Duodenum	Benedict [160]	3 fx	5cc	16.5	22.2
Duodenum	Benedict [160]	3 fx	10cc	11.4	
Duodenum	Pollom [477]	3 fx	1cc	30	
Gastrointestinal	Svedman [279]	3 fx			21 (no more than 7Gy per fraction)
Jejunum/ileum	Benedict [160]	3 fx	5cc	17.7	25.2
Large bowel	IROCK [297]	3 fx	alara minimize volume >30Gy		
Large bowel	IROCK [297]	3 fx			
Small bowel	IROCK [297]	3 fx	10	11.4	30
Small bowel	IROCK [297]	3 fx	1	24	
Small bowel	Pollom [477]	3 fx	5	24.5	
Small bowel	Pollom [477]	3 fx	2	21	
Small bowel	Senger [308]	3 fx	<5	16	27
Small bowel	Pham [316]	3 fx	0.035	30	
Small bowel	Teh [278]	3 fx			24 (no more than 8Gy per fraction)
Small bowel	Wersall [276]	3 fx			21 (no more than 7Gy per fraction)
Stomach	IROCK [297]	3 fx	<10cc	16.5	30
Stomach	IROCK [297]	3 fx	<5cc	<22.5Gy	
Stomach	Teh [278]	3 fx			24 (no more than 8Gy per fraction)
Stomach	Wersall [276]	3 fx			21
Bowel	Ponsky/Grub	4 fx	≤1	24	
Stomach	Ponsky/Grub	4 fx	≤1	22	
Colon	Benedict [160]	5 fx	20cc	25	38
Duodenum	Benedict [160]	5 fx	5cc	18	32
Duodenum	Benedict [160]	5 fx	10cc	12.5	
Duodenum	Chang [287]	5 fx	<5	18	32
Duodenum	Pollom [477]	5 fx	1	35	
Jejunum/ileum	Benedict [160]	5 fx	5cc	18.5	35
Large bowel	Chang [287]	5 fx	<20	25	38
Large bowel	IROCK [297]	5 fx	<20cc	25	38
Large bowel	IROCK [297]	5 fx			60 (BED)
Large bowel	Lo [284]	5 fx	<5	25	29
Large bowel	Rudra [303]	5 fx	0.5	36	
Large bowel	Rudra [303]	5 fx	20	25	
Small bowel	Chang [287]	5 fx	<5	19.5	35
Small bowel	Correa [289]	5 fx	D99%	24	25
Small bowel	IROCK [297]	5 fx	<5	20	30
Small bowel	IROCK [297]	5 fx			60 (BED)
Small bowel	Lo [284]	5 fx	<5	25	29
Small bowel	Pollom [477]	5 fx	2	30	
Small bowel	Pollom [477]	5 fx	5	25	
Small bowel	Rudra [303]	5 fx	5	20	35
Stomach	Chang [287]	5 fx	<10	18	32
Stomach	IROCK [297]	5 fx	<5cc	18	30

123

Stomach	IROCK [297]	5 fx			60 (BED)
Stomach	Lo [284]	5 fx	<5	27	31
Stomach	Rudra [303]	5 fx	0.5	36	
Stomach	Rudra [303]	5 fx	10	18	

6.6 Future developments

The role of radiotherapy treatment for kidney cancer management has resurfaced with great interest in the last decade, a turnaround from the poor survival gains from studies during the 1970s and 1980s[35]. The prospective reports of stereotactic radiotherapy as primary management for kidney cancers[280-283,285,286,290,311] are based on patients considered medically inoperable or have refused surgery. A pooled analysis of 223 patients treated for primary kidney cancers using a SABR technique, reported the 4-year local control, 4-year cancer-specific survival and overall survival at 97.8%, 91.9% and 70.7% respectively[479]. This is in comparison to pooled outcome results from surgery and thermal ablative techniques, which have reported 5-year cancer-specific survival and 5-year overall survival rates at 96% and 91%, respectively[486]. Compared to surgery and thermal ablative therapies, the lower overall survival data from stereotactic treatment could be attributed to the patient selection criteria (i.e. tumour too large or patient co-morbidities) rather than inferiority of technique. There are currently no published data comparing stereotactic radiotherapy of the kidneys with surgery or thermal ablation, likely due to lack of consensus on best practice guidelines for kidney SABR. The International Radiosurgery Oncology Consortium for Kidney, formed from eight international institutions with a broad experience in stereotactic kidney treatment, published common guidelines for kidney SABR treatment. The patient selection criteria, recommended by the consortium, included: 1. Previous treatment to the kidney-abdominal area is a contraindication for SABR treatment; 2. A solitary kidney is not a contraindication for treatment; 3. Pre-treatment image guidance using soft tissue or fiducial surrogates is a must; and 4. Dose constraints must prioritise small bowel as a critical organ. The report also identified areas of practice that has seen variability among institutions. These differences included: GTV to PTV margins, motion management strategies, and more importantly, dose fractionation schedule[297]. This last factor could play an important role in future studies investigating the significance of fractionation schedules on toxicity and tumour control. In the pancreatic cancer setting, compared to single fraction SBRT, a multi-fraction SBRT regimen has been shown to be superior in reducing gastrointestinal toxicity, while maintaining similar rates of local control[487]. Multi-institutional pooled analysis comparing cancer-specific survival for multi fraction treatment of kidney SABR, compared to single fraction treatment, have shown poor cancer-specific survival (HR = 1.33, p = 0.011). This analysis, however, is limited by imbalances of patient age and baseline performance status. As well, the single fraction regimen was also more commonly used for smaller tumours (mean 37.1mm +/- 10.6), compared to multi-fraction regimen which was preferred for larger tumours(mean 50.9mm +/-37.6)[479].

Technological advances in planning and treatment delivery have seen a global adoption of advanced imaging and intensity-modulated planning practices[446-448,488]. The current state-of-the-art sees the

integration of real-time imaging with IMRT planning to allow the development of online adaptive treatment. This is the ability to recalculate, re-optimise and adapt the treatment plan to the patient's anatomy as visualised on the treatment couch, directly before treatment. In the stereotactic treatment of abdominal targets, online adaptive treatment could benefit tumours that are susceptible to changes in internal organ motion. Henke *et al*[482] reported the feasibility of using an integrated MRI-linac to adapt treatment plans directly before stereotactic treatment for abdominal (liver and non-liver) targets. The protocol allowed for dose escalation or de-escalation depending on the anatomy of the day. The authors found that 81/97 (83.5%) fractions were adapted before treatment. Seventy-five per cent of the adapted plans were carried out to change a dose constraint that was exceeded by anatomy changes on the day. The most common organ to prompt an adaptive replan was the small bowel at 37/81 (45%) fractions, followed by the stomach at 22/81 (27%) fractions, and the duodenum at 14/81 (17%) of fractions. Twenty-one of 81 (26%) fractions were adapted to increase the dose coverage to the PTV. In terms of dose escalation, three of 20 (15%) patients with liver targets were able to receive a higher dose prescription than initially planned for. The median on-table treatment time was 79 minutes, ranging from 36 to 160 minutes. An online-adaptive protocol may benefit kidney SABR plans that had to sacrifice PTV coverage to meet bowel dose constraints. In our FASTRACK study, two patients did not receive treatment as the proximity of the bowel to the PTV prevented a suitable plan to be generated[317]. The need to reduce coverage to the PTV or to reduce the total dose in kidney SABR treatment is not uncommon. In one report, only 5/11 (45%) patients were able to achieve more than 90% of the volume receiving the prescription dose of 40Gy in five fractions[289]. A similar study also reported 4/16 (25%) patients able to receive a prescription dose of 40Gy in five fractions. For the remaining patients, a dose of 30 to 35Gy was used to meet constraints to organs-at-risk[287]. As for the need to re-adapt to changes in bowel organ entering the treatment field, the relatively small number (1.3%) of grade 3 to 4 bowel toxicity reported, suggests a marginal gain with organ-at-risk led adaptation[479]. One other caveat with the online adaptive process is the extended treatment time. The reported median plan-and-treat time of 79 minutes by Henke *et al*[482], is almost twice the time reported in this thesis. How the kidney motion changes over extended treatment durations will require further investigation.

As stereotactic radiotherapy is a non-invasive approach compared to surgery, preservation of kidney function post-treatment is of great interest. Siva *et al*[479] reported minimal decreases in estimated GFR post treatment which is comparable to partial nephrectomy and thermal ablative techniques[479,489]. With the ability of modern planning systems to cross-reference dose to kidney function, the establishment of dose-response-relationships is made possible. This information would help guide motion management, planning margins and beam delivery techniques to minimise radiation to non-tumour kidney tissue. Our institutional investigation (Appendix 9.5) on a dose-response effect to the kidneys used single-photon emission computed tomography (SPECT) scans to monitor kidney function at baseline and post stereotactic treatment for 21 patients. Three-dimensional images of the kidney, with voxels representing glomerular filtration rates, were co-registered with the radiotherapy treatment plan. By registering the radiation dose plan to the SPECT image, each corresponding voxel would represent the kidney function after receiving a specific dose. Based on a median follow up measurement taken at 11.8 months, the authors found a significant

relationship ($r^2 = 0.29$, $p = 0.04$) with kidney function loss and the area receiving 50% of the prescription dose[490]. This finding suggests a dose-effect at intermediate to high doses rather than lower doses as having been previously reported[160,491,492]. Yamamoto *et al*[288] also investigated renal atrophy as a function of dose for 14 patients undergoing stereotactic treatment of the kidney. Using post-treatment CT scans taken at a median of 16.9 months (range: 12 – 21.8), the authors found a median post-treatment volume of 73.4 (range 41.5 – 144.6) % remaining. Based on dose prescriptions ranging from 50 to 70Gy in ten fractions, the authors found that the volume receiving 20 to 30Gy had the strongest correlation ($r < -0.7$, $p < 0.01$) with renal atrophy. The authors also found that kidney atrophy was greater for patients without fiducial markers compared to those with fiducial markers which showed median remaining kidney volumes of 71.4% (range 61.3 – 83.4%) and 87.5% (75.6 – 96.4%) respectively ($p = 0.02$)[288]. This difference in kidney atrophy for those with and without fiducial markers, suggests an importance in motion management strategy and treatment margins used in radiotherapy treatment.

Another area of developing interest is survival prognosis based on tumour histology. Survival outcome in surgical series have suggested poorer prognosis with clear cell type kidney cancers compared to papillary/chromophobe types[493-495]. In the radiotherapy setting, there may be an opportunity to investigate the dose sensitivity of renal cell carcinomas based on their histology. One study has shown a greater percentage of patients (86%) showing complete responses to kidney SABR treatment when the histology has been of transitional cell type compared to those with renal cell type (20%)[286]. In the IROCK pooled analysis report of kidney SABR treatment outcomes, a better prognosis was observed for papillary type tumours (HR = 0.45) compared to clear cell, and worse for all other non-papillary and non-clear cell (HR = 2.08). However, this was not found to be statistically significant ($p = 0.171$)[479]. A histology-based dose-optimisation strategy has already been investigated for lung cancers showing dose threshold differences between a squamous cell and adenocarcinoma type cancers[496-498]. Future prospective studies, with pathological confirmation of disease, could inform ideal dose scheduling based on tumour pathology. For tumour histology more sensitive to high dose radiation, a lower dose prescription could be used, thereby minimising toxicity to the bowel and healthy kidney. For tumour histology that shows greater radio-resistance, a more aggressive dose approach, such as single fraction high-dose or adaptive radiotherapy, could be used.

The role of combined modality treatments for immunotherapy drugs and radiotherapy to treat primary and metastatic disease has also been investigated[499]. Compared to standard fractionation radiotherapy, high doses of radiation to tumours in animal models, have been shown to prime T-cell production in lymph nodes[500,501]. This, combined with an immunotherapeutic agent, can dramatically increase the systemic response to target cancers beyond the primary disease site, otherwise known as the abscopal effect[502]. Case study reports, describing the use of SABR treatment to primary and metastatic kidney lesions, have shown the abscopal effect triggering regression of disease located out-of-field[503-505]. Immuno-radiotherapy treatment for kidney cancer patients could potentially improve disease-free and overall survival in a manner that combination surgery and immunotherapy could not[128,506,507]. Clinical trials investigating combination

immunotherapy and SABR treatment for renal carcinomas are currently ongoing[508]. The outcome from these studies will be important to inform best practice protocols as local and distant recurrence rates for patients managed by surgery range can range between 20 to 64%[509-511].

Chapter 7

Conclusion

With the rise in kidney cancers globally, it is important to define new and safe treatment therapies. Surgery and ablative therapies are the current standards of care for early-stage kidney cancers, and more recently stereotactic ablative body radiotherapy has become a safe and feasible option for patients unsuitable for or refusing surgery. The clinical outcome for stereotactic treatment has been reported for several different delivery platforms including robotic radiosurgery, particle accelerators and linear accelerators. There are, however, minimal technical guidelines to help inform implementation on these delivery systems, specifically the linear accelerator.

The work in this thesis contributes to the field of linac-based kidney stereotactic treatment by providing technical reports focusing on motion management, 3D conformal planning and 4D image-guidance at treatment. The need to investigate these keys areas are highlighted in each chapter. The complex motion characteristic of the kidney is summarised in chapter 2. Kidney motion can vary according to breathing instructions. It can be as large as 76mm under deep breathing or be less than 5mm with shallow breathing. Controlling the amount of kidney motion can be done with devices that exert abdominal compression. In chapter 3, a dual vacuum compression system was shown to be useful to compress the abdomen, reducing overall kidney motion. In chapter 5, the same device was able to demonstrate patient intrafraction motion of less than 5mm on treatment. This supported the use of reduced planning margins to minimise dose to surrounding healthy tissue.

Compared to robotic radiosurgery and particle accelerators, achieving high dose conformality on a linear accelerator can be challenging with a 3D conformal technique. In chapter 4, the use of coplanar and non-coplanar angles, under the guidance of the R50 plan quality metric, was able to achieve intermediate dose conformality equivalent to those of IMRT and VMAT plans.

An important requirement in stereotactic ablative body radiotherapy is the verification of soft tissue targets directly before treatment. Chapter 5 demonstrated the use of CBCT technology to visualise and localise to kidney targets directly before treatment. Also, ITV margin verification using a novel tool was made at the

treatment console to measure diaphragm motion from the CBCT image. Few studies have reported the use of ITV margin verification on treatment, so this was an important and unique procedure. The dosimetric impact of a change in breathing amplitude on treatment is highlighted in a case study reported in Appendix 9.2.

The work described in this thesis can be adapted to any modern facility with a linear accelerator integrated with advanced 3D imaging capabilities. There are still many areas of ongoing technical development that could improve this linac-based approach for kidney stereotactic treatment. Breath-hold for motion management, online adaptive treatment, infraction motion monitoring using cine MRI imaging are but some of the developing technologies. Further research with these technologies could be used to answer clinical questions such as gastrointestinal and healthy kidney tissue tolerances, optimal dose fractionation schedules and the role of tumour histology and dose escalation.

Chapter 8

References

1.   Bray F, Ferlay J, Soerjomataram I, Siegel RL, Torre LA, Jemal A. Global cancer statistics 2018: GLOBOCAN estimates of incidence and mortality worldwide for 36 cancers in 185 countries. CA: A Cancer Journal for Clinicians. 2018;68(6):394-424.

2.   (AIHW) AIoHaW. Cancer data in Australia Canberra:: AIHW; 2018 [Available from: https://www.aihw.gov.au/reports/cancer/cancer-data-in-australia/.

3.   Siegel RL, Miller KD, Jemal A. Cancer statistics, 2016. CA: A Cancer Journal for Clinicians. 2016;66(1):7-30.

4.   Cancer registration statistics, England: 2017: Office for National Statistics; 2019 [Available from: https://www.ons.gov.uk/peoplepopulationandcommunity/healthandsocialcare/conditionsanddiseases/bulletins/cancerregistrationstatisticsengland/2017.

5.   Wong MCS, Goggins WB, Yip BHK, Fung FDH, Leung C, Fang Y, et al. Incidence and mortality of kidney cancer: temporal patterns and global trends in 39 countries. Scientific Reports. 2017;7(1):15698.

6.   Moreno CC, Hemingway J, Johnson AC, Hughes DR, Mittal PK, Duszak R. Changing Abdominal Imaging Utilization Patterns: Perspectives From Medicare Beneficiaries Over Two Decades. Journal of the American College of Radiology. 2016;13(8):894-903.

7.   Rosman DA, Duszak R, Wang W, Hughes DR, Rosenkrantz AB. Changing Utilization of Noninvasive Diagnostic Imaging Over 2 Decades: An Examination Family–Focused Analysis of Medicare Claims Using the Neiman Imaging Types of Service Categorization System. American Journal of Roentgenology. 2017;210(2):364-8.

8.   Barrett TW, Schierling M, Zhou C, Colfax JD, Russ S, Conatser P, et al. Prevalence of incidental findings in trauma patients detected by computed tomography imaging. The American Journal of Emergency Medicine. 2009;27(4):428-35.

9.   Pinsky PF, Dunn B, Gierada D, Nath PH, Munden R, Berland L, et al. Incidental renal tumours on low-dose CT lung cancer screening exams. Journal of Medical Screening. 2016;24(2):104-9.

10.   Porena M, Vespasiani G, Rosi P, Costantini E, Virgili G, Mearini E, et al. Incidentally detected renal cell carcinoma: role of ultrasonography. Journal of clinical ultrasound : JCU. 1992;20(6):395-400.

11.   Swensen SJ, Jett JR, Hartman TE, Midthun DE, Sloan JA, Sykes A-M, et al. Lung Cancer Screening with CT: Mayo Clinic Experience. Radiology. 2003;226(3):756-61.

12.   Hunt JD, van der Hel OL, McMillan GP, Boffetta P, Brennan P. Renal cell carcinoma in relation to cigarette smoking: Meta-analysis of 24 studies. International Journal of Cancer. 2005;114(1):101-8.

13.   Cumberbatch MG, Rota M, Catto JWF, La Vecchia C. The Role of Tobacco Smoke in Bladder and Kidney Carcinogenesis: A Comparison of Exposures and Meta-analysis of Incidence and Mortality Risks. European Urology. 2016;70(3):458-66.

14.   Wang F, Xu Y. Body mass index and risk of renal cell cancer: A dose-response meta-analysis of published cohort studies. International Journal of Cancer. 2014;135(7):1673-86.

15.   Flaherty KT, Fuchs CS, Colditz GA, Stampfer MJ, Speizer FE, Willett WC, et al. A Prospective Study of Body Mass Index, Hypertension, and Smoking and the Risk of Renal Cell Carcinoma (United States). Cancer Causes & Control. 2005;16(9):1099-106.

16.   Weikert C, Boeing H, Pischon T, Weikert S, Palli D, Vineis P, et al. Blood Pressure and Risk of Renal Cell Carcinoma in the European Prospective Investigation into Cancer and Nutrition. American Journal of Epidemiology. 2007;167(4):438-46.

17.   Abarca-Gómez L, Abdeen ZA, Hamid ZA, Abu-Rmeileh NM, Acosta-Cazares B, Acuin C, et al. Worldwide trends in body-mass index, underweight, overweight, and obesity from 1975 to 2016: a

pooled analysis of 2416 population-based measurement studies in 128·9 million children, adolescents, and adults. The Lancet. 2017;390(10113):2627-42.

18.   Prentice AM. The emerging epidemic of obesity in developing countries. International Journal of Epidemiology. 2005;35(1):93-9.

19.   Bilano V, Gilmour S, Moffiet T, d'Espaignet ET, Stevens GA, Commar A, et al. Global trends and projections for tobacco use, 1990–2025: an analysis of smoking indicators from the WHO Comprehensive Information Systems for Tobacco Control. The Lancet. 2015;385(9972):966-76.

20.   Lopez-Beltran A, Scarpelli M, Montironi R, Kirkali Z. 2004 WHO Classification of the Renal Tumors of the Adults. European Urology. 2006;49(5):798-805.

21.   Crino PB, Nathanson KL, Henske EP. The Tuberous Sclerosis Complex. New England Journal of Medicine. 2006;355(13):1345-56.

22.   Linehan WM, Srinivasan R, Schmidt LS. The genetic basis of kidney cancer: a metabolic disease. Nature Reviews Urology. 2010;7:277.

23.   Ferlay J, Ervik M, Lam F, Colombet M, Mery L, Pineros M, et al. Global Cancer Observatory: Cancer Tomorrow Lyon, France: International Agency for Research on Cancer; 2018 [Available from: https://gco.iarc.fr/tomorrow.

24.   Hock LM, Lynch J, Balaji KC. Increasing incidence of all stages of kidney cancer in the last 2 decades in the United States: an analysis of surveillance, epidemiology and end results program data. J Urol. 2002;167(1):57-60.

25.   SEER Cancer Statistics Review, 1975 - 2016 [Internet]. National Cancer Insitute. 2018. Available from: https://seer.cancer.gov/statfacts/html/kidrp.html.

26.   Levi F, Ferlay J, Galeone C, Lucchini F, Negri E, Boyle P, et al. The changing pattern of kidney cancer incidence and mortality in Europe. BJU International. 2008;101(8):949-58.

27.   Doeuk N, Guo DY, Haddad R, Lau H, Woo HH, Bariol S, et al. Renal cell carcinoma: stage, grade and histology migration over the last 15 years in a large Australian surgical series. BJU International. 2011;107(9):1381-5.

28.   Kane CJ, Mallin K, Ritchey J, Cooperberg MR, Carroll PR. Renal cell cancer stage migration. Cancer. 2008;113(1):78-83.

29.   National Cancer Database [Internet]. American College of Surgeons. 2016. Available from: https://www.facs.org/quality-programs/cancer/ncdb/publicaccess.

30.   SEER Cancer Stat Facts: Kidney and Renal Pelvis Cancer Bethesda, MD: National Cancer Institute; [Available from: https://seer.cancer.gov/statfacts/html/kidrp.html.

31.   Gill IS, Kavoussi LR, Lane BR, Blute ML, Babineau D, Colombo Jr JR, et al. Comparison of 1,800 Laparoscopic and Open Partial Nephrectomies for Single Renal Tumors. The Journal of Urology. 2007;178(1):41-6.

32.   Lane BR, Gill IS. 5-Year Outcomes of Laparoscopic Partial Nephrectomy. The Journal of Urology. 2007;177(1):70-4.

33.   Olweny EO, Park SK, Tan YK, Best SL, Trimmer C, Cadeddu JA. Radiofrequency Ablation Versus Partial Nephrectomy in Patients with Solitary Clinical T1a Renal Cell Carcinoma: Comparable Oncologic Outcomes at a Minimum of 5 Years of Follow-Up. European Urology. 2012;61(6):1156-61.

34.   Ljungberg B, Albiges L, Abu-Ghanem Y, Bensalah K, Dabestani S, Fernandez-Pello S, et al. European Association of Urology Guidelines on Renal Cell Carcinoma: The 2019 Update. Eur Urol. 2019;75(5):799-810.

35.   Tunio MA, Hashmi A, Rafi M. Need for a new trial to evaluate postoperative radiotherapy in renal cell carcinoma: a meta-analysis of randomized controlled trials. Annals of Oncology. 2010;21(9):1839-45.

36.   Zhuo JL, Li XC. Proximal nephron. Comprehensive Physiology. 2013;3(3):1079-123.

37.   SEER Cancer Stat Facts: Kidney and Renal Pelvis Cancer Bethesda, MD, USA: National Cancer Institute; [Available from: https://seer.cancer.gov/statfacts/html/kidrp.html.

38.   OpenStax. 2013. In: Anatomy and Physiology [Internet]. OpenStax. Available from: https://opentextbc.ca/anatomyandphysiology/.

39.   Eble J, Sauter G, Epstein J, Sesterhenn I, editors. Pathology and Genetics of Tumours of the Urinary System and Male Genital Organs. Lyon: IARC Press; 2004.

40.   Moch H, Cubilla AL, Humphrey PA, Reuter VE, Ulbright TM. The 2016 WHO Classification of Tumours of the Urinary System and Male Genital Organs—Part A: Renal, Penile, and Testicular Tumours. European Urology. 2016;70(1):93-105.

41.   Himmelman JG, Merrimen J, Matheson K, Theriault C, Wood LA. Accuracy of kidney cancer diagnosis and histological subtype within Canadian cancer registry data. Canadian Urological Association journal = Journal de l'Association des urologues du Canada. 2017;11(9):E326-E9.

42.   Muglia VF, Prando A. Renal cell carcinoma: histological classification and correlation with imaging findings. Radiologia brasileira. 2015;48(3):166-74.

43.   AJCC Cancer Staging Manual. Mahul B. Amin MF, editor: Springer International Publishing; 2017.

44.   Fuhrman SA, Lasky LC, Limas C. Prognostic significance of morphologic parameters in renal cell carcinoma. The American journal of surgical pathology. 1982;6(7):655-63.

45.   Campbell S, Uzzo RG, Allaf ME, Bass EB, Cadeddu JA, Chang A, et al. Renal Mass and Localized Renal Cancer: AUA Guideline. J Urol. 2017;198(3):520-9.

46.   Xing M, Kokabi N, Zhang D, Ludwig JM, Kim HS. Comparative Effectiveness of Thermal Ablation, Surgical Resection, and Active Surveillance for T1a Renal Cell Carcinoma: A Surveillance, Epidemiology, and End Results (SEER)–Medicare-linked Population Study. Radiology. 2018;288(1):81-90.

47.   Pierorazio PM, Johnson MH, Patel HD, Sozio SM, Sharma R, Iyoha E, et al. Management of Renal Masses and Localized Renal Cancer: Systematic Review and Meta-Analysis. The Journal of Urology. 2016;196(4):989-99.

48.   Huang WC, Levey AS, Serio AM, Snyder M, Vickers AJ, Raj GV, et al. Chronic kidney disease after nephrectomy in patients with renal cortical tumours: a retrospective cohort study. Lancet Oncol. 2006;7(9):735-40.

49.   Zini L, Perrotte P, Capitanio U, Jeldres C, Shariat SF, Antebi E, et al. Radical versus partial nephrectomy. Cancer. 2009;115(7):1465-71.

50.   Go AS, Chertow GM, Fan D, McCulloch CE, Hsu C-y. Chronic Kidney Disease and the Risks of Death, Cardiovascular Events, and Hospitalization. New England Journal of Medicine. 2004;351(13):1296-305.

51.   Mir MC, Derweesh I, Porpiglia F, Zargar H, Mottrie A, Autorino R. Partial Nephrectomy Versus Radical Nephrectomy for Clinical T1b and T2 Renal Tumors: A Systematic Review and Meta-analysis of Comparative Studies. European Urology. 2017;71(4):606-17.

52.   Breau RH, Crispen PL, Jimenez RE, Lohse CM, Blute ML, Leibovich BC. Outcome of Stage T2 or Greater Renal Cell Cancer Treated With Partial Nephrectomy. The Journal of Urology. 2010;183(3):903-8.

53.   Jeldres C, Patard J-J, Capitanio U, Perrotte P, Suardi N, Crepel M, et al. Partial Versus Radical Nephrectomy in Patients With Adverse Clinical or Pathologic Characteristics. Urology. 2009;73(6):1300-5.

54.   Kopp RP, Mehrazin R, Palazzi KL, Liss MA, Jabaji R, Mirheydar HS, et al. Survival outcomes after radical and partial nephrectomy for clinical T2 renal tumours categorised by R.E.N.A.L. nephrometry score. BJU International. 2014;114(5):708-18.

55.   Margulis V, Tamboli P, Jacobsohn KM, Swanson DA, Wood CG. Oncological efficacy and safety of nephron-sparing surgery for selected patients with locally advanced renal cell carcinoma. BJU International. 2007;100(6):1235-9.

56.   Mühlbauer J, Kowalewski K-F, Walach MT, Porubsky S, Wessels F, Nuhn P, et al. Partial nephrectomy preserves renal function without increasing the risk of complications compared with radical nephrectomy for renal cell carcinomas of stages pT2–3a. International Journal of Urology. 2020;n/a(n/a).

57.   Van Poppel H, Da Pozzo L, Albrecht W, Matveev V, Bono A, Borkowski A, et al. A prospective, randomised EORTC intergroup phase 3 study comparing the oncologic outcome of elective nephron-sparing surgery and radical nephrectomy for low-stage renal cell carcinoma. Eur Urol. 2011;59(4):543-52.

58.   Hemal AK, Kumar A, Kumar R, Wadhwa P, Seth A, Gupta NP. Laparoscopic versus open radical nephrectomy for large renal tumors: a long-term prospective comparison. J Urol. 2007;177(3):862-6.

59.	Seung Hyun J, Tae Gyun K, Koon Ho R, Gyung Tak S, Wan L, Jae Sung L, et al. Comparison of laparoscopic versus open radical nephrectomy for large renal tumors: a retrospective analysis of multi-center results. BJU International. 2011;107(5):817-21.

60.	Clark PE, Schover LR, Uzzo RG, Hafez KS, Rybicki LA, Novick AC. Quality of life and psychological adaptation after surgical treatment for localized renal cell carcinoma: impact of the amount of remaining renal tissue. Urology. 2001;57(2):252-6.

61.	Peyronnet B, Seisen T, Oger E, Vaessen C, Grassano Y, Benoit T, et al. Comparison of 1800 Robotic and Open Partial Nephrectomies for Renal Tumors. Annals of Surgical Oncology. 2016;23(13):4277-83.

62.	Chan DY, Cadeddu JA, Jarrett TW, Marshall FF, Kavoussi LR. LAPAROSCOPIC RADICAL NEPHRECTOMY: CANCER CONTROL FOR RENAL CELL CARCINOMA. The Journal of Urology. 2001;166(6):2095-100.

63.	Tan H-J, Norton EC, Ye Z, Hafez KS, Gore JL, Miller DC. Long-term Survival Following Partial vs Radical Nephrectomy Among Older Patients With Early-Stage Kidney Cancer. JAMA. 2012;307(15):1629-35.

64.	Albqami N, Janetschek G. Indications and contraindications for the use of laparoscopic surgery for renal cell carcinoma. Nature Clinical Practice Urology. 2006;3(1):32-7.

65.	Capitanio U, Zini L, Perrotte P, Shariat SF, Jeldres C, Arjane P, et al. Cytoreductive partial nephrectomy does not undermine cancer control in metastatic renal cell carcinoma: a population-based study. Urology. 2008;72(5):1090-5.

66.	Hennessey DB, Bolton EM, Thomas AZ, Manecksha RP, Lynch TH. The Effect of Obesity and Increased Waist Circumference on the Outcome of Laparoscopic Nephrectomy. Adv Urol. 2017;2017:3941727-.

67.	Chen K, Wang J, Dai J, Luo A, Tian Y, Guan Z, et al. Anesthetic management of radical nephrectomy in patients with renal cell carcinoma involving renal vein or inferior vena cava. Tumori Journal.0(0):0300891619839295.

68.	Fergany AF, Saad IR, Woo L, Novick AC. Open Partial Nephrectomy for Tumor in a Solitary Kidney: Experience With 400 Cases. The Journal of Urology. 2006;175(5):1630-3.

69.	Bensalah K, Sadiq A, Guille F, Lobel B, Patard JJ. [Risks and benefits of total nephrectomy in elderly patients over the age of 80]. Progres en urologie : journal de l'Association francaise d'urologie et de la Societe francaise d'urologie. 2005;15(4):632-5.

70.	FLANIGAN RC, MICKISCH G, SYLVESTER R, TANGEN C, POPPEL HV, CRAWFORD ED. Cytoreductive Nephrectomy in Patients With Metastatic Renal Cancer: A Combined Analysis. Journal of Urology. 2004;171(3):1071-6.

71.	Mickisch GH, Garin A, van Poppel H, de Prijck L, Sylvester R. Radical nephrectomy plus interferon-alfa-based immunotherapy compared with interferon alfa alone in metastatic renal-cell carcinoma: a randomised trial. Lancet. 2001;358(9286):966-70.

72.	Bhindi B, Habermann EB, Mason RJ, Costello BA, Pagliaro LC, Thompson RH, et al. Comparative Survival following Initial Cytoreductive Nephrectomy versus Initial Targeted Therapy for Metastatic Renal Cell Carcinoma. Journal of Urology. 2018;200(3):528-34.

73.	García-Perdomo HA, Zapata-Copete JA, Castillo-Cobaleda DF. Role of cytoreductive nephrectomy in the targeted therapy era: A systematic review and meta-analysis. Investig Clin Urol. 2018;59(1):2-9.

74.	Heng DYC, Wells JC, Rini BI, Beuselinck B, Lee J-L, Knox JJ, et al. Cytoreductive Nephrectomy in Patients with Synchronous Metastases from Renal Cell Carcinoma: Results from the International Metastatic Renal Cell Carcinoma Database Consortium. European Urology. 2014;66(4):704-10.

75.	Bex A, Mulders P, Jewett M, Wagstaff J, van Thienen JV, Blank CU, et al. Comparison of Immediate vs Deferred Cytoreductive Nephrectomy in Patients With Synchronous Metastatic Renal Cell Carcinoma Receiving Sunitinib: The SURTIME Randomized Clinical Trial. JAMA Oncology. 2019;5(2):164-70.

76.	Méjean A, Ravaud A, Thezenas S, Colas S, Beauval J-B, Bensalah K, et al. Sunitinib Alone or after Nephrectomy in Metastatic Renal-Cell Carcinoma. New England Journal of Medicine. 2018;379(5):417-27.

77.   Ghandour RA, Singla N, Margulis V. The use of cytoreductive nephrectomy in patients with renal cell carcinoma. Expert Review of Anticancer Therapy. 2019;19(5):405-11.

78.   Motzer RJ, Russo P. Cytoreductive Nephrectomy — Patient Selection Is Key. New England Journal of Medicine. 2018;379(5):481-2.

79.   Krokidis ME, Orsi F, Katsanos K, Helmberger T, Adam A. CIRSE Guidelines on Percutaneous Ablation of Small Renal Cell Carcinoma. CardioVascular and Interventional Radiology. 2017;40(2):177-91.

80.   Hong K, Georgiades C. Radiofrequency Ablation: Mechanism of Action and Devices. Journal of Vascular and Interventional Radiology. 2010;21(8, Supplement):S179-S86.

81.   Zagoria RJ. Imaging-guided Radiofrequency Ablation of Renal Masses. RadioGraphics. 2004;24(suppl_1):S59-S71.

82.   Gill IS, Novick AC, Soble JJ, Tak Sung G, Remer EM, Hale J, et al. Laparoscopic renal cryoablation: initial clinical series. Urology. 1998;52(4):543-51.

83.   Maria T, Georgiades C. Percutaneous Cryoablation for Renal Cell Carcinoma. Journal of kidney cancer and VHL. 2015;2(3):105-13.

84.   Tatli S, Acar M, Tuncali K, Morrison PR, Silverman S. Percutaneous cryoablation techniques and clinical applications. Diagnostic and interventional radiology (Ankara, Turkey). 2010;16(1):90-5.

85.   Gill IS, Remer EM, Hasan WA, Strzempkowski B, Spaliviero M, Steinberg AP, et al. RENAL CRYOABLATION: OUTCOME AT 3 YEARS. The Journal of Urology. 2005;173(6):1903-7.

86.   Iannuccilli JD, Dupuy DE, Beland MD, Machan JT, Golijanin DJ, Mayo-Smith WW. Effectiveness and safety of computed tomography-guided radiofrequency ablation of renal cancer: a 14-year single institution experience in 203 patients. Eur Radiol. 2016;26(6):1656-64.

87.   Johnson B, Sorokin I, Cadeddu JA. Ten-year outcomes of renal tumor radiofrequency ablation. J Urol. 2018.

88.   Best SL, Park SK, Yaacoub RF, Olweny EO, Tan YK, Trimmer C, et al. Long-Term Outcomes of Renal Tumor Radio Frequency Ablation Stratified by Tumor Diameter: Size Matters. Journal of Urology. 2012;187(4):1183-9.

89.   Breen DJ, King AJ, Patel N, Lockyer R, Hayes M. Image-guided Cryoablation for Sporadic Renal Cell Carcinoma: Three- and 5-year Outcomes in 220 Patients with Biopsy-proven Renal Cell Carcinoma. Radiology. 2018;289(2):554-61.

90.   Kelly EF, Leveillee RJ. Image guided radiofrequency ablation for small renal masses. International Journal of Surgery. 2016;36:525-32.

91.   Hasegawa T, Yamanaka T, Gobara H, Miyazaki M, Takaki H, Sato Y, et al. Radiofrequency ablation versus cryoablation for T1b renal cell carcinoma: a multi-center study. Japanese Journal of Radiology. 2018;36(9):551-8.

92.   Atwell TD, Schmit GD, Boorjian SA, Mandrekar J, Kurup AN, Weisbrod AJ, et al. Percutaneous Ablation of Renal Masses Measuring 3.0 cm and Smaller: Comparative Local Control and Complications After Radiofrequency Ablation and Cryoablation. American Journal of Roentgenology. 2013;200(2):461-6.

93.   Hui GC, Tuncali K, Tatli S, Morrison PR, Silverman SG. Comparison of Percutaneous and Surgical Approaches to Renal Tumor Ablation: Metaanalysis of Effectiveness and Complication Rates. Journal of Vascular and Interventional Radiology. 2008;19(9):1311-20.

94.   Atwell TD, Carter RE, Schmit GD, Carr CM, Boorjian SA, Curry TB, et al. Complications following 573 Percutaneous Renal Radiofrequency and Cryoablation Procedures. Journal of Vascular and Interventional Radiology. 2012;23(1):48-54.

95.   Zagoria RJ, Traver MA, Werle DM, Perini M, Hayasaka S, Clark PE. Oncologic Efficacy of CT-Guided Percutaneous Radiofrequency Ablation of Renal Cell Carcinomas. American Journal of Roentgenology. 2007;189(2):429-36.

96.   Kurup AN. Percutaneous Ablation for Small Renal Masses—Complications. Semin intervent Radiol. 2014;31(01):042-9.

97.   Sternberg CN, Davis ID, Mardiak J, Szczylik C, Wagstaff J, Salman P, et al. Pazopanib in Locally Advanced or Metastatic Renal Cell Carcinoma: Results of a Randomized Phase III Trial. 2010.

98.   Motzer RJ, Hutson TE, Cella D, Reeves J, Hawkins R, Guo J, et al. Pazopanib versus Sunitinib in Metastatic Renal-Cell Carcinoma. New England Journal of Medicine. 2013;369(8):722-31.

99.   Choueiri TK, Motzer RJ. Systemic Therapy for Metastatic Renal-Cell Carcinoma. New England Journal of Medicine. 2017;376(4):354-66.

100.   Sánchez-Gastaldo A, Kempf E, González del Alba A, Duran I. Systemic treatment of renal cell cancer: A comprehensive review. Cancer Treatment Reviews. 2017;60:77-89.

101.   Moore LE, Nickerson ML, Brennan P, Toro JR, Jaeger E, Rinsky J, et al. Von Hippel-Lindau (VHL) inactivation in sporadic clear cell renal cancer: associations with germline VHL polymorphisms and etiologic risk factors. PLoS genetics. 2011;7(10):e1002312.

102.   van Houwelingen KP, van Dijk BA, Hulsbergen-van de Kaa CA, Schouten LJ, Gorissen HJ, Schalken JA, et al. Prevalence of von Hippel-Lindau gene mutations in sporadic renal cell carcinoma: results from the Netherlands cohort study. BMC cancer. 2005;5(1):57.

103.   Kim M, Sohn M, Shim M, Choi SK, Park M, Kim E, et al. Prognostic value of vascular endothelial growth factor (VEGF), VEGF receptor 2, platelet-derived growth factor-beta (PDGF-beta), and PDGF-beta receptor expression in papillary renal cell carcinoma. Hum Pathol. 2017;61:78-89.

104.   Song SH, Jeong IG, You D, Hong JH, Hong B, Song C, et al. VEGF/VEGFR2 and PDGF-B/PDGFR-β expression in non-metastatic renal cell carcinoma: a retrospective study in 1,091 consecutive patients. Int J Clin Exp Pathol. 2014;7(11):7681-9.

105.   Ziello JE, Jovin IS, Huang Y. Hypoxia-Inducible Factor (HIF)-1 regulatory pathway and its potential for therapeutic intervention in malignancy and ischemia. Yale J Biol Med. 2007;80(2):51-60.

106.   Pick AM, Nystrom KK. Pazopanib for the treatment of metastatic renal cell carcinoma. Clinical therapeutics. 2012;34(3):511-20.

107.   Motzer RJ, Rini BI, Bukowski RM, Curti BD, George DJ, Hudes GR, et al. Sunitinib in Patients With Metastatic Renal Cell Carcinoma. JAMA. 2006;295(21):2516-24.

108.   Gore ME, Szczylik C, Porta C, Bracarda S, Bjarnason GA, Oudard S, et al. Final results from the large sunitinib global expanded-access trial in metastatic renal cell carcinoma. British Journal Of Cancer. 2015;113:12.

109.   Hutson TE, Davis ID, Machiels J-PH, Souza PLD, Rottey S, Hong B-f, et al. Efficacy and Safety of Pazopanib in Patients With Metastatic Renal Cell Carcinoma. Journal of Clinical Oncology. 2010;28(3):475-80.

110.   Battelli C, Cho DC. mTOR inhibitors in renal cell carcinoma. Therapy. 2011;8(4):359-67.

111.   Motzer RJ, Escudier B, Oudard S, Hutson TE, Porta C, Bracarda S, et al. Phase 3 trial of everolimus for metastatic renal cell carcinoma : final results and analysis of prognostic factors. Cancer. 2010;116(18):4256-65.

112.   Hudes G, Carducci M, Tomczak P, Dutcher J, Figlin R, Kapoor A, et al. Temsirolimus, Interferon Alfa, or Both for Advanced Renal-Cell Carcinoma. New England Journal of Medicine. 2007;356(22):2271-81.

113.   Belardelli F, Ferrantini M, Proietti E, Kirkwood JM. Interferon-alpha in tumor immunity and immunotherapy. Cytokine & Growth Factor Reviews. 2002;13(2):119-34.

114.   Itsumi M, Tatsugami K. Immunotherapy for Renal Cell Carcinoma. Clinical and Developmental Immunology. 2010;2010.

115.   Zitvogel L, Galluzzi L, Kepp O, Smyth MJ, Kroemer G. Type I interferons in anticancer immunity. Nature Reviews Immunology. 2015;15:405.

116.   Jiang T, Zhou C, Ren S. Role of IL-2 in cancer immunotherapy. Oncoimmunology. 2016;5(6):e1163462-e.

117.   Malek TR. The Biology of Interleukin-2. Annual Review of Immunology. 2008;26(1):453-79.

118.   Rosenberg SA. IL-2: the first effective immunotherapy for human cancer. J Immunol. 2014;192(12):5451-8.

119.   Motzer RJ, Bacik J, Murphy BA, Russo P, Mazumdar M. Interferon-alfa as a comparative treatment for clinical trials of new therapies against advanced renal cell carcinoma. Journal of clinical oncology : official journal of the American Society of Clinical Oncology. 2002;20(1):289-96.

120.   McDermott DF, Regan MM, Clark JI, Flaherty LE, Weiss GR, Logan TF, et al. Randomized Phase III Trial of High-Dose Interleukin-2 Versus Subcutaneous Interleukin-2 and Interferon in Patients With Metastatic Renal Cell Carcinoma. Journal of Clinical Oncology. 2005;23(1):133-41.

121.	Rosenberg SA, Yang JC, Topalian SL, Schwartzentruber DJ, Weber JS, Parkinson DR, et al. Treatment of 283 Consecutive Patients With Metastatic Melanoma or Renal Cell Cancer Using High-Dose Bolus Interleukin 2. JAMA. 1994;271(12):907-13.

122.	Escudier B, Bellmunt J, Négrier S, Bajetta E, Melichar B, Bracarda S, et al. Phase III Trial of Bevacizumab Plus Interferon Alfa-2a in Patients With Metastatic Renal Cell Carcinoma (AVOREN): Final Analysis of Overall Survival. Journal of Clinical Oncology. 2010;28(13):2144-50.

123.	Buchbinder EI, Desai A. CTLA-4 and PD-1 Pathways: Similarities, Differences, and Implications of Their Inhibition. American journal of clinical oncology. 2016;39(1):98-106.

124.	Massari F, Santoni M, Ciccarese C, Santini D, Alfieri S, Martignoni G, et al. PD-1 blockade therapy in renal cell carcinoma: Current studies and future promises. Cancer Treatment Reviews. 2015;41(2):114-21.

125.	Carlo MI, Voss MH, Motzer RJ. Checkpoint inhibitors and other novel immunotherapies for advanced renal cell carcinoma. Nat Rev Urol. 2016;13(7):420-31.

126.	Yang JC, Hughes M, Kammula U, Royal R, Sherry RM, Topalian SL, et al. Ipilimumab (anti-CTLA4 antibody) causes regression of metastatic renal cell cancer associated with enteritis and hypophysitis. J Immunother. 2007;30(8):825-30.

127.	Motzer RJ, Escudier B, McDermott DF, George S, Hammers HJ, Srinivas S, et al. Nivolumab versus Everolimus in Advanced Renal-Cell Carcinoma. New England Journal of Medicine. 2015;373(19):1803-13.

128.	Ghali F, Patel SH, Derweesh IH. Current Status of Immunotherapy for Localized and Locally Advanced Renal Cell Carcinoma. Journal of Oncology. 2019;2019:8.

129.	Rohde D, De Mulder PEM, Weissbach L, Osieka R, Blatter J, Jakse G. Experimental and Clinical Efficacy of $2',2'$-Difluorodeoxycytidine (Gemcitabine) against Renal Cell Carcinoma. Oncology. 1996;53(6):476-81.

130.	Longley DB, Harkin DP, Johnston PG. 5-Fluorouracil: mechanisms of action and clinical strategies. Nature Reviews Cancer. 2003;3(5):330.

131.	Walko CM, Lindley C. Capecitabine: A review. Clinical therapeutics. 2005;27(1):23-44.

132.	Kish JA, Wolf M, David Crawford E, Leimert JT, Bueschen A, Neefe JR, et al. Evaluation of low dose continuous infusion 5-fluorouracil in patients with advanced and recurrent renal cell carcinoma. A Southwest Oncology Group study. Cancer. 1994;74(3):916-9.

133.	Stadler WM, Halabi S, Rini B, Ernstoff MS, Davila E, Picus J, et al. A phase II study of gemcitabine and capecitabine in metastatic renal cancer: a report of Cancer and Leukemia Group B protocol 90008. Cancer. 2006;107(6):1273-9.

134.	Tannir NM, Thall PF, Ng CS, Wang X, Wooten L, Siefker-Radtke A, et al. A phase II trial of gemcitabine plus capecitabine for metastatic renal cell cancer previously treated with immunotherapy and targeted agents. J Urol. 2008;180(3):867-72; discussion 72.

135.	Van Veldhuizen PJ, Hussey M, Lara PN, Jr., Mack PC, Gandour-Edwards R, Clark JI, et al. A phase ii study of gemcitabine and capecitabine in patients with advanced renal cell cancer: Southwest Oncology Group Study S0312. Am J Clin Oncol. 2009;32(5):453-9.

136.	Bennouna J, Delva R, Gomez F, Lesimple T, Geoffrois L, Linassier C, et al. A phase II study with 5-fluorouracil, folinic acid and oxaliplatin (FOLFOX-4 regimen) in patients with metastatic renal cell carcinoma. Oncology. 2003;64(1):25-7.

137.	Harshman LC, Li M, Srinivas S. The combination of thalidomide and capecitabine in metastatic renal cell carcinoma -- is not the answer. Am J Clin Oncol. 2008;31(5):417-23.

138.	Marur S, Eliason J, Heilbrun LK, Dickow B, Smith DW, Baranowski K, et al. Phase II trial of capecitabine and weekly docetaxel in metastatic renal cell carcinoma. Urology. 2008;72(4):898-902.

139.	Finney R. An evaluation of postoperative radiotherapy in hypernephroma treatment—A clinical trial. Cancer. 1973;32(6):1332-40.

140.	Flocks RH, Kadesky MC. Malignant Neoplasms of the Kidney: An Analysis of 353 Patients Followed Five Years or More. Journal of Urology. 1958;79(2):196-201.

141.	Kjaer M, Iversen P, Hvidt V, Bruun E, Skaarup P, Bech Hansen J, et al. A randomized trial of postoperative radiotherapy versus observation in stage II and III renal adenocarcinoma. A study by the Copenhagen Renal Cancer Study Group. Scand J Urol Nephrol. 1987;21(4):285-9.

142.   Juusela H, Malmio K, Alfthan O, Oravisto KJ. Preoperative Irradiation in the Treatment of Renal Adenocarcinoma. Scandinavian Journal of Urology and Nephrology. 1977;11(3):277-81.
143.   van der Werf-Messing B. Carcinoma of the kidney. Cancer. 1973;32(5):1056-61.
144.   Ulutin HC, Aksu G, Fayda M, Kuzhan O, Tahmaz L, Beyzadeoglu M. The Value of Postoperative Radiotherapy in Renal Cell Carcinoma: A Single-Institution Experience. Tumori Journal. 2006;92(3):202-6.
145.   FINNEY R. The Value of Radiotherapy in the Treatment of Hypernephroma-a Clinical Trial. British Journal of Urology. 1973;45(3):258-69.
146.   Tunio MA, Hashmi A, Rafi M. Need for a new trial to evaluate postoperative radiotherapy in renal cell carcinoma: a meta-analysis of randomized controlled trials. Ann Oncol. 2010;21(9):1839-45.
147.   DiBiase SJ, Valicenti RK, Schultz D, Xie Y, Gomella LG, Corn BW. Palliative Irradiation for Focally Symptomatic Metastatic Renal Cell Carcinoma: Support for Dose Escalation Based on a Biological Model. The Journal of Urology. 1997;158(3):746-9.
148.   Onufrey V, Mohiuddin M. Radiation therapy in the treatment of me tastatic renal cell carcinoma. International Journal of Radiation Oncology • Biology • Physics. 1985;11(11):2007-9.
149.   Walsh L, Stanfield JL, Cho LC, Chang C-h, Forster K, Kabbani W, et al. Efficacy of Ablative High-Dose-per-Fraction Radiation for Implanted Human Renal Cell Cancer in a Nude Mouse Model. European Urology. 2006;50(4):795-800.
150.   Zelefsky MJ, Greco C, Motzer R, Magsanoc JM, Pei X, Lovelock M, et al. Tumor Control Outcomes After Hypofractionated and Single-Dose Stereotactic Image-Guided Intensity-Modulated Radiotherapy for Extracranial Metastases From Renal Cell Carcinoma. International Journal of Radiation Oncology*Biology*Physics. 2012;82(5):1744-8.
151.   Leung PS. The gastrointestinal system: Gastrointestinal, nutritional and hepatobiliary physiology: Springer Netherlands; 2014. 1-364 p.
152.   Stacey R, Green JT. Radiation-induced small bowel disease: latest developments and clinical guidance. Ther Adv Chronic Dis. 2014;5(1):15-29.
153.   Theis VS, Sripadam R, Ramani V, Lal S. Chronic radiation enteritis. Clin Oncol (R Coll Radiol). 2010;22(1):70-83.
154.   Bismar MM, Sinicrope FA. Radiation enteritis. Current gastroenterology reports. 2002;4(5):361-5.
155.   Emami B, Lyman J, Brown A, Cola L, Goitein M, Munzenrider JE, et al. Tolerance of normal tissue to therapeutic irradiation. International Journal of Radiation Oncology*Biology*Physics. 1991;21(1):109-22.
156.   Kavanagh BD, Pan CC, Dawson LA, Das SK, Li XA, Ten Haken RK, et al. Radiation dose-volume effects in the stomach and small bowel. Int J Radiat Oncol Biol Phys. 2010;76(3 Suppl):S101-7.
157.   Baglan KL, Frazier RC, Yan D, Huang RR, Martinez AA, Robertson JM. The dose-volume realationship of acute small bowel toxicity from concurrent 5-FU-based chemotherapy and radiation therapy for rectal cancer. International Journal of Radiation Oncology*Biology*Physics. 2002;52(1):176-83.
158.   Stanic S, Mayadev JS. Tolerance of the small bowel to therapeutic irradiation: a focus on late toxicity in patients receiving para-aortic nodal irradiation for gynecologic malignancies. International journal of gynecological cancer : official journal of the International Gynecological Cancer Society. 2013;23(4):592-7.
159.   Ling A, Furhang E, Ryemon SN, Ennis RD. Late small bowel toxicity after aggressive abdominopelvic intensity modulated radiation therapy. Adv Radiat Oncol. 2017;2(4):615-23.
160.   Benedict SH, Yenice KM, Followill D, Galvin JM, Hinson W, Kavanagh B, et al. Stereotactic body radiation therapy: The report of AAPM Task Group 101. Medical Physics. 2010;37(8):4078-101.
161.   Withers HR. Four R's of radiotherapy. Journal Name: Adv Radiat Biol, v 5, pp 241-247; Other Information: Orig Receipt Date: 31-DEC-75. 1975:Medium: X.
162.   Song CW, Park H, Griffin RJ, Levitt SH. Radiobiology of Stereotactic Radiosurgery and Stereotactic Body Radiation Therapy. In: Levitt SH, Purdy JA, Perez CA, Poortmans P, editors. Technical Basis of Radiation Therapy: Practical Clinical Applications. Berlin, Heidelberg: Springer Berlin Heidelberg; 2012. p. 51-61.

163.	Song CW, Cho LC, Yuan J, Dusenbery KE, Griffin RJ, Levitt SH. Radiobiology of stereotactic body radiation therapy/stereotactic radiosurgery and the linear-quadratic model. Int J Radiat Oncol Biol Phys. 2013;87(1):18-9.

164.	Park C, Papiez L, Zhang S, Story M, Timmerman RD. Universal survival curve and single fraction equivalent dose: useful tools in understanding potency of ablative radiotherapy. Int J Radiat Oncol Biol Phys. 2008;70(3):847-52.

165.	Siva S, Kothari G, Muacevic A, Louie AV, Slotman BJ, Teh BS, et al. Radiotherapy for renal cell carcinoma: renaissance of an overlooked approach. Nature Reviews Urology. 2017;14:549.

166.	Ramakrishna N, Rosca F, Friesen S, Tezcanli E, Zygmanszki P, Hacker F. A clinical comparison of patient setup and intra-fraction motion using frame-based radiosurgery versus a frameless image-guided radiosurgery system for intracranial lesions. Radiotherapy and Oncology. 2010;95(1):109-15.

167.	Tryggestad E, Christian M, Ford E, Kut C, Le Y, Sanguineti G, et al. Inter- and Intrafraction Patient Positioning Uncertainties for Intracranial Radiotherapy: A Study of Four Frameless, Thermoplastic Mask-Based Immobilization Strategies Using Daily Cone-Beam CT. International Journal of Radiation Oncology*Biology*Physics. 2011;80(1):281-90.

168.	Lindberg K, Nyman J, Riesenfeld Källskog V, Hoyer M, Lund JÅ, Lax I, et al. Long-term results of a prospective phase II trial of medically inoperable stage I NSCLC treated with SBRT – the Nordic experience. Acta Oncologica. 2015;54(8):1096-104.

169.	Chang JY, Senan S, Paul MA, Mehran RJ, Louie AV, Balter P, et al. Stereotactic ablative radiotherapy versus lobectomy for operable stage I non-small-cell lung cancer: a pooled analysis of two randomised trials. The Lancet Oncology. 2015;16(6):630-7.

170.	Soldà F, Lodge M, Ashley S, Whitington A, Goldstraw P, Brada M. Stereotactic radiotherapy (SABR) for the treatment of primary non-small cell lung cancer; Systematic review and comparison with a surgical cohort. Radiotherapy and Oncology. 2013;109(1):1-7.

171.	Senthi S, Haasbeek CJA, Slotman BJ, Senan S. Outcomes of stereotactic ablative radiotherapy for central lung tumours: A systematic review. Radiotherapy and Oncology. 2013;106(3):276-82.

172.	Onishi H, Shirato H, Nagata Y, Hiraoka M, Fujino M, Gomi K, et al. Stereotactic Body Radiotherapy (SBRT) for Operable Stage I Non–Small-Cell Lung Cancer: Can SBRT Be Comparable to Surgery? International Journal of Radiation Oncology*Biology*Physics. 2011;81(5):1352-8.

173.	Timmerman R, Paulus R, Galvin J, et al. STereotactic body radiation therapy for inoperable early stage lung cancer. JAMA. 2010;303(11):1070-6.

174.	Ball D, Mai GT, Vinod S, Babington S, Ruben J, Kron T, et al. Stereotactic ablative radiotherapy versus standard radiotherapy in stage 1 non-small-cell lung cancer (TROG 09.02 CHISEL): a phase 3, open-label, randomised controlled trial. The Lancet Oncology. 2019;20(4):494-503.

175.	Goodman KA, Kavanagh BD. Stereotactic Body Radiotherapy for Liver Metastases. Seminars in Radiation Oncology. 2017;27(3):240-6.

176.	Andolino DL, Johnson CS, Maluccio M, Kwo P, Tector AJ, Zook J, et al. Stereotactic body radiotherapy for primary hepatocellular carcinoma. Int J Radiat Oncol Biol Phys. 2011;81(4):e447-53.

177.	Rusthoven KE, Kavanagh BD, Cardenes H, Stieber VW, Burri SH, Feigenberg SJ, et al. Multi-Institutional Phase I/II Trial of Stereotactic Body Radiation Therapy for Liver Metastases. Journal of Clinical Oncology. 2009;27(10):1572-8.

178.	Lee MT, Kim JJ, Dinniwell R, Brierley J, Lockwood G, Wong R, et al. Phase I Study of Individualized Stereotactic Body Radiotherapy of Liver Metastases. Journal of Clinical Oncology. 2009;27(10):1585-91.

179.	Schefter TE, Kavanagh BD, Timmerman RD, Cardenes HR, Baron A, Gaspar LE. A phase I trial of stereotactic body radiation therapy (SBRT) for liver metastases. International Journal of Radiation Oncology*Biology*Physics. 2005;62(5):1371-8.

180.	Herfarth KK, Debus J, Lohr F, Bahner ML, Rhein B, Fritz P, et al. Stereotactic Single-Dose Radiation Therapy of Liver Tumors: Results of a Phase I/II Trial. Journal of Clinical Oncology. 2001;19(1):164-70.

181.	Killoran JH, Kooy HM, Gladstone DJ, Welte FJ, Beard CJ. A numerical simulation of organ motion and daily setup uncertainties: implications for radiation therapy. Int J Radiat Oncol Biol Phys. 1997;37(1):213-21.

182.   van Herk M. Errors and margins in radiotherapy. Seminars in Radiation Oncology. 2004;14(1):52-64.

183.   van Herk M, Remeijer P, Rasch C, Lebesque JV. The probability of correct target dosage: dose-population histograms for deriving treatment margins in radiotherapy. International Journal of Radiation Oncology*Biology*Physics. 2000;47(4):1121-35.

184.   Foroudi F, Pham D, Bressel M, Wong J, Rolfo A, Roxby P, et al. Bladder Cancer Radiotherapy Margins: A Comparison of Daily Alignment using Skin, Bone or Soft Tissue. Clinical Oncology. 2012;24(10):673-81.

185.   Hughes S, McClelland J, Chandler A, Adams M, Boutland J, Withers D, et al. A Comparison of Internal Target Volume Definition by Limited Four-dimensional Computed Tomography, the Addition of Patient-specific Margins, or the Addition of Generic Margins when Planning Radical Radiotherapy for Lymph Node-positive Non-small Cell Lung Cancer. Clinical Oncology. 2008;20(4):293-300.

186.   Xi M, Liu M-Z, Deng X-W, Zhang L, Huang X-Y, Liu H, et al. Defining internal target volume (ITV) for hepatocellular carcinoma using four-dimensional CT. Radiotherapy and Oncology. 2007;84(3):272-8.

187.   Lorchel F, Dumas JL, Noël A, Wolf D, Bosset JF, Aletti P. Esophageal cancer: Determination of internal target volume for conformal radiotherapy. Radiotherapy and Oncology. 2006;80(3):327-32.

188.   Underberg RWM, Lagerwaard FJ, Slotman BJ, Cuijpers JP, Senan S. Use of maximum intensity projections (MIP) for target volume generation in 4DCT scans for lung cancer. International Journal of Radiation Oncology*Biology*Physics. 2005;63(1):253-60.

189.   Ekberg L, Holmberg O, Wittgren L, Bjelkengren G, Landberg T. What margins should be added to the clinical target volume in radiotherapy treatment planning for lung cancer? Radiotherapy and Oncology. 1998;48(1):71-7.

190.   Hugo GD, Yan D, Liang J. Population and patient-specific target margins for 4D adaptive radiotherapy to account for intra- and inter-fraction variation in lung tumour position. Phys Med Biol. 2007;52(1):257-74.

191.   Sixel KE, Ruschin M, Tirona R, Cheung PCF. Digital fluoroscopy to quantify lung tumor motion: potential for patient-specific planning target volumes. International Journal of Radiation Oncology*Biology*Physics. 2003;57(3):717-23.

192.   Ruschin M, Sixel KE. Integration of digital fluoroscopy with CT-based radiation therapy planning of lung tumors. Medical Physics. 2002;29(8):1698-709.

193.   Rietzel E, Liu AK, Doppke KP, Wolfgang JA, Chen AB, Chen GTY, et al. Design of 4D treatment planning target volumes. International Journal of Radiation Oncology*Biology*Physics. 2006;66(1):287-95.

194.   Underberg RWM, Lagerwaard FJ, Cuijpers JP, Slotman BJ, van Sörnsen de Koste JR, Senan S. Four-dimensional CT scans for treatment planning in stereotactic radiotherapy for stage I lung cancer. International Journal of Radiation Oncology*Biology*Physics. 2004;60(4):1283-90.

195.   Stevens CW, Munden RF, Forster KM, Kelly JF, Liao Z, Starkschall G, et al. Respiratory-driven lung tumor motion is independent of tumor size, tumor location, and pulmonary function. International Journal of Radiation Oncology*Biology*Physics. 2001;51(1):62-8.

196.   Seppenwoolde Y, Shirato H, Kitamura K, Shimizu S, van Herk M, Lebesque JV, et al. Precise and real-time measurement of 3D tumor motion in lung due to breathing and heartbeat, measured during radiotherapy. International Journal of Radiation Oncology*Biology*Physics. 2002;53(4):822-34.

197.   Mageras GS, Pevsner A, Yorke ED, Rosenzweig KE, Ford EC, Hertanto A, et al. Measurement of lung tumor motion using respiration-correlated CT. International Journal of Radiation Oncology*Biology*Physics. 2004;60(3):933-41.

198.   Liu HH, Balter P, Tutt T, Choi B, Zhang J, Wang C, et al. Assessing Respiration-Induced Tumor Motion and Internal Target Volume Using Four-Dimensional Computed Tomography for Radiotherapy of Lung Cancer. International Journal of Radiation Oncology*Biology*Physics. 2007;68(2):531-40.

199.   Case RB, Moseley DJ, Sonke JJ, Eccles CL, Dinniwell RE, Kim J, et al. Interfraction and Intrafraction Changes in Amplitude of Breathing Motion in Stereotactic Liver Radiotherapy. International Journal of Radiation Oncology*Biology*Physics. 2010;77(3):918-25.

200.   Eccles CL, Patel R, Simeonov AK, Lockwood G, Haider M, Dawson LA. Comparison of Liver Tumor Motion With and Without Abdominal Compression Using Cine-Magnetic Resonance Imaging. International Journal of Radiation Oncology*Biology*Physics. 2011;79(2):602-8.

201.   Ge J, Santanam L, Noel C, Parikh PJ. Planning 4-Dimensional Computed Tomography (4DCT) Cannot Adequately Represent Daily Intrafractional Motion of Abdominal Tumors. International Journal of Radiation Oncology*Biology*Physics. 2013;85(4):999-1005.

202.   Kirilova A, Lockwood G, Choi P, Bana N, Haider MA, Brock KK, et al. Three-Dimensional Motion of Liver Tumors Using Cine-Magnetic Resonance Imaging. International Journal of Radiation Oncology*Biology*Physics. 2008;71(4):1189-95.

203.   Kitamura K, Shirato H, Seppenwoolde Y, Shimizu T, Kodama Y, Endo H, et al. Tumor location, cirrhosis, and surgical history contribute to tumor movement in the liver, as measured during stereotactic irradiation using a real-time tumor-tracking radiotherapy system. International Journal of Radiation Oncology*Biology*Physics. 2003;56(1):221-8.

204.   Hanley J, Debois MM, Mah D, Mageras GS, Raben A, Rosenzweig K, et al. Deep inspiration breath-hold technique for lung tumors: the potential value of target immobilization and reduced lung density in dose escalation. International Journal of Radiation Oncology*Biology*Physics. 1999;45(3):603-11.

205.   Wong JW, Sharpe MB, Jaffray DA, Kini VR, Robertson JM, Stromberg JS, et al. The use of active breathing control (ABC) to reduce margin for breathing motion. International Journal of Radiation Oncology*Biology*Physics. 1999;44(4):911-9.

206.   Engelsman M, Sharp GC, Bortfeld T, Onimaru R, Shirato H. How much margin reduction is possible through gating or breath hold? Phys Med Biol. 2005;50(3):477-90.

207.   Bloemen-van Gurp E, van der Meer S, Hendry J, Buijsen J, Visser P, Fontanarosa D, et al. Active Breathing Control in Combination With Ultrasound Imaging: A Feasibility Study of Image Guidance in Stereotactic Body Radiation Therapy of Liver Lesions. International Journal of Radiation Oncology*Biology*Physics. 2013;85(4):1096-102.

208.   Eccles C, Brock KK, Bissonnette J-P, Hawkins M, Dawson LA. Reproducibility of liver position using active breathing coordinator for liver cancer radiotherapy. International Journal of Radiation Oncology*Biology*Physics. 2006;64(3):751-9.

209.   Zhong R, Wang J, Jiang X, He Y, Zhang H, Chen N, et al. Hypofraction radiotherapy of liver tumor using cone beam computed tomography guidance combined with active breath control by long breath-holding. Radiotherapy and Oncology. 2012;104(3):379-85.

210.   Zhong R, Wang J, Zhou L, Xu F, Liu L, Zhou J, et al. Implementation of single-breath-hold cone beam CT guided hypofraction radiotherapy for lung cancer. Radiation Oncology. 2014;9(1):77.

211.   Bouilhol G, Ayadi M, Rit S, Thengumpallil S, Schaerer J, Vandemeulebroucke J, et al. Is abdominal compression useful in lung stereotactic body radiation therapy? A 4DCT and dosimetric lobe-dependent study. Physica medica : PM : an international journal devoted to the applications of physics to medicine and biology : official journal of the Italian Association of Biomedical Physics (AIFB). 2013;29(4):333-40.

212.   Heinzerling JH, Anderson JF, Papiez L, Boike T, Chien S, Zhang G, et al. Four-Dimensional Computed Tomography Scan Analysis of Tumor and Organ Motion at Varying Levels of Abdominal Compression During Stereotactic Treatment of Lung and Liver. International Journal of Radiation Oncology*Biology*Physics. 2008;70(5):1571-8.

213.   Hu Y, Zhou Y-K, Chen Y-X, Shi S-M, Zeng Z-C. 4D-CT scans reveal reduced magnitude of respiratory liver motion achieved by different abdominal compression plate positions in patients with intrahepatic tumors undergoing helical tomotherapy. Medical Physics. 2016;43(7):4335-41.

214.   Lovelock D, Zatcky J, Goodman K, Yamada Y. The Effectiveness of a Pneumatic Abdominal Compression Device in Reducing Respiratory Motion of Liver Tumors in Patients Undergoing Radiotherapy. International Journal of Radiation Oncology*Biology*Physics. 2011;81(2, Supplement):S351.

215.   Oh R, Masai N, Shiomi H, Inoue T. The "Air-Bag System": A Novel Abdominal Compression Device Collaborated with RPM System. International Journal of Radiation Oncology*Biology*Physics. 2011;81(2, Supplement):S892-S3.

216.   Wunderink W, Méndez Romero A, de Kruijf W, de Boer H, Levendag P, Heijmen B. Reduction of Respiratory Liver Tumor Motion by Abdominal Compression in Stereotactic Body Frame, Analyzed by Tracking Fiducial Markers Implanted in Liver. International Journal of Radiation Oncology • Biology • Physics.71(3):907-15.

217.   Tsang DS, Voncken FEM, Tse RV, Sykes J, Wong RKS, Dinniwell RE, et al. A Randomized Controlled Trial of Lorazepam to Reduce Liver Motion in Patients Receiving Upper Abdominal Radiation Therapy. International Journal of Radiation Oncology*Biology*Physics. 2013;87(5):881-7.

218.   Booth JT, Caillet V, Hardcastle N, O'Brien R, Szymura K, Crasta C, et al. The first patient treatment of electromagnetic-guided real time adaptive radiotherapy using MLC tracking for lung SABR. Radiotherapy and Oncology. 2016;121(1):19-25.

219.   Caillet V, Keall PJ, Colvill E, Hardcastle N, O'Brien R, Szymura K, et al. MLC tracking for lung SABR reduces planning target volumes and dose to organs at risk. Radiotherapy and Oncology. 2017;124(1):18-24.

220.   Nuyttens JJ, Prévost JB, Praag J, Hoogeman M, Van Klaveren RJ, Levendag PC, et al. Lung tumor tracking during stereotactic radiotherapy treatment with the CyberKnife: Marker placement and early results. Acta Oncologica. 2006;45(7):961-5.

221.   Wunderink W, Méndez Romero A, de Kruijf W, de Boer H, Levendag P, Heijmen B. Reduction of Respiratory Liver Tumor Motion by Abdominal Compression in Stereotactic Body Frame, Analyzed by Tracking Fiducial Markers Implanted in Liver. International Journal of Radiation Oncology*Biology*Physics. 2008;71(3):907-15.

222.   Collins BT, Erickson K, Reichner CA, Collins SP, Gagnon GJ, Dieterich S, et al. Radical stereotactic radiosurgery with real-time tumor motion tracking in the treatment of small peripheral lung tumors. Radiation Oncology. 2007;2(1):39.

223.   Poulsen PR, Worm ES, Petersen JBB, Grau C, Fledelius W, Høyer M. Kilovoltage intrafraction motion monitoring and target dose reconstruction for stereotactic volumetric modulated arc therapy of tumors in the liver. Radiotherapy and Oncology. 2014;111(3):424-30.

224.   Hyde D, Lochray F, Korol R, Davidson M, Wong CS, Ma L, et al. Spine Stereotactic Body Radiotherapy Utilizing Cone-Beam CT Image-Guidance With a Robotic Couch: Intrafraction Motion Analysis Accounting for all Six Degrees of Freedom. International Journal of Radiation Oncology*Biology*Physics. 2012;82(3):e555-e62.

225.   Mahjoubi K, Daisne JF, Deheneffe S, Huyskens D, Remouchamps V. Preliminary Results of a Randomized Study Comparing 2 Immobilization Systems for Stereotactic Body Radiation Therapy. International Journal of Radiation Oncology*Biology*Physics. 2013;87(2, Supplement):S730-S1.

226.   Siva S, Devereux T, Kron T, Gill S, MacManus M, Bressel M, et al. Vacuum immobilisation reduces tumour excursion and minimises intrafraction error in a cohort study of stereotactic ablative body radiotherapy for pulmonary metastases. Journal of Medical Imaging and Radiation Oncology. 2013:n/a-n/a.

227.   Li W, Purdie TG, Taremi M, Fung S, Brade A, Cho BCJ, et al. Effect of Immobilization and Performance Status on Intrafraction Motion for Stereotactic Lung Radiotherapy: Analysis of 133 Patients. International Journal of Radiation Oncology*Biology*Physics. 2011;81(5):1568-75.

228.   Foster R, Meyer J, Iyengar P, Pistenmaa D, Timmerman R, Choy H, et al. Localization Accuracy and Immobilization Effectiveness of a Stereotactic Body Frame for a Variety of Treatment Sites. International Journal of Radiation Oncology*Biology*Physics. 2013;87(5):911-6.

229.   Lax I, Blomgren H, Naslund I, Svanstrom R. Stereotactic radiotherapy of malignancies in the abdomen. Methodological aspects. Acta Oncol. 1994;33(6):677-83.

230.   Radiotherapy C. Iowa, USA: Civco Radiotherapy; 2019 [Available from: https://civcort.com/ro.

231.   Orfit. Wijnegem, Belgium.: Orfit Industries; 2019 [Available from: https://www.orfit.com/.

232.   Elekta. Stockholm, Sweden.: Elekta; 2019 [Available from: https://www.elekta.com/radiotherapy/treatment-solutions/patient-positioning/bodyfix.

233.   Lim DH, Yi BY, Mirmiran A, Dhople A, Suntharalingam M, D'Souza WD. Optimal beam arrangement for stereotactic body radiation therapy delivery in lung tumors. Acta Oncologica. 2010;49(2):219-24.

234. Siva S, Kirby K, Caine H, Pham D, Kron T, Te Marvelde L, et al. Comparison of Single-fraction and Multi-fraction Stereotactic Radiotherapy for Patients with 18F-fluorodeoxyglucose Positron Emission Tomography-staged Pulmonary Oligometastases. Clinical Oncology. 2015;27(6):353-61.

235. Kim S, Kim T, Ko SJ, Serago C, Smith A, Vallow LA, et al. Negative margin technique - a novel planning strategy to improve dose conformation in SBRT using dynamic conformal arc delivery. Journal of applied clinical medical physics. 2013;14(5):79-89.

236. Solberg TD, Boedeker KL, Fogg R, Selch MT, DeSalles AAF. Dynamic arc radiosurgery field shaping: a comparison with static field conformal and noncoplanar circular arcs. International Journal of Radiation Oncology*Biology*Physics. 2001;49(5):1481-91.

237. Jang SY, Lalonde R, Ozhasoglu C, Burton S, Heron D, Huq MS. Dosimetric comparison between cone/Iris-based and InCise MLC-based CyberKnife plans for single and multiple brain metastases. Journal of applied clinical medical physics. 2016;17(5):184-99.

238. Ezz A, Munro P, Porter AT, Battista J, Jaffray DA, Fenster A, et al. Daily monitoring and correction of radiation field placement using a video-based portal imaging system: A pilot study. International Journal of Radiation Oncology*Biology*Physics. 1992;22(1):159-65.

239. Leong J. Use of digital fluoroscopy as an online verification device in radiation therapy. Physics in Medicine and Biology. 1986;31(9):985-92.

240. Potters L, Gaspar LE, Kavanagh B, Galvin JM, Hartford AC, Hevezi JM, et al. American Society for Therapeutic Radiology and Oncology (ASTRO) and American College of Radiology (ACR) Practice Guidelines for Image-Guided Radiation Therapy (IGRT). International Journal of Radiation Oncology*Biology*Physics. 2010;76(2):319-25.

241. Verellen D, Ridder MD, Storme G. A (short) history of image-guided radiotherapy. Radiotherapy and Oncology. 2008;86(1):4-13.

242. van Elmpt W, McDermott L, Nijsten S, Wendling M, Lambin P, Mijnheer B. A literature review of electronic portal imaging for radiotherapy dosimetry. Radiotherapy and Oncology. 2008;88(3):289-309.

243. Gayou O, Parda DS, Johnson M, Miften M. Patient dose and image quality from mega-voltage cone beam computed tomography imaging. Medical Physics. 2007;34(2):499-506.

244. Ruchala KJ, Olivera GH, Schloesser EA, Mackie TR. Megavoltage CT on a tomotherapy system. Physics in Medicine and Biology. 1999;44(10):2597-621.

245. Pouliot J, Bani-Hashemi A, Josephine C, Svatos M, Ghelmansarai F, Mitschke M, et al. Low-dose megavoltage cone-beam CT for radiation therapy. International Journal of Radiation Oncology*Biology*Physics. 2005;61(2):552-60.

246. Jin J-Y, Ryu S, Faber K, Mikkelsen T, Chen Q, Li S, et al. 2D/3D Image fusion for accurate target localization and evaluation of a mask based stereotactic system in fractionated stereotactic radiotherapy of cranial lesions. Medical Physics. 2006;33(12):4557-66.

247. Sorcini B, Tilikidis A. Clinical application of image-guided radiotherapy, IGRT (on the Varian OBI platform). Cancer/Radiothérapie. 2006;10(5):252-7.

248. Thorson T, Prosser T. X-ray volume imaging in image-guided radiotherapy. Medical Dosimetry. 2006;31(2):126-33.

249. Jaffray DA, Drake DG, Moreau M, Martinez AA, Wong JW. A radiographic and tomographic imaging system integrated into a medical linear accelerator for localization of bone and soft-tissue targets. International Journal of Radiation Oncology*Biology*Physics. 1999;45(3):773-89.

250. Létourneau D, Wong JW, Oldham M, Gulam M, Watt L, Jaffray DA, et al. Cone-beam-CT guided radiation therapy: technical implementation. Radiotherapy and Oncology. 2005;75(3):279-86.

251. Oldham M, Létourneau D, Watt L, Hugo G, Yan D, Lockman D, et al. Cone-beam-CT guided radiation therapy: A model for on-line application. Radiotherapy and Oncology. 2005;75(3):271.E1-.E8.

252. Song WY, Kamath S, Ozawa S, Al Ani S, Chvetsov A, Bhandare N, et al. A dose comparison study between XVI® and OBI® CBCT systems. Medical Physics. 2008;35(2):480-6.

253. Dietrich L, Jetter S, Tücking T, Nill S, Oelfke U. Linac-integrated 4D cone beam CT: first experimental results. Physics in Medicine and Biology. 2006;51(11):2939-52.

254. Li T, Koong A, Xing L. Enhanced 4D cone-beam CT with inter-phase motion model. Medical Physics. 2007;34(9):3688-95.

255.   Robinson D, Liu D, Steciw S, Field C, Daly H, Saibishkumar EP, et al. An evaluation of the Clarity 3D ultrasound system for prostate localization. Journal of Applied Clinical Medical Physics. 2012;13(4):100-12.

256.   Mutic S, Dempsey JF. The ViewRay System: Magnetic Resonance–Guided and Controlled Radiotherapy. Seminars in Radiation Oncology. 2014;24(3):196-9.

257.   Fan Q, Nanduri A, Mazin S, Zhu L. Emission guided radiation therapy for lung and prostate cancers: a feasibility study on a digital patient. Med Phys. 2012;39(11):7140-52.

258.   Grills IS, Hugo G, Kestin LL, Galerani AP, Chao KK, Wloch J, et al. Image-Guided Radiotherapy via Daily Online Cone-Beam CT Substantially Reduces Margin Requirements for Stereotactic Lung Radiotherapy. International Journal of Radiation Oncology*Biology*Physics. 2008;70(4):1045-56.

259.   Den RB, Doemer A, Kubicek G, Bednarz G, Galvin JM, Keane WM, et al. Daily Image Guidance With Cone-Beam Computed Tomography for Head-and-Neck Cancer Intensity-Modulated Radiotherapy: A Prospective Study. International Journal of Radiation Oncology*Biology*Physics. 2010;76(5):1353-9.

260.   Chen AM, Yu Y, Daly ME, Farwell DG, H. Benedict S, Purdy JA. Long-term experience with reduced planning target volume margins and intensity-modulated radiotherapy with daily image-guidance for head and neck cancer. Head & Neck. 2014;36(12):1766-72.

261.   Sveistrup J, af Rosenschöld PM, Deasy JO, Oh JH, Pommer T, Petersen PM, et al. Improvement in toxicity in high risk prostate cancer patients treated with image-guided intensity-modulated radiotherapy compared to 3D conformal radiotherapy without daily image guidance. Radiation Oncology. 2014;9(1):44.

262.   Becker-Schiebe M, Abaci A, Ahmad T, Hoffmann W. Reducing radiation-associated toxicity using online image guidance (IGRT) in prostate cancer patients undergoing dose-escalated radiation therapy. Reports of Practical Oncology & Radiotherapy. 2016;21(3):188-94.

263.   Burridge N, Amer A, Marchant T, Sykes J, Stratford J, Henry A, et al. Online adaptive radiotherapy of the bladder: Small bowel irradiated-volume reduction. International Journal of Radiation Oncology*Biology*Physics. 2006;66(3):892-7.

264.   Foroudi F, Pham D, Bressel M, Wong J, Rolfo A, Roxby P, et al. Bladder cancer radiotherapy margins: a comparison of daily alignment using skin, bone or soft tissue. Clin Oncol (R Coll Radiol). 2012;24(10):673-81.

265.   Perkins CL, Fox T, Elder E, Kooby DA, Staley CA, 3rd, Landry J. Image-guided radiation therapy (IGRT) in gastrointestinal tumors. JOP : Journal of the pancreas. 2006;7(4):372-81.

266.   Brink C, Bernchou U, Bertelsen A, Hansen O, Schytte T, Bentzen SM. Locoregional Control of Non-Small Cell Lung Cancer in Relation to Automated Early Assessment of Tumor Regression on Cone Beam Computed Tomography. International Journal of Radiation Oncology*Biology*Physics. 2014;89(4):916-23.

267.   Knap MM, Hoffmann L, Nordsmark M, Vestergaard A. Daily cone-beam computed tomography used to determine tumour shrinkage and localisation in lung cancer patients. Acta Oncologica. 2010;49(7):1077-84.

268.   Purdie TG, Bissonnette J-P, Franks K, Bezjak A, Payne D, Sie F, et al. Cone-Beam Computed Tomography for On-Line Image Guidance of Lung Stereotactic Radiotherapy: Localization, Verification, and Intrafraction Tumor Position. International Journal of Radiation Oncology*Biology*Physics. 2007;68(1):243-52.

269.   Worm ES, Hansen AT, Petersen JB, Muren LP, Præstegaard LH, Høyer M. Inter- and intrafractional localisation errors in cone-beam CT guided stereotactic radiation therapy of tumours in the liver and lung. Acta Oncologica. 2010;49(7):1177-83.

270.   Sweeney RA, Seubert B, Stark S, Homann V, Müller G, Flentje M, et al. Accuracy and inter-observer variability of 3D versus 4D cone-beam CT based image-guidance in SBRT for lung tumors. Radiation Oncology. 2012;7(1):81.

271.   Dawson LA, Eccles C, Bissonnette J-P, Brock KK. Accuracy of daily image guidance for hypofractionated liver radiotherapy with active breathing control. International Journal of Radiation Oncology*Biology*Physics. 2005;62(4):1247-52.

272.   Guckenberger M, Sweeney RA, Wilbert J, Krieger T, Richter A, Baier K, et al. Image-Guided Radiotherapy for Liver Cancer Using Respiratory-Correlated Computed Tomography and Cone-Beam

Computed Tomography. International Journal of Radiation Oncology*Biology*Physics. 2008;71(1):297-304.

273.   Park JC, Park SH, Kim JH, Yoon SM, Song SY, Liu Z, et al. Liver motion during cone beam computed tomography guided stereotactic body radiation therapy. Medical Physics. 2012;39(10):6431-42.

274.   Qian G, Lowry J, Silverman P, Grosman I, Makara D, Lederman G. Stereotactic extra-cranial radiosurgery for renal cell carcinoma. International Journal of Radiation Oncology*Biology*Physics. 2003;57(2):S283.

275.   Beitler JJ, Makara D, Silverman P, Lederman G. Definitive, High-Dose-Per-Fraction, Conformal, Stereotactic External Radiation for Renal Cell Carcinoma. American Journal of Clinical Oncology. 2004;27(6):646-8.

276.   Wersäll PJ, Blomgren H, Lax I, Kälkner K-M, Linder C, Lundell G, et al. Extracranial stereotactic radiotherapy for primary and metastatic renal cell carcinoma. Radiotherapy and Oncology. 2005;77(1):88-95.

277.   Gilson B, Lederman G, Qian G, Fastaia M, Cangiane L. 2249. International Journal of Radiation Oncology*Biology*Physics. 2006;66(3):S349.

278.   Teh B, Bloch C, Galli-Guevara M, Doh L, Richardson S, Chiang S, et al. The treatment of primary and metastatic renal cell carcinoma (RCC) with image-guided stereotactic body radiation therapy (SBRT). Biomed Imaging Interv J. 2007;3(1):e6.

279.   Svedman C, Karlsson K, Rutkowska E, Sandström P, Blomgren H, Lax I, et al. Stereotactic body radiotherapy of primary and metastatic renal lesions for patients with only one functioning kidney. Acta Oncologica. 2008;47(8):1578-83.

280.   Nomiya T, Tsuji H, Hirasawa N, Kato H, Kamada T, Mizoe J, et al. Carbon Ion Radiation Therapy for Primary Renal Cell Carcinoma: Initial Clinical Experience. International Journal of Radiation Oncology*Biology*Physics. 2008;72(3):828-33.

281.   Kasuya G, Tsuji H, Nomiya T, Makishima H, Haruyama Y, Kobashi G, et al. Prospective clinical trial of 12-fraction carbon-ion radiotherapy for primary renal cell carcinoma. Oncotarget. 2019;10(1):76-81.

282.   Kaplan ID, Redrosa I, Martin C, Collins C, Wagner A. Results of a Phase I Dose Escalation Study of Stereotactic Radiosurgery for Primary Renal Tumors. International Journal of Radiation Oncology*Biology*Physics. 2010;78(3, Supplement):S191.

283.   McBride SM, Wagner AA, Kaplan ID. A Phase 1 Dose-Escalation Study of Robotic Radiosurgery in Inoperable Primary Renal Cell Carcinoma. International Journal of Radiation Oncology • Biology • Physics. 2013;87(2):S84.

284.   Lo C-H, Huang W-Y, Chao H-L, Lin K-T, Jen Y-M. Novel application of stereotactic ablative radiotherapy using CyberKnife(®) for early-stage renal cell carcinoma in patients with pre-existing chronic kidney disease: Initial clinical experiences. Oncology Letters. 2014;8(1):355-60.

285.   Ponsky L, Lo SS, Zhang Y, Schluchter M, Liu Y, Patel R, et al. Phase I dose-escalation study of stereotactic body radiotherapy (SBRT) for poor surgical candidates with localized renal cell carcinoma. Radiotherapy and Oncology. 2015;117(1):183-7.

286.   Staehler M, Bader M, Schlenker B, Casuscelli J, Karl A, Roosen A, et al. Single Fraction Radiosurgery for the Treatment of Renal Tumors. The Journal of Urology. 2015;193(3):771-5.

287.   Chang JH, Cheung P, Erler D, Sonier M, Korol R, Chu W. Stereotactic Ablative Body Radiotherapy for Primary Renal Cell Carcinoma in Non-surgical Candidates: Initial Clinical Experience. Clinical Oncology. 2016;28(9):e109-e14.

288.   Yamamoto T, Kadoya N, Takeda K, Matsushita H, Umezawa R, Sato K, et al. Renal atrophy after stereotactic body radiotherapy for renal cell carcinoma. Radiat Oncol. 2016;11:72.

289.   Correa RJM, Rodrigues GB, Chen H, Warner A, Ahmad B, Louie AV. Stereotactic Ablative Radiotherapy (SABR) for Large Renal Tumors: A Retrospective Case Series Evaluating Clinical Outcomes, Toxicity, and Technical Considerations. Am J Clin Oncol. 2018;41(6):568-75.

290.   Funayama S, Onishi H, Kuriyama K, Komiyama T, Marino K, Araya M, et al. Renal Cancer is Not Radioresistant: Slowly but Continuing Shrinkage of the Tumor After Stereotactic Body Radiation Therapy. Technology in cancer research & treatment. 2019;18:1533033818822329-.

291.   Foote M, Bailey M, Smith L, Siva S, Hegi-Johnson F, Seeley A, et al. Guidelines for safe practice of stereotactic body (ablative) radiation therapy. Journal of Medical Imaging and Radiation Oncology. 2015;59(5):646-53.

292.   Radiologists TRAaNZCo. Guidelines for Safe Practice of Stereotactic Body (Ablative) Radiation Therapy. Sydney, Australia: The Royal Australian and New Zealand College of Radiologists; 2015.

293.   Consortium US. Stereotactic Ablative Body Radiotherapy (SABR): A Resource

United Kingdom: SABR Consortium; 2019. Report No.: 6.1 Contract No.: 6.1.

294.   Sahgal A, Roberge D, Schellenberg D, Purdie TG, Swaminath A, Pantarotto J, et al. The Canadian Association of Radiation Oncology Scope of Practice Guidelines for Lung, Liver and Spine Stereotactic Body Radiotherapy. Clinical Oncology. 2012;24(9):629-39.

295.   Potters L, Kavanagh B, Galvin JM, Hevezi JM, Janjan NA, Larson DA, et al. American Society for Therapeutic Radiology and Oncology (ASTRO) and American College of Radiology (ACR) Practice Guideline for the Performance of Stereotactic Body Radiation Therapy. International Journal of Radiation Oncology*Biology*Physics. 2010;76(2):326-32.

296.   Pan H, Simpson DR, Mell LK, Mundt AJ, Lawson JD. A survey of stereotactic body radiotherapy use in the United States. Cancer. 2011;117(19):4566-72.

297.   Siva S, Ellis RJ, Ponsky L, Teh BS, Mahadevan A, Muacevic A, et al. Consensus statement from the International Radiosurgery Oncology Consortium for Kidney for primary renal cell carcinoma. Future Oncology. 2016;12(5):637-45.

298.   Song R, Tipirneni A, Johnson P, Loeffler RB, Hillenbrand CM. Evaluation of respiratory liver and kidney movements for MRI navigator gating. Journal of Magnetic Resonance Imaging. 2011;33(1):143-8.

299.   Stam MK, Vulpen Mv, Barendrecht MM, Zonnenberg BA, Intven M, Crijns SPM, et al. Kidney motion during free breathing and breath hold for MR-guided radiotherapy. Physics in Medicine and Biology. 2013;58(7):2235.

300.   Sonier M, Chu W, Korol RM. Evaluation of Immobilization on Target Localization for Image-Guided Kidney/Adrenal SBRT. International Journal of Radiation Oncology*Biology*Physics. 2014;90(1, Supplement):S898-S9.

301.   West K, Russo M, Brown E, Barry T, Hargrave C, Pryor D. Evaluation of kidney motion with and without a pneumatic abdominal compression belt: Considerations for stereotactic radiotherapy. J Med Imaging Radiat Oncol. 2018;62(1):128-32.

302.   Prins FM, Stemkens B, Kerkmeijer LGW, Barendrecht MM, de Boer HJ, Vonken E-JPA, et al. Intrafraction Motion Management of Renal Cell Carcinoma With Magnetic Resonance Imaging-Guided Stereotactic Body Radiation Therapy. Practical Radiation Oncology. 2019;9(1):e55-e61.

303.   Rudra S, Fischer-Valuck B, Pachynski R, Daly M, Green O. Magnetic Resonance Image Guided Stereotactic Body Radiation Therapy to the Primary Renal Mass in Metastatic Renal Cell Carcinoma. Advances in Radiation Oncology. 2019.

304.   Centers DoR. Status of Radiation Therapy Equipment: IAEA; [Available from: https://dirac.iaea.org/Query/Map2?mapId=2.

305.   Svedman C, Sandström P, Pisa P, Blomgren H, Lax I, Kälkner K-M, et al. A prospective Phase II trial of using extracranial stereotactic radiotherapy in primary and metastatic renal cell carcinoma. Acta Oncologica. 2006;45(7):870-5.

306.   Kuo JS, Yu C, Petrovich Z, Apuzzo MLJ. The CyberKnife Stereotactic Radiosurgery System: Description, Installation, and an Initial Evaluation of Use and Functionality. Neurosurgery. 2003;53(5):1235-9.

307.   Accuray. Cyberknife Treatment Delivery System: Technical Specifications 2018 [Available from: https://www.accuray.com/wp-content/uploads/cyberknife-treatment-delivery-system_-technical-specifications.pdf.

308.   Senger C, Conti A, Kluge A, Pasemann D, Kufeld M, Acker G, et al. Robotic stereotactic ablative radiotherapy for renal cell carcinoma in patients with impaired renal function. BMC Urology. 2019;19(1):96.

309.   Peddada AV, Anderson D, Blasi OC, McCollough K, Jennings SB, Monroe AT. Nephron Sparing Robotic Radiosurgical Therapy for Primary Renal Cell Carcinoma: Single Institution Experience and Review of the Literature. Advances in Radiation Oncology. 2019.

310.   Staehler M, Fürweger C, Kufeld M, Karl A, Roosen A, Stief C, et al. Cyberknife radiosurgery of a renal pelvis tumor to avoid renal dialysis2010.

311.   Grubb W, Ponsky L, Lo SS, Traughber BJ, Jr., Zhang Y, Liu Y, et al. Dose Escalation to 60 Gy in 3 Fractions with Stereotactic Body Radiation Therapy (SBRT) for Poor Surgical Candidates with Localized Renal Cell Carcinoma: Expansion of a Phase I Study. International Journal of Radiation Oncology • Biology • Physics. 2018;102(3):e91.

312.   Nelson RG, Tuttle KR. The New KDOQI[TM] Clinical Practice Guidelines and Clinical Practice Recommendations for Diabetes and CKD. Blood Purification. 2007;25(1):112-4.

313.   Correa RJM, Louie AV, Zaorsky NG, Lehrer EJ, Ellis R, Ponsky L, et al. The Emerging Role of Stereotactic Ablative Radiotherapy for Primary Renal Cell Carcinoma: A Systematic Review and Meta-Analysis. European Urology Focus. 2019;5(6):958-69.

314.   Correa RJM, Ahmad B, Warner A, Johnson C, MacKenzie MJ, Pautler SE, et al. A prospective phase I dose-escalation trial of stereotactic ablative radiotherapy (SABR) as an alternative to cytoreductive nephrectomy for inoperable patients with metastatic renal cell carcinoma. Radiation Oncology. 2018;13(1):47.

315.   Zaorsky NG, Lehrer EJ, Kothari G, Louie AV, Siva S. Stereotactic ablative radiation therapy for oligometastatic renal cell carcinoma (SABR ORCA): a meta-analysis of 28 studies. European urology oncology. 2019;2(5):515-23.

316.   Pham D, Thompson A, Kron T, Foroudi F, Kolsky MS, Devereux T, et al. Stereotactic Ablative Body Radiation Therapy for Primary Kidney Cancer: A 3-Dimensional Conformal Technique Associated With Low Rates of Early Toxicity. International Journal of Radiation Oncology*Biology*Physics. 2014(0).

317.   Siva S, Pham D, Kron T, Bressel M, Lam J, Tan TH, et al. Stereotactic ablative body radiotherapy for inoperable primary kidney cancer: a prospective clinical trial. BJU International. 2017:n/a-n/a.

318.   Pham D, Kron T, Foroudi F, Schneider M, Siva S. A Review of Kidney Motion Under Free, Deep and Forced-shallow Breathing Conditions: Implications for Stereotactic Ablative Body Radiotherapy Treatment. Technol Cancer Res Treat. 2013.

319.   Seer Cancer Statistics Review 2012 [

320.   Flanigan RC, Salmon SE, Blumenstein BA, Bearman SI, Roy V, McGrath PC, et al. Nephrectomy Followed by Interferon Alfa-2b Compared with Interferon Alfa-2b Alone for Metastatic Renal-Cell Cancer. New England Journal of Medicine. 2001;345(23):1655-9.

321.   Kjaer M, Frederiksen PL, Engelholm S. Postoperative radiotherapy in stage II and III renal adenocarcinoma. A randomized trial by the Copenhagen renal cancer study group. International Journal of Radiation Oncology*Biology*Physics. 1987;13(5):665-72.

322.   Timmerman RD. Surgery Versus Stereotactic Body Radiation Therapy for Early-Stage Lung Cancer: Who's Down for the Count? Journal of Clinical Oncology. 2010;28(6):907-9.

323.   Kavanagh BD, Schefter TE, Cardenes HR, Stieber VW, Raben D, Timmerman RD, et al. Interim analysis of a prospective phase I/II trial of SBRT for liver metastases. Acta Oncologica. 2006;45(7):848-55.

324.   Siva S, Pham D, Gill S, Corcoran NM, Foroudi F. A systematic review of stereotactic radiotherapy ablation for primary renal cell carcinoma. BJU International. 2012:no-no.

325.   Gray HM. Anatomy of the human body. 30th ed. Philadelphia: Lea & Febiger; 1985.

326.   Keall PJ, Mageras GS, Balter JM, Emery RS, Forster KM, Jiang SB, et al. The management of respiratory motion in radiation oncology report of AAPM Task Group 76. Medical Physics. 2006;33(10):3874-900.

327.   Plathow C, Zimmermann H, Fink C, Umathum R, Schöbinger M, Huber P, et al. Influence of different breathing maneuvers on internal and external organ motion: Use of fiducial markers in dynamic MRI. International Journal of Radiation Oncology*Biology*Physics. 2005;62(1):238-45.

328.   Barnes EA, Murray BR, Robinson DM, Underwood LJ, Hanson J, Roa WH. Dosimetric evaluation of lung tumor immobilization using breath hold at deep inspiration. International journal of radiation oncology, biology, physics. 2001;50(4):1091-8.

329.   Han K, Cheung P, Basran PS, Poon I, Yeung L, Lochray F. A comparison of two immobilization systems for stereotactic body radiation therapy of lung tumors. Radiotherapy and Oncology. 2010;95(1):103-8.

330.   Moorrees J, Bezak E. Four dimensional CT imaging: a review of current technologies and modalities. Australas Phys Eng Sci Med. 2012;35(1):9-23.

331.   Kim YS, Park SH, Ahn SD, Lee JE, Choi EK, Lee S-w, et al. Differences in abdominal organ movement between supine and prone positions measured using four-dimensional computed tomography. Radiotherapy and Oncology. 2007;85(3):424-8.

332.   Lee S, Yang DS, Choi MS, Kim CY. Development of Respiratory Motion Reduction Device System (RMRDs) for Radiotherapy in Moving Tumors. Japanese Journal of Clinical Oncology. 2004;34(11):686-91.

333.   Katoh N, Onimaru R, Sakuhara Y, Abo D, Shimizu S, Taguchi H, et al. Real-time tumor-tracking radiotherapy for adrenal tumors. Radiotherapy and Oncology. 2008;87(3):418-24.

334.   Moerland MA, van den Bergh ACM, Bhagwandien R, Janssen WM, Bakker CJG, Lagendijk JJW, et al. The influence of respiration induced motion of the kidneys on the accuracy of radiotherapy treatment planning, a magnetic resonance imaging study. Radiotherapy and Oncology. 1994;30(2):150-4.

335.   Schwartz LH, Richaud J, Buffat L, Touboul E, Schlienger M. Kidney mobility during respiration. Radiotherapy and Oncology. 1994;32(1):84-6.

336.   Suramo I, Paivansalo M, Myllyla V. Cranio-caudal movements of the liver, pancreas and kidneys in respiration. Acta radiologica: diagnosis. 1984;25(2):129-31.

337.   Ahmad NR, Huq MS, Corn BW. Respiration-induced motion of the kidneys in whole abdominal radiotherapy: implications for treatment planning and late toxicity. Radiotherapy and Oncology. 1997;42(1):87-90.

338.   Aruga T, Itami J, Aruga M, Nakajima K, Shibata K, Nojo T, et al. Target volume definition for upper abdominal irradiation using CT scans obtained during inhale and exhale phases. International Journal of Radiation Oncology*Biology*Physics. 2000;48(2):465-9.

339.   Balter JM, Ten Haken RK, Lawrence TS, Lam KL, Robertson JM. Uncertainties in CT-based radiation therapy treatment planning associated with patient breathing. International Journal of Radiation Oncology*Biology*Physics. 1996;36(1):167-74.

340.   Draney MT, Zarins CK, Taylor CA. Three-Dimensional Analysis of Renal Artery Bending Motion During Respiration. Journal of Endovascular Therapy. 2005;12(3):380-6.

341.   Wysocka B, Kassam Z, Lockwood G, Brierley J, Dawson LA, Buckley CA, et al. Interfraction and Respiratory Organ Motion During Conformal Radiotherapy in Gastric Cancer. International Journal of Radiation Oncology*Biology*Physics. 2010;77(1):53-9.

342.   Boucher L, Rodrigue S, Lecomte R, Bénard F. Respiratory Gating for 3-Dimensional PET of the Thorax: Feasibility and Initial Results. Journal of Nuclear Medicine. 2004;45(2):214-9.

343.   Brandner ED, Wu A, Chen H, Heron D, Kalnicki S, Komanduri K, et al. Abdominal organ motion measured using 4D CT. International Journal of Radiation Oncology*Biology*Physics. 2006;65(2):554-60.

344.   Bussels B, Goethals L, Feron M, Bielen D, Dymarkowski S, Suetens P, et al. Respiration-induced movement of the upper abdominal organs: a pitfall for the three-dimensional conformal radiation treatment of pancreatic cancer. Radiotherapy and Oncology. 2003;68(1):69-74.

345.   Davies SC, Hill AL, Holmes RB, Halliwell M, Jackson PC. Ultrasound quantitation of respiratory organ motion in the upper abdomen. British Journal of Radiology. 1994;67(803):1096-102.

346.   Gawthrop JB, Gill S. The use of respiratory-correlated four-dimensional CT where kidney motion has the potential to impact upon the radiotherapy planning process. Journal of Medical Imaging and Radiation Oncology. 2012;56(6):689-95.

347.   Giraud P, Yorke E, Ford EC, Wagman R, Mageras GS, Amols H, et al. Reduction of organ motion in lung tumors with respiratory gating. Lung Cancer. 2006;51(1):41-51.

348.	Goldstein SD, Ford EC, Duhon M, McNutt T, Wong J, Herman JM. Use of Respiratory-Correlated Four-Dimensional Computed Tomography to Determine Acceptable Treatment Margins for Locally Advanced Pancreatic Adenocarcinoma. International Journal of Radiation Oncology*Biology*Physics. 2010;76(2):597-602.

349.	Hallman JL, Mori S, Sharp GC, Lu H-M, Hong TS, Chen GTY. A Four-Dimensional Computed Tomography Analysis of Multiorgan Abdominal Motion. International Journal of Radiation Oncology*Biology*Physics. 2012;83(1):435-41.

350.	Siva S, Pham D, Bressel M, Gill S, Herschtal A, Dang K, et al. Analysis of Potential Surrogates for Kidney Motion Verification Imaging and its Implications for Stereotactic Radiation Therapy of the Kidney. International Journal of Radiation Oncology*Biology*Physics. 2012;84(3, Supplement):S423.

351.	Tai A, Liang Z, Erickson B, Li XA. Management of Respiration-Induced Motion With 4-Dimensional Computed Tomography (4DCT) for Pancreas Irradiation. International Journal of Radiation Oncology*Biology*Physics. 2013(0).

352.	van Sörnsen de Koste JR, Senan S, Kleynen CE, Slotman BJ, Lagerwaard FJ. Renal mobility during uncoached quiet respiration: An analysis of 4DCT scans. International Journal of Radiation Oncology*Biology*Physics. 2006;64(3):799-803.

353.	Nazmy MS, Khafaga Y, Mousa A, Khalil E. Cone beam CT for organs motion evaluation in pediatric abdominal neuroblastoma. Radiotherapy and Oncology. 2012;102(3):388-92.

354.	Pai Panandiker AS, Sharma S, Naik MH, Wu S, Hua C, Beltran C, et al. Novel Assessment of Renal Motion in Children as Measured via Four-Dimensional Computed Tomography. International Journal of Radiation Oncology*Biology*Physics. 2012;82(5):1771-6.

355.	Fletcher ME, Stack C, Ewart M, Davies CJ, Ridley S, Hatch DJ, et al. Respiratory compliance during sedation, anesthesia, and paralysis in infants and young children. Journal of Applied Physiology. 1991;70(5):1977-82.

356.	Bancalari E, Clausen J. Pathophysiology of changes in absolute lung volumes. European Respiratory Journal. 1998;12(1):248-58.

357.	Simpson DR, Lawson JD, Nath SK, Rose BS, Mundt AJ, Mell LK. Utilization of Advanced Imaging Technologies for Target Delineation in Radiation Oncology. Journal of the American College of Radiology. 2009;6(12):876-83.

358.	Khoo VS, Dearnaley DP, Finnigan DJ, Padhani A, Tanner SF, Leach MO. Magnetic resonance imaging (MRI): considerations and applications in radiotherapy treatment planning. Radiotherapy and Oncology. 1997;42(1):1-15.

359.	Cai J, Chang Z, Wang Z, Segars WP, Yin F-F. Four-dimensional magnetic resonance imaging (4D-MRI) using image-based respiratory surrogate: A feasibility study. Medical Physics. 2011;38(12):6384-94.

360.	Teh B, Bloch C, Galli-Guevara M, Doh L, Richardson S, Chiang S, et al. The treatment of primary and metastatic renal cell carcinoma (RCC) with image-guided stereotactic body radiation therapy (SBRT). Biomed Imaging Interv J. 2007;3(1):e6. doi: 10.2349/biij.3.1.e6. Epub 007 Jan 1.

361.	Pham D, Kron T, Foroudi F, Siva S. Effect of different breathing patterns in the same patient on stereotactic ablative body radiotherapy dosimetry for primary renal cell carcinoma: A case study. Medical dosimetry : official journal of the American Association of Medical Dosimetrists. 2013.

362.	Bohris C, Stief CG, Strittmatter F. Improvement of SWL Efficacy: Reduction of the Respiration-Induced Kidney Motion by Using an Abdominal Compression Plate. Journal of Endourology. 2015;30(4):411-6.

363.	Hoon Jung S, Min Yoon S, Ho Park S, Cho B, Won Park J, Jung J, et al. Four-dimensional dose evaluation using deformable image registration in radiotherapy for liver cancer. Medical Physics. 2013;40(1):011706.

364.	Pham D, Kron T, Styles C, Whitaker M, Bressel M, Foroudi F, et al. The Use of Dual Vacuum Stabilization Device to Reduce Kidney Motion for Stereotactic Radiotherapy Planning. Technology in cancer research & treatment. 2014.

365.	Yamashita H, Yamashita M, Futaguchi M, Takenaka R, Shibata S, Yamamoto K, et al. Individually wide range of renal motion evaluated by four-dimensional computed tomography. SpringerPlus. 2014;3(1):1-7.

366.   Abhilash RH, Chauhan S, Che MV, Ooi C-C, Bakar RA, Lo RHG. Quantitative Study on the Effect of Abnormalities on Respiration-Induced Kidney Movement. Ultrasound in Medicine & Biology. 2016;42(7):1681-8.

367.   Van Gelder R, Wong S, Le A, Podreka A, Briggs A, Haddad C, et al. Experience with an abdominal compression band for radiotherapy of upper abdominal tumours. Journal of Medical Radiation Sciences. 2018;65(1):48-54.

368.   Damato AL, Brown J, Lee LJ, Viswanathan AN. Changes in Kidney Position and Dose Due to Respiratory Motion in Gynecologic Patients Receiving Extended Field Intensity Modulated Radiation Therapy. International Journal of Radiation Oncology • Biology • Physics.90(1):S879.

369.   Tai A, Liang Z, Erickson B, Li XA. Management of Respiration-Induced Motion With 4-Dimensional Computed Tomography (4DCT) for Pancreas Irradiation. International Journal of Radiation Oncology*Biology*Physics. 2013;86(5):908-13.

370.   R. HS, Shirley YLM, Jr. WJC, O. CR, W. TB. Quantification of the Range of Motion of Kidney and Ureteral Stones During Shockwave Lithotripsy in Conscious Patients. Journal of Endourology. 2016;30(4):406-10.

371.   West K, Russo M, Brown E, Barry T, Hargrave C, Pryor D. Evaluation of kidney motion with and without a pneumatic abdominal compression belt: Considerations for stereotactic radiotherapy. Journal of Medical Imaging and Radiation Oncology. 2018;62(1):128-32.

372.   Cusumano D, Dhont J, Boldrini L, Chiloiro G, Teodoli S, Massaccesi M, et al. Predicting tumour motion during the whole radiotherapy treatment: a systematic approach for thoracic and abdominal lesions based on real time MR. Radiotherapy and Oncology. 2018;129(3):456-62.

373.   Pham D, Kron T, Bressel M, Foroudi F, Hardcastle N, Schneider M, et al. Image guidance and stabilization for stereotactic ablative body radiation therapy (SABR) treatment of primary kidney cancer. Practical Radiation Oncology. 2015;5(6):e597-e605.

374.   Huijskens SC, van Dijk IWEM, de Jong R, Visser J, Fajardo RD, Ronckers CM, et al. Quantification of renal and diaphragmatic interfractional motion in pediatric image-guided radiation therapy: A multicenter study. Radiotherapy and Oncology. 2015;117(3):425-31.

375.   Uh J, Krasin MJ, Li Y, Li X, Tinkle C, Lucas JT, Jr., et al. Quantification of Pediatric Abdominal Organ Motion With a 4-Dimensional Magnetic Resonance Imaging Method. International Journal of Radiation Oncology • Biology • Physics. 2017;99(1):227-37.

376.   Christian B, G. SC, Frank S. Improvement of SWL Efficacy: Reduction of the Respiration-Induced Kidney Motion by Using an Abdominal Compression Plate. Journal of Endourology. 2016;30(4):411-6.

377.   Baba F, Shibamoto Y, Tomita N, Ikeya-Hashizume C, Oda K, Ayakawa S, et al. Stereotactic body radiotherapy for stage I lung cancer and small lung metastasis: evaluation of an immobilization system for suppression of respiratory tumor movement and preliminary results. Radiation Oncology. 2009;4(1):15.

378.   Bengua G, Ishikawa M, Sutherland K, Horita K, Yamazaki R, Fujita K, et al. Evaluation of the Effectiveness of the Stereotactic Body Frame in Reducing Respiratory Intrafractional Organ Motion Using the Real-Time Tumor-Tracking Radiotherapy System. International Journal of Radiation Oncology*Biology*Physics. 2010;77(2):630-6.

379.   Bouilhol G, Ayadi M, Rit S, Thengumpallil S, Schaerer J, Vandemeulebroucke J, et al. Is abdominal compression useful in lung stereotactic body radiation therapy? A 4DCT and dosimetric lobe-dependent study. Physica Medica. 2013;29(4):333-40.

380.   Kontrisova K, Stock M, Dieckmann K, Bogner J, Pötter R, Georg D. Dosimetric comparison of stereotactic body radiotherapy in different respiration conditions: A modeling study. Radiotherapy and Oncology. 2006;81(1):97-104.

381.   Molinelli S, de Pooter J, Romero AM, Wunderink W, Cattaneo M, Calandrino R, et al. Simultaneous tumour dose escalation and liver sparing in Stereotactic Body Radiation Therapy (SBRT) for liver tumours due to CTV-to-PTV margin reduction. Radiotherapy and Oncology. 2008;87(3):432-8.

382.   Whitaker M, Franich R, Whitaker J, Kron T. A software tool to assess patient suitability for respiratory gated radiotherapy using breathing patterns obtained with different methods. Journal of Medical Imaging and Radiation Oncology. 2009;53:Suppl, A190.

383.   Siva S, Devereux T, Kron T, Gill S, Macmanus M, Bressel M, et al. Vacuum immobilisation reduces tumour excursion and minimises intrafraction error in a cohort study of stereotactic ablative body radiotherapy for pulmonary metastases. Journal of Medical Imaging and Radiation Oncology. 2013.

384.   Jiang SB. Technical aspects of image-guided respiration-gated radiation therapy. Medical Dosimetry. 2006;31(2):141-51.

385.   Kirkbride P, Cooper T. Stereotactic Body Radiotherapy. Guidelines for Commissioners, Providers and Clinicians: a National Report. Clinical Oncology. 2011;23(3):163-4.

386.   Timmerman R, Galvin J, Michalski J, Straube W, Ibbott G, Martin E, et al. Accreditation and quality assurance for Radiation Therapy Oncology Group: Multicenter clinical trials using Stereotactic Body Radiation Therapy in lung cancer. Acta Oncologica. 2006;45(7):779-86.

387.   Liu R, Buatti JM, Howes TL, Dill J, Modrick JM, Meeks SL. Optimal number of beams for stereotactic body radiotherapy of lung and liver lesions. International Journal of Radiation Oncology*Biology*Physics. 2006;66(3):906-12.

388.   Dong P, Lee P, Ruan D, Long T, Romeijn E, Yang Y, et al. 4π Non-Coplanar Liver SBRT: A Novel Delivery Technique. International Journal of Radiation Oncology*Biology*Physics. 2013;85(5):1360-6.

389.   Ewing MM, DesRosiers C, Fakiris AJ, DeBliek CR, Kiszka DN, Stinson ER, et al. Conformality Study for Stereotactic Radiosurgery of the Lung. Medical Dosimetry. 2011;36(1):14-20.

390.   Weksberg DC, Palmer MB, Vu KN, Rebueno NC, Sharp HJ, Luo D, et al. Generalizable Class Solutions for Treatment Planning of Spinal Stereotactic Body Radiation Therapy. International Journal of Radiation Oncology*Biology*Physics. 2012;84(3):847-53.

391.   Takeda A, Ohashi T, Kunieda E, Sanuki N, Enomoto T, Takeda T, et al. Comparison of clinical, tumour-related and dosimetric factors in grade 0–1, grade 2 and grade 3 radiation pneumonitis after stereotactic body radiotherapy for lung tumours. The British Journal of Radiology. 2012;85(1013):636-42.

392.   Son SH, Choi BO, Ryu MR, Kang YN, Jang JS, Bae SH, et al. Stereotactic Body Radiotherapy for Patients With Unresectable Primary Hepatocellular Carcinoma: Dose-Volumetric Parameters Predicting the Hepatic Complication. International Journal of Radiation Oncology*Biology*Physics. 2010;78(4):1073-80.

393.   Pan CC, Kavanagh BD, Dawson LA, Li XA, Das SK, Miften M, et al. Radiation-Associated Liver Injury. International Journal of Radiation Oncology*Biology*Physics. 2010;76(3, Supplement):S94-S100.

394.   Xiao Y, Papiez L, Paulus R, Timmerman R, Straube WL, Bosch WR, et al. Dosimetric Evaluation of Heterogeneity Corrections for RTOG 0236: Stereotactic Body Radiotherapy of Inoperable Stage I-II Non–Small-Cell Lung Cancer. International Journal of Radiation Oncology*Biology*Physics. 2009;73(4):1235-42.

395.   Hurkmans C, Cuijpers J, Lagerwaard F, Widder J, van der Heide U, Schuring D, et al. Recommendations for implementing stereotactic radiotherapy in peripheral stage IA non-small cell lung cancer: report from the Quality Assurance Working Party of the randomised phase III ROSEL study. Radiation Oncology. 2009;4(1):1.

396.   Lo SS, Sahgal A, Chang EL, Mayr NA, Teh BS, Huang Z, et al. Serious Complications Associated with Stereotactic Ablative Radiotherapy and Strategies to Mitigate the Risk. Clinical Oncology. 2013;25(6):378-87.

397.   Grimm J, LaCouture T, Croce R, Yeo I, Zhu Y, Xue J. Dose tolerance limits and dose volume histogram evaluation for stereotactic body radiotherapy2011.

398.   Sweeney R, Seubert B, Stark S, Homann V, Muller G, Flentje M, et al. Accuracy and inter-observer variability of 3D versus 4D cone-beam CT based image-guidance in SBRT for lung tumors. Radiation Oncology. 2012;7(1):81.

399.   Balter JM, Dawson LA, Kazanjian S, McGinn C, Brock KK, Lawrence T, et al. Determination of ventilatory liver movement via radiographic evaluation of diaphragm position. International Journal of Radiation Oncology*Biology*Physics. 2001;51(1):267-70.

400.   Fowler JF. The linear-quadratic formula and progress in fractionated radiotherapy. The British Journal of Radiology. 1989;62(740):679-94.

401.   Ning S, Trisler K, Wessels BW, Knox SJ. Radiobiologic studies of radioimmunotherapy and external beam radiotherapy in Vitro and in Vivo in human renal cell carcinoma xenografts. Cancer. 1997;80(S12):2519-28.

402.   Siva S, Pham D, Gill S, Bressel M, Dang K, Devereux T, et al. An analysis of respiratory induced kidney motion on four-dimensional computed tomography and its implications for stereotactic kidney radiotherapy. Radiation Oncology. 2013;8(1):248.

403.   Pham D, Kron T, Foroudi F, Siva S. Effect of different breathing patterns in the same patient on stereotactic ablative body radiotherapy dosimetry for primary renal cell carcinoma: A case study. Medical Dosimetry. 2013;38(3):304-8.

404.   Sonier M, Chu W, Korol RM. Evaluation of Immobilization on Target Localization for Image-Guided Kidney/Adrenal SBRT. International Journal of Radiation Oncology • Biology • Physics. 2014;90(1):S898-S9.

405.   Foster R, Meyer J, Iyengar P, Pistenmaa D, Timmerman R, Choy H, et al. Localization Accuracy and Immobilization Effectiveness of a Stereotactic Body Frame for a Variety of Treatment Sites. International Journal of Radiation Oncology • Biology • Physics. 2013;87(5):911-6.

406.   Bibault J-E, Prevost B, Dansin E, Mirabel X, Lacornerie T, Lartigau E. Image-Guided Robotic Stereotactic Radiation Therapy with Fiducial-Free Tumor Tracking for Lung Cancer. Radiation Oncology. 2012;7(1):102.

407.   Jackson P, Foroudi F, Pham D, Hofman M, Hardcastle N, Callahan J, et al. Short communication: timeline of radiation-induced kidney function loss after stereotactic ablative body radiotherapy of renal cell carcinoma as evaluated by serial 99mTc-DMSA SPECT/CT. Radiation Oncology. 2014;9(1):253.

408.   Lee DYY, Stuart KE, editors. Survey of SBRT Patterns of Practice and Future Demands in Australia and New Zealand. RANZCR 2015 Annual Scientific Meeting; 2015; Adelaide, South Australia: The Royal Australian and New Zealand College of Radiologists.

409.   Distefano G, Baker A, Scott AJD, Webster GJ, Group obotUSCQA. Survey of stereotactic ablative body radiotherapy in the UK by the QA group on behalf of the UK SABR Consortium. The British Journal of Radiology. 2014;87(1037):20130681.

410.   Nagata Y, Kimura T, Murakami Y, Kenjo M, Kaneyasu Y, Doi Y, et al. Survey of Stereotactic Body Radiation Therapy in Japan. International Journal of Radiation Oncology • Biology • Physics. 2013;87(2):S726.

411.   Siva S, MacManus M, Ball D. Stereotactic Radiotherapy for Pulmonary Oligometastases: A Systematic Review. Journal of Thoracic Oncology. 2010;5(7):1091-9 10.7/JTO.0b013e3181de7143.

412.   Høyer M, Swaminath A, Bydder S, Lock M, Méndez Romero A, Kavanagh B, et al. Radiotherapy for Liver Metastases: A Review of Evidence. International Journal of Radiation Oncology*Biology*Physics. 2012;82(3):1047-57.

413.   Petrelli F, Comito T, Barni S, Pancera G, Scorsetti M, Ghidini A. Stereotactic body radiotherapy for colorectal cancer liver metastases: A systematic review. Radiotherapy and Oncology. 2018;129(3):427-34.

414.   Chawla S, Schell MC, Milano MT. Stereotactic Body Radiation for the Spine: A Review. American Journal of Clinical Oncology. 2013;36(6):630-6.

415.   Sahgal A, Bilsky M, Chang EL, Ma L, Yamada Y, Rhines LD, et al. Stereotactic body radiotherapy for spinal metastases: current status, with a focus on its application in the postoperative patient. Journal of neurosurgery Spine. 2011;14(2):151-66.

416.   Lei Y, Geng Z, Guo-Jun W, He W, Jian-Lin Y. Prognostic significance of survivin expression in renal cell cancer and its correlation with radioresistance. Molecular and Cellular Biochemistry. 2010;344(1):23-31.

417.   Siva S, Pham D, Kron T, Bressel M, Lam J, Tan TH, et al. Stereotactic ablative body radiotherapy for inoperable primary kidney cancer: a prospective clinical trial. BJU International. 2017;120(5):623-30.

418.   Mageras GS, Yorke E, Rosenzweig K, Braban L, Keatley E, Ford E, et al. Fluoroscopic evaluation of diaphragmatic motion reduction with a respiratory gated radiotherapy system. Journal of applied clinical medical physics. 2001;2(4):191-200.

419.	Timmerman R, Papiez L, McGarry R, Likes L, DesRosiers C, Frost S, et al. Extracranial stereotactic radioablation*: Results of a phase i study in medically inoperable stage i non-small cell lung cancer. CHEST Journal. 2003;124(5):1946-55.

420.	Sonier M, Chu W, Lalani N, Erler D, Cheung P, Korol R. Evaluation of kidney motion and target localization in abdominal SBRT patients. Journal of Applied Clinical Medical Physics. 2016;17(6):429-33.

421.	Clements N, Kron T, Franich R, Dunn L, Roxby P, Aarons Y, et al. The effect of irregular breathing patterns on internal target volumes in four-dimensional CT and cone-beam CT images in the context of stereotactic lung radiotherapy. Med Phys. 2013;40(2):021904.

422.	Pollock S, Keall R, Keall P. Breathing guidance in radiation oncology and radiology: A systematic review of patient and healthy volunteer studies. Medical Physics. 2015;42(9):5490-509.

423.	Yamamoto T, Langner U, Loo BW, Jr., Shen J, Keall PJ. Retrospective analysis of artifacts in four-dimensional CT images of 50 abdominal and thoracic radiotherapy patients. International journal of radiation oncology, biology, physics. 2008;72(4):1250-8.

424.	Brook OR, Gourtsoyianni S, Mendiratta-Lala M, Mahadevan A, Siewert B, Sheiman RR. Safety Profile and Technical Success of Imaging-Guided Percutaneous Fiducial Seed Placement With and Without Core Biopsy in the Abdomen and Pelvis. American Journal of Roentgenology. 2012;198(2):466-70.

425.	Kim JH, Hong SS, Kim JH, Park HJ, Chang Y-W, Chang AR, et al. Safety and Efficacy of Ultrasound-Guided Fiducial Marker Implantation for CyberKnife Radiation Therapy. Korean J Radiol. 2012;13(3):307-13.

426.	Kothary N, Heit JJ, Louie JD, Kuo WT, Loo Jr BW, Koong A, et al. Safety and Efficacy of Percutaneous Fiducial Marker Implantation for Image-guided Radiation Therapy. Journal of Vascular and Interventional Radiology. 2009;20(2):235-9.

427.	Slagowski JM, Colbert LE, Cazacu IM, Singh BS, Martin R, Koay EJ, et al. Evaluation of the Visibility and Artifacts of 11 Common Fiducial Markers for Image Guided Stereotactic Body Radiation Therapy in the Abdomen. Practical Radiation Oncology. 2020.

428.	Khashab MA, Kim KJ, Tryggestad EJ, Wild AT, Roland T, Singh VK, et al. Comparative analysis of traditional and coiled fiducials implanted during EUS for pancreatic cancer patients receiving stereotactic body radiation therapy. Gastrointest Endosc. 2012;76(5):962-71.

429.	Dawson LA, Brock KK, Kazanjian S, Fitch D, McGinn CJ, Lawrence TS, et al. The reproducibility of organ position using active breathing control (ABC) during liver radiotherapy. International Journal of Radiation Oncology*Biology*Physics. 2001;51(5):1410-21.

430.	Hubie C, Shaw M, Bydder S, Lane J, Waters G, McNabb M, et al. A randomised comparison of three different immobilisation devices for thoracic and abdominal cancers. Journal of Medical Radiation Sciences. 2017;64(2):90-6.

431.	Sonier M, Chu W, Lalani N, Erler D, Cheung P, Korol R. Implementation of a volumetric modulated arc therapy treatment planning solution for kidney and adrenal stereotactic body radiation therapy. Medical Dosimetry. 2016;41(4):323-8.

432.	Balasubramanian A, Shamsuddin R, Cheung Y, Sawant A, Prabhakaran B, editors. Exploring Baseline Shift Prediction in Respiration Induced Tumor Motion. 2014 IEEE International Conference on Healthcare Informatics; 2014 15-17 Sept. 2014.

433.	Shaw E, Kline R, Gillin M, Souhami L, Hirschfeld A, Dinapoli R, et al. Radiation Therapy Oncology Group: radiosurgery quality assurance guidelines. Int J Radiat Oncol Biol Phys. 1993;27(5):1231-9.

434.	Feuvret L, Noël G, Mazeron J-J, Bey P. Conformity index: A review. International Journal of Radiation Oncology*Biology*Physics. 2006;64(2):333-42.

435.	Paddick I, Lippitz B. A simple dose gradient measurement tool to complement the conformity index. 2006;105(Supplement):194.

436.	Benedict SH, Yenice KM, Followill D, Galvin JM, Hinson W, Kavanagh B, et al. Stereotactic body radiation therapy: the report of AAPM Task Group 101. Med Phys. 2010;37(8):4078-101.

437.	Yaparpalvi R, Garg MK, Shen J, Bodner WR, Mynampati DK, Gafar A, et al. Evaluating which plan quality metrics are appropriate for use in lung SBRT. The British Journal of Radiology. 2018;91(1083):20170393.

438.   Orton CG, Chungbin S, Klein EE, Gillin MT, Schultheiss TE, Sause WT. Study of lung density corrections in a clinical trial (RTOG 88-08). Radiation Therapy Oncology Group. Int J Radiat Oncol Biol Phys. 1998;41(4):787-94.

439.   Bezjak A. Seamless phase I/II study of stereotactic lung radiotherapy (SBRT) for early stage, centrally located, non-small cell lung cancer (NSCLC) in medically inoperable patients. In: Bradley J, editor. Philadelphia, PA: RTOG; 2012.

440.   Lee J, Dean C, Patel R, Webster G, Eaton DJ. Multi-center evaluation of dose conformity in stereotactic body radiotherapy. Physics and Imaging in Radiation Oncology. 2019;11:41-6.

441.   Timmerman R, McGarry R, Yiannoutsos C, Papiez L, Tudor K, DeLuca J, et al. Excessive Toxicity When Treating Central Tumors in a Phase II Study of Stereotactic Body Radiation Therapy for Medically Inoperable Early-Stage Lung Cancer. Journal of Clinical Oncology. 2006;24(30):4833-9.

442.   Narayanasamy G, Desai D, Morrill S, Zhang X, Galhardo E, Maraboyina S, et al. Technical Note: A planning technique to lower normal tissue toxicity in lung SBRT plans based on two likely dependent RTOG metrics. Medical Physics. 2018;45(5):2325-8.

443.   Hoffman D, Dragojević I, Hoisak J, Hoopes D, Manger R. Lung Stereotactic Body Radiation Therapy (SBRT) dose gradient and PTV volume: a retrospective multi-center analysis. Radiation Oncology. 2019;14(1):162.

444.   Toesca DAS, Koong AJ, von Eyben R, Koong AC, Chang DT. Stereotactic body radiation therapy for adrenal gland metastases: Outcomes and toxicity. Advances in Radiation Oncology. 2018;3(4):621-9.

445.   Kumar R, Wild AT, Ziegler MA, Hooker TK, Dah SD, Tran PT, et al. Stereotactic body radiation therapy planning with duodenal sparing using volumetric-modulated arc therapy vs intensity-modulated radiation therapy in locally advanced pancreatic cancer: A dosimetric analysis. Medical Dosimetry. 2013;38(3):243-50.

446.   Barber J, Vial P. SU-F-T-296: Modulated Therapy Down Under: A Survey of IMRT & VMAT Physics Practice in Australia and New Zealand. Medical Physics. 2016;43(6Part17):3531-.

447.   Frenzel T, Krüll A. The use of IMRT in Germany. Strahlentherapie und Onkologie. 2015;191(11):821-6.

448.   Mell LK, Roeske JC, Mundt AJ. A survey of intensity-modulated radiation therapy use in the United States. Cancer. 2003;98(1):204-11.

449.   Tai A, Christensen JD, Gore E, Khamene A, Boettger T, Li XA. Gated Treatment Delivery Verification With On-Line Megavoltage Fluoroscopy. International Journal of Radiation Oncology*Biology*Physics. 2010;76(5):1592-8.

450.   Li R, Mok E, Chang DT, Daly M, Loo BW, Diehn M, et al. Intrafraction Verification of Gated RapidArc by Using Beam-Level Kilovoltage X-Ray Images. International Journal of Radiation Oncology*Biology*Physics. 2012;83(5):e709-e15.

451.   Takahashi W, Yamashita H, Kida S, Masutani Y, Sakumi A, Ohtomo K, et al. Verification of planning target volume settings in volumetric modulated arc therapy for stereotactic body radiation therapy by using in-treatment 4-dimensional cone beam computed tomography. Int J Radiat Oncol Biol Phys. 2013;86(3):426-31.

452.   Kundapur V, Venugopal N. Verification of ITV Margins Using Four Dimensional CBCT. International Journal of Radiation Oncology • Biology • Physics. 2017;99(2):E681.

453.   Santoso AP, Song KH, Qin Y, Gardner SJ, Liu C, Chetty IJ, et al. Evaluation of gantry speed on image quality and imaging dose for 4D cone-beam CT acquisition. Radiat Oncol. 2016;11:98.

454.   Shimohigashi Y, Araki F, Maruyama M, Yonemura K, Nakaguchi Y, Kai Y, et al. Image quality of four-dimensional cone-beam computed tomography obtained at various gantry rotation speeds for liver stereotactic body radiation therapy with fiducial markers. Phys Med. 2018;45:19-24.

455.   Kothary N, Heit JJ, Louie JD, Kuo WT, Loo BW, Koong A, et al. Safety and Efficacy of Percutaneous Fiducial Marker Implantation for Image-guided Radiation Therapy. Journal of Vascular and Interventional Radiology. 2009;20(2):235-9.

456.   Bissonnette JP, Balter PA, Dong L, Langen KM, Lovelock DM, Miften M, et al. Quality assurance for image-guided radiation therapy utilizing CT-based technologies: a report of the AAPM TG-179. Med Phys. 2012;39(4):1946-63.

457.	Zhong R, Wang J, Zhou L, Xu F, Liu L, Zhou J, et al. Implementation of single-breath-hold cone beam CT guided hypofraction radiotherapy for lung cancer. Radiation Oncology (London, England). 2014;9:77-.

458.	Pham D, Maxim P, Diehn M, Loo BW. Individualised stereotactic ablative radiotherapy for lung cancers: report on patients using bio‐visual feedback for gated VMAT FFF treatment. Journal of Medical Radiation Sciences; Saturday 30 March, 2019

Wiley Online Library; 2019. p. 36-79.

459.	Creach KM, El Naqa I, Bradley JD, Olsen JR, Parikh PJ, Drzymala RE, et al. Dosimetric predictors of chest wall pain after lung stereotactic body radiotherapy. Radiotherapy and Oncology. 2012;104(1):23-7.

460.	Murray L, Karakaya E, Hinsley S, Naisbitt M, Lilley J, Snee M, et al. Lung stereotactic ablative radiotherapy (SABR): dosimetric considerations for chest wall toxicity. The British Journal of Radiology. 2016;89(1058):20150628.

461.	Stephans KL, Djemil T, Tendulkar RD, Robinson CG, Reddy CA, Videtic GMM. Prediction of Chest Wall Toxicity From Lung Stereotactic Body Radiotherapy (SBRT). International Journal of Radiation Oncology*Biology*Physics. 2012;82(2):974-80.

462.	Thibault I, Chiang A, Erler D, Yeung L, Poon I, Kim A, et al. Predictors of Chest Wall Toxicity after Lung Stereotactic Ablative Radiotherapy. Clinical Oncology. 2016;28(1):28-35.

463.	Dunlap NE, Cai J, Biedermann GB, Yang W, Benedict SH, Sheng K, et al. Chest Wall Volume Receiving >30 Gy Predicts Risk of Severe Pain and/or Rib Fracture After Lung Stereotactic Body Radiotherapy. International Journal of Radiation Oncology*Biology*Physics. 2010;76(3):796-801.

464.	Tinkle CL, Shiao SL, Weinberg VK, Lin AM, Gottschalk AR. Comparison of stereotactic body radiotherapy and conventional external beam radiotherapy in renal cell carcinoma. Journal of Clinical Oncology. 2015;33(7_suppl):434-.

465.	Chang DT, Swaminath A, Kozak M, Weintraub J, Koong AC, Kim J, et al. Stereotactic body radiotherapy for colorectal liver metastases. Cancer. 2011;117(17):4060-9.

466.	Goodman KA, Wiegner EA, Maturen KE, Zhang Z, Mo Q, Yang G, et al. Dose-Escalation Study of Single-Fraction Stereotactic Body Radiotherapy for Liver Malignancies. International Journal of Radiation Oncology*Biology*Physics. 2010;78(2):486-93.

467.	Scorsetti M, Arcangeli S, Tozzi A, Comito T, Alongi F, Navarria P, et al. Is Stereotactic Body Radiation Therapy an Attractive Option for Unresectable Liver Metastases? A Preliminary Report From a Phase 2 Trial. International Journal of Radiation Oncology*Biology*Physics. 2013;86(2):336-42.

468.	Meyer JJ, Foster RD, Lev-Cohain N, Yokoo T, Dong Y, Schwarz RE, et al. A Phase I Dose-Escalation Trial of Single-Fraction Stereotactic Radiation Therapy for Liver Metastases. Annals of Surgical Oncology. 2016;23(1):218-24.

469.	Gao S, Chang JY, Welsh J, Komaki R, Balter P. Influence of the Couch and Immobilization Device used during Stereotactic Body Radiotherapy on Skin Dose. International Journal of Radiation Oncology • Biology • Physics. 2009;75(3):S682.

470.	Peng Y. SU-D-211-01: Effect of Immobilization/support Devices and Air Gap on Skin Doses for Stereotactic Body Radiotherapy with Abdominal Compression Device. Med Phys. 2012;39(6Part3):3610.

471.	Hoyer M, Roed H, Traberg Hansen A, Ohlhuis L, Petersen J, Nellemann H, et al. Phase II study on stereotactic body radiotherapy of colorectal metastases. Acta Oncol. 2006;45(7):823-30.

472.	Hoyer M, Roed H, Sengelov L, Traberg A, Ohlhuis L, Pedersen J, et al. Phase-II study on stereotactic radiotherapy of locally advanced pancreatic carcinoma. Radiotherapy and Oncology. 2005;76(1):48-53.

473.	Koong AC, Le QT, Ho A, Fong B, Fisher G, Cho C, et al. Phase I study of stereotactic radiosurgery in patients with locally advanced pancreatic cancer. International Journal of Radiation Oncology*Biology*Physics. 2004;58(4):1017-21.

474.	Murphy JD, Christman-Skieller C, Kim J, Dieterich S, Chang DT, Koong AC. A Dosimetric Model of Duodenal Toxicity After Stereotactic Body Radiotherapy for Pancreatic Cancer. International Journal of Radiation Oncology*Biology*Physics. 2010;78(5):1420-6.

475.	LaCouture TA, Xue J, Subedi G, Xu Q, Lee JT, Kubicek G, et al. Small Bowel Dose Tolerance for Stereotactic Body Radiation Therapy. Seminars in Radiation Oncology. 2016;26(2):157-64.

476.	Goldsmith C, Price P, Cross T, Loughlin S, Cowley I, Plowman N. Dose-Volume Histogram Analysis of Stereotactic Body Radiotherapy Treatment of Pancreatic Cancer: A Focus on Duodenal Dose Constraints. Seminars in Radiation Oncology. 2016;26(2):149-56.

477.	Pollom EL, Chin AL, Diehn M, Loo BW, Chang DT. Normal Tissue Constraints for Abdominal and Thoracic Stereotactic Body Radiotherapy. Seminars in Radiation Oncology. 2017;27(3):197-208.

478.	Carr KE. Effects of radiation damage on intestinal morphology. International Review of Cytology. 208: Academic Press; 2001. p. 1-119.

479.	Siva S, Louie AV, Warner A, Muacevic A, Gandhidasan S, Ponsky L, et al. Pooled analysis of stereotactic ablative radiotherapy for primary renal cell carcinoma: A report from the International Radiosurgery Oncology Consortium for Kidney (IROCK). Cancer. 2018;124(5):934-42.

480.	Pollom EL, Deng L, Pai RK, Brown JM, Giaccia A, Loo BW, et al. Gastrointestinal Toxicities With Combined Antiangiogenic and Stereotactic Body Radiation Therapy. International Journal of Radiation Oncology*Biology*Physics. 2015;92(3):568-76.

481.	Barney BM, Markovic SN, Laack NN, Miller RC, Sarkaria JN, Macdonald OK, et al. Increased bowel toxicity in patients treated with a vascular endothelial growth factor inhibitor (VEGFI) after stereotactic body radiation therapy (SBRT). Int J Radiat Oncol Biol Phys. 2013;87(1):73-80.

482.	Henke L, Kashani R, Robinson C, Curcuru A, DeWees T, Bradley J, et al. Phase I trial of stereotactic MR-guided online adaptive radiation therapy (SMART) for the treatment of oligometastatic or unresectable primary malignancies of the abdomen. Radiotherapy and Oncology. 2018;126(3):519-26.

483.	Smitsmans MH, Pos FJ, de Bois J, Heemsbergen WD, Sonke JJ, Lebesque JV, et al. The influence of a dietary protocol on cone beam CT-guided radiotherapy for prostate cancer patients. Int J Radiat Oncol Biol Phys. 2008;71(4):1279-86.

484.	Weiss E, Wu J, Sleeman W, Bryant J, Mitra P, Myers M, et al. Clinical Evaluation of Soft Tissue Organ Boundary Visualization on Cone-Beam Computed Tomographic Imaging. International Journal of Radiation Oncology*Biology*Physics. 2010;78(3):929-36.

485.	Noel CE, Parikh PJ, Spencer CR, Green OL, Hu Y, Mutic S, et al. Comparison of onboard low-field magnetic resonance imaging versus onboard computed tomography for anatomy visualization in radiotherapy. Acta Oncol. 2015;54(9):1474-82.

486.	Xing M, Kokabi N, Zhang D, Ludwig JM, Kim HS. Comparative Effectiveness of Thermal Ablation, Surgical Resection, and Active Surveillance for T1a Renal Cell Carcinoma: A Surveillance, Epidemiology, and End Results (SEER)-Medicare-linked Population Study. Radiology. 2018;288(1):81-90.

487.	Pollom EL, Alagappan M, von Eyben R, Kunz PL, Fisher GA, Ford JA, et al. Single- versus Multifraction Stereotactic Body Radiation Therapy for Pancreatic Adenocarcinoma: Outcomes and Toxicity. International Journal of Radiation Oncology*Biology*Physics. 2014;90(4):918-25.

488.	Simpson DR, Lawson JD, Nath SK, Rose BS, Mundt AJ, Mell LK. A survey of image-guided radiation therapy use in the United States. Cancer. 2010;116(16):3953-60.

489.	Patel HD, Pierorazio PM, Johnson MH, Sharma R, Iyoha E, Allaf ME, et al. Renal Functional Outcomes after Surgery, Ablation, and Active Surveillance of Localized Renal Tumors: A Systematic Review and Meta-Analysis. Clinical journal of the American Society of Nephrology : CJASN. 2017;12(7):1057-69.

490.	Siva S, Jackson P, Kron T, Bressel M, Lau E, Hofman M, et al. Impact of stereotactic radiotherapy on kidney function in primary renal cell carcinoma: Establishing a dose–response relationship. Radiotherapy and Oncology. 2016;118(3):540-6.

491.	Dawson LA, Kavanagh BD, Paulino AC, Das SK, Miften M, Li XA, et al. Radiation-Associated Kidney Injury. International Journal of Radiation Oncology*Biology*Physics. 2010;76(3, Supplement):S108-S15.

492.	Hanna GG, Murray L, Patel R, Jain S, Aitken KL, Franks KN, et al. UK Consensus on Normal Tissue Dose Constraints for Stereotactic Radiotherapy. Clinical Oncology. 2018;30(1):5-14.

493.	Cheville JC, Lohse CM, Zincke H, Weaver AL, Blute ML. Comparisons of outcome and prognostic features among histologic subtypes of renal cell carcinoma. The American journal of surgical pathology. 2003;27(5):612-24.

494.	Nguyen DP, Vertosick EA, Corradi RB, Vilaseca A, Benfante NE, Touijer KA, et al. Histological subtype of renal cell carcinoma significantly affects survival in the era of partial nephrectomy. Urologic oncology. 2016;34(6):259.e1-.e2598.

495.	Teloken PE, Thompson RH, Tickoo SK, Cronin A, Savage C, Reuter VE, et al. Prognostic Impact of Histological Subtype on Surgically Treated Localized Renal Cell Carcinoma. The Journal of Urology. 2009;182(5):2132-6.

496.	Hörner-Rieber J, Bernhardt D, Dern J, König L, Adeberg S, Paul A, et al. Histology of non-small cell lung cancer predicts the response to stereotactic body radiotherapy. Radiotherapy and Oncology. 2017;125(2):317-24.

497.	Nikolaev A, Benda RK, Shang CY, Schramm A, Watson S, Kasper ME, et al. Significance of Tumor Cell Histology for Local Control of Early-Stage Non-Small Cell Lung Cancer Treated With Stereotactic Body Radiation Therapy: A Stratified Retrospective Analysis. International Journal of Radiation Oncology • Biology • Physics. 2016;96(2):E424.

498.	Shiue K, Cerra-Franco A, Shapiro R, Estabrook N, Mannina EM, Deig CR, et al. Histology, Tumor Volume, and Radiation Dose Predict Outcomes in NSCLC Patients After Stereotactic Ablative Radiotherapy. Journal of Thoracic Oncology. 2018;13(10):1549-59.

499.	Tselis N, Chatzikonstantinou G. Treating the Chameleon: Radiotherapy in the management of Renal Cell Cancer. Clin Transl Radiat Oncol. 2019;16:7-14.

500.	Lee Y, Auh SL, Wang Y, Burnette B, Wang Y, Meng Y, et al. Therapeutic effects of ablative radiation on local tumor require CD8+ T cells: changing strategies for cancer treatment. Blood. 2009;114(3):589-95.

501.	Lugade AA, Moran JP, Gerber SA, Rose RC, Frelinger JG, Lord EM. Local radiation therapy of B16 melanoma tumors increases the generation of tumor antigen-specific effector cells that traffic to the tumor. J Immunol. 2005;174(12):7516-23.

502.	Ge X, Zhu H, Dai W, Sun X. Stereotactic body radiotherapy in the era of radiotherapy with immunotherapy. Journal of thoracic disease. 2016;8(11):2968-70.

503.	LaPlant Q, Deselm C, Lockney NA, Hsieh J, Yamada Y. Potential abscopal response to dual checkpoint blockade in RCC after reirradiation using dose-painting SBRT. Practical Radiation Oncology. 2017;7(6):396-9.

504.	Xie G, Gu D, Zhang L, Chen S, Wu D. A rapid and systemic complete response to stereotactic body radiation therapy and pembrolizumab in a patient with metastatic renal cell carcinoma. Cancer Biology & Therapy. 2017;18(8):547-51.

505.	Van de Walle M, Demol J, Staelens L, Rottey S. Abscopal effect in metastatic renal cell carcinoma. Acta Clinica Belgica. 2017;72(4):245-9.

506.	Barata PC, Rini BI. Treatment of renal cell carcinoma: Current status and future directions. CA: A Cancer Journal for Clinicians. 2017;67(6):507-24.

507.	Meissner MA, McCormick BZ, Karam JA, Wood CG. Adjuvant therapy for advanced renal cell carcinoma. Expert Review of Anticancer Therapy. 2018;18(7):663-71.

508.	Kang J, Demaria S, Formenti S. Current clinical trials testing the combination of immunotherapy with radiotherapy. Journal for ImmunoTherapy of Cancer. 2016;4(1):51.

509.	Dabestani S, Beisland C, Stewart GD, Bensalah K, Gudmundsson E, Lam TB, et al. Long-term Outcomes of Follow-up for Initially Localised Clear Cell Renal Cell Carcinoma: RECUR Database Analysis. European Urology Focus. 2018.

510.	Dabestani S, Thorstenson A, Lindblad P, Harmenberg U, Ljungberg B, Lundstam S. Renal cell carcinoma recurrences and metastases in primary non-metastatic patients: a population-based study. World journal of urology. 2016;34(8):1081-6.

511.	Lam JS, Shvarts O, Leppert JT, Pantuck AJ, Figlin RA, Belldegrun AS. Postoperative surveillance protocol for patients with localized and locally advanced renal cell carcinoma based on a validated prognostic nomogram and risk group stratification system. The Journal of Urology. 2005;174(2):466-72.

Chapter 9

Appendices

The following section include papers that have been authored/co-authored outside of the thesis program. They are directly related to the theme of kidney stereotactic therapy and where appropriate, have been referenced in the discussion.

9.1 A systematic review of stereotactic radiotherapy ablation for primary renal cell carcinoma

A systematic review of stereotactic radiotherapy ablation for primary renal cell carcinoma

BJUI

Shankar Siva*[‡], Daniel Pham*, Suki Gill*, Niall M. Corcoran[§] and Farshad Foroudi*[†‡]

*Division of Radiation Oncology and Cancer Imaging, Peter MacCallum Cancer Centre, [†]Department of Pathology, University of Melbourne, [‡]Sir Peter MacCallum Department of Oncology, University of Melbourne, Melbourne, Vic., and [§]Departments of Urology and Surgery, Royal Melbourne Hospital and the University of Melbourne, Parkville, Vic., Australia

Study Type – Therapy (systematic review)
Level of Evidence 1a

What's known on the subject? and What does the study add?
At present, little is known about the role of stereotactic ablative body radiotherapy in the treatment of primary renal cell carcinoma. The published evidence to date totals 126 patients worldwide. The majority of evidence is retrospective in nature.

The present study adds context to the current literature by providing an overall summary of the evidence.

OBJECTIVE

- To critically assess the use of stereotactic ablative body radiotherapy (SABR) for the treatment of primary renal cell carcinoma with particular focus on local control and toxicity outcomes.

METHODS

- A systematic search on PubMed was performed in January 2012 independently by two radiation oncologists using structured search terms.
- Secondary manual searches were performed on citations in relevant publications and abstracts in major radiotherapy journals.
- Outcomes, techniques, biological doses and scientific rigour of the studies were analysed.

RESULTS

- In total 10 publications (seven retrospective and three prospective) were

identified. A wide range of techniques, doses and dose fractionation schedules were found.
- A total of 126 patients were treated with between one and six fractions of SABR. Median or mean follow-up ranged from 9 to 57.5 months. A weighted local control was reported of 93.91% (range 84%–100%).
- The weighted rate of severe grade 3 or higher adverse events was 3.8% [range 0%–19%]. The weighted rate of grade 1–2 minor adverse events was 21.4% (range 0%–93%). The most commonly employed fractionation schedule was 40 Gy delivered over five fractions.

CONCLUSIONS

- Current literature suggests that SABR for primary renal cell carcinoma can be

delivered with promising rates of local control and acceptable toxicity.
- However, there was insufficient evidence to recommend a consensus view for dose fractionation or technique.
- This indicates the need for further prospective studies assessing the role of this technique in medically inoperable patients.

KEYWORDS

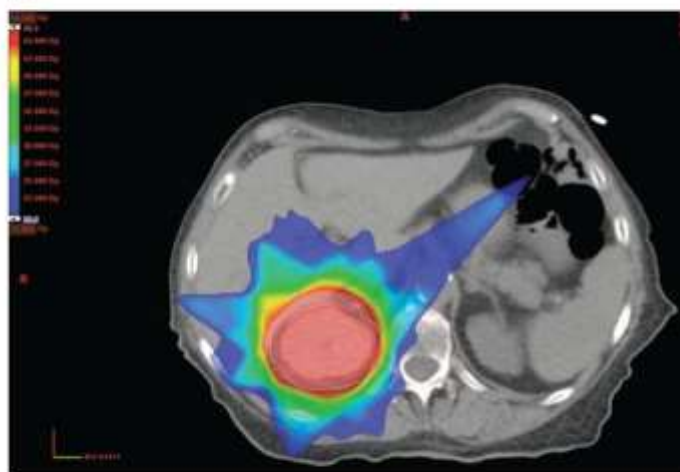stereotactic, renal cell, kidney, radiosurgery, radiotherapy

INTRODUCTION

RCC is the ninth most common cancer in Australia [1] and the eighth most common cancer in the UK [2]. It affects predominantly the older population with a median age at diagnosis of 65 years, with a slight male preponderance. According to the American Cancer Society kidney cancer incidence rates increased by 4.1% per year in men and 3.3% per year in women between 2004 and 2008 [3]. It is postulated that the increasing incidence of RCC is largely incidental and due to the more frequent use of abdominal imaging with ultrasound and CT. For those who require treatment, surgery, either as a radical nephrectomy or more preferably as a nephron-sparing partial nephrectomy, is the standard of care for primary disease. However, given the demographics of

FIG. 1. A representative 10-field SABR plan with a prescription dose of 42 Gy in three fractions (Peter MacCallum Cancer Centre). The right kidney RCC is contoured in red, with the radiotherapy planning target volume contoured in cyan. The dose colour wash depicts the 20 Gy (blue) to 46.5 Gy (red) dose spread.

FIG. 2. A fully awake patient vacuum immobilized in the Elekta BodyFix® system (Medical Intelligence, Schwabmünchen, Germany) at the Peter MacCallum Cancer Centre.

[9,11]. The very large hypofractionated doses used in SABR can be given safely because (i) the treated volumes are small with tight margins and (ii) the technique employs a large number of beams (eight or more), which individually contribute a small dose along their path but together result in a much larger dose where they intersect and are summed at the locus of the cancer. (Fig. 2). A specific challenge for SABR/SRS in the kidney is respiratory-synchronous organ motion. Common strategies employed to ameliorate respiratory induced uncertainty include respiratory gating of the beam delivery [13], with or without breath hold techniques [12], and tumour tracking of the beam using a robotic-arm-mounted linear accelerator [13]. Additional efforts to reduce total tumour excursion are commonplace and include abdominal compression or patient coaching for shallow breathing [14].

A linear quadratic equation [15] is often used to estimate cell survival to radiation. A linear quadratic equation is used to calculate biological equivalent doses (BEDs) between the various fractionation schemes reported below, as this allows a direct comparison of effective doses for early effects to tumour and normal tissues. However, at very large doses per fraction, radiotherapy becomes tissue ablative and may not follow conventional radiobiological rules [16]; thus, the absolute values of the BED calculations reported here should be interpreted with caution.

patients with RCC, many older patients have comorbidities which may preclude them from major surgery. Alternative strategies such as cryotherapy, radiofrequency ablation (RFA) and stereotactic radiosurgery have emerged as potentially curative treatment approaches for patients who refuse or are unsuitable for surgery.

Stereotactic ablative body radiotherapy (SABR) is a novel, potentially curative treatment approach for inoperable primary RCC. 'Radiosurgery' was a term first coined by Swedish neurosurgeon Lars Leksell [4] in the 1950s to describe single-dose ablative radiotherapy delivered to brain lesions via stereotaxy. The term stereotaxis applies to the realization of tumour position via the use of coordinates derived from external surrogate markers or fiducials. These fiducials allow the determination of tumour coordinates in the sagittal, coronal and axial planes. This principle has been extrapolated to the stereotactic delivery of severely hypofractionated treatments to body targets. Lax et al. [5] developed the first stereotactic body frame to enclose the body from head to mid-femoral region with vacuum stabilization to provide high surface contact (Fig. 1). There is an established role for the use of stereotactic radiotherapy in

the treatment of tumours in the brain [6], lung [2,7,8], liver [9] and spine [2,10]. Several reports of both single-fraction stereotactic radiosurgery (SRS) and fractionated SABR techniques have emerged in the treatment of primary kidney RCC. In contrast to RFA and cryotherapy, SABR and SRS are capable of treating both larger tumours and those adjacent to collecting vessels and ureteric ducts. Additionally, these novel techniques are non-invasive and delivered whilst the patient is fully awake.

BASIC PRINCIPLES OF STEREOTACTIC TREATMENT

Stereotactic techniques represent a revolutionary departure from conventional radiotherapy. Typical fractionation for curative intent treatment of epithelial tumours generally involves the use of 30 or more small doses of 1.8–2 Gy per fraction, delivered 5 days a week over many weeks. This is in order to maximize the therapeutic window between tumour cell kill and normal tissue repair in the context of relatively large and imprecise fields. In contrast, recent work with hypofractionated SABR/SRS has resulted in the use of fraction sizes of up to 25 Gy delivered to the upper abdomen

The term 'radiosurgery' to describe single-fraction ablative radiotherapy is misleading as it does not involve surgery at all. It could be argued that 'radioablation' is a more appropriate term. Similarly, the definition of stereotaxis has been somewhat loosely applied throughout the literature. The need

TABLE 1 Summary of studies assessing SABR in primary RCC tabulated in chronological order

Author, year of publication	Patients	Study design	Follow-up median or mean	Dose/fractionation	Outcome – crude local control (%)	Estimated 3-year local control	Overall survival, median	BED estimated by RCC type		Toxicity
								Calc-1 $\alpha/\beta = 6.1$	Calc-2 $\alpha/\beta = 2.6$	
Qian et al 2003 [44]	20	Retrospective	13	8 Gy × 5	93%	96	Not reported	86.4	93.1	Not reported
Beitler et al 2004 [45]	9	Retrospective	26.7	6 Gy × 5, 7 Gy × 6	100%	100	4 of 9 patients alive	84.6–86.4	155.1–163.1	30% grade 1–2, nil grade 3+
Wersäll et al 2005 [34]	8	Retrospective	37	8 Gy × 5, 10 Gy × 4, 15 Gy × 3	100%	100	Median survival 58 months	86.4–142.8	163.1–304.6	20% grade 1–2, 10% grade 3, nil grade 4+
Gilson et al 2006 [46]	11	Retrospective	17	Median 8 Gy × 5	94%	90	Not reported	86.4	93.1	Not reported
Svedman et al 2006 [47]	5	Prospective phase II	52	8 Gy × 4, 10 Gy × 4, 15 Gy × 2, 15 Gy × 3	80%	91	Median survival 32 months	69.1–142.8	130.4–304.6	89% grade 1–2, 4% grade 3
Teh et al 2007 [41]	2	Retrospective	9	24–40 Gy in 3–4 fractions	100%	100	Not reported	51.8–103.7	97.6–135.7	Not reported
Svedman et al 2008 [40]	7	Retrospective	28	10 Gy × 3 or 10 Gy × 4	86%	91	Not reported	73.46–98.0	145.4–193.8	50% grade 3–2, nil else
Nomiya et al 2008 [23]	10	Retrospective	67.5	Median 4.5 Gy × 16	100%	100	5-year overall survival 74%	11.9	106.9	10% grade 4 toxicity, no other toxicities > grade 1
Kaplan et al 2009 [21]	12	Prospective phase I	Not reported	Max 13 Gy × 3	84%	Not reported	Not reported	112.5	234	Nil
Ponsky and Vricella [22], ongoing†	20	Prospective phase I	Not reported	Max 16 Gy in 3 fractions	Not reported	Not reported	Not reported	158.3	343.4	Nil

†Additional information through personal correspondence

for fiducial surrogates for precise tumour localization has been largely replaced by image-guided radiotherapy using tumour visualization, although the term stereotactic is still often used. Image-guided radiotherapy involves the use of some method of direct or indirect radiological localization of the tumour in the treatment room immediately before or during treatment delivery [17]. This may be with volumetric soft tissue imaging devices attached to the treatment machine or with implanted radio-opaque fiducials that are detectable by orthogonal kilovoltage X-rays. In this review of the literature, we shall consider all definitions of stereotactic radiotherapy and radiosurgery published to date. A large proportion of published reports regarding SABR address the treatment of both primary and metastatic RCC lesions. This review will focus only on the reported outcomes of those patients treated for primary disease.

PATIENTS AND METHODS

A systematic literature search was performed using PubMed for the period from January 1995 to February 2012. The search employed the following structured search terms: 'kidney neoplasms [MeSH] AND (radiotherapy[Title] OR radiosurgery[Title] OR stereotactic[Title] OR radiation[Title]) NOT (metastases[Title] OR metastasis[Title]) NOT brain[Title]'. This yielded 161 publications. Papers were subsequently independently reviewed by two radiation oncologists (SS and FF) for relevance. A secondary search was performed using recovered paper citations and an abstract search of the major North American and European radiotherapy journals: the *International Journal of Radiation Oncology, Biology and Physics* and *Radiotherapy and Oncology*. Where multiple publications existed for a single institution, outcome data from only the most recent or most relevant papers were included. However, previously published information regarding treatment techniques were considered if this gave useful additional information. Where publications reported outcomes for both primary and secondary RCC, only the former patients were considered. In total, 10 clinical studies and two preclinical studies were identified. Relevant clinical information concerning

tumour characteristics, treatment techniques, duration of patient follow-up, treatment-related toxicities and radiobiological information is tabulated chronologically in Table 1. Two-year overall survival and local control data, when not reported, were extrapolated from reported time points assuming a constant hazard. Weighted crude local control rate and mean 2-year local control rate were calculated using the average of each of the categories with respect to the contribution of the number of patients within each study. The BED of each treatment was calculated using the α/β estimates of the two common RCC cell lines Caki-1 and A498 as investigated by Ning et al. [18].

RESULTS: PRECLINICAL EVIDENCE

Stereotactic radioablative approaches have been evaluated in both porcine and murine models in the literature. Walsh et al. [19] injected nude mice with the A498 line of human RCC cells and subsequently irradiated 12 mice with seven mice observed as unirradiated controls. This group used a fractionated SABR approach, with three fractions of 16 Gy delivered weekly. All except one mouse completed all 3 weeks of treatment, and this mouse died of unknown cause without evidence of radiation toxicity. Whilst tumour volume in control mice progressively increased, the irradiated tumours decreased to <30% of the initial volume. Tumours in mice sacrificed 4 weeks after treatment demonstrated no mitotic activity.

The radioablative effect of stereotactic irradiation was also evaluated in a porcine model in an earlier study by Ponsky et al. [20]. In this model, eight pigs and 16 kidneys were irradiated with single-fraction SRS in a dose escalation study from 24 Gy to 40 Gy. A hypothetical renal 'target' was irradiated whilst the pigs were anaesthetized, and subsequently the kidneys were harvested at 4, 6 and 8 weeks after treatment. This group demonstrated a sharp demarcation of fibrosis at a gross and microscopic level between the renal 'targets' and surrounding normal parenchyma. After 8 weeks, the 'targets' showed complete fibrosis with relative sparing of surrounding renal tissue. At the time of kidney harvest there was no gross evidence of injury to the surrounding organs

or body wall, renal blood vessels or the collecting system.

RESULTS: CLINICAL EVIDENCE

A total of 10 published studies were reviewed and 126 patients were identified treated for primary RCC (Table 1). Three studies were prospective in nature, whilst the other seven were retrospective. Kaplan et al. [21] and Ponksy and Vricella [22] used a robotic arm-held linear accelerator system in their respective phase I studies, and Nomiya et al. [23] reported the use of a heavy carbon-ion particle accelerator, whilst all other studies used conventional gantry-operated linear accelerators. None of the groups restricted or excluded tumours based on proximity to collecting vessels or renal vasculature. Reporting institutions cited no size restrictions. There were no reports of pathological confirmation of tumour response through post-treatment biopsy, which is consistent with routine clinical practice after radiation therapy.

Of the 10 published clinical studies, techniques and dose fractionation schedules varied widely. Three, four and five fraction approaches were most commonly reported. The most commonly employed fractionation schedule was 40 Gy delivered over five fractions. The median or mean follow-up of reported series ranged between 9 and 57.5 months. Crude local control was commonly reported, with individual reports ranging from 84% to 100%. The crude weighted local control rate and 2-year estimated weighted local control rate were 93.1% and 92.9% respectively. Overall survival was inconsistently reported in these series. The most common reported toxicities were fatigue and nausea, followed by radiation dermatitis and enteritis. Rates of severe toxicity (grade 3+) were very low, although in one study a 19% rate was recorded [24]. Nomiya et al. [23] reported one late grade 4 skin toxicity. The weighted rate of severe toxicity was 3.8%, and the weighted rate of minor toxicity (grade 1–2) was 21.4%.

DISCUSSION

A common preconception is that RCC is resistant to radiotherapy. This notion was challenged in the neoadjuvant setting through an early report of improved

disease-free survival in one surgeon's series in the 1960s [25]. However, subsequent clinical trials throughout the 1970s and 1980s failed to demonstrate any increase in survival with external beam radiation delivered in the neoadjuvant or adjuvant setting [26–29]. A meta-analysis of seven randomized controlled trials and 735 patients treated with postoperative radiotherapy was recently published [30]. Pooled results from these trials showed a significant reduction of locoregional failure in patients treated with postoperative radiotherapy ($P < 0.001$) but no difference in overall survival ($P = 0.29$). Currently the role of conventional radiotherapy for primary RCC is limited, possibly to patients with poor pathological features who are at high risk of tumour recurrence [31].

Research from Stanford University suggests that the inherent radioresistance of RCC may only exist at low doses per fraction. Ning et al. [18] performed clonogenic survival assays with two human RCC cell lines (Caki-1 and A498). The cells were irradiated with 0–15 Gy and surviving fractions were calculated. At doses used in conventional radiotherapy (1.8–2 Gy per fraction) there was only a small proportion of cell kill observed in either cell line. However, at doses above 6 Gy per fraction an exponential rate of cell kill was noted, suggesting that radiotherapy may be profoundly effective in RCC when used at high doses per fraction. Considerable evidence for this effectiveness can be demonstrated in the well established stereotactic literature for RCC metastases to the brain, in which multiple studies consistently report local control rates of 90% or higher [32–37].

When considering the dose fractionation schedules employed by the groups assessed in this literature review, a very high BED is certainly achieved through SABR. BED calculations are commonly used to compare dose fractionation schedules in radiotherapy [38]. The BED is based on the α/β ratio, which expresses a tumour or tissue sensitivity to a specified dose [15]. The BEDs of the different schedules used have been calculated in Table 1 by using the estimated α/β ratios of the Caki-1 and A498 RCC cell lines (6.9 and 2.6 respectively) [18]. The estimated BED ranged widely in the studies between 86.4 Gy and 159.3 Gy for the Caki-1 cell line. Similarly, the estimated BED

ranged between 163.1 Gy and 343.4 Gy for the A498 cell line. In contrast, a hypothetical conventionally fractionated long course of radiotherapy (e.g. 60 Gy in 30 fractions delivered over 6 weeks) would only achieve a BED of 77.4 Gy and 106.1 Gy for the Caki-1 and A498 cell lines respectively. It is clear that the BEDs achieved with SABR and SRS techniques are an order of magnitude greater than can be achieved with conventional radiotherapy techniques. The caveat to these comparisons is that BED calculations may not be reliable at the severely hypofractionated doses in the SABR and SRS techniques, given that preclinical models did not account for such high doses per fraction.

Clinical evidence to date supports the assertion that high tumour control rates with minimal associated toxicities can be achieved using high dose per fraction stereotactic techniques. Individual reports of crude local control ranged from 84% to 100%. The crude weighted local control rate and 2-year estimated weighted local control rate were 93.1% and 92.9% respectively. These results are comparable with other ablative techniques, with a recent meta-analysis indicating that local tumour progression was 5.2% after renal cryoablation and 12.9% after RFA [39]. Survival, when reported, was difficult to interpret in the context of the patient demographics. Most patients were medically inoperable with multiple comorbidities and most patient deaths occurred with the renal disease controlled. Treatment delivery was well tolerated with minimal severe toxicities. The weighted severe (grade 3+) toxicity rate in these series was 3.81% with no study reporting a patient death.

There have been no reports of clinically relevant renal dysfunction secondary to SABR. The potential for nephron injury in humans kidneys after SABR has been most eloquently researched in a series of seven patients with only one functioning kidney published by Svedman et al. [40]. These patients were subsequently treated with SABR in the remaining kidney, with a maximum reported follow-up of 6 years. Five of the seven patients had no change in renal function. In one patient serum creatinine increased from 120 μmol/L to 150–160 μmol/L after 2 years of follow-up. In the other patient, creatinine levels increased by 20% during the 6-year

follow-up period, without medical or dialysis intervention required. None of the patients developed hypertension over the 6-year follow-up period. In another series by Teh et al. [41] asymptomatic elevations in serum creatinine were observed in patients 52 months after renal SABR. In light of this the QUANTEC group consensus guidelines for dose constraints in radiotherapy recommended no dose constraint be applied for the kidney during SABR [42]. The QUANTEC group suggested that 'one hypothesis [is] that nearly complete sparing of a substantial volume of normal kidney is associated with preservation of renal function' [42]. An alternative hypothesis is that late renal nephropathy may manifest at a later date (up to 10+ years after SABR); however, current data are not yet mature enough to support this hypothesis and it may not be relevant in the medically inoperable patient cohort.

There was insufficient evidence in this review to support that any one delivery system was clinically superior to another. The conventional gantry-operated linear accelerator was most commonly used in these reports and has the advantage of being readily accessible in most radiotherapy centres. The Cyberknife® (Accuray, Sunnyvale, CA, USA) is a robotic arm-held linear accelerator, allowing many degrees of freedom to deliver over 100 beamlets, which permits the high dose regions to conform tightly to the target area. However, the system is expensive, may require several hours to deliver each dose of radiation (limiting patient throughput) and usually requires the insertion of radio-opaque fiducials to assist tumour tracking. The use of a heavy carbon-ion particle accelerator (reported by Nomiya et al. [23]) represents a highly specialized solution to radiotherapy delivery, which takes advantage of the distinct dosimetric advantages of heavy particle radiation over conventional X-ray therapy. However, this system is not readily available for medical use outside Japan. Irrespective of the system used to deliver SABR or SRS similar clinical results were achieved.

Although SABR and SRS techniques are still an emerging modality for the treatment of primary RCC, high reported rates of tumour control and low toxicity are promising. In particular, stereotactic radiotherapy techniques are non-invasive and are not

limited to smaller tumours or to those in close proximity to hilar structures. They are delivered without anaesthesia whilst the patient is fully awake. These attributes are particularly attractive when considering alternative modalities for the treatment of inoperable primary RCC, such as cryotherapy or RFA. At present, there is insufficient evidence to recommend a consensus view for the optimal dose/fractionation, technique or delivery system. There is only limited scientifically rigorous prospective evidence at this time. Further well designed prospective trials are required to validate the available literature.

ACKNOWLEDGEMENTS

CONFLICT OF INTEREST

None declared.

REFERENCES

1 **AIHW.** *Cancer in Australia: An Overview.* Canberra, ACT: AIHW, 2008; Cancer Series no. 46, Cat. no. CAN 42

2 **Ryu SI, Chang SD, Kim DH et al.** Image-guided hypo-fractionated stereotactic radiosurgery to spinal lesions. *Neurosurgery* 2001; **49**: 838–46

3 **American Cancer Society.** *Cancer Facts & Figures 2011.* Atlanta, NJ: American Cancer Society, 2011

4 **Leksell L.** The stereotaxic method and radiosurgery of the brain. *Acta Chir Scand* 1951; **102**: 316–9

5 **Lax I, Blomgren H, Näslund I, Svanström R.** Stereotactic radiotherapy of malignancies in the abdomen: methodological aspects. *Acta Oncol* 1994; **33**: 677–83

6 **Andrews DW, Scott CB, Sperduto PW et al.** Whole brain radiation therapy with or without stereotactic radiosurgery boost for patients with one to three brain metastases: phase III results of the RTOG 9508 randomised trial. *Lancet* 2004; **363**: 1665–72

7 **Timmerman R, Paulus R, Galvin J et al.** Stereotactic body radiation therapy for

inoperable early stage lung cancer. JAMA 2010; 303: 1070–6

8 Siva S, MacManus M, Ball D. Stereotactic radiotherapy for pulmonary oligometastases: a systematic review. J Thoracic Oncol 2010; 5: 1091–9

9 Herfarth KK, Debus J, Lohr F et al. Stereotactic single-dose radiation therapy of liver tumors: results of a phase I/II trial. J Clin Oncol 2001; 19: 164–70

10 Pan H, Simpson DR, Mell LK, Mundt AJ, Lawson JD. A survey of stereotactic body radiotherapy use in the United States. Cancer 2011; 117: 4566–72

11 Mahadevan A, Miksad R, Goldstein M et al. Induction gemcitabine and stereotactic body radiotherapy for locally advanced nonmetastatic pancreas cancer. Int J Radiat Oncol Biol Phys 2011; 81: e615–22

12 Hanley J, Debois MM, Mah D et al. Deep inspiration breath-hold technique for lung tumors: the potential value of target immobilization and reduced lung density in dose escalation. Int J Radiat Oncol Biol Phys 1999; 45: 603–11

13 Murphy MJ. Tracking Moving Organs in Real Time. Amsterdam: Elsevier, 2004: 91–100

14 Ozhasoglu C, Murphy MJ. Issues in respiratory motion compensation during external-beam radiotherapy. Int J Radiat Oncol Biol Phys 2002; 52: 1389–99

15 Fowler JF. The linear-quadratic formula and progress in fractionated radiotherapy. Br J Radiol 1989; 62: 679–94

16 Guerrero M, Li XA. Extending the linear-quadratic model for large fraction doses pertinent to stereotactic radiotherapy. Phys Med Biol 2004; 49: 4825–35

17 Dawson LA, Jaffray DA. Advances in image-guided radiation therapy. J Clin Oncol 2007; 25: 938–46

18 Ning S, Trisler K, Wessels BW, Knox SJ. Radiobiologic studies of radioimmunotherapy and external beam radiotherapy in vitro and in vivo in human renal cell carcinoma xenografts. Cancer 1997; 80: 2519–28

19 Walsh L, Stanfield JL, Cho LC et al. Efficacy of ablative high-dose-per-fraction radiation for implanted human renal cell cancer in a nude mouse model. Eur Urol 2006; 50: 795–800

20 Ponsky L, Crownover R, Rosen M et al. Initial evaluation of cyberknife technology for extracorporal renal tissue ablation. Urology 2003; 61: 498–501

21 Kaplan ID, Redrosa I, Martin C, Collins C, Wagner A. Results of a phase I dose escalation study of stereotactic radiosurgery for primary renal tumors. Int J Radiat Oncol Biol Phys 2009; 78: S191–S

22 Ponsky L, Vricella G. Radiosurgery for renal tumors. In Ponsky LE, Fuler DB, Meier RM, Ma C eds, Robotic radiosurgery treating prostate cancer and related genitourinary applications. Berlin: Springer-Verlag, 2012: 179–84

23 Nomiya T, Tsuji H, Hirasawa N et al. Carbon ion radiation therapy for primary renal cell carcinoma: initial clinical experience. Int J Radiat Oncol Biol Phys 2008; 72: 828–33

24 Wersäll PJ, Blomgren H, Lax I et al. Extracranial stereotactic radiotherapy for primary and metastatic renal cell carcinoma. Radiother Oncol 2005; 77: 88–95

25 Riches E. The place of radiotherapy in the management of parenchymal carcinoma of the kidney. J Urol 1966; 95: 313–7

26 Juusela H, Malmio K, Alfthan O, Oravisto KJ. Preoperative irradiation in the treatment of renal adenocarcinoma. Scand J Urol Nephrol 1977; 11: 277–81

27 Kjaer M, Iversen P, Hvidt V et al. A randomized trial of postoperative radiotherapy versus observation in stage II and III renal adenocarcinoma. Scand J Urol Nephrol 1987; 21: 285–9

28 Kjaer M, Frederiksen PL, Engelholm S. Postoperative radiotherapy in stage II and III renal adenocarcinoma. A randomized trial by the Copenhagen Renal Cancer Study Group. Int J Radiat Oncol Biol Phys 1987; 13: 665–72

29 Finney R. The value of radiotherapy in the treatment of hypernephroma, a clinical trial. Br J Urol 1973; 45: 258–69

30 Tunio MA, Hashmi A, Rafi M. Need for a new trial to evaluate postoperative radiotherapy in renal cell carcinoma: a meta-analysis of randomized controlled trials. Ann Oncol 2010; 21: 1839–45

31 Michalski JM. Kidney, renal pelvis, and ureter. In Perez CA, Brady LW, Halperin EC, Schmidt-Ullrich R eds, Principles and Practice of Radiation Therapy. Philadelphia, PA: Lippincott Williams & Wilkins, 2004: 1649–63

32 Sheehan JP, Sun MH, Kondziolka D, Flickinger J, Lunsford LD. Radiosurgery in patients with renal cell carcinoma metastasis to the brain: long-term outcomes and prognostic factors influencing survival and local tumor control. J Neurosurg 2003; 98: 342–9

33 Payne BR, Prasad D, Szeifert G, Steiner M, Steiner L. Gamma surgery for intracranial metastases from renal cell carcinoma. J Neurosurg 2000; 92: 760–5

34 Goyal LK, Suh JH, Reddy CA, Barnett GH. The role of whole brain radiotherapy and stereotactic radiosurgery on brain metastases from renal cell carcinoma. Int J Radiat Oncol Biol Phys 2000; 47: 1007–12

35 Amendola BE, Wolf A, Coy SR, Amendola MA. Radiosurgery as palliation for brain metastases: a retrospective review of 72 patients harboring multiple lesions at presentation. J Neurosurg 2002; 97: 511–4

36 Schoggl A, Kitz K, Ertl A, Dieckmann K, Saringer W, Koos WT. Gamma-knife radiosurgery for brain metastases of renal cell carcinoma: results in 23 patients. Acta Neurochir 1998; 140: 549–55

37 Mori Y, Kondziolka D, Flickinger JC, Logan T, Lunsford LD. Stereotactic radiosurgery for brain metastasis from renal cell carcinoma. Cancer 1998; 83: 344–53

38 Lee SP, Leu MY, Smathers JB, McBride WH, Parker RG, Withers HR. Biologically effective dose distribution based on the linear quadratic model and its clinical relevance. Int J Radiat Oncol Biol Phys 1995; 33: 375–89

39 Kunkle DA, Uzzo RG. Cryoablation or radiofrequency ablation of the small renal mass. Cancer 2008; 113: 2671–80

40 Svedman C, Karlsson K, Rutkowska E et al. Stereotactic body radiotherapy of primary and metastatic renal lesions for patients with only one functioning kidney. Acta Oncol 2008; 47: 1578–83

41 Teh B, Bloch C, Galli-Guevara M et al. The treatment of primary and metastatic renal cell carcinoma (RCC) with image-guided stereotactic body radiation therapy (SBRT). Biomed Imaging Interv J 2007; 3: e6

42 Dawson LA, Kavanagh BD, Paulino AC et al. Radiation-associated kidney injury. Int J Radiat Oncol Biol Phys 2010; 76: S108–15

43 Ramsey CR, Scaperoth D, Arwood D, Oliver AL. Clinical efficacy of respiratory gated conformal radiation therapy. *Med Dosim* 1999; **24**: 115–9

44 Qian G, Lowry J, Silverman P, Grosman I, Makara D, Lederman G. Stereotactic extra-cranial radiosurgery for renal cell carcinoma. *Int J Radiat Oncol Biol Phys* 2003; **57**: S283

45 Beitler JJ, Makara D, Silverman P, Lederman G. Definitive, high-dose-per-fraction, conformal, stereotactic external radiation for renal cell carcinoma. *Amer J Clin Oncol* 2004; **27**: 646

46 Gilson B, Lederman G, Qian G, Fastaia M, Cangiane L. 2249: Hypo-fractionated Stereotactic Extra-Cranial Radiosurgery (HFSR) for Primary and Metastatic Renal Cell Carcinoma. *Int J Radiat Oncol Biol Phys* 2006; **66**: S349

47 Svedman C, Sandstrom P, Pisa P *et al.* A prospective Phase II trial of using extracranial stereotactic radiotherapy in primary and metastatic renal cell carcinoma. *Acta Oncol* 2006; **45**: 870–5

Correspondence: Shankar Siva, Peter MacCallum Cancer Centre – Radiation Oncology, St Andrews Street East Melbourne, East Melbourne, Vic. 3002, Australia. e-mail: shankar.siva@petermac.org

Abbreviations: **RF**, radiofrequency ablation; **SABR**, stereotactic ablative body radiotherapy; **SRS**, stereotactic radiosurgery.

164

Effect of different breathing patterns in the same patient on stereotactic ablative body radiotherapy dosimetry for primary renal cell carcinoma: A case study

Daniel Pham, C.M.D., R.T.T.,* Tomas Kron, Ph.D.,† Farshad Foroudi, F.R.A.N.Z.C.R.,‡ and Shankar Siva, F.R.A.N.Z.C.R.‡

*Radiotherapy Services, Peter MacCallum Cancer Centre, East Melbourne, Victoria, Australia; †Physical Sciences, Peter MacCallum Cancer Centre, East Melbourne, Victoria, Australia; and ‡Radiation Oncology, Peter MacCallum Cancer Centre, East Melbourne, Victoria, Australia

ARTICLE INFO

ABSTRACT

Stereotactic ablative body radiotherapy (SABR) for primary renal cell carcinoma (RCC) targets requires motion management strategies to verify dose delivery. This case study highlights the effect of a change in patient breathing amplitude on the dosimetry to organs at risk and target structures. A 73-year-old male patient was planned for receiving 26 Gy of radiation in 1 fraction of SABR for a left primary RCC. The patient was simulated with four-dimensional computed tomography (4DCT) and the tumor internal target volume (ITV) was delineated using the 4DCT maximum intensity projection. However, the initially planned treatment was abandoned at the radiation oncologist's discretion after pretreatment cone-beam CT (CBCT) motion verification identified a greater than 50% reduction in superior to inferior diaphragm motion as compared with the planning 4DCT. This patient was resimulated with respiratory coaching instructions. To assess the effect of the change in breathing on the dosimetry to the target, each plan was recalculated on the data set representing the change in breathing condition. A change from smaller to larger breathing showed a 46% loss in planning target volume (PTV) coverage, whereas a change from larger breathing to smaller breathing resulted in an 8% decrease in PTV coverage. ITV coverage was similarly reduced by 8% in both scenarios. This case study highlights the importance of tools to verify breathing motion prior to treatment delivery. 4D image guided radiation therapy verification strategies should focus on not only verifying ITV margin coverage but also the effect on the surrounding organs at risk.

Crown Copyright © 2013 Published by Elsevier Inc. on behalf of American Association of Medical Dosimetrists.

Introduction

Stereotactic ablative body radiotherapy (SABR) for primary renal cell targets has been shown to provide 2-year local control rates between 80% and 100%.[1] To deliver doses to abdominal targets accurately, motion management strategies can be adapted to all phases of an SABR program. Methods of motion management include four-dimensional computed tomography (4DCT) for target volume delineation[2] or breath control devices[3] and abdominal compression devices[4,5] to minimize breathing-motion uncertainties. Advances in imaging technology have provided pretreatment verification of target motion using 4D cone beam CT (CBCT)[7,8] or surrogates of breathing motion.[6] Pretreatment target verification in SABR aims to ensure adequate target coverage with target volumes derived at planning. We describe a scenario in which a change in breathing pattern lead to inadequate target coverage and excess dose to surrounding tissue. We aim to explore the dosimetric consequences of treatment delivery in the same patient with 2 different breathing patterns captured on nonconsecutive days.

Case Report

A 73-year-old man was referred with a 4-cm clear cell renal cell carcinoma at the midpole of the left kidney. The patient was immobilized with his arms up using the Elekta BodyFIX dual vacuum technology (Stockholm, Sweden) and underwent a 4D CT

Reprint requests to: Daniel Pham, C.M.D., R.T.T., Radiotherapy Services, Peter MacCallum Cancer Centre, 32/100 Union Road, Ascot Vale, East Melbourne, Victoria 3032, Australia.
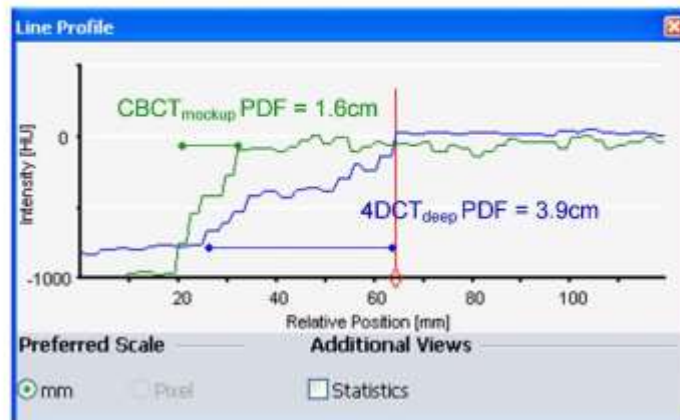E-mails: Daniel.Pham@petermac.org, daniel.pham@radiotherapy.edu.au

Fig. 1. Assessment of the right diaphragm motion using a line profile to measure the width of the probability density function. Graphical display on the Eclipse image browser shows the difference in the gradient between the planning 4DCT_deep and the CBCT_mockup. (Color version of figure is available online.)

scan on a Philips Brilliance Big Bore CT scanner (Philips Medical Systems, Cleveland, OH). Eclipse v8.9 (Varian Medical System, Palo Alto, CA) was used to create an 8-field 3D conformal plan prescribing 26 Gy to the minimum surrounding isodose of 75% to ensure that the planning target volume (PTV) D99 received a minimum of 100% dose. As per normal practice in our institution for SABR, the patient attended a mock-up session to verify beam angle, image quality, and breathing motion. Pretreatment internal target volume (ITV) verification used the line profile tool on the Varian OBI (v1.4) to measure the width of the probability density function to measure the range of diaphragm motion. This method has been adopted from a technique described by Guckenberger et al.[6] The breathing motion on treatment was discovered to be half of the planned value (Fig. 1). At this point, concern regarding dosimetric implications of this change in breathing pattern prompted the attending radiation oncologist to abandon the SABR treatment. Upon further investigation, it was discovered that the patient was breathing deeply of his own volition during the planning 4DCT without the knowledge of the planning therapist. A new 4DCT was requested with the patient advised to breathe normally (Fig. 2).

Both the initial and subsequent 4DCTs, referenced as 4DCT_deep and 4DCT_normal, were contoured by a single radiation oncologist

delineating the target and organs at risk for each. Two plans were created Plan_deep and Plan_normal representing optimization to each respective 4DCT data set. To evaluate the dosimetric consequences of a change in breathing motion, Plan_deep and Plan_normal were both recalculated on 4DCT_normal and 4DCT_deep, respectively. The isocenter position in each plan was corrected by matching the planned left kidney contour to the imaged kidney structure. This represents the online matching scenario where the kidney is used as a matching surrogate for the target volume.

Results

Four plans were made available for analysis with the dose to target volumes and organs at risk summarized in Table 1. The dose to PTV and ITV were reduced by 14% and 8% when Plan_deep was recalculated on the 4DCT_normal data set. For the Plan_normal, the PTV and ITV were reduced by 46% and 8% when recalculated on the 4DCT_deep data set. Small bowel, stomach, and skin dose increased when the Plan_deep was recalculated on the shallower data set. There was a reduction or no change in dose to the organs at risk when the Plan_normal was recalculated on the larger breathing data set.
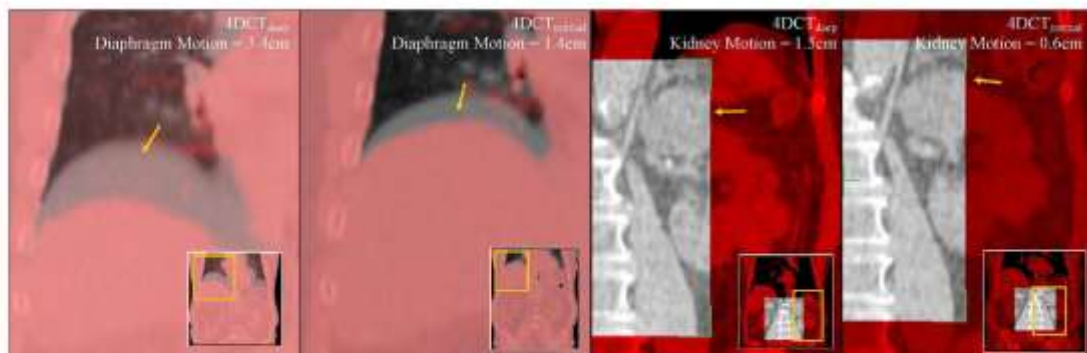

Fig. 2. Max expiration and max inspiration data set blended in Eclipse to show the peak-to-peak motion of the right diaphragm and left kidney for the deep-breathing planning 4DCT_deep and the normal breathing 4DCT_normal. (Color version of figure is available online.)

166

Table 1

Planning parameters from original deep-breathing data set (1) and shallow free-breathing data set (2). Change in planning parameters considered if Plan$_{deep}$ was recalculated on free-breathing shallow 4DCT data set (3) and if Plan$_{shallow}$ was recalculated on deep-breathing 4DCT data set (4)

	Dose to target volumes and OAR (prescription 26 Gy in 1 fraction)			
	(1) Plan$_{deep}$ on 4DCT$_{deep}$	(2) Plan$_{normal}$ on 4DCT$_{normal}$	(3) Plan$_{deep}$ on 4DCT$_{normal}$	(4) Plan$_{normal}$ on 4DCT$_{deep}$
PTV (D99)	107%	103%	93%	57%
ITV (D99)	123%	115%	115%	107%
Small bowel (V$_{30 cc}$)	5.7 Gy	6.3 Gy	6.5 Gy	5.9 Gy
Stomach	0.2 Gy	2.16 Gy	2.7 Gy	0.2 Gy
Spinal canal	8.1 Gy	7.8 Gy	8.1 Gy	7.7 Gy
Skin	13.4 Gy	13.3 Gy	14.7 Gy	12.5 Gy
Liver (V$_{700 cc}$)	0.1 Gy	0.1 Gy	0.1 Gy	0.1 Gy

OAR = organs at risk.

Small bowel dose increased by 1.5 Gy when Plan$_{deep}$ is recalculated on 4DCT$_{shallow}$ reaching the maximum dose tolerance allowed on the protocol (Fig. 2). When the Plan$_{shallow}$ is recalculated on the 4DCT$_{deep}$, this dose is reduced by 1.2 Gy. Dose to the stomach, liver, spinal canal, and skin did not change beyond dose tolerance (Fig. 3).

Discussion

Stereotactic dose delivery to abdominal targets should include motion management strategies prior to treatment delivery. Target volume reconstruction on CBCT images may not represent the entire planned volume[7] under different motion conditions. This can be a concern when using planning contours to register to CBCT reconstructed targets. Motion-assessment tools such as 4D CBCT and diaphragm motion evaluation[6,8] have been used to reduce this area of uncertainty. Our institution has used diaphragm motion as a surrogate for ITV margin verification for patients undergoing stereotactic treatment to the kidney. Ten patients have been treated using this protocol with only the 1 case showing a significantly large breathing deviation. Although no further intrafraction verification of breathing change is in place, this patient was immobilized using the BodyFIX dual vacuum technology which has been shown to provide reduction in tumor motion for lung patients[4] as well as intrafraction motion of < 1 mm SD.[9]

Breathing pattern changes from larger to smaller and vice versa can affect target dose coverage reducing the PTV coverage in both scenarios. With larger breathing anatomic changes is not only in the superior to inferior direction but also medial-lateral and anterior to posterior directions. Figure 4 shows a 0.5-cm difference in the lateral edge of the ITV/PTV relative to the lateral aspect of kidney organ. As the entire kidney is used as a surrogate matching target for the ITV position, it is important that the anatomic relationship between the ITV and the kidney organ does not change when using this form of image verification. The data indicates an increase in the dose to mobile structures (stomach,
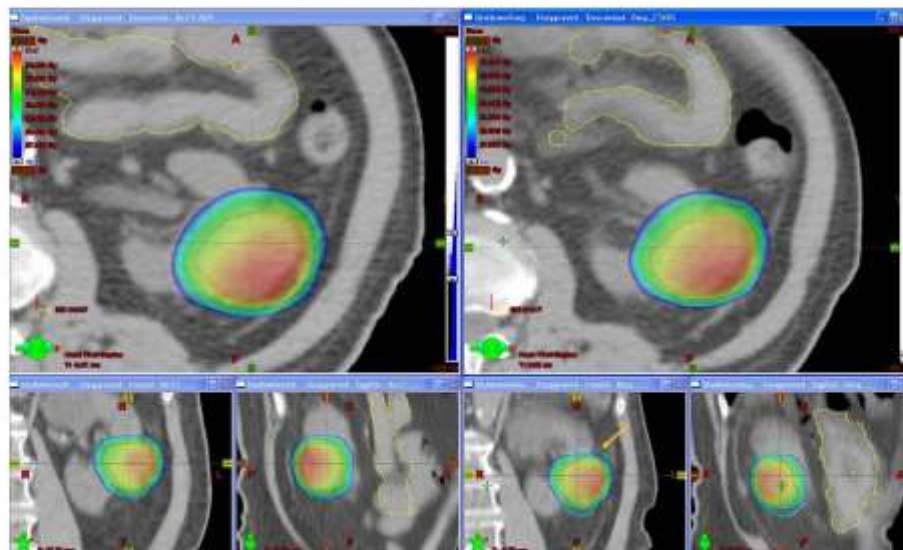

Fig. 3. Dose coverage on PTV for the Plan$_{normal}$ calculated on 4DCT$_{normal}$ data set (left) and the dose coverage to the PTV when the Plan$_{normal}$ is recalculated on the 4DCT$_{deep}$ data set (right). Dose coverage is compromised at the superior to inferior level because of larger motion (arrow). (Color version of figure is available online.)

Fig. 4. Dose coverage of PTV for the Plan$_{deep}$ calculated on 4DCT$_{deep}$ data set (left) and the dose coverage to the PTV when the Plan$_{deep}$ is recalculated on the 4DCT$_{normal}$ data set (right). Dose coverage is compromised and increased dose to small bowel (arrows). (Color version of figure is available online.)
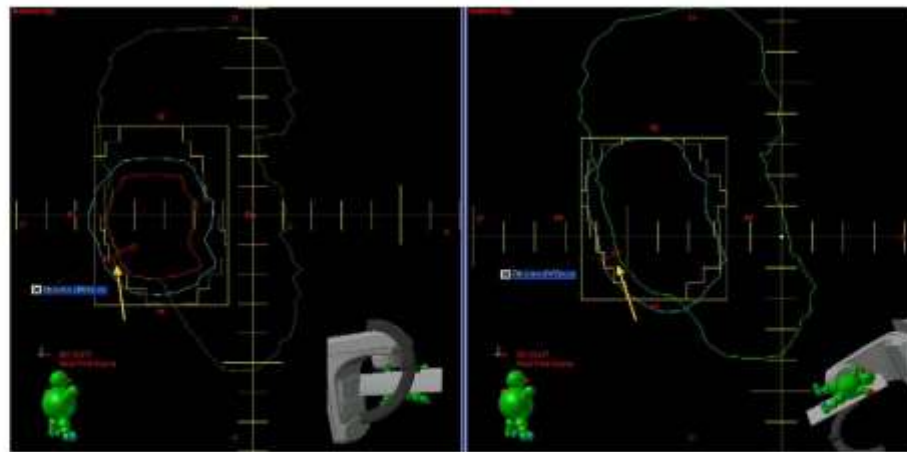

Fig. 5. Beam's eye view of field angle 245° showing a 0.5-cm change in position (arrow) of the PTV/ITV relative to the ipsilateral kidney organ. The field coverage of the Plan$_{deep}$ when matched to 4DCT$_{normal}$ (left) and similarly of Plan$_{normal}$ when matched to 4DCT$_{deep}$ (right) can be compromised when matching to the entire kidney organ surrogate. (Color version of figure is available online.)

skin, and small bowel) when dose is delivered to a condition when the breathing is more shallow. This assumes that there is minimal contribution from interfraction organ motion (Fig. 5).

Free breathing, deep breathing, and compressed breathing can show kidney motion range of up to 2.4 cm,[10] 6.6 cm,[11] and 0.5 cm,[12] respectively. It is important therefore for the dosimetrist and radiation therapist to ensure that patient breathing is consistent. Communication to patients about their breathing requirements from the planning stages should have treatment verification protocols to maintain consistency. Although it is difficult to define a breathing discrepancy threshold, therapists should be aware that PTV margins are reduced around the ITV structure. Education and training for therapists to be aware of this can provide intervention opportunities at treatment to ensure correct dose delivery.

Conclusions

This case study illustrates the effect of breathing changes in stereotactic body radiotherapy for primary kidney targets. A larger- or smaller-than-planned breathing change on treatment would not only affect PTV coverage but could also potentially increase the dose to surrounding organs at risk.

References

1. Siva, S.; Pham, D.; Gill, S.; et al. A systematic review of stereotactic radiotherapy ablation for primary renal cell carcinoma. *BJU Int.* **110**(11b):E737–43; 2012.
2. Xi, M.; Liu, M.-Z.; Deng, X.-W.; et al. Defining internal target volume (ITV) for hepatocellular carcinoma using four-dimensional CT. *Radiother. Oncol.* **84**(3):272–8; http://dx.doi.org/10.1016/j.radonc.2007.07.021.
3. Zhong, R.; Wang, J.; Jiang, X.; et al. Hypofraction radiotherapy of liver tumor using cone beam computed tomography guidance combined with active breath control by long breath-holding. *Radiother. Oncol.* **104**(3):379–85, http://dx.doi.org/10.1016/j.radonc.2011.11.007.
4. Han, K.; Cheung, P.; Basran, P.S.; et al. A comparison of two immobilization systems for stereotactic body radiation therapy of lung tumors. *Radiother. Oncol.* **95**(1):103–8, http://dx.doi.org/10.1016/j.radonc.2010.01.025.

5. Lee, S.; Yang, D.S.; Choi, M.S.; et al. Development of respiratory motion reduction device system (RMRDs) for radiotherapy in moving tumors. Jpn. J. Clin. Oncol. **34**(11):686–91; 2004.

6. Guckenberger, M.; Sweeney, R.A.; Wilbert, J.; et al. Image-guided radiotherapy for liver cancer using respiratory-correlated computed tomography and cone-beam computed tomography. Int. J. Radiat. Oncol. Biol. Phys. **71**(1):297–304, http://dx.doi.org/10.1016/j.ijrobp.2008.01.005.

7. Wang, Z.; Yin, F.; Yoo, S.; et al. SU-EE-A1-04: Verifying internal target volume using cone-beam CT for stereotactic body radiotherapy treatment. Med. Phys. **33**(6):1991; 2006.

8. Rit, S.; van Herk, M.; Zijp, L.; et al. Quantification of the variability of diaphragm motion and implications for treatment margin construction. Int. J. Radiat. Oncol. Biol. Phys. **82**(3):e399–407, http://dx.doi.org/10.1016/j.ijrobp.2011.06.1986.

9. Li, W.; Sahgal, A.; Foote, M.; et al. Impact of immobilization on intrafraction motion for spine stereotactic body radiotherapy using cone beam computed tomography. Int. J. Radiat. Oncol. Biol. Phys. **84**(2):520–6, http://dx.doi.org/10.1016/j.ijrobp.2011.12.039.

10. Bussels, B.; Goethals, L.; Feron, M.; et al. Respiration-induced movement of the upper abdominal organs: A pitfall for the three-dimensional conformal radiation treatment of pancreatic cancer. Radiother. Oncol. **68**(1):69–74, http://dx.doi.org/10.1016/S0167-8140(03)00133-6.

11. Moerland, M.A.; van den Bergh, A.C.M.; Bhagwandien, R.; et al. The influence of respiration induced motion of the kidneys on the accuracy of radiotherapy treatment planning, a magnetic resonance imaging study. Radiother. Oncol. **30**(2):150–4, http://dx.doi.org/10.1016/0167-8140(94)90045-0.

12. Heinzerling, J.H.; Anderson, J.F.; Papiez, L.; et al. Four-dimensional computed tomography scan analysis of tumor and organ motion at varying levels of abdominal compression during stereotactic treatment of lung and liver. Int. J. Radiat. Oncol. Biol. Phys. **70**(5):1571–8, http://dx.doi.org/10.1016/j.ijrobp.2007.12.023.

RESEARCH **Open Access**

An analysis of respiratory induced kidney motion on four-dimensional computed tomography and its implications for stereotactic kidney radiotherapy

Shankar Siva[1,2,6*†], Daniel Pham[3†], Suki Gill[1], Mathias Bressel[4], Kim Dang[3], Thomas Devereux[3], Tomas Kron[2,5] and Farshad Foroudi[1,2]

Abstract

Background and purpose: Stereotactic ablative body radiotherapy (SABR) is an emerging treatment modality for primary renal cell carcinoma. To account for respiratory-induced target motion, an internal target volume (ITV) concept is often used in treatment planning of SABR. The purpose of this study is to assess patterns of kidney motion and investigate potential surrogates of kidney displacement with the view of ITV verification during treatment.

Material and methods: Datasets from 71 consecutive patients with free breathing four-dimensional computed tomography (4DCT) planning scans were included in this study. The displacement of the left and right hemi-diaphragm, liver dome and abdominal wall were measured and tested for correlation with the displacement of the both kidneys and patient breathing frequency.

Results: Nine patients were excluded due to severe banding artifact. Of 62 evaluable patients, the median age was 68 years, with 41 male patients and 21 female patients. The mean (range) of the maximum, minimum and average breathing frequency throughout the 4DCTs were 20.1 (11–38), 15.1 (9–24) and 17.3 (9–27.5) breaths per minute, respectively. The mean (interquartile range) displacement of the left and right kidneys was 0.74 cm (0.45-0.98 cm) and 0.75 cm (0.49-0.97) respectively. The amplitude of liver-dome motion was correlated with right kidney displacement ($r=0.52$, $p<0.001$), but not with left kidney displacement ($p=0.796$). There was a statistically significant correlation between the magnitude of right kidney displacement and that of abdominal displacement ($r=0.36$, $p=0.004$), but not the left kidney ($r=0.24$, $p=0.056$). Hemi-diaphragm displacements were correlated with kidney displacements respectively, with a weaker correlation for the left kidney/left diaphragm ($r=0.45$, [95% CI 0.22 to 0.63], $p=<0.001$) than for the right kidney/right diaphragm ($r=0.57$, [95% CI 0.37 to 0.72], $p=<0.001$).

Conclusions: For the majority of patients, maximal left and right kidney displacement is subcentimeter in magnitude. The magnitude of kidney motion cannot be reliably estimated from the diaphragmatic, liver dome or abdominal wall surrogates. One explanation may be that the kidneys are not uniformly in contact with the surrogates investigated in this study. Further investigation is required before surrogates of kidney displacement are used for clinical SABR delivery.

Keywords: Kidney, Stereotactic, 4DCT, Respiratory motion, Radiation, ITV margin

* Correspondence: shankar.siva@petermac.org
†Equal contributors
[1]Department of Radiation Oncology, Peter MacCallum Cancer Centre, Melbourne, Australia
[2]Sir Peter MacCallum Department of Oncology, University of Melbourne, Melbourne, Australia
Full list of author information is available at the end of the article

Introduction

Renal cell carcinoma (RCC) is one of the 10 most common cancers in men and women, with incidence rates increasing by 4.1% per year in men and 3.3% per year in women between 2004 and 2008 [1]. Whilst surgery is the standard of care for primary disease [2], stereotactic ablative body radiotherapy (SABR) has emerged as potentially curative treatment approaches for patients who refuse or are unsuitable for surgery. A recent systematic review reports that local control rates from SABR in primary RCC are excellent, ranging from 84%-100% [3]. However, given the potential risk of severe toxicity to surrounding normal organs susceptible to hypofractionated radiotherapy (such as small bowel), significant consideration must be given to limit dose to normal tissue. One strategy to limit risk is to utilize rigorous image guidance methods for SABR delivery. Integral to this aim is the ability to mitigate geometric uncertainty arising from the target kidney motion.

A major challenge in the image guidance process is intrafractional kidney displacement due to respiration. Renal tumours are often of similar density to the surrounding normal kidney and can be difficult to visualize using cone beam CT (CBCT). The use of contrast enhancing agents is often contraindicated by the pre-existing renal dysfunction that is prevalent in this patient population. In light of challenging imaging conditions, one potential strategy to account for kidney motion is treatment planning using the internal target volume (ITV) concept [4]. In order to validate the appropriateness of ITV margins constructed at planning, surrogates of tumor displacement can be matched at the time of treatment delivery. These surrogates include the diaphragm as visualized using fluoroscopic kilovoltage (kV) imaging, or external markers placed on the abdominal wall. The use of external markers is often favored due to the advantages of real-time tracking and a reduction in undesirable excess ionizing radiation to the patient [5]. When using 3D on board imaging with CBCT, a novel and as yet unexplored potential surrogate is the excursion of the liver dome. However, the validity of the use of any surrogate of kidney position is predicated on validating a robust relationship between the kidneys and surrounding organ motion.

The purpose of this study is to assess the relationship of kidney displacement with clinically relevant surrogates that can be easily measured at the time of the treatment planning CT. The surrogates investigated in this study include the anterior abdominal wall, the diaphragms, and the probability density function (PDF) of the liver dome (previously described by Guckenberger et al. [6]). These relationships have implications for radiotherapy planning and treatment delivery, as typical SABR plans using an ITV concept employ a very narrow margin to the final planning target volume (PTV). As such, these plans rely heavily on accurate quantification of both

target position and displacement. We investigated if the displacement of these surrogates can be used to confirm the magnitude of displacement of the kidney and therefore serve to validate the appropriateness of the ITV margin used for kidney SABR. The central hypothesis of this study is that the magnitude of kidney displacement correlates to the PDF width.

Materials and methods

This is a retrospective study of 71 consecutive patients who had 4DCT planning scans including partial or full view of the left and right kidneys at a single institution. Nine patient datasets were excluded due to excessive banding artifact. Of the remaining 62 patients, 53 had thoracic tumors and 9 patients had liver tumors. The median age was 68 years, with 41 male patients and 21 female patients. This study had independent review board (IRB) approval at the Peter MacCallum Cancer Centre.

Patients were scanned in the arms up position under relaxed free-breathing conditions without any compression devices. A respiratory sorted four-dimensional computed tomography (4DCT) dataset was generated using the Philips Brilliance® CT scanner coupled with a Philips Bellows system® as surrogate marker for breathing phase (Philips Medical Systems, Best, The Netherlands). The bellows system consists of an elasticised belt worn around the abdomen that expands and contracts with respiratory motion. A pressure transducer converts the variation of pressure in the bellows into a voltage signal, which is digitized and transmitted to the CT scanner. The resultant data is presented as a trace demonstrating respiratory motion and calculated number of breaths per minute. The calculated respiratory rate is used to select an appropriate pitch for couch motion during CT scanning. Typically, the respiratory trace was observed for a period of approximately one minute to ensure inter-cycle stability prior to CT acquisition. The CT scanner was commissioned to acquire 4DCT scans in helical mode, and to bin the CT slices into 10 phases for image reconstruction. The patients were imaged using 140 kVp, 3 mm slice thickness, 3 mm increment, and 0.44 s rotation time, and images were reconstructed with ~3.5 mm^3 voxel resolution (3 mm slice thickness × 1.0742 mm pixel spacing). The 4DCT scan acquisition was approximately 90 seconds in duration, typically incorporating information from 18–27 patient breaths. From the respiratory-sorted imaging datasets, the maximum expiration and inspiration phases were identified and subsequently exported to the treatment planning system for analysis. This methodology cannot account for irregularity of the breathing cycle. However, in most motion management techniques, including the Internal Target Volume delineation used in our centre, the accurate identification of the extremes of breathing is of greater importance.
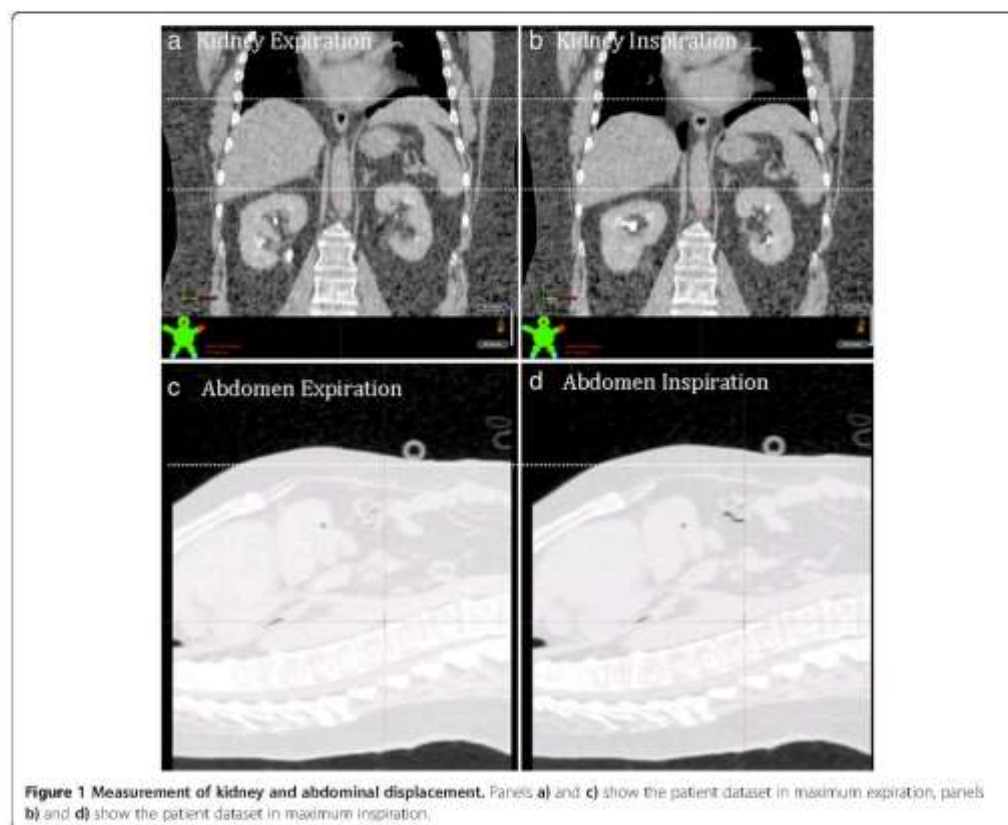
All measurements were performed on an Eclipse* workstation v 8.9 (Varian Medical Systems, Palo Alto, CA) using standardized abdominal window/level settings. Left and right diaphragm displacement was measured using a predefined coronal reference plane: The most anterior aspect of the T12 vertebral body, at midline and mid-vertebral height. Cranio-caudal kidney apex displacements were viewed across axial, sagittal and coronal CT for the maximum displacement (Figure 1). The magnitude of displacement of the abdominal wall was measured in the ventero-dorsal plane. The magnitude of displacement was defined as the difference between maximum and minimal organ position throughout all viewed datasets. To quantify liver dome displacement, a line profile tool was used to display and visualize the liver dome's probability density function (PDF) at the coronal reference plane. This measurement was performed on the 4DCT reconstructed *averaged* CT dataset (which is a composite of all 10 respiratory phases, equivalent of a slow CT scan).

A line profile tool was used to measure the PDF width displaying the Hounsfield Unit variation due to liver dome motion. This technique was adapted from that previously described [6] to measure liver excursion in CBCT datasets during online image guidance of SABR.

A Pearson correlation coefficient was subsequently used to test the liver dome PDF width for correlation with the displacement of kidneys and abdominal wall (Figure 2). The width of the PDF, and right and left kidneys were also correlated to the breathing frequency from each recorded breathing trace recorded from the 4DCT scans using a Pearson statistic.

Results

Under free breathing conditions the mean displacement as identified on 4DCT of the left and right kidney were 0.74 cm (range 0.10-2.15 cm) and 0.75 cm (range 0.11-1.92 cm) respectively. The mean displacement of the left and right hemi-diaphragms were 1.34 cm (range 0.27-2.76 cm)
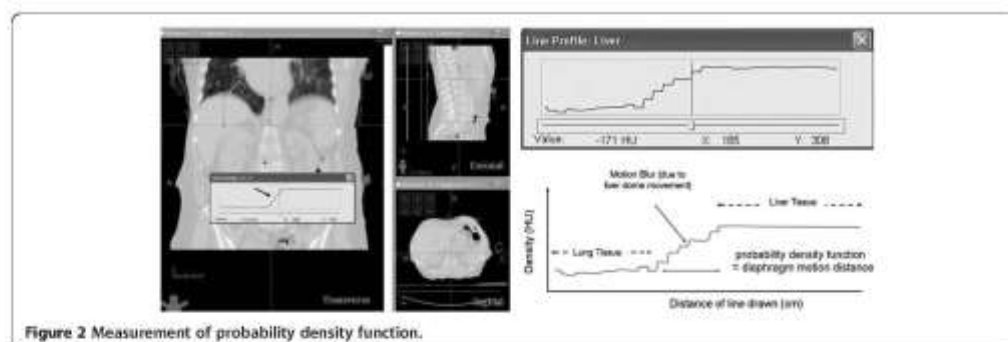

Figure 1 Measurement of kidney and abdominal displacement. Panels a) and c) show the patient dataset in maximum expiration, panels b) and d) show the patient dataset in maximum inspiration.

Figure 2 Measurement of probability density function.

and 1.45 cm (range 0.45-3.26 cm) respectively. The mean displacement of the anterior abdominal wall (abdomen) was 0.57 cm (range 0–1.06 cm) (Table 1).

Both left and right hemi-diaphragm displacements were correlated with left and right kidney displacements respectively, with a slightly weaker correlation for the left kidney/left diaphragm ($r=0.45$, [95% CI 0.22 to 0.63], $p=<0.001$) than for the right kidney/right diaphragm ($r=0.57$, [95% CI 0.37 to 0.72], $p=<0.001$). The width of the PDF showed a statistically significant correlation with right kidney displacement ($r=0.52$ [95% CI 0.31 to 0.68], $p<0.001$) (Figure 3), but not with left kidney displacement ($r=-0.08$ [95% CI −0.33 to 0.17], $p=0.796$) nor abdominal wall displacement ($r=-0.18$ [95% CI −0.07 to 0.42], ($p=0.151$). There was a statistically significant correlation between the magnitude of right kidney displacement and that of abdominal displacement ($r=0.36$ [95% CI 0.12 to 0.57], $p=0.004$) (Figure 4). However the correlation between magnitude of left kidney displacement and abdominal wall displacement had only approached statistical significance ($r=0.24$ [95% CI −0.01 to 0.47], $p=0.056$). Age was not associated with either the left kidney ($r=0.05$ [95% CI −0.20 to 0.29], $p=0.710$) or right kidney ($r=-0.08$ [95% CI −0.33 to 0.17], $p=0.517$) displacement. The mean (±standard deviation) of left and right kidney motion was 0.95 cm (±0.63 cm) and 0.83 cm (±0.39 cm) respectively for

patients with liver tumors and was 0.61 cm (±0.41 cm) and 0.74 cm (±0.40 cm) respectively for patients with thoracic tumors. The magnitude of left and right kidney displacement was not statistically different between patients with liver tumors and those with thoracic tumors (student's t-test, $p=0.257$ and $p=0.519$ respectively). Similarly, tumor site (thoracic versus liver) did not affect abdominal displacement nor PDF measurement ($p=0.259$ and $p=0.180$ respectively).

The patient breathing frequency was recorded as a maximum, minimum and average in breaths per minute (bpm) from the breathing trace acquired at the time of the 4DCT. Of the 61 evaluable breathing traces, the mean (range) of the maximum, minimum and average breathing frequency was 20.1 (11–38) bpm, 15.1 (9–24) bpm and 17.3 (9–27.5) bpm respectively. The average breathing frequency showed a negative correlation with the magnitude of the PDF ($r=-0.124$, [95% CI −0.554 to −0.110, $p=0.006$) and the right kidney displacement ($r=-0.112$, [95% CI −0.541 to −0.090], $p=0.008$). However, breathing frequency was not correlated to left kidney displacement ($r=-0.23$, [95% CI −0.44 to 0.05], $p=0.120$) (Figure 5 a-c).

Discussion

There is a resurgent interest in radiotherapy use for primary RCC since the advent of hypofractionated SABR

Table 1 Descriptive statistics of measured organ displacement

Parameter	Organ displacement (cm)					
	Left kidney	Right kidney	Left diaphragm	Right diaphragm	Abdomen	Liver dome (PDF)
Mean	0.74	0.75	1.34	1.45	0.57	1.56
Standard Dev	0.44	0.40	0.50	0.55	0.25	0.53
Median	0.61	0.69	1.27	1.38	0.56	1.49
Minimum	0.10	0.11	0.27	0.45	0.00	0.74
Maximum	2.15	1.92	2.76	3.26	1.06	2.91
Interquartile range	0.45-0.98	0.49-0.97	1.07-1.56	1.08-1.77	0.41-0.74	1.17-1.85
90th percentile	1.33	1.30	2.12	2.21	0.98	2.33

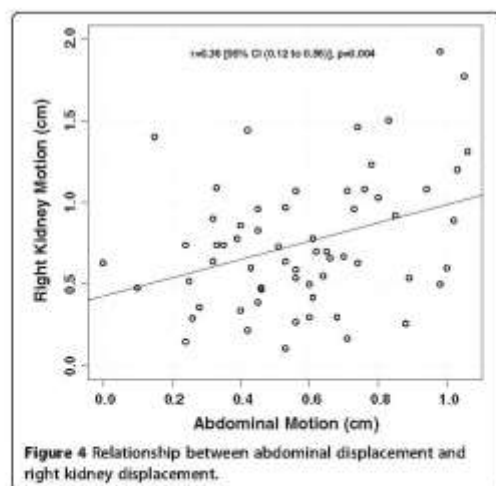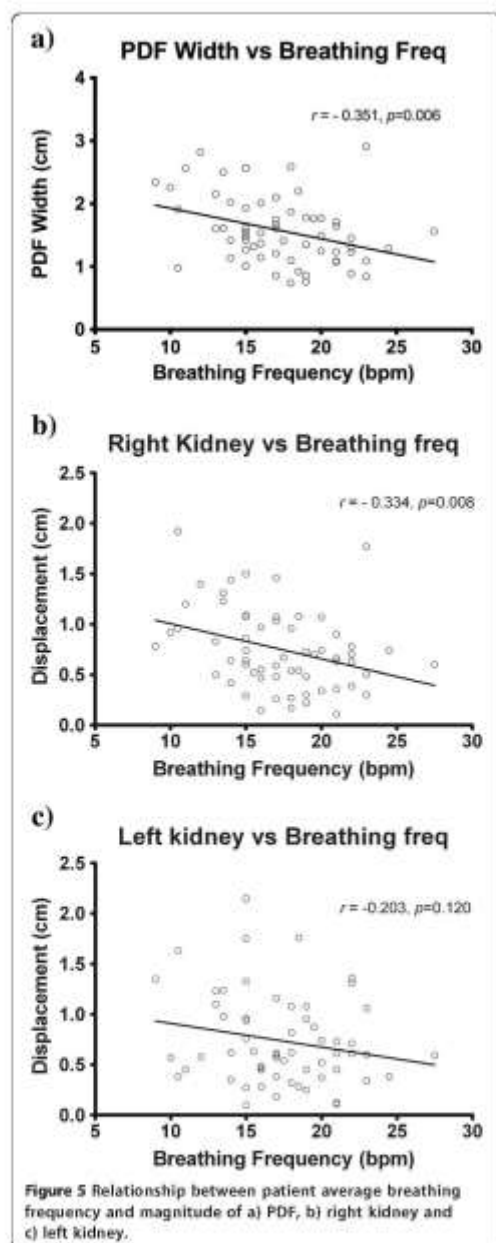**Figure 3** Relationship between pdf width and right kidney displacement.
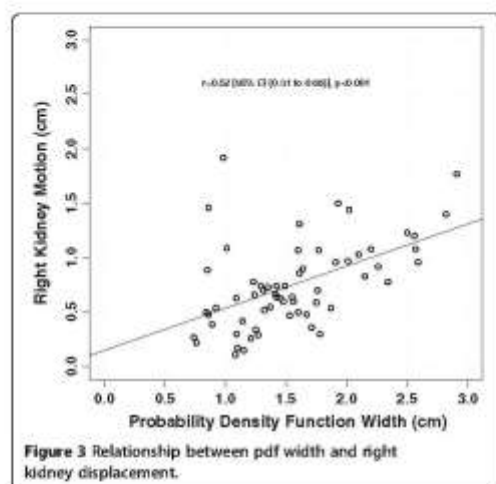
techniques. Several treatment strategies have been developed to account for target motion, including respiratory gated delivery or delivery to the entire volume of tumor excursion. The latter strategy uses fields that incorporate the internal target volume (ITV), which encompasses the gross tumor volume in addition to an internal margin for tumor motion [4]. Understanding the amplitude of motion expected in either kidney is important in determining appropriate radiotherapy margins as typical SABR planning target volumes (PTVs) have a very narrow margin applied to the respective ITV, typically around 5 mm or less [7,8]. An understanding of a population average of motion is critical as breathing motion is complex, variable,

Figure 4 Relationship between abdominal displacement and right kidney displacement.

and known to change over time at an individual level with transient instabilities [9]. Our population of patients showed a mean amplitude motion of 0.74 cm and 0.75 cm for both the left and right kidneys respectively, with 75 percent of patients having subcentimeter maximum kidney excursion. However, 10 percent of patients had greater than 1.33 cm and 1.30 cm of motion for the left and right kidneys respectively.

A consequence of the use of an ITV concept for treatment (as opposed to gated radiotherapy delivery) is an increase in the amount of normal tissue irradiated in order to account for tumor motion. In the context of the kidney however, this motion relates to a relatively large organ typically measuring 3 cm by 6 cm by 12 cm [10]. The kidney is an organ that functions in a radiobiological sense in a parallel rather than serial fashion for the expression of radiation toxicity such as hypertension or loss of renal function. A relatively small respiratory induced organ motion in the context of a large parallel functioning volume may mitigate the consequences of non-gated treatment delivery. This view is reinforced by historically low risks of clinical toxicity after SABR for renal cell carcinoma. Interestingly, symptomatic kidney injury has not been reported after SABR to kidney targets to date. The QUANTEC consensus group publication [11] suggests that "one hypothesis is that nearly complete sparing of a substantial volume of the kidney should be associated with compensatory effects and preservation of renal function, despite the delivery of focal high doses". The low risk of clinical toxicity after SABR to the kidney has been most eloquently researched in a study published by Svedman et al. [12]. This study assessed the effect of SABR in patients with only one functioning kidney with up to 6-years of follow up. Five of the seven patients had no change in renal function. Two patients had mild asymptomatic increases in renal function, without the need for medical or dialysis intervention. None of the patients developed hypertension. In the context of low clinical risk of renal toxicity, and given that the large majority of patients in our study had subcentimeter kidney motion, our group suggests that SABR delivery with an ITV concept may be a reasonable strategy for the majority of these patients. However, in select patients with large respiratory excursion, strategies to reduce the internal tumor motion (such as respiratory training [13] or abdominal compression [14]) may be warranted to reduce the integral dose to surrounding normal tissue.

This study presents the largest series to date assessing patient kidney motion. Previous smaller studies have used a variety of different imaging modalities under varying breathing conditions. These studies have demonstrated a broad range of values for kidney displacement. An early study demonstrated in 14 patients that kidney motion measured by radiographs under forced deep breathing

Figure 5 Relationship between patient average breathing frequency and magnitude of a) PDF, b) right kidney and c) left kidney.

conditions ranged between 0.1-3.2 cm and 0.3-2.1 cm in the right and left kidneys respectively [15]. Moerland et al. [16] found that forced breathing can induce movement as large as 6.6 cm in the left kidney and 8.6 cm in the

right kidney in a study using magnetic resonance imaging (MRI). Under free breathing conditions using MRI in 12 patients, Bussels et al. [17] demonstrated a mean cranio-caudal displacement of the right kidney and left kidney of 1.61 cm and 1.69 cm respectively. A study by Wysocka et al. [18] using serial non-gated CTs in 22 patients treated for gastric cancer showed a median (range) free breathing cranio-caudal displacement of 0.6 cm (0–3.7 cm) and 0.8 cm (0.2–3.5 cm) in the left and right kidneys respectively, and a displacement of 0.6 cm (0–2.8 cm) for the diaphragm. Kim et al. [19] studied 9 healthy volunteers with 4DCT scans in the supine position showed mean kidney motion of 1.2 cm and mean hepatic dome motion of 1.7 cm. The largest report of kidney motion using 4DCT prior to our study was from Van Sörnsen de Koste [20] in an investigation of 54 patients, 49 with lung tumors and 5 with liver tumors. Mean (range) cranio-caudal mobility was observed to be 0.98 cm (0.25-3.00 cm) for the left kidney and 0.9 cm (0.25-2.05 cm) for the right kidney. Similarly, our series demonstrated a similar mean (range) of displacement for both the left and right kidney, at 0.74 cm (0.10-2.15 cm) and 0.75 cm (0.11-1.92 cm) respectively.

The use of the PDF for assessment of liver dome motion from the *average* reconstruction of the planning 4DCT is a relatively novel technique. We have extrapolated this technique from that described by Guckenberger et al. [6] to interpret respiratory excursion of the liver on CBCT) Our own group's experience within the context of the FASTRACK prospective clinical trial (*ClinicalTrials.gov Identifier*: NCT01676428) indicates that kidney tumor image guidance can be particularly challenging when using online 3D CBCT techniques, particularly without the aid of implanted fiducials or contrast agents. During the treatment delivery workflow, should the kidney and tumor ITV not match to pre-treatment estimates, confirmation of the appropriateness of the ITV margin selected can be theoretically achieved through measurement of surrogate organ displacement. This present study suggests that the PDF width has only moderate correlation with right kidney displacement ($r=0.52$, $p<0.001$) and no correlation with the left kidney ($p=0.151$). Based on these results, the PDF width does not allow for reliable matching of respiratory induced kidney displacement. On a practical level, our study suggests that liver dome excursion should not be used as a surrogate for kidney target displacement as has been previously reported for liver targets [6].

In our study population there was a correlation between abdominal wall motion and right kidney displacement ($p=0.004$), however no significant correlation between abdominal motion and left kidney displacement ($p=0.056$). A similar de-coupling effect of breathing and organ motion was demonstrated for the left kidney in our study when assessing for patient breathing frequency. The breathing frequency was inversely correlated to the PDF and right

kidney motion (p=0.006 and p=0.008 respectively), confirming the intuitive assumption that patients with more shallow, rapid breathing patterns have smaller respiratory induced organ excursion. In contrast, breathing frequency did not correlate with left kidney motion (p=0.120). Our hypothesis for this phenomenon is that the intimate association of the liver may constrain kidney motion on the right, whereas in contrast the left kidney largely floats within the perinephric fat, bounded only by Gerota's fascia. Therefore the left kidney motion and relationship with surrounding upper abdominal organs may not be as rigidly conformal as the right kidney. On a practical level, this dissociation raises the concern that current evidence supporting the use of external surrogates for indirect tumor matching in lung and liver tumors may not be directly applicable to the context of SABR kidney treatments. This is an area in need of further investigation. The weak inter-patient correlation noted in this study, despite the large sample size, indicates that abdominal marker displacement is also an inadequate surrogate for kidney displacement.

A potential weakness of this study is that the 4DCT datasets are acquired for each scan over a relatively short time in the context of the clinical treatment times required for SABR kidney. Future studies utilizing long acquisition scanning techniques with high spatial resolution (such as cine MRI) or repeated 4DCTs would be necessary to fully elucidate the patterns of motion of upper abdominal organs over periods that more closely match that of treatment delivery. Baseline shifts of the liver and kidney displacement have been observed with a median shift of 6.5 mm and 6.6 mm respectively over longer breathing periods (Wysocka 2010). A baseline shift in patient breathing can potentially confound the verification of the PDF width. A 4D image guidance protocol to verify breathing motion should take this into consideration. For example, a 3D CBCT of the diaphragm dome can be matched to bony anatomy of the planning CT before assessment of the PDF width. Verification of the location of the maximum inspiration and expiration of the liver dome as well as its magnitude can ensure that a large baseline shift has not occurred. The use of planar imaging can also allow the entire range of diaphragm motion to be observed in order to verify displacement as well as maximum inspiration and expiration positions. However in a free breathing protocol, our clinic has experienced technical limitations in using fluoroscopic imaging in this context due to user variability in the measurement of liver dome displacement. For the present time the PDF width still serves as a useful tool to compare the patient's depth of respiration on the planning CT and the pre-treatment CBCT.

Conclusion

Kidney motion during respiration for the majority of patients is subcentimeter in magnitude and justifies the use of an ITV for treatment delivery. In a small minority kidney motion can be significant and poses a potential technical limitation in the delivery of stereotactic image guided radiotherapy. Neither the abdominal wall nor the liver dome were found to be adequate surrogates of kidney displacement in our study, and diaphragmatic displacement was only moderately correlated. Therefore, these organs should not be used to estimate the appropriateness of kidney ITV margins unless validated in an individual patient.

Consent

Written informed consent was obtained from the patient for the publication of this report and any accompanying images.

Author details
¹Department of Radiation Oncology, Peter MacCallum Cancer Centre, Melbourne, Australia. ²Sir Peter MacCallum Department of Oncology, University of Melbourne, Melbourne, Australia. ³Radiation Therapy Services, Peter MacCallum Cancer Centre, Melbourne, Australia. ⁴Department of Biostatistics and Clinical Trials, Peter MacCallum Cancer Centre, Melbourne, Australia. ⁵Department of Physical Sciences, Peter MacCallum Cancer Centre, Melbourne, Australia. ⁶Peter MacCallum Cancer Centre, Locked Bag 1, A'Beckett Street, East Melbourne, Victoria 8006, Australia.

References
1. Coates PJ, Rundle JK, Lorimore SA, Wright EG: Indirect macrophage responses to ionizing radiation: implications for genotype-dependent bystander signaling. Cancer Res 2008, 68:450–456.
2. Ljungberg B, Cowan NC, Hanbury DC, Hora M, Kuczyk MA, Merseburger AS, Patard JJ, Mulders PFA, Sinescu IC: EAU guidelines on renal cell carcinoma: the 2010 update. Eur Urol 2010, 58:398–406.
3. Siva S, Pham D, Gill S, Corcoran NM, Foroudi F: A systematic review of stereotactic radiotherapy ablation for primary renal cell carcinoma. BJU Int 2012. doi: 10.1111/j.1464-410X.2012.11550.x.
4. ICRU: Report 62 Prescribing, Recording and Reporting Photon Beam Therapy (Supplement to ICRU Report 50). Bethesda, MD: International Commission on Radiation Units and Measurements; 1999.
5. Schweikard A, Glosser G, Bodduluri M, Murphy MJ, Adler JR: Robotic motion compensation for respiratory movement during radiosurgery. Comput Aided Surg 2000, 5:263–277.
6. Guckenberger M, Sweeney RA, Wilbert J, Krieger T, Richter A, Baier K, Mueller G, Sauer O, Flentje M: Image-guided radiotherapy for liver cancer using respiratory-correlated computed tomography and cone-beam computed tomography. Int J Radiat Oncol Biol Phys 2008, 71:297–304.
7. Underberg RWM, Lagerwaard FJ, Cuijpers JP, Slotman BJ, van Sörnsen de Koste JR, Senan S: Four-dimensional CT scans for treatment planning in stereotactic radiotherapy for stage I lung cancer. Int J Radiat Oncol Biol Phys 2004, 60:1283–1290.
8. Siva S, Chesson B, Aarons Y, Clements N, Kron T, MacManus M, Ball D: Implementation of a lung radiosurgery program: technical considerations and quality assurance in an Australian institution. J Med Imaging Radiat Oncol 2012, 56(3):354–361.

9. Ozhasoglu C, Murphy MJ: Issues in respiratory motion compensation during external-beam radiotherapy. *Int J Radiat Oncol Biol Phys* 2002, **52**:1389–1399.

10. Warwick R, Dyson M, Bannister L: *Gray's anatomy. In Book Gray's anatomy (Editor ed.^eds.)*. City. London: Churchill Livingstone; 2005.

11. Dawson LA, Kavanagh BD, Paulino AC, Das SK, Miften M, Li XA, Pan C, Ten Haken RK, Schultheiss TE: Radiation-associated kidney injury. *Int J Radiat Oncol Biol Phys* 2010, **76**:S108–S115.

12. Svedman C, Karlsson K, Rutkowska E, Sandström P, Blomgren H, Lax I, Wersäll P: Stereotactic body radiotherapy of primary and metastatic renal lesions for patients with only one functioning kidney. *Acta Oncol* 2008, **47**:1578–1583.

13. Kini VR, Vedam SS, Keall PJ, Patil S, Chen C, Mohan R: Patient training in respiratory-gated radiotherapy. *Med Dosim* 2003, **28**:7–11.

14. Heinzerling JH, Anderson JF, Papiez L, Boike T, Chien S, Zhang G, Abdulrahman R, Timmerman R: Four-dimensional computed tomography scan analysis of tumor and organ motion at varying levels of abdominal compression during stereotactic treatment of lung and liver. *Int J Radiat Oncol Biol Phys* 2008, **70**:1571–1578.

15. Ahmad N, Huq M, Corn B: Respiration-induced motion of the kidneys in whole abdominal radiotherapy: implications for treatment planning and late toxicity. *Radiother Oncol* 1997, **42**:87–90.

16. Moerland M, van den Bergh A, Bhagwandien R, Janssen W, Bakker C, Lagendijk J, Battermann J: The influence of respiration induced motion of the kidneys on the accuracy of radiotherapy treatment planning, a magnetic resonance imaging study. *Radiother Oncol* 1994, **30**:150–154.

17. Bussels B, Goethals L, Feron M, Bielen D, Dymarkowski S, Suetens P, Haustermans K: Respiration-induced movement of the upper abdominal organs: a pitfall for the three-dimensional conformal radiation treatment of pancreatic cancer. *Radiother Oncol* 2003, **68**:69–74.

18. Wysocka B, Kassam Z, Lockwood G, Brierley J, Dawson LA, Buckley CA, Jaffray D, Cummings B, Kim J, Wong R: Interfraction and respiratory organ motion during conformal radiotherapy in gastric cancer. *Int J Radiat Oncol Biol Phys* 2010, **77**:53–59.

19. Kim YS, Park SH, Ahn SD, Lee JE, Choi EK, Lee S, Shin SS, Yoon SM, Kim JH: Differences in abdominal organ movement between supine and prone positions measured using four-dimensional computed tomography. *Radiother Oncol* 2007, **85**:424–428.

20. Van Sörnsen de Koste JR, Senan S, Kleynen CE, Slotman BJ, Lagerwaard FJ: Renal mobility during uncoached quiet respiration: An analysis of 4DCT scans. *Int J Radiat Oncol Biol Phys* 2006, **64**:799–803.

177

9.4 A planning study investigating dual-gated volumetric arc stereotactic treatment of primary renal cell carcinoma

A planning study investigating dual-gated volumetric arc stereotactic treatment of primary renal cell carcinoma

Thomas Devereux, R.T.T.,[*] Daniel Pham, R.T.T.,[*] Tomas Kron, Ph.D.,[††] Farshad Foroudi, F.R.A.N.Z.C.R.,[‖§] Jeremy Supple, B.Sc. Hons.,[‖] and Shankar Siva, F.R.A.N.Z.C.R.[§]

[*]Radiation Therapy Services, Peter MacCallum Cancer Centre, Melbourne, Australia; [†]Department of Physical Sciences, Peter MacCallum Cancer Centre, Melbourne, Australia; [‡]Sir Peter MacCallum Department of Oncology, Melbourne University, Melbourne, Australia; [§]Radiation Oncology and Cancer Imaging, Peter MacCallum Cancer Centre, Melbourne, Australia; and [‖]School of Applied Sciences, Royal Melbourne Institute of Technology, Melbourne, Australia

ARTICLE INFO

ABSTRACT

This is a planning study investigating the dosimetric advantages of gated volumetric-modulated arc therapy (VMAT) to the end-exhale and end-inhale breathing phases for patients undergoing stereotactic treatment of primary renal cell carcinoma. VMAT plans were developed from the end-inhale (VMATinh) and the end-exhale (VMATexh) phases of the breathing cycle as well as a VMAT plan and 3-dimensional conformal radiation therapy plan based on an internal target volume (ITV) (VMATitv). An additional VMAT plan was created by giving the respective gated VMAT plan a 50% weighting and summing the inhale and exhale plans together to create a summed gated plan. Dose to organs at risk (OARs) as well as comparison of intermediate and low-dose conformity was evaluated. There was no difference in the volume of healthy tissue receiving the prescribed dose for the planned target volume (PTV) (CI100%) for all the VMAT plans; however, the mean volume of healthy tissue receiving 50% of the prescribed dose for the PTV (CI50%) values were 4.7 ($\pm$ 0.2), 4.6 ($\pm$ 0.2), and 4.7 ($\pm$ 0.6) for the VMATitv, VMATinh, and VMATexh plans, respectively. The VMAT plans based on the exhale and inhale breathing phases showed a 4.8% and 2.4% reduction in dose to 30 cm^3 of the small bowel, respectively, compared with that of the ITV-based VMAT plan. The summed gated VMAT plans showed a 6.2% reduction in dose to 30 cm^3 of the small bowel compared with that of the VMAT plans based on the ITV. Additionally, when compared with the inhale and the exhale VMAT plans, a 4% and 1.5%, respectively, reduction was observed. Gating VMAT was able to reduce the amount of prescribed, intermediate, and integral dose to healthy tissue when compared with VMAT plans based on an ITV. When summing the inhale and exhale plans together, dose to healthy tissue and OARs was optimized. However, gating VMAT plans would take longer to treat and is a factor that needs to be considered.

Crown Copyright © 2015 Published by Elsevier Inc. on behalf of American Association of Medical Dosimetrists

Introduction

For patients diagnosed with primary renal cell carcinoma (RCC), the primary form of treatment is surgical resection. However, because this disease occurs generally in an elderly population with multiple comorbidities, surgery is not always a viable option.[1,2] Alternative options include ablative therapies such as cryoablation and radiofrequency ablation.[2,3] These techniques are still invasive, delivered either laparoscopically or percutaneously, and as such carry associated risks and potential for morbidity.

Noninvasive ablative techniques using high-dose-per-fraction radiation have recently been investigated for the treatment of primary RCC. Historically, RCCs are considered radioresistant to conventional radiation therapy (RT), with RT typically being reserved for palliation only.[4] However, this notion has recently been challenged by the delivery of large-dose-per-fraction RT enabled by the advent of stereotactic ablative body radiotherapy (SABR). The potential toxicity of the large radiation doses involved is mitigated using image guidance, advanced planning techniques, and immobilization devices.[5] In the context of primary RCC, SABR has achieved local control rates in the order of 80% to 100%.[4]

Reprint requests to: Thomas Devereux, R.T.T., Peter MacCallum Cancer Centre, Locked Bag No. 1 A' Beckett Street, Victoria 8006, Australia.
E-mail: thomas.devereux@petermac.org

SABR treatment can be delivered via open fields 3-dimensional conformal RT (3DCRT) or dynamic multileaf collimator delivery, which includes intensity-modulated RT (IMRT) and volumetric-modulated arc therapy (VMAT). When compared with static dose delivery, the dynamic alternative can offer superior conformity of the prescription dose to the target with reduced dose to critical structures.[6,7] However, organs and tumors in the upper abdomen, such as the liver and the kidneys, can experience considerable motion caused by respiration, which limits the reduction of margins on the tumor.[8] This in turn causes greater amounts of healthy tissue to receive radiation and increases the risk of geographic miss of the target volume.[9]

Therefore, SABR treatment planning in the abdominal region requires motion management. There are a number of methods to take into account organ motion, including compression plates, breath-hold, and time-resolved 4D computed tomography (CT) scans.[10] A common planning method is to use the concept of the internal target volume (ITV), which provides treatment of the target throughout the breathing cycle.[11] Alternatively, gating is another technique used to account for motion by delivering treatment during a specific part of the breathing phase. The 4DCT-based gated planning study by Gabrys et al.,[12] in 2010, for liver tumors found a significant correlation between dose and volume reduction in the organs at risk (OARs). In addition, a preclinical evaluation of respiratory-gated delivery of VMAT by Nicolini et al.[13] concluded that there is potential for VMAT to be delivered in conjunction with respiratory gating.

The purpose of this study was to assess the dosimetric advantages of gated VMAT plans compared with that of VMAT plans based on ITVs. In addition, it was proposed that by combining both the end-exhale and end-inhale phases of a patient's breathing cycle into a "summed" plan dose to healthy tissue and OARs can be optimized further. Therefore, the secondary objective of this study was to investigate whether there were any dosimetric benefits to combining the gated plans for each patient into a "summed gated" VMAT plan. This would provide some insight into motion-adaptive RT.

Methods

Patient cohort

Patients enrolled into an ethics-approved pilot study of Focal Ablative Stereotactic Radiosurgery for Cancers of the Kidney (FASTRACK; clinical trials.gov ID NCT01676428) were the subjects of this study. FASTRACK is a pilot study investigating the feasibility of treatment of primary RCC using a stereotactic dose for treatment on a conventional linac. Patients with primary RCC < 5 cm in size were planned to receive a single fraction of SABR. A cohort of 5 sequentially treated patients with primary RCC who received a 26-Gy dose in a single fraction were identified and formed the basis of this planning study.

Immobilization and simulation

All patients were immobilized with the BodyFIX whole-body double-vacuum system (Medical Intelligence, Schwabmünchen, Germany) and underwent a 4DCT on a Philips Brilliance Big Bore CT scanner (Philips Medical Systems, Cleveland, OH) and were positioned supine with their arms above their head. The 4DCT scans for each patient were reconstructed into 10 time bins, 0% to 90%, using respiratory phase binning and exported to a computer planning system (Eclipse v11.31; Varian Medical Systems, Palo Alto, CA). One of the patients had a deep-breathing 4D CT scan and a normal-breathing 4D scan, which are labeled accordingly. The deep-breathing scan was taken at the patient's own volition during the initial planning appointment without the knowledge of the planning therapist. A change in breathing amplitude was detected at a mock-up treatment session, and it was decided that a new 4D scan that was more representative of the patient's normal-breathing pattern was required. Therefore, both the scans were used for this study's purpose and were labeled accordingly.

Contouring

An ITV was contoured based on the 4D maximum-intensity projection data set. A 5-mm expansion around the ITV was used to generate the planning target

volume (PTV). Maximum-inhale and maximum-exhale data sets were also selected based on the 10 time bins (generally 0% and 50%, respectively), and a gross tumor volume (GTV) was contoured based on each of these data sets and labeled GTV inhale (GTVinh) and GTV exhale (GTVexh). A 5-mm expansion was also placed around the GTVinh and GTVexh to generate the respective PTVs. Furthermore, OARs were contoured on the time-weighted average data set and on the maximum-inhale and maximum-exhale data sets independently; these organs included the small bowel, stomach, liver, skin, and spinal cord.

Planning technique and dose calculation

3-Dimensional conformal RT

3DCRT plans were created for each patient on the Eclipse treatment planning system (Varian Medical Systems, Palo Alto, CA) and calculated using an Analytical Anisotropic Algorithm, v11.03. A minimum of 6 coplanar and a minimum of 2 noncoplanar fields with a combination of 6/18 MV were used with a prescription to the minimum surrounding isodose to ensure that 99% of the PTV received 100% of the dose. These plans were used clinically as part of the previously mentioned FASTRACK trial and have been included in the results as the clinically used plan but are not meant for comparison and are not the focus of this study.

VMAT plans

For each patient, 4 VMAT plans were developed and were labeled in relation to the relevant target volume. These plans include a plan based on an ITV (VMATitv), a plan based on the patient's maximum-inhale (VMATinh) breathing phase, and a plan based on the maximum-exhale (VMATexh) breathing phase. The VMATitv, VMATinh, and VMATexh plans were calculated independently on their associated data sets. The relevant volumes that were contoured on each of these data sets were then used to optimize the plan and report dose. In addition, a fourth VMAT plan was created, whereby the plans based on the inhale and exhale breathing phases were given a 50/50 weighting and summed together to create a summed gated plan (VMATsum). This plan was calculated using the time-weighted average data set, and the relevant dose for OARs from the VMATsum plan were reported from the contours based on the average data set.

As a separate analysis in the optimization of the summed gating technique, the inhale and exhale plans were summed with alternate weightings for the patient who showed the largest kidney motion. A 75/25 weighting was given to the exhale and inhale phases and vice versa, to assess the optimization of the summed gating plan. To simulate gating on both the inhale and the exhale phases, dose for the VMATsum plan was calculated on the time-weighted average scan. This method does not yield accurate dose information in the region of the target owing to dose inhomogeneities within, and steep dose gradients around, the PTV. As such, target doses were not reported for the VMATsum plan.

Plans were generated using the Eclipse treatment planning system (Varian Medical Systems, Palo Alto, CA) based on 6-MV photon beams for Varian Clinac iX Linear Accelerator (Varian Medical Systems, Palo Alto, CA). The modulated arcs consisted of 359°, with a clockwise (CW) rotation for the VMATexh plans and counterclockwise (CCW) for the VMATinh plans. This was done to allow for "realistic" multiple-gated arc delivery. Collimators were placed on a 45° angle for the CW and 315° angle for the CCW rotation. Arc plans were optimized using Progressive Resolution Optimizer 3 (RapidArc Varian Medical Systems, Palo Alto). Dose calculations were performed with a grid resolution of 2.5 mm using Analytical Anisotropic Algorithm, v11.03 (Varian Medical Systems, Palo Alto, CA).

Dose prescription

The prescription dose was 26 Gy in a single fraction to the covering isodose, with 99% of the PTV receiving the full prescription dose with no limit on the maximum dose within the PTV. Optimization constraints were also placed on the following OARs: subcutaneous skin, spinal cord, liver, small bowel, and stomach; organ constraints are listed in Table 2.

Table 1
Patient descriptive

Patient	Sex	Age	Location	Centroid motion (cm)
1	M	74		
Normal			Left	0.3
Deep			Left	1.6
2	M	84	Left	1.3
3	M	82	Right	0.6
4	M	43	Left	0.4
5	F	74	Right	0.3

Centroid motion is the amount of craniocaudal motion of the center of the affected kidney.

180

Table 2
Mean dose (Gy) + standard deviation for OARs and trial constraints

Plan	30 cm³ small bowel	SD (±)	Stomach	SD (±)	Skin	SD (±)	Spinal cord	SD (±)	Liver	SD (±)
Trial constraint	30 cm³ < 12.5 Gy		5 cm³ < 22.5 Gy		Max dose < 18 Gy		12 Gy point dose		700 cm³ < 15 Gy	
VMATitv	6.22	1.99	2.58	2.70	9.93	4.08	7.06	1.37	0.64	0.94
VMATinh	6.07	1.68	2.80	2.68	9.35	3.39	6.77	1.42	0.60	0.89
VMATexh	5.92	1.77	2.61	2.79	9.42	3.61	7.08	1.72	0.60	0.83
VMATsum	5.83	1.69	2.60	2.75	9.02	3.25	6.93	1.60	0.59	0.84
3DCRT	4.81	2.32	2.43	4.20	12.01	2.18	7.97	3.15	0.66	1.14

SD = standard deviation.

Dosimetric analysis

PTV minimum (PTV$_{min}$) and maximum were dose-volume metrics recorded, with PTV$_{min}$ defined as dose to 99% of the PTV and PTV maximum defined by 3% of the highest dose within the PTV. Moreover, the volume of healthy tissue receiving high dose (CI100%), intermediate dose (CI50%), and low dose (CI10%) was used to evaluate the conformity of the plan for the target volume. This technique of measuring the volume of healthy tissue receiving dose for the target volume has been reported in previous literature as a tool to score plans.[14,15]

Results

In this study, we planned treatment for 5 patients: 3 with left-sided kidney lesions and 2 with right-sided kidney lesions. Of these 5 patients, 4 were male and 1 was a female, the median age was 74 years (range: 43 to 84 years) (Table 1). The centroid motion of the affected kidney is also described, with a median craniocaudal motion of 0.8 cm (range: 0.3 to 1.6 cm) (Table 1). The median volumes for the ITV, GTVinh, and GTVexh were 25.2 cm³ (range: 7.2 to 58.5 cm³), 24.5 cm³ (range: 6.7 to 54.8 cm³), and 22.3 cm³ (range: 6.5 to 63 cm³), respectively.

Dose comparison of the gated VMAT technique against the nongated VMAT technique

Averaged cumulative dose-volume histograms are shown in Fig. 1. There was no difference in PTV$_{min}$ coverage for the VMATinh plans compared with the VMATitv plans; however, for the VMATexh plan, the minimum dose coverage was 26.8 Gy (± 1.77). In addition, there was no difference in the CI100% for all the VMAT plans; however, the mean CI50% values were 4.7 (± 0.2), 4.6 (± 0.2), and 4.7 (± 0.6) for the VMATitv, VMATinh, and VMATexh plans, respectively. The VMAT plans, based on the exhale and inhale breathing phases, showed a 4.8% and 2.4% reduction in dose to 30 cm³ of the small bowel compared with that of the ITV-based VMAT plan. Moreover, when compared with the VMATitv plans, the amount of healthy tissue receiving 100% of the prescribed dose and 50% of the prescribed dose was reduced by an average of 12% and 8% when planning VMAT on the inhale and exhale breathing phases, respectively. The integral dose to healthy tissue was reduced by 11% and 6% when compared with the VMATitv plans. Figure 2 indicates the average dose cloud volumes of healthy tissue receiving 26-, 13-, and 2.6-Gy doses.

Dose comparison of the summed gated VMAT techniques against the standard gated and the nongated techniques

The summed gated VMAT plans showed a 6.2% reduction in dose to 30 cm³ of the small bowel when compared with the VMAT plans based on the ITV. Additionally, when compared with the inhale and the exhale VMAT plans, a 4% and 1.5% reduction was observed, respectively. Likewise, the dose to skin was less, with a mean reduction of 0.9, 0.3, and 0.4 Gy when associated with the VMATitv, VMATinh, and VMATexh plans, respectively. This was observed together with a decrease in 100% of the prescribed dose to healthy tissue; it was reduced by a mean of 27%, 19%, and 23.5% when compared with the VMATitv, VMATinh, and VMATexh plans, respectively (Fig. 2).

Exploratory analysis of the time-weighted gating VMAT technique against the summed gated techniques

For patient 1 (deep), the amount of healthy tissue receiving the prescribed dose was 21.89 and 22.84 cm³ for the 75inh/25exh and the 25inh/75exh summed gated plans, respectively; this is compared with 19.33 cm³ for the 50/50 summed gated plan. Moreover, the amount of healthy tissue receiving 13-Gy dose was 200.9 and 203.26 cm³ for the 75inh/25exh and the 25inh/75exh summed gated plans. The dose received by the small bowel was 4.6 and 5 Gy for the 75inh/25exh and the 25inh/75exh summed gated plans. This is compared with 6.5-Gy for the 50/50 VMAT summed gated plan. Figure 3 shows the average maximum dose to the small bowel for each variation of the VMAT summed gated plans and the 26, 13, and 2.6 Gy dose cloud volumes.

Dose comparison of the nongated VMAT technique against forward planned 3DCRT

The mean minimum doses for the VMATitv and the 3DCRT plans were 26.8 Gy (± 0.6) and 27.8 Gy (± 0.8), respectively. The mean CI100% for the VMATitv plans was 1.2 (± 0.6 Gy) compared with 1.4 (± 0.2 Gy) for the 3DCRT plans. Furthermore, the CI50% was improved by an average of 8% for the VMAT plans compared with that of the 3DCRT plans, with mean values of 4.7 (± 0.3) and 5.1 (± 1.4), respectively. The dose to the small bowel was increased for the VMATitv plans with a mean maximum dose of 6.2 Gy (± 2.0) compared with 4.8 Gy (± 2.3), the dose to the stomach also increased for the VMATitv plans compared with the 3DCRT plans. In addition, the VMATitv plans reduced the amount of healthy tissue receiving 100% and 50% of the prescribed dose by an average of 14% and 1.5%, respectively. Alternatively, the amount of healthy tissue receiving 10% of the prescribed dose was on average 29% more for the VMATitv plans compared with the 3DCRT plans.

Discussion

The small sample size used for this study prevented any robust conclusions being made. From our institutions' experience, enrolling patients in this cohort is a slow process, as SABR is a novel modality for treatment.[4] Hence, the purpose of this study was to publish a unique technique with a unique cohort of patients, which would contribute to a wider knowledge of SABR in the context of RCC.

VMAT was chosen for the comparison of plans in different phases of the breathing cycle as it was hoped that this would introduce the least operator bias, as no beam directions must be identified. The VMAT plan also has the benefit of producing highly conformal dose distribution with an added benefit of decreased treatment times.[16] Its use in the context of SABR has been reported for early-stage lung lesions with the advantage of sparing OARs when compared with techniques such as IMRT and 3DCRT.[17,18] More specifically, for lesions in the abdomen, Wang et al.[19]
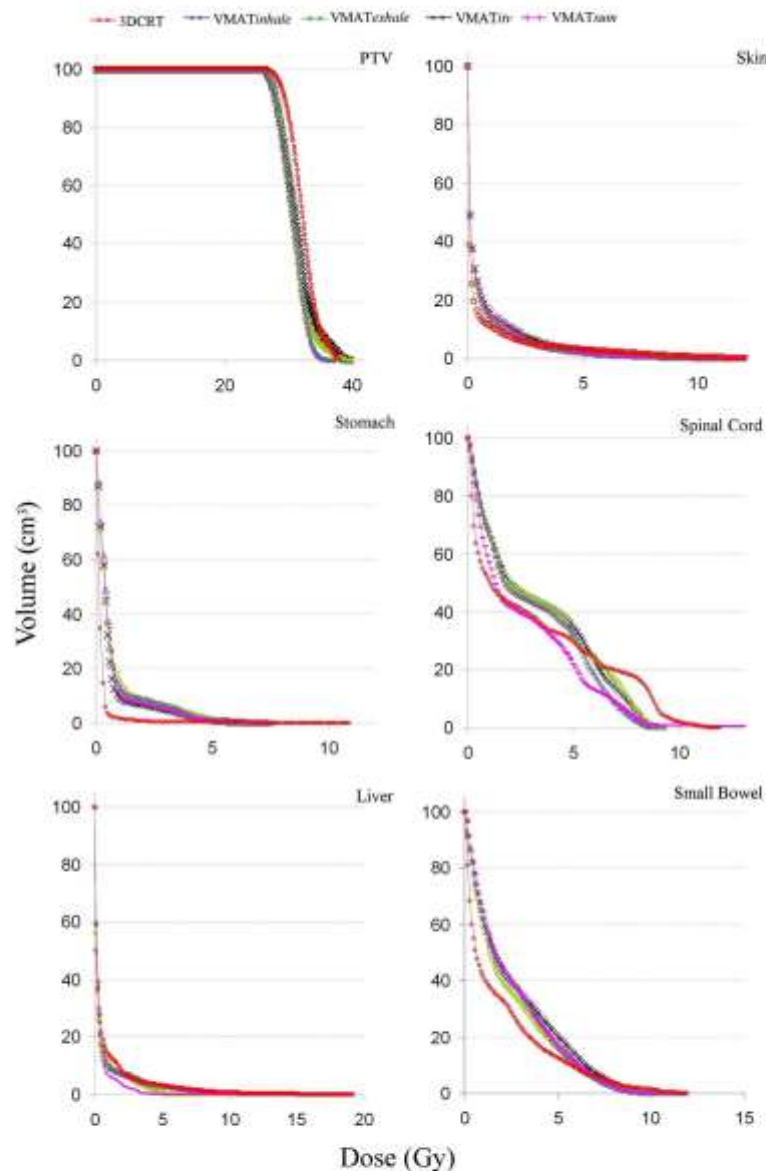
181

Fig. 1. Average cumulative dose-volume histograms for PTV and OARs. (Color version of figure is available online.)

reported superior dose conformity and OAR sparing for the VMAT plans along with IMRT plans when compared with the 3DCRT plans for gastric cancers. In this study, all the VMAT plans and the 3DCRT plans were able to achieve the minimum dose for the relevant PTVs.

Regarding dose to OAR, the dose to 30 cm³ of the small bowel was higher for the VMAT plans when compared with that of the 3DCRT plans. This seems to contradict the previously mentioned literature that suggests the VMAT plan is superior in reducing dose to OARs.[10] However, this perhaps can be because during the

optimization process, the emphasis was on 0% of this organ to receive a 12.5-Gy dose rather than limiting it to 30 cm³. This can be seen in Fig. 1, where the maximum point dose is lower for the VMAT plans for the small bowel when compared with the 3DCRT plans. Moreover, the maximum dose to the stomach, although still well below the tolerance for this OAR, was higher than that of the 3DCRT plans. Otherwise, the VMAT plan was able to reduce dose to the spinal cord and skin.

Moreover, for dose to healthy tissue, the VMATitv plans were able to reduce the amount receiving the prescribed dose and the
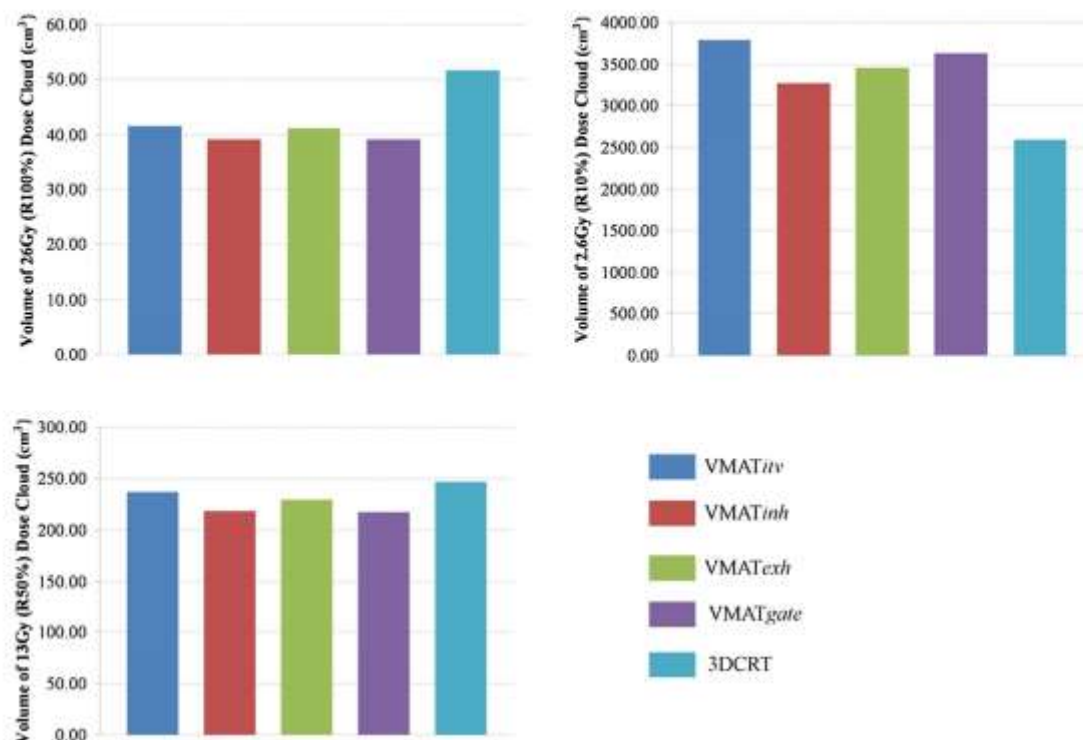
Fig. 2. Average dose clouds to healthy tissue for 100%, 50%, and 10% of the prescription dose. (Color version of figure is available online.)

intermediate dose. However, the integral dose received by healthy tissue was increased when compared with the 3DCRT plans. From the results, an increase in the integral dose delivered to healthy tissue was observed. This is in accordance with much of the previously published literature about the VMAT plans, which have shown an increase in integral dose when compared with fixed-field techniques.[30] This planning study shows no difference, and the increase in low dose received by healthy tissue is something to consider when deciding to use the VMAT plan in similar cases.[20]

A contributing factor to the volume of healthy tissue receiving dose is organ motion. Organs in the abdomen, such as the kidney and the liver, are subject to respiratory-induced motion; this has been reported in literature previously with the recommendation of motion management techniques.[9] A previous study at our institution regarding kidney motion was conducted using 71 consecutive 4D data sets; the results showed a median craniocaudal motion of 0.61 cm (range: 0.10 to 2.15 cm) and 0.69 cm (range: 0.11 to 1.92 cm) for the left and the right kidney, respectively.[21] Similarly, for the 5 patients, the median craniocaudal motion under free-breathing conditions was 0.8 cm (range: 0.3 to 1.6 cm). Regarding treatment planning, the motion caused by respiration results in additional margins being placed on the target, which consequentially increases the amount of healthy tissue receiving radiation.[22]

One such way to account for this and potentially reducing the amount of tissue receiving integral dose is gating. Gating stereotactic radiation treatment of lung lesions has been well published in literature, with results showing less healthy tissue receiving the prescribed dose, which effectively would reduce lung toxicity for patients.[23] A French study of 401 patients in 2011 reported a

significant reduction in mean lung dose due to respiratory gating and concluded that it is a viable strategy to reduce lung toxicity.[24] Similarly, the present study shows a reduction in the healthy tissue receiving the prescribed dose, which was 50% and 10% of the prescribed dose for the VMATinh plans and the VMATexh plans, respectively, when compared with the VMATitv plans. Interestingly, the volume of healthy tissue receiving the prescribed dose, 50% and 10% of the prescribed dose, was less in the VMATinh plans compared with the VMATexh plans. This reduction could be because the VMATinh plans were planned with a CCW arc compared with a CW arc for the VMATexh plans. However, other planning studies have shown that using the maximum-inhale phase of the breathing cycle further reduces dose to healthy lung tissue when compared with the exhale phase, which can be attributed to the expansion of the lung volume during the inhalation process. The same may be true here; the expansion of the abdomen during inhalation could have resulted in a reduction of integral dose.[25,26]

The true benefit of gating can be witnessed in the deep-breathing scan for patient 1, where both the inspiration and expiration plans show the healthy tissue receiving a reduction in dose. Furthermore, the small bowel, which is the main OAR of concern in these cases, is receiving less dose than that of the VMAT plan based on the ITV. In this scan, the affected kidney is shown to move 1.6 cm in the craniocaudal direction, which is concordant to previous gating planning studies that suggest that gating is of benefit when the target exhibits large amounts of motion.[26-28]

Alternatively, we have also previously demonstrated that a large amplitude of kidney motion can be observed within the BodyFIX device when treating primary kidney lesions with SABR.[28]
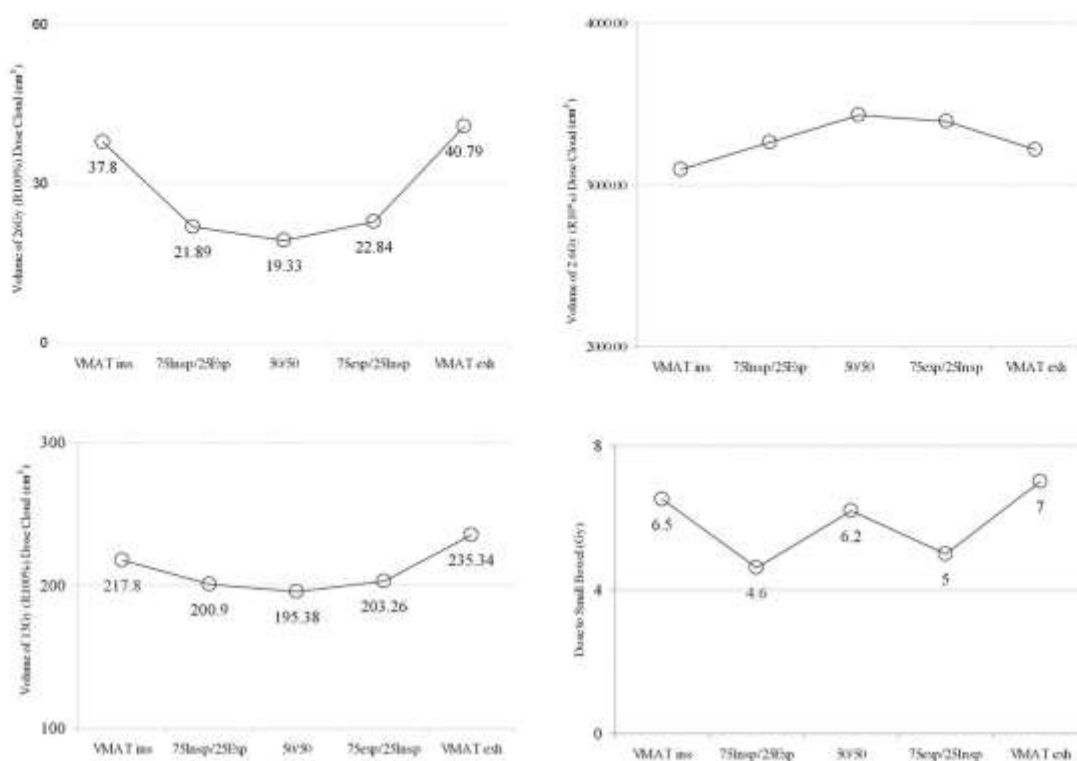
183

Fig. 3. Plan modeling showing dose to the small bowel and the amount of healthy tissue receiving 100%, 50%, and 10% of the prescription dose.

This is in contradiction to literature, including our own, that suggests vacuum immobilization reduces respiratory-induced motion and has the potential of significant potential clinical effect.[28,29] In these selected cases, consideration of gated delivery may derive a potential benefit to these patients.

However, it is unexpected for most patients to exhibit renal motion greater than a centimeter, and therefore gating may be unnecessary. A study conducted by Siva et al.[21] analyzing respiratory-induced motion to the kidney in patients not immobilized using the BodyFIX system showed a mean displacement of the kidney to be 0.7 cm. This is in concordance with the fact that this cohort of patients were simulated and treated within the BodyFIX may have confounded the results. Therefore, the combination of respiratory-motion reduction techniques and respiratory gating may only be necessary in selected patients.[28]

Moreover, when compared with the other VMAT techniques, the VMATsum plan shows an improvement for the volume of healthy tissue receiving the prescribed dose and 50% of the prescribed dose; yet, this is at the expense of the maximum dose to the small bowel. To optimize the dose to the small bowel and the amount of healthy tissue receiving the dose, the summed plan was weighted differently to determine a more favorable option. For patient 1 (deep), 2 additional plans were created, where the inspiration and expiration plans were summed with a 75% and 25% weighting and vice versa. Figure 3 shows that by adjusting the weighting of the summed VMAT plan, the maximum dose to the small bowel can be reduced and, concurrently, the amount of healthy tissue receiving the dose can be minimized. Some literature has suggested that an increase in the integral dose

throughout healthy tissue results in an increased chance of carcinogenesis.[30] Considering some patients can expect longevity should their cancer be controlled, then, minimizing radiation deposition to healthy tissue through summed gating techniques could be beneficial.

Finally, the gated VMAT plans were planned with a 10% duty cycle, which adds time to the treatment and of course negate the benefit of VMAT planning and treatment. A preclinical evaluation conducted by Nicolini et al.[13] reported the time differences for different gating conditions. The authors concluded that a 15-Gy fraction with short duty cycles and 45 beam interruptions, where the target moves outside the "gate" and the beam is switched off, results in a treatment delivery time of 7 to 8 minutes. This cohort of patients were planned for receiving a 26-Gy dose in a single fraction with a 10% duty cycle; therefore, this would result in a large number of beam interruptions and hence a significantly longer treatment time. Niccolini et al.[13] recommended keeping interruptions below 20 per arc to reduce treatment times, as it has been shown that increasing treatment times results in a greater chance of intrafraction motion. Therefore, the benefits of VMAT gating must be weighed up with the amount of time required to deliver the treatment and a potential reduction in accuracy.

It should also be noted that calculating dose for the VMATsum plan on the average-intensity projection gives a simplistic estimate of the accumulated dose resulting from gating on both the maximum-inhale and the maximum-exhale breathing phases. Although the dose summation reflects doses to static structures correctly, the dose to moveable and deformable structures has to be interpreted with caution. To more accurately estimate the

accumulated dose distribution, time-dependent geometric changes in patient anatomy must be explicitly accounted for. This may be achieved via quasi-4D dose accumulation calculations based on deformable image registration. However, that is outside the scope of this work and is the basis of a forthcoming study.

Conclusions

The results of this study indicate that planning VMAT to a single phase of a patient's breathing cycle can reduce the volume of the prescribed dose and the intermediate dose received by healthy tissue. The biggest advantages are seen when the tumor is highly mobile; in this case, it may be of benefit to combine exhale- and inhale-based VMAT plans into a combined plan that optimizes dose to healthy tissue. The results from the summation of gated VMAT plans in this study need to be interpreted with caution, and a further study involving deformable image registration should be conducted. Finally, the dosimetric benefits gained by gating VMAT plans must be balanced against the time it takes to deliver. More investigations need to be carried out to determine the benefit of gated VMAT planning in the context of SABR, in particular its ability to reduce toxicity to the affected kidney.

References

1. Svedman, C.; Karlsson, K.; Rutkowska, E.; et al. Stereotactic body radiotherapy of primary and metastatic renal lesions for patients with only one functioning kidney. Acta Oncol. 47(8):1578–83; 2008.
2. Teh, B.; Bloch, C.; Galli-Guevara, M.; et al. The treatment of primary and metastatic renal cell carcinoma (RCC) with image-guided stereotactic body radiation therapy (SBRT). Biomed. Imaging Interv. J. 3(1):e6; 2007.
3. Van Poppel, H.; Becker, F.; Cadeddu, J.A.; et al. Treatment of localised renal cell carcinoma. Eur. Urol. 60(4):662–72; 2011.
4. Siva, S.; Pham, D.; Gill, S.; et al. A systematic review of stereotactic radiotherapy ablation for primary renal cell carcinoma. BJU Int. 110(11):E737–43; 2012.
5. Siva, S.; MacManus, M.; Ball, D. Stereotactic radiotherapy for pulmonary oligometastases: a systematic review. J. Thorac. Oncol. 5(7):1091–9, http://dx.doi.org/10.1097/JTO.0b013e3181de7143.
6. Webb, S. Intensity-modulated radiation therapy (IMRT): a clinical reality for cancer treatment, "any fool can understand this". Br. J. Radiol. 78(special_-issue_2):564–72; 2005.
7. Otto, K. Volumetric modulated arc therapy: IMRT in a single gantry arc. Med. Phys. 35(1):310–7; 2007.
8. Pham, D.; Kron, T.; Foroudi, F.; et al. A review of kidney motion under free, deep and forced-shallow breathing conditions: implications for stereotactic ablative body radiotherapy treatment. Technol. Cancer Res. Treat. 13(4):315–23; 2014.
9. Keall, P.J.; Mageras, G.S.; Balter, J.M.; et al. The management of respiratory motion in radiation oncology report of AAPM Task Group 76a. Med. Phys. 33(10):3874–900; 2006.
10. Benedict, S.H.; Yenice, K.M.; Followill, D.; et al. Stereotactic body radiation therapy: the report of AAPM Task Group 101. Med. Phys. 37(8):4078; 2010.
11. Morgan-Fletcher, S. ICRU Report 62. Prescribing, recording, and reporting photon beam therapy (Supplement to ICRU Report 50). Br. J. Radiol. 74 (879):294; 2001.
12. Gabrys, D.; Kulik, R.; Trela, K.; et al. Dosimetric comparison of liver tumour radiotherapy in all respiratory phases and in one phase using 4DCT. Radiother. Oncol. 100(3):360–4; 2011.
13. Nicolini, G.; Vanetti, E.; Clivio, A.; et al. Pre-clinical evaluation of respiratory-gated delivery of volumetric modulated arc therapy with RapidArc. Phys. Med. Biol. 55(12):N347; 2010.
14. Feuvret, L.; Noël, G.; Mazeron, J.-J.; et al. Conformity index: a review. Int. J. Radiat. Oncol. Biol. Phys. 64(2):333–42; 2006.
15. Paddick, I. A simple scoring ratio to index the conformity of radiosurgical treatment plans. J. Neurosurg. 93(suppl. 3):219–22; 2000.
16. Teoh, M.; Clark, C.H.; Wood, K.; et al. Volumetric modulated arc therapy: a review of current literature and clinical use in practice. Br. J. Radiol. 84 (1007):967–96; 2011.
17. Vladimir, Valakh; Philip, Chan; D'Adamo, K.; et al. Early-stage central lung cancer and volumetric modulated arc therapy: a dosimetric case study with literature review. Anticancer Res. 33:4493–6; 2013.
18. McGrath, S.D.; Matuszak, M.M.; Yan, D.; et al. Volumetric modulated arc therapy for delivery of hypofractionated stereotactic lung radiotherapy: a dosimetric and treatment efficiency analysis. Radiother. Oncol. 95(2):153–7; 2010.
19. Wang, X.; Li, G.; Zhang, Y.; et al. Single-arc volumetric-modulated arc therapy (sVMAT) as adjuvant treatment for gastric cancer: dosimetric comparisons with three-dimensional conformal radiotherapy (3D-CRT) and intensity-modulated radiotherapy (IMRT). Med. Dosim. 38(4):395–400; 2013.
20. Kumar, R.; Wild, A.T.; Ziegler, M.A.; et al. Stereotactic body radiation therapy planning with duodenal sparing using volumetric-modulated arc therapy vs intensity-modulated radiation therapy in locally advanced pancreatic cancer: a dosimetric analysis. Med. Dosim. 38(3):243–50; 2013.
21. Siva, S.; Pham, D.; Gill, S.; et al. An analysis of respiratory induced kidney motion on four-dimensional computed tomography and its implications for stereotactic kidney radiotherapy. Radiat. Oncol. 8(1):248; 2013.
22. Guckenberger, M.; Kavanagh, A.; Webb, S.; et al. A novel respiratory motion compensation strategy combining gated beam delivery and mean target position concept—a compromise between small safety margins and long duty cycles. Radiother. Oncol. 98(3):317–22; 2011.
23. Xi, M.; Zhang, L.; Liu, M.Z.; et al. Dosimetric analysis of respiratory-gated radiotherapy for hepatocellular carcinoma. Med. Dosim. 36(2):213–8; 2011.
24. Giraud, P.; Morvan, E.; Claude, L.; et al. Respiratory gating techniques for optimization of lung cancer radiotherapy. J. Thorac. Oncol. 6(12):2058–68, http://dx.doi.org/10.1097/JTO.0b013e3182307ec2.
25. Biancia, C.D.; Yorke, E.; Chui, C.-S.; et al. Comparison of end normal inspiration and expiration for gated intensity modulated radiation therapy (IMRT) of lung cancer. Radiother. Oncol. 75(2):149–56; 2005.
26. Saito, T.; Sakamoto, T.; Oya, N. Comparison of gating around end-expiration and end-inspiration in radiotherapy for lung cancer. Radiother. Oncol. 93(3):430–5; 2009.
27. Starkschall, G.; Forster, K.M.; Kitamura, K.; et al. Correlation of gross tumor volume excursion with potential benefits of respiratory gating. Int. J. Radiat. Oncol. Biol. Phys. 60(4):1291–7; 2004.
28. Pham, D.; Kron, T.; Foroudi, F.; et al. Effect of different breathing patterns in the same patient on stereotactic ablative body radiotherapy dosimetry for primary renal cell carcinoma: a case study. Med. Dosim. 38(3):304–8; 2013.
29. Siva, S.; Devereux, T.; Kron, T.; et al. Vacuum immobilisation reduces tumour excursion and minimises intrafraction error in a cohort study of stereotactic ablative body radiotherapy for pulmonary metastases. J. Med. Imaging Radiat. Oncol. 58(2):244–52; 2014.

9.5 Impact of stereotactic radiotherapy on kidney function in primary renal cell carcinoma: Establishing a dose–response relationship

Contents lists available at ScienceDirect

Radiotherapy and Oncology

Renal SBRT

Impact of stereotactic radiotherapy on kidney function in primary renal cell carcinoma: Establishing a dose–response relationship

Shankar Siva [a,b,*], Price Jackson [a], Tomas Kron [a,b], Mathias Bressel [c], Eddie Lau [a,b,d], Michael Hofman [a,b], Mark Shaw [a], Sarat Chander [a], Daniel Pham [a], Nathan Lawrentschuk [e], Lih-Ming Wong [f], Jeremy Goad [e], Farshad Foroudi [a]

[a] Division of Radiation Oncology and Cancer Imaging, Peter MacCallum Cancer Centre; [b] Sir Peter MacCallum Department of Oncology, University of Melbourne; [c] Department of Biostatistics and Clinical Trials, Peter MacCallum Cancer Centre; [d] Department of Radiology, University of Melbourne; [e] Division of Cancer Surgery, Peter MacCallum Cancer Centre; and [f] Department of Surgery, University of Melbourne, Australia

ARTICLE INFO

ABSTRACT

Background and purpose: To evaluate renal dysfunction after stereotactic ablative body radiotherapy (SABR) for inoperable primary renal cell carcinoma (RCC) using nuclear medicine assessments.
Materials and methods: In a prospective clinical trial, patients received single fraction renal SABR (26 Gy) for tumours <5 cm, or fractionated SABR (3 × 14 Gy) for tumours >5 cm. Global and regional glomerular filtration rate (GFR) was calculated through ^{51}Cr-EDTA and ^{99m}Tc-DMSA SPECT/CT, respectively, at baseline and post-treatment (14, 90 days and at 1-year). Regional loss in function was correlated to the absolute and biologically effective doses (BED) delivered.
Results: In 21 patients the mean (range) tumour size was 48 mm (21–75 mm). The mean ± SD GFR at baseline was 52 ± 24 ml/min. Net change in mean GFR was +0.6 ± 11.3, +3.2 ± 14.5 and −8.7 ± 13.4 ml/min ($p = 0.03$) at 2 weeks, 3 months and 1 year, respectively. For every 10 Gy of physical dose delivered, an exponential decline in affected kidney GFR was observed at 39% for 26 Gy/1 fraction and 25% for 42 Gy/3 fractions. When normalised to BED$_{3Gy}$, the dose–response relationship for each treatment prescription was similar with a plateau beyond 100 Gy. The R50% conformity index correlated with GFR loss ($p = 0.04$). No patient required dialysis.
Conclusions: SABR results in clinically acceptable and dose-dependent renal dysfunction at 1-year. Sparing functional kidney from high-dose regions (>50% isodoses) may help reduce risk of functional loss.
© 2016 Elsevier Ireland Ltd. All rights reserved. Radiotherapy and Oncology 118 (2016) 540–546

The standard of care for fit patients with localised kidney cancer is surgical resection. This may involve removing either the tumour (partial nephrectomy) or the entire kidney and surrounding tissues (i.e. radical nephrectomy). Renal cell carcinoma (RCC) predominantly affects the older population with a median age at diagnosis of 65 years [1]. However, in this patient population, a proportion of patients are not able to tolerate surgery due to medical co-morbidities. Additionally, patients undergoing partial or radical nephrectomy for renal cancer experience post-operative nephron loss. This may result in *de novo* chronic kidney disease or decline of pre-existing renal dysfunction [2–6], which in turn may result in significantly increased risk of mortality [7].

In light of these factors several alternatives are available for those patients who are not suitable for extirpative therapies.

Radiofrequency ablation (RFA) involves either percutaneous or intra-operative insertion of electrodes to affect thermal ablation of the renal mass [8]. Cryoablation typically delivered via a laparoscopic approach, involves supercooled liquid introduced in order to create an iceball that results in ablation of the mass. The use of RFA is limited to treating smaller renal masses (<4 cm) as well as those away from the ureter and renal pelvis due to the risk of heat sink effects, stricture and/or fistula developing [9]. Both of these techniques are invasive and may have issues that arise where patients are on anticoagulation or where an ability to remain still and/or undergo anaesthesia for these options may not be possible.

Stereotactic Ablative Body Radiotherapy (SABR) is an emerging alternative treatment option for patients with inoperable primary RCC. It is non-invasive, does not necessitate hospital admission, and is typically associated with low toxicity rates and excellent local control rates in the context of both primary [10] and metastatic RCC [11–13]. SABR may have comparable local effectiveness to RFA or cryotherapy, with a systematic review of available data

* Corresponding author at: Peter MacCallum Cancer Centre, Locked Bag 1 A'Beckett Street, Parkville 8006, Australia.
E-mail address: shankar.siva@petermac.org (S. Siva).

reporting local progression rates of 6.1% [10]. Unlike RFA or cryotherapy, SABR does not have specific limitations relating to tumour size or position relative to pelvic calyceal structures. One drawback is that tumour biopsy confirmation has not been mandated in past series. Modern reports since the systematic review indicate very infrequent severe treatment related toxicities using both single and multi-fraction approaches [14,15]. As yet it is not completely understood what the relationship is between kidney function loss and SABR dose delivered. A preliminary report of patients with a solitary functioning kidney suggested minimal clinically significant impact to renal function after SABR, with five of seven patients with a solitary kidney reporting no change in renal function [16]. No patient required intervention with renal replacement therapy. A more recent case report used split function nuclear medicine assessments to demonstrate SABR induced renal cortical perfusion loss in a patient treated with single fraction SABR to a solitary kidney. Again in this case, there was no need for dialysis or medical intervention due to the associated renal dysfunction [17].

The purpose of this translational substudy is to prospectively evaluate radiation induced renal impairment in patients receiving SABR for primary RCC. In particular, we hypothesised that radiation-induced renal dysfunction is dose-dependent and that the effects of ablative doses of radiation can be modelled in this patient cohort. By evaluating the dose–response relationship of SABR to the kidney we aim to be able to inform clinical decision-making into the impact of a proposed treatment plan in patients receiving SABR for primary RCC.

Materials and methods

Patients

The study received institutional ethical review board approval and was conducted as a translational substudy of a registered prospective clinical trial (clinicaltrials.gov identifier: NCT01676428). Eligible patients were medically inoperable, technically high risk for surgery or declined surgery, with an ECOG performance status of 0–2 inclusive. Patients with previous high-dose radiotherapy to the upper abdomen were excluded from the study. Patients underwent serial renal function assessments through serum biochemistry (global assessment) and nuclear medicine scintigraphy (regional assessment) before and after SABR.

Radiotherapy treatment details

Patients with tumours of ≤5 cm received a single fraction of 26 Gy, whilst patients with tumours >5 cm received 42 Gy in 3 fractions. As human RCC cell lines have been observed to have α/β values estimated to be 2.6 Gy or 6.9 Gy depending on the cell line (55) the two fractionation schedules were designed to be relatively isoeffective – at an α/β of 6.9 Gy, 26 Gy/1 = 123 Gy and 42 Gy/3 = 127 Gy, whilst at an α/β of 2.6 Gy, 26 Gy/1 = 286 Gy and 42 Gy/3 = 268 Gy. All patients underwent a 4D CT scan on a Brilliance 16 slice CT scanner (Philips Andover Mass) using the Philips bellows to reconstruct the data into 3 mm slices that were binned into 10 phases of breathing. Patients were setup supine in a dual vacuum stabilisation system (BodyFIX™, Elekta, Stockholm). An average pressure of 72 mbar (50–100) was used to immobilise patients using both the thoracic and pelvic setup. The averaged CT dataset was reconstructed into a 3 mm slice dataset that was imported into Eclipse (v11.03) for contouring and dose calculation. The maximum inspiration and expiration datasets were used to define the internal target volume (ITV) with a 5 mm planning target volume (PTV) margin applied to the ITV.

All patients were planned on an Eclipse v11.030 (Varian, Palo Alto) workstation using the analytical anisotropic algorithm (AAA; v 11.03) for the final dose calculation.

SPECT imaging & glomerular filtration rate

In 21 patients, ^{99m}Tc-DMSA SPECT/CT images (200 MBq injected activity) and GFR by ^{51}Cr-EDTA plasma clearance were recorded concurrently at baseline (1 month pre-treatment), and at 2-weeks, 3-months and when available approximately 1-year post-treatment (median 11.8 months). Two patients were excluded from regional dose–response analysis based on inconsistencies in their baseline GFR measure with corresponding eGFR and post-treatment renal function data (likely due to poor hydration or diuretic intake at the time of Cr-51 EDTA sampling/administration). In one patient onset of renal vein thrombus with subsequent total kidney dysfunction occurred prior to the three-month and one-year assessments. Two patients died between three-month and one-year of follow up. The final long-term follow up cohort with available datasets therefore consisted of fifteen patients (8 single-fraction, 7 three-fraction).

Individual kidney function was calculated from baseline and follow-up ^{51}Cr-EDTA which measures global function and then scaled according to DMSA SPECT-derived split function. This enabled examination of radiation-induced function deficit confined solely to the irradiated kidney and evaluation of compensatory effect in the contralateral kidney. Regional renal function was quantified based on measured GFR and proportion of total DMSA uptake using the integrated counts for a volume-of-interest comprising the kidneys on SPECT imaging. Each voxel's contribution to total renal function [GFR: (ml/min) per ml tissue] was then calculated based on the derived scaling factor. The low dose CT component of the SPECT/CT images were co-registered to the pre-therapy planning CT and dose prescription image sets. Fused SPECT/CTs were aligned by deformable registration of anatomical (CT) volumes with the MIM software package (version 6.1, MIM Software Inc, Cleveland OH, USA). Radiotherapy treatment planning structures were utilised for segmentation of healthy renal tissue [Kidney minus Internal Target Volume (ITV)] [18]. Healthy renal tissue was then divided based on radiation isodose zone in 2 Gy increments. Quantified dose regions were compared between baseline and follow-up scans in order to calculate change in local renal function according to prescribed isodose zone from treatment planning. A pictorial representation of the workflow is depicted in Fig. 1.

Dose–response was determined per patient as the percent loss in function relative to the baseline scan for each isodose region within the affected kidney. To generate a curve of mean dose–response based on all patient data, each point was weighted for the volume enclosed in a patient's relative isodose bin. Tissue response was evaluated based on physical dose (Gy) and Biological Effective Dose (BED) for an α/β value of 3 Gy. BED was used for evaluating similarity of tissue response between fractionation regimes. Linear and exponential regression curves were fit to the physical dose and BED response data, respectively. Based on the common use of the 50% isodose (R50%) as plan quality parameter [19,20] and a previously observed case of renal dysfunction in regions above the 50% isodose threshold [17], the correlation of regional change in GFR with the volume receiving 50% of dose was assessed using Pearson statistic. Comparison of GFR loss between treated and non-irradiated kidney was evaluated by paired t-test. One patient had a solitary kidney due to previous contralateral nephrectomy and therefore was analysed for affected kidney dose–response effects only. Creatinine change over time was modelled using linear mixed models with patients included as random effect.
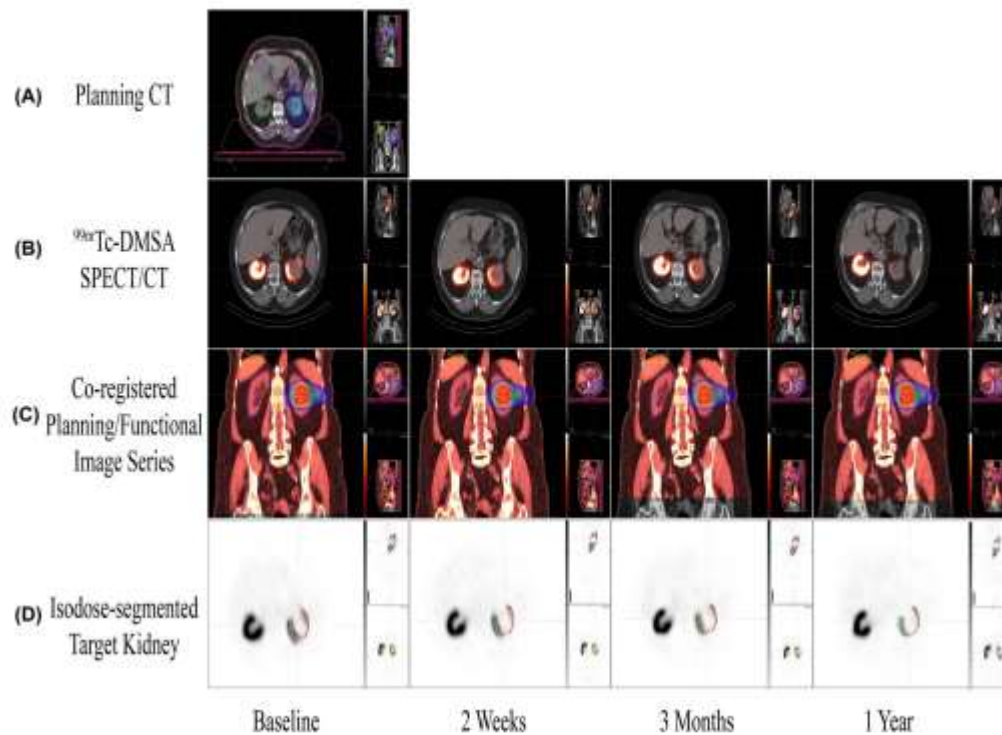
Fig. 1. Workflow of dose–response analysis methodology – (A) Planning CT scan with organ structures and isodose distributions (B) Hybrid SPECT/CT DMSA images across serial timepoints (C) Co-registered planning CT with SPECT/CT DMSA images (D) DMSA tracer activity segmented by isodose regions encompassing the treated kidney.

Serum creatinine assessments

The biochemical effect of treatment on global renal function (as determined by serum creatinine) was compared by modelling the trajectory of function change pre-treatment to the post-SABR rate of function change. Patients had all available serum creatinine assessments recorded 12 months prior to treatment and subsequently on post-treatment assessments at 3-monthly intervals. Change in serum creatinine from immediately pre-treatment to 1-year post-treatment was compared using a paired t-test. To assess whether the rate of global renal function loss was affected by treatment delivery, a piecewise linear mixed model was used to assess the change in slope with patients as a random effect, time from RT as a fixed effect and the maximum between time and zero (i.e. the time post RT representing change in slope) as a fixed effect.

Results

Study population

In total, 21 patients were included in this study, with a median follow-up of 1.1 years. Pre-treatment patient characteristics can be found in Table 1. This was a patient population with significant comorbidities and pre-existing renal dysfunction with a median Charlson comorbidity score of 9 (range 3–12), mean ± standard deviation (SD) serum creatinine of 131 ± 28 μmol/L and calculated GFR of 52 ± 24 ml/min. Nine of the patients were referred for the clinical trial due to the perceived high risk of post-operative dialysis. One patient was treated with a solitary kidney in the context of previous nephrectomy.

Table 1
Patient characteristics (n = 21).

Characteristic	Value
Age (y), median (range)	77 (41–91)
Site	
Left Kidney	10
Right Kidney	11
Sex	
Male	14
Female	7
Tumour size (mm), mean (range)	48 (21–75)
Dose prescription	
42 Gy in 3 fractions	10
26 Gy in 1 fraction	11
T stage	
1a	6
1b	14
3	1
ECOG performance status	
0	12
1	5
2	4
Charlson Co-morbidity Score, median (range)	9, (3–12)
Reason for referral	
Medically inoperable	9
Need for post-op dialysis	9
Declined surgery	3
Mean dose (±sd) to kidney by prescription	
42 Gy in 3 fractions	10.0 ± 3.4 Gy
26 Gy in 1 fraction	24.8 ± 7.5 Gy

188

Effect of SABR on renal function

No appreciable global renal function change was observed using ^{51}Cr-EDTA calculated GFR at 2 weeks or 3 months post-SABR. The mean GFR ± SD was 52 ± 24 ml/min at baseline. There was a net change in measured mean GFR at 2 weeks of +0.6 ± 11.3 ml/min and at 3 months + 3.2 ± 14.5 ml/min. In the subset of patients with further delayed imaging, ~1 year, there was a mean change in renal filtration rate of −8.7 ± 13.4 ml/min ($p = 0.03$). Split renal function in the irradiated kidney declined from a median 53.9% at baseline to 51.8%, 51.5%, and 43.9% (all p-values < 0.01) at two weeks, 3 months, and one year, respectively. In the contralateral non-irradiated kidney, localised GFR increased by a mean of of 12.3 ± 25.3% ml/min from baseline ($p < 0.01$). Change in kidney GFR was significantly different between irradiated and non-irradiated organs ($p < 0.01$). Fig. 2 demonstrates a waterfall plot of change in GFR in the treated and contralateral kidney at a per-patient level. Despite deliberate avoidance of beam entry points traversing the contralateral kidney (when patients had two kidneys in situ), 35.7% (5/14) of contralateral kidneys demonstrated loss of renal function at 1-year, indicative of decline independent of radiation in the context of pre-existing nephropathy. The remaining 64.2% (9/14) of contralateral kidneys demonstrated relative gain in function post-irradiation at 1-year.

Regional effects of irradiation

Regional effects of irradiation in the normal kidney were associated with dose delivered. A representative example of dose–response relationship for a typical patient is shown in Fig. 3. No appreciable local radiation damage is apparent at 2-weeks or 3-months. The patient displays a common pattern of late-onset regional nephropathy where a local DMSA perfusion deficit is clearly evident only in the high-dose regions of renal tissue. At the 1-year late time-point, quantitative assessment indicates that renal perfusion remains stable from baseline for regions receiving less than 10 Gy in a single fraction. Based on volume-weighted tissue response in each dose zone, an apparent exponential decline in regional function was observed with escalating physical radiation dose (Fig. 4). In single-fraction treatment, dose–response to normal kidney follows approximately an exponential decline with respect to percentage of local baseline function; losing an additional 39%

function within the irradiated region for each increasing 10 Gy of physical dose. In three fractions, a similar shape was observed, however losing 25% per 10 Gy of increased total physical dose. Reduction in GFR in the late follow-up cohort demonstrated linear correlation with the R50% volume ($r^2 = 0.29$, $p = 0.04$). Normalising the two treatment arms according to BED using an α/β ratio of 3 demonstrated an exponential shape for preserved DMSA perfusion with a dose dependent region (0–100 Gy$_{BED}$) followed by an approximate plateau above 100 Gy$_{BED}$. This is described by the equation:

$$GFR = a * e^{-b*BED} + c$$

where GFR is the preserved local contribution to glomerular filtration rate according to DMSA SPECT imaging and a & b are the coefficients for the bi-exponential decline in local tracer uptake according to radiation dose and c is a parameter to describe residual perfusion to high dose regions (>100 Gy$_{BED}$).

Global effects of Irradiation

No patient required renal replacement therapy during the study period. The mean serum creatinine was worse 1-year post SBRT at 162 umol/L as compared to the baseline level of 131 μmol/L ($p = 0.02$). The average change in creatinine within 12 months before treatment was −0.59 ± 0.43 μmol/L/month ($p = 0.176$) indicating that there was no significant change in creatinine, on average, in the 12 months preceding treatment. For the 12-month period after treatment, the slope of change in creatinine increased by 3.85 ± 0.74 μmol/L/month ($p < 0.01$) resulting on a rate of change in creatinine post SABR treatment of 3.26 μmol/L/month ($p < 0.01$), Supplementary Fig.

Discussion

In this study we describe a dose-dependent relationship with regional kidney dysfunction secondary to radiation nephritis. Nephron sparing was observed at two weeks and three months after SABR, but late regional loss in function was observed at 1-year post treatment. We observed regional kidney dysfunction to be exponentially associated with physical delivered dose. Importantly, when normalising to BED using an α/β value of 3, both
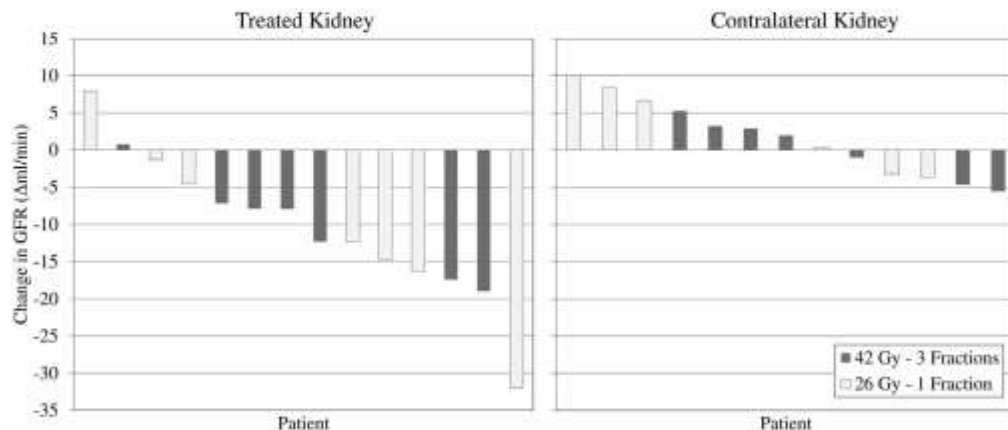

Fig. 2. Waterfall plots of change in renal function for irradiated and contralateral kidneys as assessed at 1-year depicted at an individual per kidney level. Isolated GFR values are determined based on ^{51}Cr–EDTA clearance and ^{99m}Tc-DMSA SPECT split function. A pronounced deficit is evident in the treated kidney. There is no visually apparent distinction between treatment arms (26 Gy/1 or 42 Gy/3).
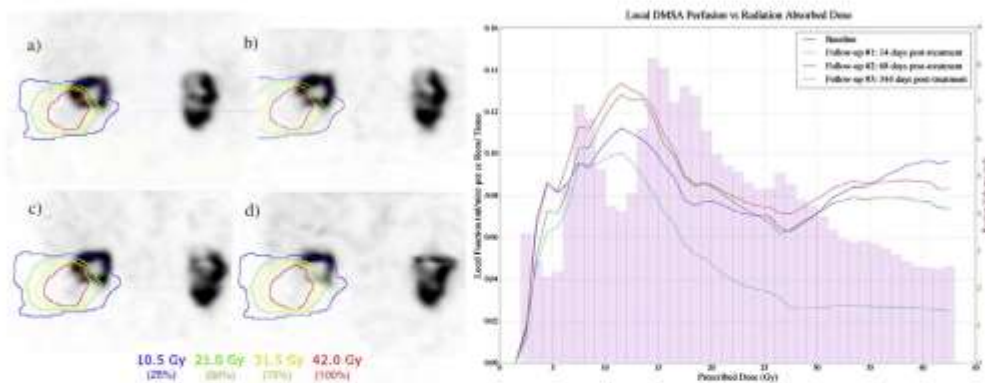
189

Fig. 3. Coronal view of DMSA SPECT of the right kidney for patient receiving 42 Gy in 3 fraction for a 6 cm lesion to the inferior pole. Scans at (a) baseline, (b) 2 weeks, (c), 3 months, (d), and 1 year are presented along with a plot of renal function to each isodose bin as determined on functional imaging. Temporal image assessment of this patient indicates that the severity of renal function deficit in the high dose zone increases with increasing radiation dose and does not present until after three months post-treatment. Renal perfusion is largely preserved in regions receiving less than 10 Gy.
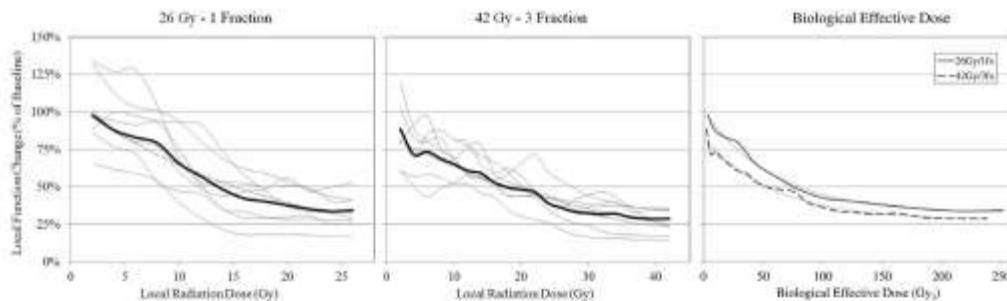

Fig. 4. Local radiation dose–response curves for 26 Gy/1 and 42/3 Gy treatment cohorts based on late imaging DMSA SPECT imaging assessment. Per-patient curves are shown in grey plotted for percentage of baseline function in local dose bin. Mean cohort response for single fraction (black) and multi-fraction (dash) are presented, normalised by BED. In both treatment groups, dose–response appears as an exponential decline.

single and multi-fraction SABR displayed similar dose–response relationships. According to a report by the National Kidney Foundation, the ideal assessment of kidney toxicity is GFR [21]. Overall in this patient cohort which included some patients with pre-existing kidney disease, we found a statistically significant change in mean global calculated GFR of -9.1 ml/min from a baseline of 54 ml/min ($p = 0.03$), with a decrease in split function of the irradiated kidney by 10.0% at 1 year. Importantly, no renal replacement therapies were required in this patient cohort, despite pre-existing kidney disease.

Presently, our understanding of the pathophysiology of radiation induced nephropathy and relationship with delivered radiotherapy dose is incomplete. A recent report from Quantitative Analyses of Normal Tissue Effects in the Clinic (QUANTEC) group did not recommend any specific constraints for dose to the kidney in the context of SABR [22]. In this report, Dawson et al. suggested that "one hypothesis [is] that nearly complete sparing of a substantial volume of normal kidney is associated with preservation of renal function". However, asymptomatic deteriorations in renal function without the need for medical or dialysis interventions have been noted after SABR by both Svedman et al. [16] and Teh et al. [23]. We also observed a loss of renal function secondary to SABR concordant with these reports. In the context of conventionally fractionated

radiotherapy, Kost et al. [24] used sequential scintigraphy patients receiving abdominal RT to demonstrate a dose–response relationship, with the effective dose to result in 5% loss of function ranging between 3 Gy and 6 Gy. More recently, May et al. [25] showed that in those patients receiving conventionally fractionated chemoradiation to the abdomen that split renal function decreased from 49.8% pre-radiation to 41.3% >12 months post-radiation ($p = 0.02$). We found a similar (if slightly larger) magnitude of decline in our cohort in which the split renal function of the kidney directly irradiated fell from 54.5% at baseline to 43.9% ($p < 0.01$). The cohort described by May et al. [25] had normal kidney function, and observed a decline in creatinine clearance from 90.67 ml/min pre-radiation to 82.23 ml/min and 74.54 ml/min at 6–12 months and >12 months post-radiation ($p < 0.01$). The percentage volume of irradiated kidney in that goup receiving $\geqslant 25$ Gy and 40 Gy were significantly associated with $\geqslant 5\%$ decrease in relative renal function ($p = 0.039$ and $p = 0.044$ respectively).

Our study demonstrates dose dependent deterioration of kidney function in the irradiated kidneys of those patients receiving SABR, with a loss of 25–39% of activity observed on SPECT for every 10 Gy of physical delivered dose (depending on the dose/fractionation schedule). Qualitatively there was evidence of residual DMSA uptake even to regions of kidney receiving ablative doses. This

model best accounts for the observed tracer perfusion in these regions. It is not clear whether DMSA retention in high-dose areas is related to true cell viability or a structural effect from the remaining vascular structures. When biologically normalised using an α/β ratio of 3, both single and multi-fraction SABR had a similar dose–response relationship, described as bi-exponential, or a two-phase decline and approximate plateau above 100 Gy BED (Fig. 4). The 42 Gy in 3 fraction cohort is downwardly shifted in amplitude across the range of measured dose values, which is possibly attributed to physiological factors relating to larger tumour size in this patient group. Our present findings are derived using a free-breathing technique and treatment delivered using an ITV concept. Thus, the observed dose–response relationship may be slightly different in the context of tumour tracked or respiratory-gated delivery. A prospective clinical trial [26] is underway evaluating the effect of conventionally fractionated radiotherapy to the upper abdomen on nephron dysfunction. The results of this study, when available, will further inform our understanding of the dose–response relationship of radiotherapy and nephron loss.

Nephron loss and renal dysfunction secondary to extirpation and other ablative techniques have been previously quantified. In a randomised study comparing elective nephron-sparing surgery and radical nephrectomy, the mean loss of eGFR was 16.6 ml/min for partial nephrectomy, and 23.5 ml/min after radical nephrectomy [27,28]. In a series spanning 1997–2009 at the Clevelend Clinic, patients with pre-existing chronic kidney disease (defined as an eGFR < 60 ml/min) the annual decline in eGFR was 4.7% after surgical resection [5]. Nephrectomy in these patients resulted in a mean ± SD eGFR of 37 ± 11 ml/min. Studies evaluating renal dysfunction after RFA or cryotherapy in patients with pre-existing chronic kidney disease are limited. Meaningful comparisons are particularly challenging, as resultant renal dysfunction is proportional to tumour size and volume of ablation zones [29]. Most series report outcomes from only small renal masses of typical average sizes ranging 2–3 cm in diameter, whereas the mean size in our cohort was 4.8 cm. In one study 16 patients with a solitary functioning kidney were treated with a decrease in the mean GFR from 54.2 ml/min per minute pre-ablation to 47.5 ml/min at a mean F/U of 30.7 months [30]. By comparison to both surgical and RFA series, in our cohort we observed a decrease from pre-treatment to post-treatment calculated GFR of 52 ml/min to 43 ml/min. However, selection of patients for these various treatments differs widely in both patient and tumour characteristics and hence comparisons post treatment renal dysfunction are purely hypothesis generating. Whilst loss in renal function appeared to qualitatively plateau at 1-year in this series, further late assessments are warranted.

There are several limitations of our study to acknowledge. We considered our methodology to provide an accurate measure of regional renal function by integrating ^{51}Cr-EDTA GFR and DMSA SPECT/CT results as compared to scaling by activity- and body weight-scaled counts per voxel or against a reference in the non-irradiated kidney. Although ^{51}Cr-EDTA measures of renal function remain the clinical standard, they are susceptible to daily variation due to patient hydration and other physiological factors. That influences the calculated SPECT scaling factor, but should not affect estimations of *regional* function change, that is relative nephrotoxicity in high- and low-dose zones. Based on our experience, it may be helpful to utilise quantitative SPECT imaging (ie calibrated for measurement of voxel intensity in activity of ^{99m}Tc in Bq/ml) as another technique for comparison. Additionally, localised dose assessment is limited by the resolving power of SPECT imaging, which is approximately at 10 mm resolution. In the case of SABR where steep dose gradients are expected in surrounding normal kidney, a technique with higher spatial resolution should be evaluated. One such technique recently proposed for GFR assessment is ^{68}Ga-EDTA PET/CT, which also allows fully quantitative assessment

of tracer activity [31]. Despite these limitations, the authors are confident that conclusions drawn regarding regional radiation dose–response and the timeline for nephrotoxicity are representative of the physiological processes investigated.

Our findings suggest that techniques to improve overall treatment precision may be worthwhile in reducing functional loss. This is due to the relationship between high-dose regions delivered and renal dysfunction. Importantly, this data may help inform estimations of kidney function loss secondary to SABR prior to treatment delivery. There was a significant correlation with the common plan quality index, R50%, and nephron loss, which may provide a practical and easily applicable planning aid to reduce kidney injury. The clinical impact of techniques such as respiratory gating/tracking, and heavy particle therapy may warrant further investigation in this context. Nevertheless, using our treatment technique, SABR for primary RCC appears to result in clinically acceptable loss in renal function in the short to medium term. Given the small sample size, we were unable to account for the effects of tumour size and location on subsequent functional loss. Future studies should evaluate pre-treatment characteristics in order to better inform individual patient risk of nephron loss including ongoing functional assessment in order to investigate the long-term evolution of renal dysfunction after SABR.

Conflicts of interest statement

No disclosures.

Acknowledgment

Appendix A. Supplementary data

Supplementary data associated with this article can be found, in the online version, at http://dx.doi.org/10.1016/j.radonc.2016.01.027.

References

[1] Torre LA, Bray F, Siegel RL, Ferlay J, Lortet-Tieulent J, Jemal A. Global cancer statistics, 2012. CA Cancer J Clin 2015;65:87–108.
[2] Siegel R, Naishadham D, Jemal A. Cancer statistics, 2013. CA Cancer J Clin 2013;63:11–30.
[3] Malcolm JB, Bagrodia A, Derweesh IH, et al. Comparison of rates and risk factors for developing chronic renal insufficiency, proteinuria and metabolic acidosis after radical or partial nephrectomy. BJU Int 2009;104:476–81.
[4] Kim SP, Thompson RH, Boorjian SA, et al. Comparative effectiveness for survival and renal function of partial and radical nephrectomy for localized renal tumors: a systematic review and meta-analysis. J Urol 2012;188:51–7.
[5] Demirjian S, Lane BR, Derweesh IH, Takagi T, Fergany A, Campbell SC. Chronic kidney disease due to surgical removal of nephrons: relative rates of progression and survival. J Urol 2014.
[6] Huang WC, Levey AS, Serio AM, et al. Chronic kidney disease after nephrectomy in patients with renal cortical tumours: a retrospective cohort study. Lancet Oncol 2006;7:735–40.
[7] Go AS, Chertow GM, Fan D, McCulloch CE, Hsu C-Y. Chronic kidney disease and the risks of death, cardiovascular events, and hospitalization. N Engl J Med 2004;351:1296–305.
[8] Zagoria RJ, Hawkins AD, Clark PE, et al. Percutaneous CT-guided radiofrequency ablation of renal neoplasms: factors influencing success. Am J Roentgenol 2004;183:201–7.
[9] Kunkle DA, Uzzo RG. Cryoablation or radiofrequency ablation of the small renal mass. Cancer 2008;113:2671–80.
[10] Siva S, Pham D, Gill S, Corcoran NM, Foroudi F. A systematic review of stereotactic radiotherapy ablation for primary renal cell carcinoma. BJU Int 2012;110:E737–743.
[11] Loh J, Davis ID, Martin JM, Siva S. Extracranial oligometastatic renal cell carcinoma: current management and future directions. Future Oncol 2014;10:761–74.

[12] Kothari G, Foroudi F, Gill S, Corcoran NM, Siva S. Outcomes of stereotactic radiotherapy for cranial and extracranial metastatic renal cell carcinoma: a systematic review. Acta Oncol 2014;1–10.

[13] Ponsky L, Lo SS, Zhang Y, et al. Phase I dose-escalation study of stereotactic body radiotherapy (SBRT) for poor surgical candidates with localized renal cell carcinoma. Radiother Oncol 2015;117:183–7.

[14] Staehler M, Bader M, Schlenker B, et al. Single fraction radiosurgery for the treatment of renal tumors. J Urol 2015;193:771–5.

[15] Pham D, Thompson A, Kron T, et al. Stereotactic ablative body radiation therapy for primary kidney cancer: a 3-dimensional conformal technique associated with low rates of early toxicity. Int J Radiat Oncol Biol Phys 2014;90:1061–8.

[16] Svedman C, Karlsson K, Rutkowska E, et al. Stereotactic body radiotherapy of primary and metastatic renal lesions for patients with only one functioning kidney. Acta Oncol 2008;47:1578–83.

[17] Jackson P, Foroudi F, Pham D, et al. Short communication: timeline of radiation-induced kidney function loss after stereotactic ablative body radiotherapy of renal cell carcinoma as evaluated by serial 99mTc-DMSA SPECT/CT. Radiat Oncol 2014;9:253.

[18] Morgan-Fletcher SL. Prescribing, Recording and Reporting Photon Beam Therapy (Supplement to ICRU Report 50), ICRU Report 62. ICRU, pp. ix+52, 1999 (ICRU Bethesda, MD) $65.00 ISBN 0-913394-61-0. Br J Radiol 2001;74:294.

[19] Hurkmans CW, Cuijpers JP, Lagerwaard FJ, et al. Recommendations for implementing stereotactic radiotherapy in peripheral stage IA non-small cell lung cancer: report from the Quality Assurance Working Party of the randomised phase III ROSEL study. Radiat Oncol 2009;4:19138400.

[20] Siva S, Kirby K, Caine H, et al. Comparison of single-fraction and multi-fraction stereotactic radiotherapy for patients with F-fluorodeoxyglucose positron emission tomography-staged pulmonary oligometastases. Clin Oncol (R Coll Radiol) 2015;27:353–61.

[21] Levey AS, Eckardt K-U, Tsukamoto Y, et al. Definition and classification of chronic kidney disease: a position statement from Kidney Disease: Improving Global Outcomes (KDIGO). Kidney Int 2005;67:2089–398.

[22] Dawson LA, Kavanagh BD, Paulino AC, et al. Radiation-associated kidney injury. Int J Radiat Oncol Biol Phys 2010;76:S108–15.

[23] Teh B, Bloch C, Galli-Guevara M, et al. The treatment of primary and metastatic renal cell carcinoma (RCC) with image-guided stereotactic body radiation therapy (SBRT). Biomed Imaging Interv J 2007;3:e6.

[24] Köst S, Dörr W, Keinert K, Glaser F-H, Endert G, Herrmann T. Effect of dose and dose-distribution in damage to the kidney following abdominal radiotherapy. Int J Radiat Biol 2002;78:695–702.

[25] May KS, Yang GY, Khushalani NI, et al. Association of Technetium99m MAG-3 renal scintigraphy with change in creatinine clearance following chemoradiation in the abdomen in patients with gastrointestinal malignancies. J Gastrointestinal Oncol 2010;1:7.

[26] Lopez-Gaitan J, Ebert MA, Robins P, et al. Radiotherapy of abdomen with precise renal assessment with SPECT/CT imaging (RAPRASI): design and methodology of a prospective trial to improve the understanding of kidney radiation dose response. BMC Cancer 2013;13:381.

[27] Van Poppel H, Da Pozzo L, Albrecht W, et al. A prospective, randomised eortc intergroup phase 3 study comparing the oncologic outcome of elective nephron-sparing surgery and radical nephrectomy for low-stage renal cell carcinoma. Eur Urol 2011;59:543–52.

[28] Scosyrev E, Messing EM, Sylvester R, Van Campbell S, Poppel H. Renal function after nephron-sparing surgery versus radical nephrectomy: results from EORTC randomized trial 30904. Eur Urol 2014;65:372–7.

[29] Park SY, Park BK, Kim CK. Thermal ablation in renal cell carcinoma: what affects renal function? Int J Hyperther 2012;28:729–34.

[30] Raman JD, Thomas J, Lucas SM, et al. Radiofrequency ablation for T1a tumors in a solitary kidney: promising intermediate oncologic and renal function outcomes. Canadian J Urol 2008;15:3980–5.

[31] Hofman MS, Binns D, Johnston V. Ga-68 EDTA PET/CT imaging and plasma clearance for glomerular filtration rate (GFR) quantification: comparison to conventional Cr-51 EDTA. J Nucl Med 2015;114:147843.

9.6 Out-of-field in vivo dosimetry using TLD in SABR for primary kidney cancer involving mixed photon fields

Original paper

Out-of-field in vivo dosimetry using TLD in SABR for primary kidney cancer involving mixed photon fields

CrossMark

P. Lonski [a,b,*], S. Keehan [b], S. Siva [c], D. Pham [c], R.D. Franich [b], M.L. Taylor [b], T. Kron [a,b]

[a] Department of Physical Sciences, Peter MacCallum Cancer Centre, Melbourne, Australia
[b] RMIT University, Melbourne, Australia
[c] Division of Radiation Oncology and Cancer Imaging, Peter MacCallum Cancer Centre, Melbourne, Australia

ABSTRACT

Purpose: To assess out-of-field dose using three different variants of LiF thermoluminescence dosimeters (TLD) for ten patients who underwent stereotactic ablative body radiotherapy (SABR) for primary renal cell carcinoma (RCC) and compare with treatment planning system (TPS) dose calculations.
Methods and materials: Thermoluminescent dosimeter (TLD) measurements were conducted at 20, 30, 40 and 50 cm from isocentre on ten patients undergoing SABR for primary RCC. Three types of high-sensitivity LiF:Mg,Cu,P TLD material with different ^{6}Li/^{7}Li isotope ratios were used. Patient plans were calculated using Eclipse Anisotropic Analytical Algorithm (AAA) for clinical evaluation and recalculated using Pencil Beam Convolution (PBC) algorithm for comparison.
Results: Both AAA and PBC showed diminished accuracy for photon doses at increasing distance out-of-field. At 50 cm, measured photon dose was 0.3 cGy normalised to a 10 Gy prescription on average with only small variation across all patients. This is likely due to the leakage component of the out-of-field dose. The ^{6}Li-enriched TLD materials showed increased signal attributable to additional neutron contribution.
Conclusion: LiF:Mg,Cu,P TLD containing ^{6}Li is sensitive enough to measure out-of-field dose 50 cm from isocentre however will over-estimate the photon component of out-of-field dose in high energy treatments due to the presence of thermal neutrons. ^{7}Li enriched materials which are insensitive to neutrons are therefore required for accurate photon dosimetry. Neutron signal has been shown here to increase with MUs and is higher for patients treated using certain non coplanar beam arrangements. Further work is required to convert this additional neutron signal to dose.

© 2017 Associazione Italiana di Fisica Medica. Published by Elsevier Ltd. All rights reserved.

1. Introduction

With promising rates of local control and acceptable toxicity [1,2], stereotactic ablative body radiotherapy (SABR) is emerging as an alternative for treatment of primary renal cell carcinoma (RCC) in medically inoperable patients. SABR is characterised by high doses (typically > 8 Gy) per fraction delivered in few (typically 1–5) fractions. Previous work has demonstrated favourable early outcomes using a minimum of 8 beams with a mix of 6- and 18-MV photons [2], with 18 MV being important for skin sparing in many cases. Treatment precision is ensured through the use of advanced patient setup and immobilisation techniques in conjunction with image guidance. These immobilisation devices however are often bulky and can reduce the skin sparing effect. Additionally, patients with RCC referred for SABR are often not fit for surgery and may have large abdominal girth resulting in large patient separation, which can compromise dose conformity and further reduce skin sparing. Posteriorly located lesions pose additional challenges in terms of skin sparing. While the use of high energy (>10 MV) photon beams improves skin sparing, there is a degree of concern raised regarding incidental neutron production in the medical linear accelerator.

While modern radiotherapy treatment techniques such as SABR are able to achieve a high degree of conformality to a targeted region, a small yet inevitable component of radiation dose reaches untargeted healthy tissues beyond the useful treatment beam. This additional radiation, termed 'out-of-field' dose, arises from patient scatter, leakage dose from the medical linear accelerator, and scatter from the machine head and collimating devices. Out-of-field dose in radiotherapy has gained substantial interest in recent years

* Corresponding author at: Peter MacCallum Cancer Centre, Locked Bag 5, A'Beckett St, Victoria 8006, Australia.
E-mail address: Peta.Lonski@petermac.org (P. Lonski).

[3], owing to improved life expectancies post-treatment with modern management strategies. The risk of developing a second primary cancer following radiotherapy has been studied extensively; the systematic review by Murray et al. [4] showed an increased risk of radiation induced cancer in prostate radiotherapy across several studies. Further, this risk was shown to increase over time.

Commercially available radiotherapy treatment planning systems do not model out-of-field dose accurately. Several groups have measured out-of-field photon dose for conventional radiotherapy of various treatment sites, including liver [5], brain [6], prostate [7] and breast [8]. If accurate knowledge of out-of-field dose is required, direct measurement is necessary. Out-of-field dose may have relevance for long term risk assessment particularly in cases where patient outlook is favourable. This may be the case in primary kidney cancer, as the 5-year survival for operable patients with organ-confined disease is above 80% [9].

The high dose per fraction associated with SABR treatments provided a unique opportunity to explore out of field dose owing to the higher absolute dose at out-of-field locations compared to conventional fractionation schedules. The present work describes the use of highly sensitive TLD material for out-of-field in vivo dosimetry in SABR treatments involving mixed photon fields. We demonstrate how this method has been used to assess out-of-field photon dose and compare with treatment planning system (TPS) calculations on ten patients undergoing SABR for primary kidney cancer. The relative contribution of neutron signal is also assessed.

2. Methods and materials

All reported doses refer to absorbed dose due to photons herein, as assessed using TLD 700H. TLD measurements were conducted along midline on ten consecutive patients treated with SABR for primary kidney cancer. All patients underwent a 4-dimensional CT scan using a Brilliance 16-slice scanner (Philips Medical Systems, Eindhoven, Netherlands) for internal target volume (ITV) determination. Treatment planning was performed using Eclipse (v11.03, Varian Medical Systems, Palo Alto, CA). Patients were treated following a clinical protocol approved by the Peter MacCallum Cancer Centre ethics review board with 3D conformal radiotherapy to a prescribed dose of 26 Gy in 1 fraction (lesion size < 5 cm) or 42 Gy in 3 fractions using a mix of 6 and 18 MV photon beams. Non coplanar beams were employed as appropriate to optimise planning target volume (PTV) coverage and normal tissue sparing. Treatment parameters are summarised in Table 1. One patient who was treated to 24 Gy in a single fraction to the sacrum (Patient 11) is included in Table 1 for comparison to a treatment using only

6 MV photons. TLD measurements for neutrons were performed on this patient where no neutron signal is expected. This allows the TLD signal from low-energy irradiation to be compared with that in a high-energy radiation field where neutrons are present.

Measurements were conducted out-of-field for a single fraction at 20, 30, 40 and 50 cm from beam central axis (as defined at gantry and couch angles of 0 degrees herein) midline along the inferior direction (ie, beginning at the abdomen with TLDs placed at 10 cm intervals towards feet). All patients were treated on a Varian 21-iX medical linear accelerator (Varian Medical Systems, Palo Alto, CA).

The TLD material used in this work was LiF:Mg,Cu,P, which was chosen for its high sensitivity. This allowed in vivo measurements to be conducted in low-dose regions (order of cGy or less) at relatively large distances out-of-field. LiF:Mg,Cu,P is approximately 30 times more sensitive than LiF:Mg,Ti [10]. In addition, previous work using synchrotron radiation has demonstrated minimal energy dependence for this material, with a maximum deviation of 15% caused by an over-response to a relatively narrow range of photon energies at approximately 80 keV in the range between 15 keV and 18 MV, making it a useful detector for out-of-field measurements involving a component of low energy scatter. TLDs were calibrated in a 6 MV beam ($TPR_{20,10} = 0.67$) under reference conditions (10 cm × 10 cm square field at depth of maximum dose in solid water with full backscatter provided). The linear accelerator was calibrated using an ionisation chamber with a calibration traceable to a primary standards lab. Standard TLDs from the same batch as patient TLDs were irradiated to a known photon dose. Sensitivity factor corrections were applied to individual TLD chips. Photon dose was calculated using a ratio of TLD signal from a known dose to TLD signal from in vivo measurements. Patient TLDs and standard TLDs were read out together using a Harshaw 5500 automatic reader. For LiF:Mg,Cu,P, the use of multiple chips for each measurement as well as careful calibration is reported to yield an overall uncertainty of 4% at the 95% confidence level for a single measurement [11]. This is a Type B uncertainty estimated from previous experience using our system which includes maintaining thermal history of TLDs in a batch, use of an automated reader which performs a pre-read anneal, application of sensitivity factors for individual chips, and careful handling procedures.

Three different variants of LiF:Mg,Cu,P were used at each measurement point, each with different $^6Li/^7Li$ isotope ratios. The ^6Li-enriched, or $^6LiF:Mg,Cu,P$ ('600H') variation comprises approximately 95.6% ^6Li. The ^7Li-enriched, or $^7LiF:Mg,Cu,P$ ('700H') material contains less than 0.07% ^6Li. The response of 600H and 700H material is almost identical for photons and electrons however the higher cross-section for thermal neutrons of ^6Li makes 600H more sensitive to thermal and thermalised neutrons, leading to an additional signal upon readout. The use of $^6Li/^7Li$ TLD pairs for

Table 1
Summary of key treatment parameters.

Patient no. (prescription)	Treatment fields (non coplanar)	Mean jaw field size [X Y cm]	MU at 6 MV per fraction	MU at 18 MV per fraction (% of total)
1 (26 Gy/1)	9 (3)	6 × 6	1782	2695 (60%)
2 (42 Gy/3)	9 (4)	7 × 6	1082	1136 (51%)
3 (26 Gy/1)	9 (2)	7 × 4	3652	897 (20 %)
4 (42 Gy/3)	10 (5)	8 × 7	0	2106 (100%)
5 (42 Gy/3)	10 (3)	7 × 6	1048	1667 (61%)
6 (26 Gy/1)	10 (2)	5 × 6	3463	1568 (31%)
7 (42 Gy/3)	9 (4)	7 × 9	1059	999 (49%)
8 (42 Gy/3)	11 (4)	6 × 8	1554	889 (36%)
9 (42 Gy/3)	9 (5)	7 × 7	0	1868 (100%)
10 (42 Gy/3)	10 (4)	6 × 5	1280	1025 (45%)
11* (24 Gy/1)	8 (5)	6 × 5	4978	0 (0%)
Mean	**10 (4)**	**7 × 7**	**1809**	**1520 (59%)**

* Patient 11 was treated at 24 Gy to the sacrum using only 6 MV photons. This patient is included to compare an 18 MV only treatment with a 6 MV only treatment, since all RCC patients had at least one 18 MV beam.

neutron detection has been discussed by other groups [12–15] who used TLD 600 and 700 material, comprised of LiF: Mg,Ti. The high sensitivity material used in this work enabled out-of-field measurements to be conducted in vivo at locations far from the radiation field, up to 50 cm from isocentre. The 700H material is relatively insensitive to neutrons with the energy spectrum which reaches the patient plane [16,17], and the small concentration of 6Li in 700H material has been shown to produce negligible neutron signal from the spectrum produced by a Varian 21-EX [18]. The response of the 700H material can therefore be used to assess photon dose. The third material ('100H') contains natural Li (approximately 7.5% ^{6}Li) and was also included at each measurement point. The thermoluminescent (TL) response linearity range of LiF:Mg,Cu,P extends from 10 μGy up to 10 Gy [19]. For photon dose, TLD signal was converted to dose by comparing the 700H thermoluminescence signal from in vivo measurements to TLD signal from chips in the same batch given a known dose under reference conditions. A pre-read anneal was used to minimise effects of fading. Photon dose measurements were compared to treatment planning system calculations at identical measurement locations. TLDs were placed in custom made Perspex 'buildup domes' which were designed to accommodate three TLD chips ($1 \times 3 \times 3$ mm in size) with minimal angular dependence, providing approximately 1 cm buildup material (photons) and moderation (neutrons). Buildup domes are illustrated in Fig. 1a. A triplet of 600H, 700H and 100H TLD material was included at each measurement point. The domes were not oriented in any particular direction when positioned. The neutron signal was taken as the difference in response between the 600H and 700H TLDs at each point.

3. Results

3.1. Limit of detection

The limit of detection was assessed for each TLD material using readings from 5 un-irradiated chips from each set, several days after being annealed in a TLD oven. The limit of detection may be expressed as:

$$x_L = \bar{x} + k \cdot s$$

where x_L is the smallest measure that can be detected with reasonable certainty, $\bar{x}$ is the mean of blank (un-irradiated) readings, s is

the standard deviation of the blank readings. The coverage factor k was chosen to be 3 for a confidence of 99%. Background readings were of the order of 10 ± 5 nC, reflecting environmental radiation over one to two days, which was typical for in vivo measurement readout delay time. The limit of detection for each material type is estimated to be approximately 1 μGy, well below the dose levels measured in vivo.

3.2. Reproducibility

Measurement reproducibility was investigated at identical points for a fractionated treatment of 42 Gy in 3 fractions. Fig. 1b shows mean TLD signal for all three fractions and the standard uncertainty is shown by the error bars. The relative standard uncertainty for each TL material was within 18, 14, 18 and 8% over 3 fractions at 20, 30, 40 and 50 cm from beam central axis respectively. From the measurements on the example patient from Fig. 1b, the dose gradient can be estimated to be 0.15 cGy/cm between 20 and 30 cm, 0.04 cGy/cm between 30 and 40 cm, and 0.02 cGy/cm between 40 and 50 cm. Positioning accuracy of the TLD domes is estimated to be within ±2 mm. The inset shows the mean resulting neutron signal measured for 3 fractions, which showed a relative standard uncertainty of 15, 10, 9 and 6% over 3 fractions at 20, 30, 40 and 50 cm respectively, indicated by the error bars.

3.3. TLD response in 6, 18 MV treatments

TLD measurements conducted on an example patient treated using only 18 MV photons (Patient 4) were compared with measurements for a sacrum patient treated with only 6 MV photons (Patient 11). The TL signal from each material is shown in Fig. 2 for these patients. The difference between the 600H and 700H material was found to be negligible within the measurement uncertainties for the patient treated using 6 MV, which is consistent with the absence of neutrons as expected for this energy. For the patient treated with only 18 MV photons, an increased response attributable to neutrons can be seen from the 600H and 100H materials. 600H produced the greatest signal due to its higher concentration of ^{6}Li. Comparing the relative TL signal from these two patients demonstrates a non-negligible neutron component of the TL signal for the 18 MV case, making 700H essential for
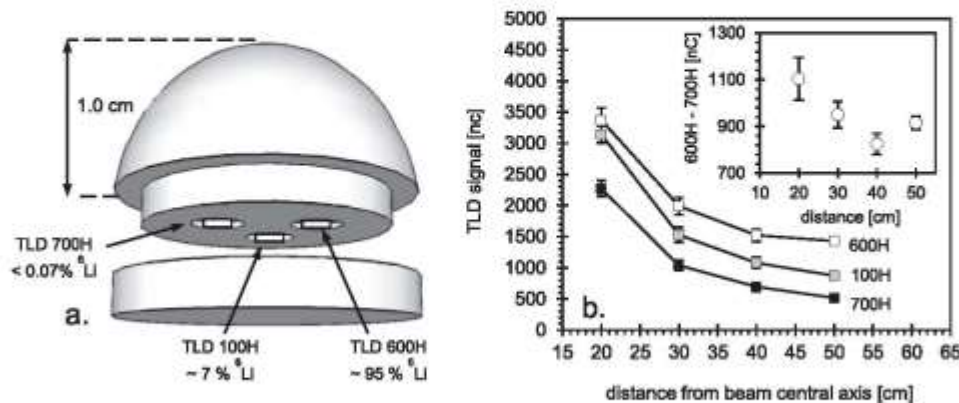

Fig. 1. a. Schematic of Perspex buildup domes used to accommodate three TLDs at each measurement location. The concentration of ^{6}Li isotope, which has a higher cross section for thermal neutrons, is indicated for each material. b. Mean TL response over 3 fractions for one patient. Error bars show the standard error at each point for all TL materials (not visible at 50 cm due to the small standard error). The mean resulting neutron signal and standard error (error bars) is shown in the inset.
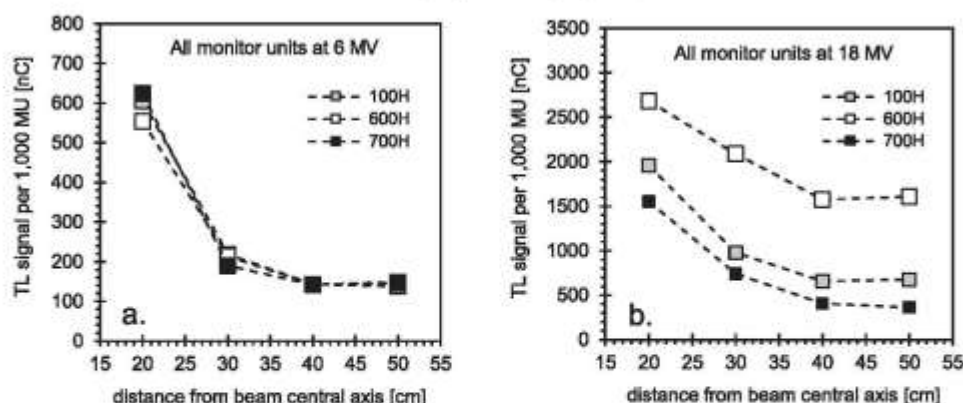
Fig. 2. TL signal measured out-of-field for each material as a function of distance from beam central axis for two SABR patients, one treated using only 6 MV (a) and the other with only 18 MV photons (b). TL signal is scaled per 1000 monitor units and readout uncertainties of 3% are indicated by symbol size.

accurate assessment of photon dose in high energy photon dosimetry. Photon dose can be determined using the 700H material and for the example patients shown in Fig. 2, the measured doses at 20, 30, 40 and 50 cm were 1.48, 0.45, 0.34 and 0.35 cGy per 10 Gy prescribed dose for the patient treated with only 6 MV and 2.48, 1.28, 0.67 and 0.65 cGy per 10 Gy prescribed dose for the patient treated using only 18 MV. For these two patients, the out-of-field dose for 18 MV was on average a factor of 2 higher than for 6 MV, though this does not take into consideration differences in field sizes, patient geometry, couch or gantry angles.

3.4. Photon doses

The out-of-field photon component was assessed using the response of the 700H material, which is insensitive to neutrons. Both PBC and AAA were found to under estimate the out of field photon dose. In most cases, no dose estimate was provided by the treatment planning system at the measurement points owing to the large distance from the treatment volume. Fig. 3 shows a
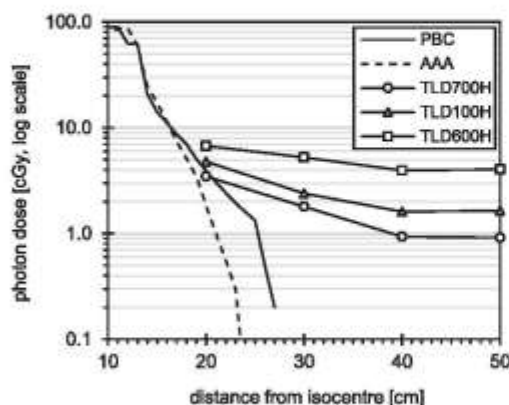

Fig. 3. Out-of-field dose measurements for a single fraction comparing 700 H TLD measurements with the PBC and AAA dose calculation algorithms for Patient 4. Both the 100 H and 600 H materials can be seen to over-estimate out-of-field dose due to their higher ⁶Li concentrations, making them sensitive to thermal neutrons.

dose pattern out-of-field comparing Eclipse calculations to out-of-field TLD measurements for a typical patient. Both AAA and PBC can be seen to underestimate photon dose out-of-field at points beyond approximately 22 cm. The degree by which the planning system underestimates out-of-field dose increases at larger distances. The 700H material provides a measurement of photon dose while the 600H and 100H material show increased response due to their increased sensitivity to thermal neutrons.

If not accounted for, additional TLD signal due to neutrons increased the apparent photon dose. Using the response of the 700H material to calculate 'true' photon dose, apparent photon dose from the 100H and 600H material was calculated. Over response of the natural Li (100H) material was 22% (range 2–51), 40% (range 9–99), 59% (range 27–92) and 66% (range 24–120) on average at 20, 30, 40 and 50 cm from isocentre, respectively. The over response for the 600H material was higher at 54 (range 11–94), 117 (range 50–224), 196 (range 85–324) and 231 (range 92–418) % respectively. The measured photon doses as assessed using 700H are shown for all patients in Fig. 4b.

Out-of-field photon dose as measured using 700H was assessed as a function of relative contribution of 18 MV monitor units to the overall treatment. Measured doses were scaled to a common prescribed dose of 10 Gy and are shown in Fig. 4a with the unscaled doses shown in Fig. 4b. At 50 cm, the measured dose for a 10 Gy prescription was 0.3 cGy on average with only small variation across all patients. The trendline for 50 cm demonstrates a near-constant dose 'bath' that may be attributable to leakage radiation from the linear accelerator, which is largely independent of field size and the magnitude of the measured dose would be consistent with International Electrotechnical Commission (IEC) recommendations for maximum allowable leakage radiation for medical linear accelerators.

3.5. Assessment of neutron signal

The difference between the raw 700H and 600H TLD response is taken as an additional signal due to neutrons. Fig. 5 shows neutron signal detected in vivo for ten SABR patients as a function of number of monitor units (MU) delivered at 18 MV. The measured neutron signal is shown for points at 20, 30, 40 and 50 cm from beam central axis. Neutron signal increases with number of MUs for each measurement location. No such correlation between neutron
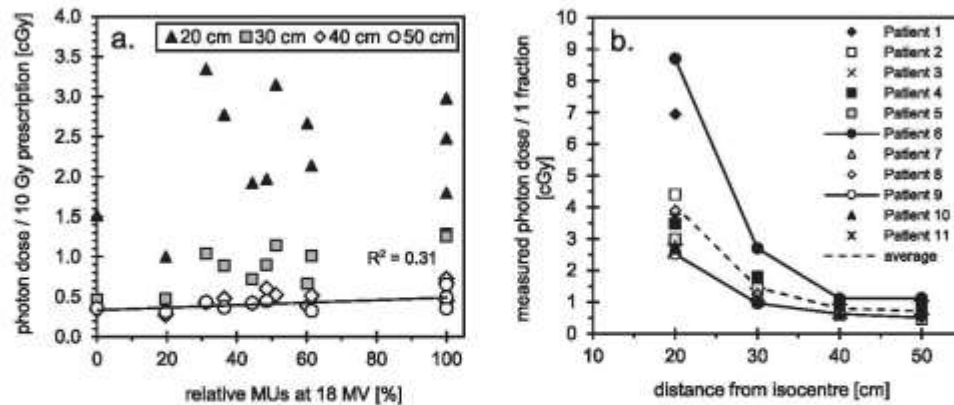
Fig. 4. (a) Measured photon dose at 20, 30, 40 and 50 cm from isocentre for 10 SABR patients as a function of relative contribution of 18 MV monitor units, scaled to a 10 Gy prescription. Trend line is included for 50 cm and (b) unscaled photon doses for all patients measured using 700 H, with treatment parameters for each patient shown in Table 1. Lines for patients measuring the highest dose (Patient 6), lowest dose (Patient 9) are shown along with the mean dose for all patients (dashed line).
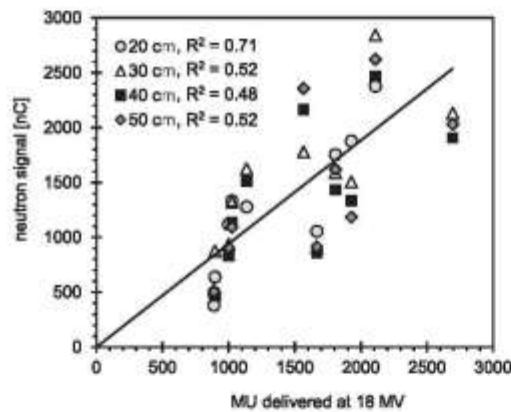

Fig. 5. Neutron signal measured in vivo along midline at 20, 30, 40 and 50 cm from beam central axis on ten patients undergoing SABR. Neutron signal is taken as the difference between 600 H and 700 H TLD response and increases with number of monitor units (MU) delivered at 18 MV.
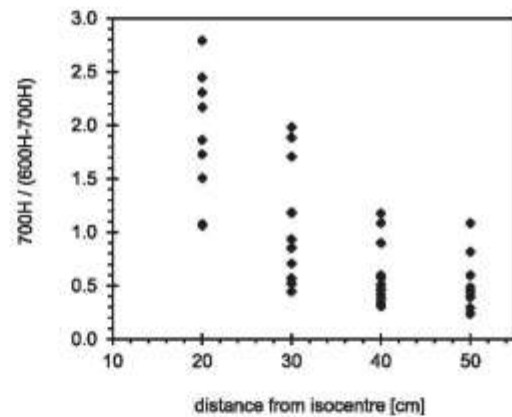

Fig. 6. Photon TL signal relative to neutron signal as a function of increasing distance from beam central axis for 10 SABR patients.

signal and either field size or source-surface distance was observed within the patient cohort.

The photon contribution to TL signal out-of-field (TLD 700H), relative to neutron signal (difference of the TLD 600H reading and TLD 700H reading), is shown in Fig. 6 as a function of distance from the beam central axis. Relative photon signal can be seen to decrease with increasing distance from the treatment field. The cross-over point where neutron TLD signal begins to dominate over photon TLD signal occurs at distances >30 cm from beam central axis.

Per thousand monitor units, the mean jaw-defined field size and patient size as assessed in terms of anterior-posterior as well as left-right separation at the level of the PTV did not make a significant difference to neutron signal (two-tail $p = 0.97$ and 0.91, respectively). The work of Sohrabi et al. (2016) [20] also shows that for out-of-field neutron measurements, field size does not correlate with neutron equivalent dose. Neutrons are not well collimated by field-shaping components made from high atomic number materi-

als with low neutron absorption cross sections. Neutrons tend to be scattered elastically with little energy loss to the recoil nuclei. There was a slight increase in neutron signal for shorter mean SSD but this was not significant ($p = 0.07$). Geometrical assessment of non coplanar beams showed that neutron signal was generally higher for patients who received at least one non coplanar beam delivered anteriorly from the patient inferior direction (i.e., side of the linac head positioned directly above the TLDs, creating an acute angle between linac gantry and the patient plane) at 18 MV. In this arrangement the side of the linac head is in close proximity to the TLDs. On average, mean neutron signal across all measurement locations was a factor of 2 greater received at least one 18 MV beam delivered at an anterior-inferior gantry angle, which was significant (two-tail $t = 2.57$, $p < 0.001$).

To further investigate this apparent correlation between angle, TLD measurements were made in the linac gantry and treatment couch geometries outlined in Fig. 7. TLD buildup domes were aligned along the couch with solid water backscatter material provided. Increased neutron signal was detected with the linac head
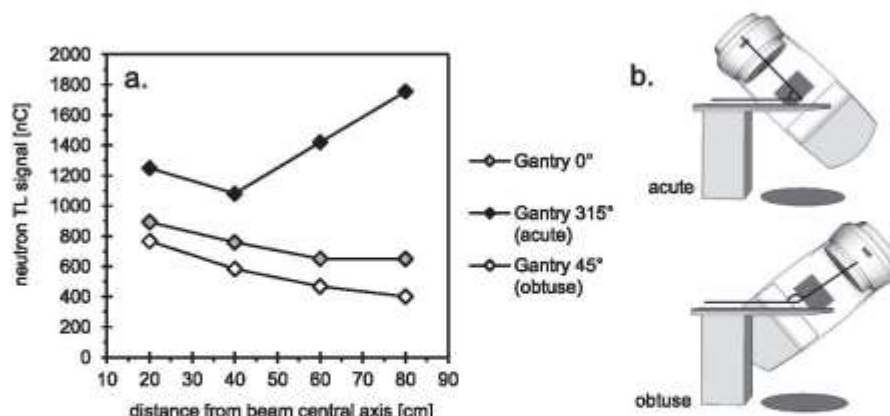
Fig. 7. a. Neutron signal measured along the patient plane at increasing distance from linac isocentre for three different linac/couch angle configurations. b. Schematic depicting the acute and obtuse configurations used. A considerable increase in neutron signal is observed in the case of an acute angle between linac gantry and patient plane, with the side of the linac head in closer proximity to the TLDs.

forming an acute angle with the patient couch, as was observed within the patient cohort. The measured photon dose was found to decrease exponentially for all three geometries. Photon dose from the gantry 45 degree geometry (ie, obtuse angle) was found to have the highest dose overall. An increase in photon dose between 40 cm and 80 cm was observed for the gantry 315 degree geometry but to a much smaller extent compared to the reported neutron signal; ratios of photon dose measured at 60 and 80 cm to that measured at 40 cm were 1.3 and 1.7 for photons. For neutrons, the ratios were 1.7 and 26.4 (Fig. 7a), indicating a stronger increase in neutron signal compared to photons.

4. Discussion

Modern management strategies and sophisticated radiotherapy techniques have led to improved patient outcomes and longer life expectancies. As such, increased attention has been turned to the potentially harmful long-term effects of incidental irradiation of untargeted healthy tissues during radiotherapy. Neutrons are of particular concern owing to the higher biological damage, up to a factor of 20 [21], compared to photons. Neutron production occurs within high atomic number materials contained within the medical linear accelerator when operated above ~10 MV. The use of treatment beams at these higher energies is necessary in many cases particularly in SABR for RCC where immobilisation devices can compromise the skin sparing effect.

High sensitivity LiF:Mg,Cu,P TLD material allowed assessment of out-of-field dose at locations far from the treatment field. For in vivo photon dosimetry, the use of TLD materials containing ^{6}Li including standard 100H leads to an over-response in high energy photon treatments where neutrons are produced [22]. Isolation of the neutron component using combinations of ^{6}Li and ^{7}Li enriched TLDs allows distinction of neutron and photon associated signal in mixed neutron and photon fields. An increased neutron signal with number of monitor units delivered at 18 MV has been demonstrated in vivo in the current patient cohort (Fig. 5). This finding is consistent with the work by Romero-Exposito et al., who have demonstrated a linear increase in measured neutrons with linac MU for different accelerator models [23]. This work demonstrates this application in vivo. Interpretation of the measured signal, however, is complex. Calibration factors for neutron dosimetry are

strongly dependent on the incident energy spectrum. Thus, for dosimetry of photo-neutrons produced by a medical linear accelerator where the neutron spectrum differs significantly from those produced by standard neutron sources, determining an accurate dose response calibration factor experimentally presents a significant challenge. It should be emphasised that the results shown in the present work do not explicitly account for differences in TLD sensitivity with changing neutron spectrum. Patterns in neutron signal at out-of-field locations may change when a correction can be derived for changes in sensitivity. Further work is required to determine the thermal neutron spectrum out-of-field for the measurement scenarios in the present work.

Aside from being a neutron detector, rather than dosimeter, TLD has some additional advantages and drawbacks. The key advantage is assessment of out-of-field photon dose, arising from linac leakage and scatter, obtained in the same measurement. It is only in the context of this photon dose that the neutron component can be interpreted. Drawbacks however include the laborious nature of proper TLD handling and readout, delayed readout, requirement of specialist procedures and in particular the requirement of specialised TLD material. With careful handling and readout procedures, TLD was shown to be very reproducible for photon dosimetry at out-of-field locations, with the largest variation occurring at measurement points closest to the primary beam (see Fig. 1b). With the reproducibility improving at larger distances, positioning uncertainties may be assumed to be the dominant contributor to inter-fraction variations, since the dose gradient is steeper closer to the beam.

Within this patient cohort, the use of 6 or 18 MV showed no trend in out-of-field dose at 20 cm, where scatter is dominant (Fig. 4). Measured dose at 50 cm from isocentre was 0.4 cGy (standard deviation of 0.1 cGy) for a 10 Gy prescription regardless of beam energy, consistent in magnitude with 0.1% of the primary beam at 1.0 m distance from the target stated in IEC recommendations [24] for leakage from the linear accelerator. This is further supported by the similar doses measured for both 6- and 18-MV treatments in this region. Leakage was observed to be the main contributor to out-of-field dose beyond 40 cm from isocentre. The use of oblique gantry angles was found to be associated with increased neutron signal. Fig. 7 shows a phantom irradiation replicating a similar geometry, further demonstrating that increased neutron signal is observed beneath the side of the linac head. From

the patient data, this increase is not observed in the case of photons. It is unclear why this increase beneath the linac head occurs for neutrons but not for photons however one may speculate that different interactions within materials in the linac head may play a role, since photons are attenuated by high atomic number materials but these same materials have a low neutron absorption cross section.

TLD 700H material was found to be essential for assessing out-of-field dose at locations, particularly at 40 cm and beyond from treatment isocentre. The over-response of 600H due to neutrons in high energy treatments was demonstrated, with an over-estimation of photon dose by a factor of 4 in some cases. These findings are similar in magnitude to the work by Kry et al. [22] who demonstrated an over-response of 487% on average for TLD 100 at out-of-field locations up to 50 cm from central axis using 18 MV fields. The use of multiple TLD compositions enabled assessment of the relative neutron signal along the patient plane compared with that of photons. From our measurements we conclude that linac gantry and couch combinations which place the patient directly beneath the side of the linac head could be avoided or assigned lower beam weighting where possible at high energies, since the detected neutron signal was highest for these beam arrangements. However this should only be considered in cases where comparable PTV coverage and acceptable doses to critical structures can still be achieved. This is a relatively simple planning strategy which could be implemented clinically to reduce overall neutron exposure at no real cost to plan quality or delivery.

5. Conclusion

This work demonstrates that LiF:Mg,Cu,P exhibits sufficient sensitivity to assess out-of-field dose at locations far from the radiation treatment field in vivo for patients treated with SABR using 6 and 18 MV photons. The use of TLD materials containing ^{6}Li for out-of-field in vivo dosimetry including standard 100H will result in over-estimation of photon doses in high energy radiotherapy if additional signal due to neutrons is not taken into account, with over-estimates as high as 418% for 600H and 66% for 100H at 50 cm from the field reported in this work. 700H can be used to discern photon dose in vivo during high energy SABR with adequate spatial resolution at distances far from the treatment field without additional signal from neutrons, and is essential in order to accurately assess photon dose in high energy radiotherapy using LiF-type TLD. Out-of-field photon doses have been presented for 10 SABR patients at locations up to 50 cm from the treatment field. In these regions, the treatment planning system was found to under-estimate the photon dose. ^{6}Li/^{7}Li TLD pairs may be used to discern additional signal due to neutron interactions within the TLD material, although interpretation of measured TL signal is complex and further work is required to better understand the link between neutron energy deposition and dose in TL materials.

References

[1] Siva S, Pham D, Gill S, et al. A systematic review of stereotactic radiotherapy ablation for primary renal cell carcinoma. BJUI 2012;110:E737–43.
[2] Pham D, Thompson A, Kron T, Foroudi F, Kolsky MS, Devereux T, et al. Stereotactic ablative body radiation therapy for primary kidney cancer: A 3-dimensional conformal technique associated with low rates of early toxicity. Int J Radiat Oncol Biol Phys 2014.
[3] Taylor ML, Kron T. Consideration of the radiation dose delivered away from the treatment field to patients in radiotherapy. J Med Phys 2011;36(2):59–71.
[4] Murray L, Henry A, Hoskin P, et al. Second primary cancers after radiation for prostate cancer: a systematic review of the clinical data and impact of treatment technique. Radiother Oncol 2014;110:213–28.
[5] Howell RM, Scarboro SB, Taddei PJ, Krishnan S, Kry SF, Newhauser WD. Methodology for determining doses to in-field, out-of-field and partially in-field organs for late effects studies in photon radiotherapy. Phys Med Biol 2010;55:7009–23.
[6] Taylor ML, Franich RD, Kron T. Assessment of out-of-field dose in radiotherapy of brain lesions in children. Int J Radiat Oncol Biol Phys 2011;79(3):927–33.
[7] Kry SF, Salehpour M, Followill D, Stovall M, Kuban D, White A. Out-of-field photon and neutron dose equivalents from step-and-shoot intensity-modulated radiation therapy. Int J Radiat Oncol Biol Phys 2005;62(4):1204–16.
[8] Lonski P, Taylor ML, Hackworth W, Phipps A, Franich RD, Kron T. In vivo verification of radiation dose delivered to healthy tissue during radiotherapy for breast cancer. J Phys Conf Ser 2014;489:012015.
[9] Cancer.org. Survival rates for kidney cancer by stage American Cancer Society; 2014. [online] Available at: http://www.cancer.org/cancer/kidneycancer/detailedguide/kidney-cancer-adult-survival-rates [Accessed 4 Dec. 2014].
[10] Kron T. Thermoluminescence dosimetry and its applications in medicine—part 1: physics, materials and equipment. Aust Phys Eng Sci Med 1994;17:175–99.
[11] Duggan L, Hood C, Warren-Forward H, Haque M, Kron T. Variations in dose response with x-ray energy of LiF:Mg, Cu, P thermoluminescence dosimeters: implications for clinical dosimetry. Phys Med Biol 2004;49:3831–45.
[12] Esposito A, Bedogni R, Lembo L, Morelli M. Determination of the neutron spectra around an 18 MV medical LINAC with a passive Bonner sphere spectrometer based on gold foils and TLD pairs. Radiat Meas 2008;43:1038–43.
[13] La Tessa C, Berger T, Kaderka R, et al. Characterization of the secondary neutron field produced during treatment of an anthropomorphic phantom with x-rays, protons and carbon ions. Phys Med Biol 2014;59:8.
[14] Reft C, Runkel-Muller R, Myrianthopoulos L. In vivo and phantom measurements of the secondary photon and neutron doses for prostate patients undergoing 18 MV IMRT. Med Phys 2006;33(10):3734–42.
[15] Howell RM, Ferenci MS, Hertel NE, Fullerton GD. Investigation of secondary neutron dose for 18 MV dynamic MLC IMRT delivery. Med Phys 2005;32(3):786–93.
[16] Kry SF et al. Neutron spectra and dose equivalents calculated in tissue for high-energy radiation therapy. Med Phys 2009;36(4):1244–50.
[17] Barquero R et al. Neutron spectra and dosimetric features around an 18 MV linac accelerator. Health Phys 2005;88(1):48–58.
[18] Keehan S et al. Accuracy of calibration of lithium-6 and -7 enriched LiF TLDs for neutron measurements in high energy radiotherapy. Med Phys 2015;42:3351.
[19] Moscovitch M. Personnel dosimetry using LiF:Mg, Cu, P. Rad Prot Dosim 1999;85:49–56.
[20] Sohrabi M, Hakimi A, Mahdavi SR. A novel position-sensitive mega-size dosimeter for photoneutrons in high-energy X-ray medical accelerators. Phys Med 2016;32:778–86.
[21] International Commission on Radiological Protection (ICRP). The 2007 Recommendations of the International Commission on Radiological Protection. ICRP Publication 103, Ann. ICRP 2007; 37.
[22] Kry SF, Price M, Followill D, Mourtada F, Salehpour M. The use of LiF (TLD-100) as an out-of-field dosimeter. JACMP 2007;8:169–75.
[23] Riesem-Expósito M, Sánchez-Nieto B, Terrón JA, et al. Commissioning the neutron production of a Linac: development of a simple tool for second cancer risk estimation. Med Phys 2015;42:276.
[24] International Electrotechnical Commission (IEC) Safety of medical electrical equipment, Part 2: particular requirements for medical electron accelerators in the range 1–50 MeV, Publication 601-2-1. IEC, Geneva; 1981.

BJUI
BJU International

Stereotactic ablative body radiotherapy for inoperable primary kidney cancer: a prospective clinical trial

Shankar Siva*,†, Daniel Pham*, Tomas Kron*,†, Mathias Bressel*, Jacqueline Lam*, Teng Han Tan*, Brent Chesson*, Mark Shaw*, Sarat Chander*, Suki Gill*,‡, Nicholas R. Brook§, Nathan Lawrentschuk*,¶, Declan G. Murphy*,† and Farshad Foroudi*,¶

*Peter MacCallum Cancer Centre, Melbourne, Vic., Australia, †Sir Peter MacCallum Department of Oncology, University of Melbourne, Melbourne, Vic. Australia, ‡Sir Charles Gairdner Hospital, Nedlands Perth, WA, Australia, §Royal Adelaide Hospital, Adelaide, SA, Australia, and ¶Olivia Newton John Cancer Centre, Heidelberg, Vic., Australia

Objective

To assess the feasibility and safety of stereotactic ablative body radiotherapy (SABR) for renal cell carcinoma (RCC) in patients unsuitable for surgery. Secondary objectives were to assess oncological and functional outcomes.

Materials and Methods

This was a prospective interventional clinical trial with institutional ethics board approval. Inoperable patients were enrolled, after multidisciplinary consensus, for intervention with informed consent. Tumour response was defined using Response Evaluation Criteria In Solid Tumors v1.1. Toxicities were recorded using Common Terminology Criteria for Adverse Events v4.0. Time-to-event outcomes were described using the Kaplan–Meier method, and associations of baseline variables with tumour shrinkage was assessed using linear regression. Patients received either single fraction of 26 Gy or three fractions of 14 Gy, dependent on tumour size.

Results

Of 37 patients (median age 78 years), 62% had T1b, 35% had T1a and 3% had T2a disease. One patient presented with bilateral primaries. Histology was confirmed in 92%. In total, 33 patients and 34 kidneys received all prescribed SABR fractions (89% feasibility). The median follow-up was 24 months. Treatment-related grade 1–2 toxicities occurred in 26 patients (78%) and grade 3 toxicity in one patient (3%). No grade 4–5 toxicities were recorded and six patients (18%) reported no toxicity. Freedom from local progression, distant progression and overall survival rates at 2 years were 100%, 89% and 92%, respectively. The mean baseline glomerular filtration rate was 55 mL/min, which decreased to 44 mL/min at 1 and 2 years ($P < 0.001$). Neutrophil:lymphocyte ratio correlated to % change in tumour size at 1 year, $r^2 = 0.45$ ($P < 0.001$).

Conclusion

The study results show that SABR for primary RCC was feasible and well tolerated. We observed encouraging cancer control, functional preservation and early survival outcomes in an inoperable cohort. Baseline neutrophil:lymphocyte ratio may be predictive of immune-mediated response and warrants further investigation.

Keywords

ablation, clinical trial, nephron-sparing, stereotactic ablative body radiotherapy, radiation, renal cell carcinoma, #KidneyCancer, #kcsm

Introduction

Renal cell carcinoma is the 8th most common cancer worldwide [1] and continues to increase in incidence and lethality. According to the American Cancer Society, kidney cancer incidence rates increased by 4.1% per year in men and 3.3% per year in women between 2004 and 2008 [2]. Surgery is the standard of care for primary RCC; however, many patients are in an older age group [3] and have associated medical comorbidities that may preclude them from extirpative therapies. Patients undergoing partial (PN) or radical nephrectomy (RN) experience postoperative nephron loss, which may result in *de novo* chronic kidney disease or advancement of pre-existing renal dysfunction [4].

Non-surgical definitive treatment options for this population of patients are limited. Radiofrequency ablation (RFA) and

cryotherapy are two common thermal ablation techniques that have specific limitations. They are typically limited to small renal masses and are generally restricted to lesions located away from the ureter and vascular structures because of the risk of heat sink effects, stricture and/or fistula development [5]. With larger tumours there is a significant risk of haemorrhage, which can require major intervention to control. Both of these techniques are invasive, adding to complication risk and issues with managing anticoagulative medications.

By contrast, stereotactic ablative body radiotherapy (SABR) is a non-invasive treatment option for patients deemed unsuitable for surgical intervention. SABR is delivered to patients whilst fully awake and in a single or few outpatient treatment sessions. SABR is well established in the treatment of cancers in the lung, liver and spine. Whilst the approach is still emerging in the kidney, it is not technically limited by tumour proximity to central pelvic-calyceal structures or to small renal masses [6]; however, there is a paucity of prospective data to support the routine adoption of SABR for primary inoperable RCC [7]. In this context we conducted a prospective clinical trial of SABR for this disease setting. The primary purpose of the present study was to assess the feasibility and safety of this approach using conventional linear accelerators without fiducial marker insertion, an approach readily translatable to radiotherapy departments worldwide.

Materials and Methods
Patient Population

This was an institutional ethics board-approved single institutional prospective clinical trial (clinicaltrials.gov ID NCT01676428) conducted at the Peter MacCallum Cancer Centre. All patients signed informed consent. Eligible patients were enrolled between 2012 and 2014 and were aged >18 years, had Eastern Cooperative Oncology Group (ECOG) performance scores of 0–2 inclusive and had a single lesion within the target kidney. Patients were medically inoperable, were in the high-risk group for surgery (because of likelihood of post-surgical dialysis) or refused surgery. Patients were excluded when receiving systemic therapy prior to or concurrent with SABR, or when having previously received high-dose radiotherapy to the upper abdomen. Biopsy confirmation was attempted in all patients when possible. Patients with small renal masses (T1a disease) were evaluated closely for the need for treatment factoring for existing comorbidites; these patients had documented growth on serial imaging, and/or were symptomatic with haematuria or pain. Multidisciplinary tumour board consensus was required before active intervention was recommended. Bloods were taken for haematology (including neutrophil and lymphocyte count) and electrolyes (including creatinine) at baseline and at each clinical visit.

Study Objectives

The primary objective was to assess the feasibility of treatment, as defined by successfully delivering the treatment plan as prescribed and achieving the nominated dose constraints. Secondary objectives were to assess: (1) treatment-related adverse events; (2) freedom from local progression; (3) freedom from distant progression; and (4) overall survival. A further exploratory objective was to identify possible predictors of change in tumour size after 1 year of SABR.

Study Protocol

Trial investigations occurred every 3 months after treatment with data close-out after all patients completed a minimum of 12 months' potential follow-up. Investigations included serum urea and electrolytes and estimated GFR (eGFR) using Chronic Kidney Disease Epidemiology Collaboration (CKD-EPI) formula calculations, CT of the chest and abdomen and clinical review with adverse event reporting. All Response Evaluation Criteria In Solid Tumors v1.1 (RECIST) [8] tumour measurements were performed by a single experienced radiologist (T.T.).

For primary RCCs <5 cm in size (maximum dimension) a single treatment of 26 Gy was delivered. For RCCs of ≥ 5 cm (maximum dimension) 42 Gy in three fractions was delivered on non-consecutive days. All treatments were delivered on conventional c-arm linear accelerators, either Varian Truebeam STx or Trilogy (Varian, Palo Alto, CA, USA). All patients were immobilized using an Elekta Bodyfix dual vacuum device (Medical Intelligence, Schwabmünchen, Germany). Radiotherapy treatment delivery techniques have been previously described in detail [9]. The motion encompassing internal target volume was constructed using four-dimensional CT simulation. A 5-mm expansion was given to derive the planning target volume (PTV). The peak dose within the internal target volume was typically 125% of the prescribed dose, with target coverage of the PTV being 95–99% by the prescription isodose.

Statistical Methods

Patient demographics, baseline characteristics and treatment details are described using descriptive statistics. Ninety-five percent exact two-sided CIs were used to assess the primary objective of feasibility. Treatment-related toxicities were graded using the National Cancer Institute Common Terminology Criteria for Adverse Events (CTCAE) v4.0. Toxicities were reported separately for the acute period (up to 90 days from SABR treatment) and late period (beyond 90 days from SABR treatment). Freedom from local progression, freedom from distant progression and overall survival were estimated using the Kaplan–Meier method with

corresponding 95% CIs. Freedom from local progression, freedom from distant progression and overall survival rates were calculated from the date of first SABR treatment. Local progression was defined using RECIST v1.1. The percentage change in tumour size (maximum diameter in axial and transverse directions) and volume from baseline was calculated for each CT assessment. Linear regression was used to assess candidate prognostic variables (histological grade, target volume, dose and neutrophil:lymphocyte ratio) for change in tumour size from baseline to 1 year after SABR.

The proportion of patients who developed new-onset chronic kidney disease (CKD), as defined by eGFR < 60 mL/min, was described. Estimate of change in eGFR in 1 year with 95% CI was provided from a linear mixed model with time as a fixed effect and patient as a random effect. This process was repeated for the subset of patients with/without pre-existing CKD and by number of risk factors for CKD. Average GFR loss from baseline to 1 and 2 years was estimated with 95% CIs.

Results

In the 2-year accrual period 37 eligible patients signed informed consent. These patient characteristics are shown in Table 1. T1a disease accounted for 35% of cases, with T1b in 62% and T2a in 3% of cases. Histological confirmation was achieved in 92% of kidneys (n = 34). Of these cases, tumour necrosis in the pathological specimen was noted in 33 (97%), and no cases demonstrated sarcomatoid differentiation. Medical risk factors for CKD included diabetes in 14 (38%), hypertension in 24 (65%) and cardiovascular disease in 19 patients (51%). The Charlson comorbidity score was ≥6 in 28 patients (76%), with 11 patients referred because they were at technically high risk of post-surgical dialysis (30%) with a complex tumour in a dominant functioning kidney. Only one patient in the cohort refused surgery as the reason for enrolment (Charlson comorbidity score 1).

Of the 37 patients who fulfilled eligibility criteria, 33 patients received all study treatments to 34 primary RCCs, resulting in a feasibility rate of 89% (95% CI 73–94). Of the 4/37 patients for which treatment was not delivered, one patient with a pulmonary embolus prior to SABR died after an international flight and two could not meet planned dose constraints. One further patient completed only two of three planned fractions because of social difficulties. Acute and late treatment-related toxicities are shown in Table 2. One patient (3%) had a treatment-related grade 3 toxicity (fatigue), 26 (78%) reported grade 1–2 treatment-related toxicity as worst grade and six patients (18%) reported no treatment-related side effects. There was no treatment-related mortality, and no grade 4 toxicities were recorded.

Radiotherapy treatment characteristics were as follows: 17 patients were prescribed 26 Gy in a single fraction; and 17

Table 1 Patient characteristics.

| Characteristic	
Median (range) age, years	78 (42–91)
Sex, n (%)	
Female	9 (24)
Male	28 (76)
T stage, n (%)	
1a	13 (35)
1b	23 (62)
2a	1 (3)
Tumour size largest dimension, mm	
Mean (SD)	49.2 (12.6)
Median (range)	48 (21–75)
Neutrophil:lymphocyte ratio (baseline)	
Mean (SD)	4.6 (6.5)
Laterality, n (%)	
Bilateral	1 (3)
Left	18 (49)
Right	18 (49)
Histological grade, n (%)	
I	3 (9)
II	20 (59)
III	1 (3)
Not otherwise specified	10 (29)
Histological subtype	
Clear-cell	30 (88)
Mixed	1 (3)
Papillary/chromophilic	3 (9)
Diabetes	
No	23 (62)
Yes	14 (38)
Hypertension	
No	13 (35)
Yes	24 (65)
Cardiovascular disease	
No	18 (49)
Yes	19 (51)
Charlson comorbidity score	
1–2	2 (5)
4–6	7 (19)
6	7 (19)
7	9 (24)
8	6 (16)
9–11	6 (16)

were prescribed 42 Gy in three fractions. For single-fraction and three-fraction SABR, the PTV was a median (interquartile range [IQR]) of 77.2 (51.8–89.4) cc and 166.8 (133.1–214.2) cc, respectively. The mean PTV dose as a percentage of the prescription dose was a median (IQR) of 122 (117–124)% and 117 (110–120])%, respectively. The minimum PTV dose as a percentage of the prescription dose was a median (IQR) of 92 (88–96)% and 81 (58–93)%, respectively.

Oncological outcomes are shown in Figs 1 and 2. The freedom from local progression rates at 1 and 2 years were100%. One patient progressed locally with concurrent distant progression at 28 months after treatment. The freedom from distant progression rates at 1 and 2 years were 97% (95% CI 91–100) and 89% (95% CI 78–100), respectively. The 1- and 2-year overall survival rates were

Table 2 Treatment-related adverse events according to period (acute and late) and overall.

Adverse event	Acute (≤90 days after SABR)			Late (>90 days after SABR)			Overall		
	Grade 1	Grade 2	Grade 3	Grade 1	Grade 2	Grade 3	Grade 1	Grade 2	Grade 3
Abdominal pain	0	0	0	0	1	0	0	1	0
Back pain	0	0	0	0	0	0	0	0	0
Chest wall pain	5	0	0	12	0	0	15	0	0
Dermatitis	2	0	0	0	0	0	2	0	0
Diarrhoea	3	0	0	1	0	0	3	0	0
Dizziness	0	0	0	0	0	0	0	0	0
Dizzy	0	0	0	0	0	0	0	0	0
Dyspnoea	0	1	0	2	0	0	2	1	0
Fatigue	11	6	0	7	0	1	14	5	1
Gastritis	1	1	0	1	0	0	2	1	0
Haematuria	0	0	0	3	1	0	3	1	0
Left flank pain	0	0	0	0	0	0	0	0	0
Nausea	5	2	0	2	0	0	5	2	0
Pneumonia	0	0	0	0	0	0	0	0	0
Right flank pain	1	0	0	0	0	0	1	0	0
Skin induration	0	0	0	1	0	0	1	0	0
At least one event, n (%)	11 (33)	7 (21)	0	17 (52)	2 (6)	1 (3)	19 (58)	7 (21)	1 (3)

SABR, stereotactic ablative body radiotherapy.

Fig. 1 Time to local progression at per-patient level.
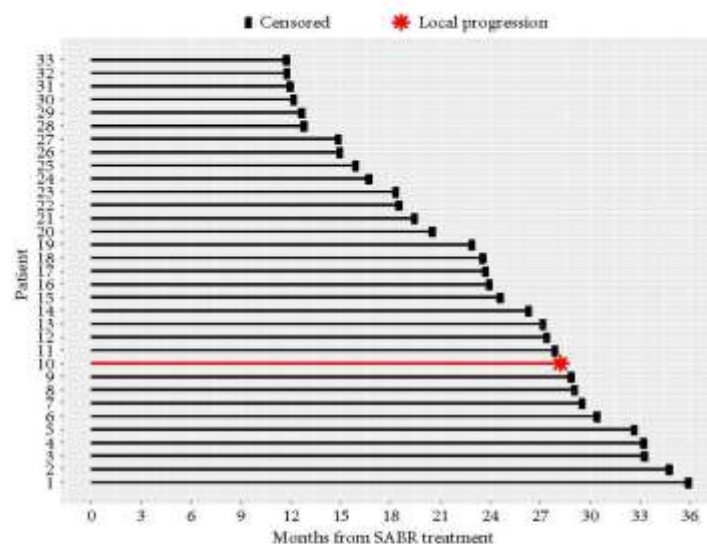
100% and 92% (95% CI 81–100), respectively. At last follow-up, four patients had partial responses and 28 had stable disease, as defined by RECIST criteria. Objective tumour size reduction at 1 year was observed in 61% of RCCs after SABR. In the univariate analysis describing % change in tumour size from baseline to 1 year (Table 3), only a lower neutrophil:lymphocyte ratio was significantly associated with tumour shrinkage ($r^2 = 0.45$, $P < 0.001$). A representative image of tumour shrinkage after therapy is shown in Fig. 3.

The baseline mean (range) eGFR was 55 (18–97) mL/min. At 1 year the eGFR was reduced by 11 mL/min (95% CI 6–17), and in the subset of nine patients who were assessed at 2 years, there was a similar reduction from baseline by 11 mL/min (95% CI 3–19). Whilst the change in eGFR was statistically significant at 1 year ($P < 0.001$) using linear mixed models, the slopes of change in eGFR in patients with pre-existing CKD were not different from patients without pre-existing CKD

Fig. 2 (A) Overall survival. (B) Freedom from distant progression. Dashed lines represent 95% CIs.
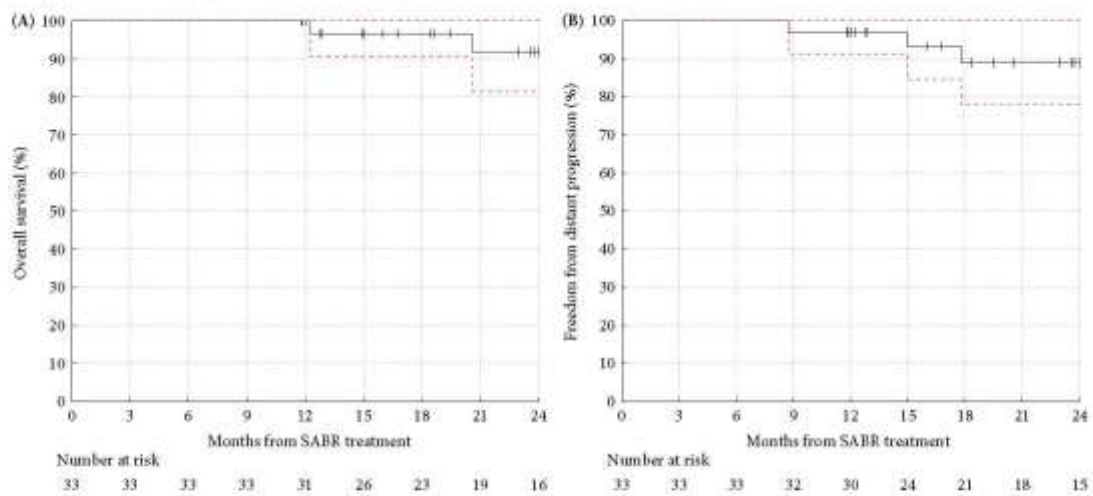
Table 3 Univariate analysis of % change in tumour size from baseline to 1 year after SABR.

Variable	Mean ± SD	r²	Coefficient ± SE	P
Histological grade				
NOS and I	−4.22 ± 9.38		1	0.318
II and III	−9.07 ± 13.43		−6.84 ± 4.73	
Minimum target dose (%)		0.02	−0.10 ± 0.14	0.475
Mean target dose (%)		0.01	−0.16 ± 0.26	0.551
PTV, cc		0.01	0.02 ± 0.03	0.627
Baseline tumour volume		0.00	−0.02 ± 0.04	0.806
Neutrophil/lymphocyte ratio		0.46	4.67 ± 1.02	<0.001

NOS, not otherwise specified; PTV, planned target volume.

Fig. 3 Representative image depicting maximum dimensions of a right-sided Fuhrman grade 2 primary RCC at baseline (left) and 1 year after SABR (right), demonstrating typical appearance of tumour shrinkage without change in contrast enhancement characteristics.

(difference in slopes of −2.1 mL/min (95% CI −5.3 to 1.1; $P = 0.196$). The slopes by the number of risk factors for CKD was also not statistically significant ($P = 0.536$).

Discussion

The present study has demonstrated the safety and efficacy of a conventional linear accelerator based technique for the

204

treatment of primary inoperable RCC. The majority (65%) of tumours treated were large renal masses (>4 cm). We observed grade 3 toxicity rates of 3% (transient fatigue) and no grade 4–5 toxicities. Importantly, most patients sustained only transient minor side effects (78%) or no treatment-related side effects (18%). Freedom from local progression at 2 years was 100%, with freedom from distant progression and overall survival being 89% and 92%, respectively. These results compare favourably with the existing largely retrospective literature suggesting local control rates ranging between 84 and 100%, with similarly low rates of associated toxicity [10]. A recent prospective phase 1 trial of 19 patients and a prospective series of 29 patients with primary RCC [11,12] corroborate the findings of infrequent treatment-related side effects (< 5% grade 3+ toxicities). Most of the existing literature is from groups using the Cyberknife™ (Accuray, Sunnyvale, CA, USA), a specialized robotic stereotactic radiotherapy delivery system. This system necessitates the insertion of fiducial markers for tumour tracking, an intervention that is invasive and associated with the risk of tumour haemorrhage. Importantly, our results were derived using conventional radiotherapy linear accelerators that are ubiquitous in modern radiotherapy departments worldwide, supporting the generalizability of our results internationally.

The majority (65%) of patients treated in our cohort had primary RCC > 4 cm in size. A major advantage of SABR over thermal ablation is the capacity to treat larger masses, as RFA and microwave ablation (MWA) are typically limited to the treatment of smaller small renal masses (< 4 cm). Whilst cryotherapy has the capacity to treat larger tumours, both complication rate and efficacy appear to be reduced. A multivariable analysis of outcomes in 99 patients undergoing laparoscopic cryoablation from the Netherlands determined that whilst lesion complexity did not prognosticate for risk of complications, tumour size >3.5 cm did [13]. Tumour control also appears to correlate to size, with a study in 124 patients from Washington University [14] of percutaneous cryoablation reporting a 2-year disease-free survival rate of 85%, with tumour size >3 cm being predictive of recurrence on multivariable analysis. Overall, one meta-analysis [15] reported a similar proportion of clinical efficacy for cryoablation at 89% vs RFA at 90%, whilst another [16] suggested better local tumour control of 94.8% after cryoablation compared with 87.1% after RFA. These rates are similar to those in the present series (despite the treatment of T1b and T2 disease) and to other literature on SABR for primary RCC [10]. Importantly SABR has a protocol and is thus not dependent on technician experience or learning curve, increasing the likelihood of reproducibility outside of major academic centres.

An important consideration with regard to ablative interventions for primary RCC is the ability to conserve nephrons and renal function. At the last recorded clinical visit, up to 3 years after SABR, no patient required renal replacement therapy. Both SABR and thermal ablative techniques affect a rim of surrounding normal kidney [17,18]. Meaningful comparisons are particularly challenging, as resultant renal dysfunction is proportional to tumour size and volume of ablation zones [19]. Most series of thermal ablation report outcomes from only small renal masses of typical average sizes, ranging from 2 to 3 cm in diameter, with very limited prospectively collected renal function outcomes. In one prospective study of 102 patients randomized to MWA vs PN, the mean tumour sizes were 3.1 and 2.8 cm, respectively. The mean eGFR for the MWA arm dropped by 7 mL/min from a baseline value of 130 mL/min, and dropped by 25 mL/min from a baseline value of 113 mL/min in the PN arm [20]. In a further study of 541 patients randomized between RN and PN [21], the median tumour size was 3.0 cm. During the first year after surgery, mean eGFR was 52.7 mL/min in the RN arm and 66.8 mL/min in the PN arm. The proportion reaching a postoperative eGFR was <60 mL/min was 85.7% with RN and 64.7% with PN. By comparison, the median tumour size treated in this trial was 4.8 cm, and the mean pre-treatment eGFR was already significantly impaired at 55 mL/min. The average post-treatment reduction was to 44 mL/min, and no patient required dialysis. In the 14 patients with an initial eGFR of >60 mL/min, new-onset eGFR of <60 mL/min occurred in 10 patients (71.4%). Importantly, this proportion of new-onset CKD was similar to that of PN in the surgical series discussed above (64.7%), and lower than that of RN (85.7%) [21]. Our cohort had significant medical risk factors for CKD, including diabetes in 38%, hypertension in 65% and cardiovascular disease in 51% of patients. Thus, whilst it is difficult to compare treatment approaches given the differences in tumour size, patient comorbidities and pre-existing renal dysfunction, in the context of the alternative therapeutic interventions of surgery and thermal ablation we observed a similar and clinically acceptable preservation of renal function after SABR, consistent with previous reports [11,12].

An exploratory finding of this study was the inverse correlation observed between neutrophil:lymphocyte ratio and tumour response to SABR. Raised levels of circulating neutrophils in peripheral blood is considered to be a biomarker of a chronic inflammatory state within the host, whilst depressed lymphocyte levels are considered to be reflective of a reduced capacity to mount an inflammatory response to cancer [22]. Although it is recognized that SABR is highly effective at RCC control in preclinical [23] and clinical studies [24], this efficacy may not be solely attributable to higher biological radiation dose. Indeed, it is possible that some of the efficacy of SABR is directly attributable to immune stimulating properties [25]. RCC is a

highly immunogenic tumour that has shown impressive responses to immunotherapy [26] as well as 'abscopal' or out-of-field distant tumour responses to radiotherapy with or without immunotherapy [25]. It may be that the association between lower neutrophil:lymphocyte ratio and tumour shrinkage is a correlate of lymphocyte-mediated adaptive immune response in the irradiated primary. This suggests possible utility as a novel and easily accessible predictive biomarker of response to therapy in patients undergoing SABR for primary RCC. This finding warrants further investigation and validation in future studies.

Radiological response assessment after SABR using CT criteria represents several challenges. Post-ablative radiotherapy effects in the tumour and adjacent normal tissues can evolve over years [27], and in the more common application of SABR for lung tumours, functional imaging with positron emission tomography can detect metabolic responses that long predate any CT apparent morphological changes [28]; however, positron emission tomography does not have an established role in the context of primary RCC. Presence of tumour cells on biopsy after ablative radiation can also be unreliable, such as in the context of prostate brachytherapy, where positive biopsies can occur up to 2 years post-therapy but do not correlate to biochemical disease control [29]. Whilst residual post-radiation tissue within the treated field is expected, tumour progression on CT imaging is not, and thus progression is typically used as a surrogate for treatment failure.

The present study has several limitations. First and foremost, because this is an early-phase clinical trial, longer-term follow-up is required to establish robust efficacy outcomes in this cohort. Secondly, the treatment of small renal masses may be criticized by some, with expected growth rates of 0.25 cm per year [30] and low metastatic potential [31]. As described the patients in the present study had already demonstrated progression and/or symptoms after initial active surveillance, and treatment was recommended only once comorbidities had been carefully balanced by a multidisciplinary tumour board. Furthermore the vast majority of tumours included in the present study were larger masses indicating the feasibility of SABR in masses not amenable to thermal ablative techniques. Additionally, histological confirmation was not achieved in all cases (8%). Finally, the observed post-treatment decline in GFR was modest but, again, longer-term data would be reassuring in order to evaluate functional outcomes.

In conclusion, SABR for both small and large primary RCC is well tolerated. We observed encouraging cancer control, functional preservation and survival in an inoperable cohort. Baseline neutrophil:lymphocyte ratio may be predictive of immune-mediated response and warrants further investigation. The findings of this study have been used to inform the design of an international phase II clinical trial under the auspices of the TransTasman Radiation Oncology Group (TROG 15.03 FASTRACK, clinicaltrials.gov ID NCT02613819). This study is designed with the purpose of validating the efficacy of our treatment technique in a multi-institutional setting.

Acknowledgements

Conflict of Interest

None declared.

References

1 Znaor A, Lortet-Tieulent J, Laversanne M, Jemal A, Bray F. International variations and trends in renal cell carcinoma incidence and mortality. Eur Urol 2015; 67: 519–30

2 Siegel R, Naishadham D, Jemal A. Cancer statistics, 2013. CA Cancer J Clin 2013; 63: 11–30

3 Ljungberg B, Campbell SC, Choi HY et al. The epidemiology of renal cell carcinoma. Eur Urol 2011; 60: 615–21

4 Demirjian S, Lane BR, Derweesh IH, Takagi T, Fergany A, Campbell SC. Chronic kidney disease due to surgical removal of nephrons: relative rates of progression and survival. J Urol 2014; 192: 1057–63

5 Van Poppel H, Becker F, Cadeddu JA et al. Treatment of localised renal cell carcinoma. Eur Urol 2011; 60: 662–72

6 Siva S, Ellis RJ, Ponsky L et al. Consensus statement from the International Radiosurgery Oncology Consortium for Kidney for primary renal cell carcinoma. Fut Oncol 2016; 12: 637–45

7 Siva S, Daniels CP, Ellis RJ, Ponsky L, Lo SS. Stereotactic ablative body radiotherapy for primary kidney cancer: what have we learned from prospective trials and what does the future hold? Fut Oncol 2016; 12: 601–6

8 Eisenhauer E, Therasse P, Bogaerts J et al. New response evaluation criteria in solid tumours: revised RECIST guideline (version 1.1). Eur J Cancer 2009; 45: 228–47

9 Pham D, Thompson A, Kron T et al. Stereotactic ablative body radiation therapy for primary kidney cancer: a 3-dimensional conformal technique associated with low rates of early toxicity. Int J Radiat Oncol Biol Phys 2014; 90: 1061–8

10 Siva S, Pham D, Gill S, Corcoran NM, Foroudi F. A systematic review of stereotactic radiotherapy ablation for primary renal cell carcinoma. BJU Int 2012; 110: E737–43

11 Ponsky L, Lo SS, Zhang Y et al. Phase I dose-escalation study of stereotactic body radiotherapy (SBRT) for poor surgical candidates with localized renal cell carcinoma. Radiother Oncol 2015; 117: 183–7

12 Staehler M, Bader M, Schlenker B et al. Single fraction radiosurgery for the treatment of renal tumors. J Urol 2015; 193: 771–5

13 Lagerveld BW, Brenninkmeijer M, van der Zee JA, van Haarst EP. Can RENAL and PADUA nephrometry indices predict complications of laparoscopic cryoablation for clinical stage T1 renal tumors? J Endourol 2014; 28: 464–71

14 Kim EH, Tanagho YS, Bhayani SB, Saad NE, Benway BM, Figenshau RS. Percutaneous cryoablation of renal masses: Washington University experience of treating 129 tumours. BJU Int 2013; 111: 872–9

15 El Dib R, Touma NJ, Kapoor A. Cryoablation vs radiofrequency ablation for the treatment of renal cell carcinoma: a meta-analysis of case series studies. *BJU Int* 2012; 110: 510–6

16 Kunkle DA, Uzzo RG. Cryoablation or radiofrequency ablation of the small renal mass. *Cancer* 2008; 113: 2671–80

17 Kutikov A, Kunkle DA, Uzzo RG. Focal therapy for kidney cancer: a systematic review. *Curr Opin Urol* 2009; 19: 148–53

18 Siva S, Jackson P, Kron T et al. Impact of stereotactic radiotherapy on kidney function in primary renal cell carcinoma: Establishing a dose-response relationship. *Radiother Oncol* 2016; 118: 540–6

19 Park SY, Park BK, Kim CK. Thermal ablation in renal cell carcinoma: what affects renal function? *Int J Hyperth* 2012; 28: 729–34

20 Guan W, Bai J, Liu J et al. Microwave ablation versus partial nephrectomy for small renal tumors: intermediate-term results. *J Surg Oncol* 2012; 106: 316–21

21 Scosyrev E, Messing EM, Sylvester R, Campbell S, Van Poppel H. Renal function after nephron-sparing surgery versus radical nephrectomy: results from EORTC randomized trial 30904. *Eur Urol* 2014; 65: 372–7

22 Coffelt SB, Wellenstein MD, de Visser KE. Neutrophils in cancer: neutral no more. *Nat Rev Cancer* 2016; 16: 431–46

23 Ning S, Trisler K, Wessels BW, Knox SJ. Radiobiologic studies of radioimmunotherapy and external beam radiotherapy in vitro and in vivo in human renal cell carcinoma xenografts. *Cancer* 1997; 80: 2519–28

24 Kothari G, Foroudi F, Gill S, Corcoran NM, Siva S. Outcomes of stereotactic radiotherapy for cranial and extracranial metastatic renal cell carcinoma: a systematic review. *Acta Oncol* 2015; 54: 148–57

25 Reynders K, Illidge T, Siva S, Chang JY, De Ruysscher D. The abscopal effect of local radiotherapy: using immunotherapy to make a rare event clinically relevant. *Cancer Treat Rev* 2015; 41: 503–10

26 Park SS, Dong H, Liu X et al. PD-1 Restrains Radiotherapy-Induced Abscopal Effect. *Cancer Immunol Res* 2015; 3: 610–9

27 Huang K, Palma DA. Follow-Up of Patients after Stereotactic Radiation for Lung Cancer: A Primer for the Nonradiation Oncologist. *J Thorac Oncol* 2015; 10: 412–9

28 Siva S, Callahan JW, Kron T et al. Respiratory-gated (4D) FDG-PET detects tumour and normal lung response after stereotactic radiotherapy for pulmonary metastases. *Acta Oncol* 2015; 54: 1105–12

29 D'Alimonte L, Helou J, Sherman C et al. The clinical significance of persistent cancer cells on prostate biopsy after high-dose-rate brachytherapy boost for intermediate-risk prostate cancer. *Brachytherapy* 2015; 14: 309–14

30 Mason RJ, Abdolell M, Trottier G et al. Growth kinetics of renal masses: analysis of a prospective cohort of patients undergoing active surveillance. *Eur Urol* 2011; 59: 863–7

31 Jewett MA, Mattar K, Basiak J et al. Active surveillance of small renal masses: progression patterns of early stage kidney cancer. *Eur Urol* 2011; 60: 39–44

Correspondence: Dr Shankar Siva, Peter MacCallum Cancer Centre, 305 Grattan Street, Melbourne, Vic. 3000, Australia.

e-mail: shankar.siva@petermac.org

Abbreviations: SABR, stereotactic ablative body radiotherapy; PN, partial nephrectomy; RN, radical nephrectomy; RFA, radiofrequency ablation; eGFR, estimated GFR; RECIST, Response Evaluation Criteria In Solid Tumors; CTCAE, Common Terminology Criteria for Adverse Events; CKD, chronic kidney disease; PTV, planning target volume; IQR, interquartile range; MWA, microwave ablation.